THE UNIVERSITY OF
SYDNEY

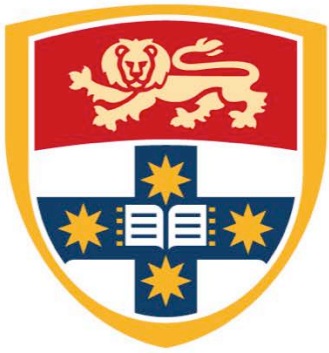

Structural and Functional Studies of Cardiac Myosin Binding Protein – C and Cofilin

Joo-Mee Hwang

A thesis submitted for the degree of
Doctor of Philosophy (Medicine)

Discipline of Pathology
Faculty of Medicine
The University of Sydney
Sydney, Australia

August, 2013

Declaration

In accordance with the laws of The University of Sydney the author declares that: this thesis describes original research performed within the Discipline of Pathology at The University of Sydney and The Institute of Molecular Biophysics at Florida State University between February 2007 and August 2012. All the results reported herein were the work of the author, except acquisition of NMR spectra, which were performed in collaboration with Prof Tim Logan, Florida State University.

This work has not been submitted for any other degree at this or any other institution.

Joo-Mee Hwang

August, 2013

Acknowledgements

First and foremost, I would like to acknowledge my supervisors, Dr Brett Hambly and Dr Murat Kekic, for their ceaseless guidance and encouragement. I am privileged to say I have worked under the most supportive and approachable academics.

Special thanks must go to Prof. Peter Fajer, Prof. Tim Logan and their lab members, whom have not only guided me in my PhD project but also for welcoming me to the States and making my visit memorable and fun. I would also like to thank Dr Deepak Chhabra for his advice on cofilin, Dr Adrian Tchen for rabbit muscle and Dr Alistair Edwards for his expertise and time in assisting with the mass spectrometry work.

Enormous thanks must go to Dr Cecily Oakley, Yaxin Lu, Komal Prabhu and Nasim Nik Tavakoli. My time here is full of memories with all of you guys. You were all there for me through my ups and downs and I truly couldn't have done this without any of you. Thank you very much.

I would also like to thank my special friends for their friendship and support. You guys know who you are. Thank you very much for putting up with me and most importantly, for not talking about my PhD whenever I am not in the mood for it.

Finally, I would like to express my gratitude to my family. Dad, thank you very much for your unstinting support and sense of humour. Mum, your perpetual care and immense support brought me where I am now. My lovely sister, Joo-Hee, I cannot thank you enough for your boundless support and encouragement. Thank you all!

Summary

Muscle is one of the most specialised and organised units in our body. Its ability to generate force via the complex interaction of many different muscle proteins is widely accepted. While the basic mechanism of force generation in vertebrate muscle is well understood, the precise structure and function of numerous other proteins that also contribute in muscle contraction and cell motility, such as cardiac myosin binding protein C (cMyBP-C) and cofilin, remain unclear. Therefore, greater understanding of the structure and function of these proteins will enhance our understanding and management of muscle related diseases, such as familial hypertrophic cardiomyopathy (FHC). Additionally, mutations in cardiac myosin binding protein C are known to be the most common cause of FHC.

Thus, the aims of this thesis are to 1). Construct a fragment of cMyBP-C and its FHC mutants and to assess their structural and functional roles and, 2). Design cofilin mutants suitable for selective labelling with extrinsic fluorescent spectroscopic probes to assess its structural and functional role.

The fragment of cMyBP-C examined in this thesis is C1 + linker (C1-L). C1 is an immunoglobulin domain of cMyBP-C with the lengthy linker region joining the two immunoglobulin domains, C1 and C2. While the structures of C1 and C2 are known, the structure of the linker region is unknown. However, homology modelling of the linker region suggests the presence of some α-helix in the C-terminal half of the linker, while the N-terminal half of the linker consists of minimal secondary structure and most likely a significant amount of random coil. Thus, the C1-L construct was used to gain further insight into the structure of the linker region by using nuclear magnetic resonance (NMR) spectroscopy. This study revealed the linker region is largely unstructured with significant α-helical content.

Along with the structural analysis, functional analysis was also performed using C1-L and its FHC mutant constructs. cMyBP-C has been shown to bind to myosin, actin and titin, however, the specific binding site(s) remain to be determined. cMyBP-C includes an N-terminal region, which projects out from the thick filament and is believed to be able to interact with both actin and the myosin crossbridge. Of this N-terminal region, domains C1 and C2 and the motif (linker) region connecting the two domains (collectively denoted as C1-C2) were analysed in this thesis. This

region is of special interest as its cardiac isoform (related to FHC) contains multiple phosphorylation sites (C1-C2 is phosphorylated in response to α and ß adrenergic stimulation) and controls S2 binding, which in turn allows an increase in systolic force. Phosphorylation may also regulate actin binding, thus making this region a crucial component of cMyBP-C function. Furthermore, the C2 domain alone has been shown to have minimal capacity to bind to actin, raising the question whether the minimum functional unit is the C1 domain and motif (linker). Our data showed that C1-L is capable of binding to both F-actin and myosin with a similar affinity to the full C1-C2 construct, albeit with a weak, μmolar affinity. These data are consistent with the hypothesis that the C2 domain makes little contribution to binding to F-actin or myosin. Additionally, our data have shown that FHC mutations result in reduced binding to F-actin, suggesting that, at least in part, these mutations may exert their effects on sarcomeric function by inhibiting normal physiological interactions with F-actin during the contractile cycle.

Another actin binding protein, cofilin, was studied in this thesis. Cofilin is important for the regulation of the actin cytoskeleton. It is capable of binding to and severing F-actin filaments, but the molecular basis for these functions is poorly understood, due to a paucity of structural data on the quaternary complex. A recent computational model has been proposed which we sought to test. We inserted mutant residues into the sequence of cofilin to facilitate the specific and unique labelling of cofilin residues with spectroscopic probes, to gain structural and functional insights in the cofilin-actin interaction.

We successfully mutated and expressed four mutant cofilins, each containing unique spectroscopic probe sites. During this process, we discovered the apparent sensitivity of the structure of cofilin to mutagenesis. Mutagenesis led one N-terminal cofilin mutant to abolish G-actin binding, whilst still permitting F-actin binding. On the other hand, mutations at others sites showed no effect on the binding of cofilin to both G- and F-actin. These data allowed us to postulate which regions of cofilin are involved in actin binding. Additionally, inter-molecular distance measurements between actin and cofilin were undertaken, using fluorescence resonance energy transfer (FRET) spectroscopy. Our data provide strong confirmation for the proposed computational model of the cofilin-F-actin complex.

List of Abbreviations

A	Adenine
ABP	Actin binding protein
ACEC	Animal Care and Ethics Committee
ADF	Actin depolymerisation factor
ADP	Adenosine diphosphate
APS	Ammonium persulphate
ATP	Adenosine triphosphate
ATPase	Adenosine triphosphatase
A.U.	Absorbance units
BSA	Bovine serum albumin
C	Cytosine
Ca^{2+}	Calcium
$CaCl_2$	Calcium chloride
cAMP	Cyclic adenosine monophosphate
CD	Circular dichroism
cMyBP-C	cardiac myosin binding protein-C
C1-L	C1 + linker
C1-C2	C1 + linker + C2
DABMI	4-Dimethylaminophenylazophenyl-4'-maleimide
DHNBS (HNB)	Dimethyl(2-hydroxy-5-nitrobenzyl) sulphonium bromide
DNA	Deoxyribonucleic acid
dNTP	Deoxyribonucleotide triphosphate
ds	Double stranded
DTT	Dithiothreitol
ECG	Echocardiography
E. coli	*Escherichia coli*
EDTA	Ethylenediaminetetraacetic acid.
FHC	Familial hypertrophic cardiomyopathy
Fn	Fibronectin
G	Guanine
GST	Glutathione-S-transferase
HCl	Hydrochloric acid
H & E	Hematoxylin and eosin
HMM	Heavy meromyosin
IAEDANS	5-({2-[(iodoacetyl) amino] ethyl}amino) naphthalene-1-sulfonic acid
IgI	Immunoglobulin of the 'I' set
IPTG	Isopropyl β-D-1-thiogalactopyranoside
KCl	Potassium chloride
LB	Luria-Bertani
LMM	Light meromyosin
MALDI-TOF MS	Matrix-assisted laser desoption ionisation time-of-flight mass spectrometry
Mg^{2+}	Magnesium
$MgCl_2$	Magnesium chloride
MRE	Mean residue ellipticity
MRW	Mean residue weight

MS	Mass spectrometry
mS/cm	MilliSiemens per centimetre
MyBP-C	Myosin binding protein C
MW	Molecular weight
NaCl	Sodium chloride
NaN_3	Sodium azide
NaOH	Sodium hydroxide
NMR	Nuclear magnetic resonance
NP-40	Nonylphenyl-polyethylene glycol, nonidet P-40
OD	Optical density
PBS	Phosphate buffered saline
PEVK	Proline, glutamine, valine and lysine
PCR	Polymerase chain reaction
pET	Plasmid for expression by T7 RNA polymerase
Pi	Inorganic phosphate
PIP	Phosphatidylinositol 4-phosphate
PIP2	Phosphatidylinositol 4,5-bis-phosphate
PKA	Protein kinase
PMSF	Phenylmethylsulphonylfluoride
RNA	Ribonucleic acid
SCD	Sudden cardiac death
SDS-PAGE	Sodium dodecyl sulphate polyacrylamide gel electrophoresis
SUMO	Small ubiquitin-like modifier
SUPAMAC	Sydney University and Prince Alfred Hospital Macromolecular Analysis Centre
S1	Subfragment 1, N-terminal heads
S2	C-terminal ends, the tails
T	Thymine
TAE	Tris-acetate-EDTA
TEMED	N,N,N’,N’-trimethylenediamine
Tm	Tropomyosin
Tn	Troponin
TnC	Troponin C
TnI	Troponin I
TnT	Troponin T
UV	Ultraviolet
WHO	World Health Organisation

Amino Acids

Alanine	Ala	A	Glycine	Gly	G	Proline	Pro	P
Arginine	Arg	R	Histidine	His	H	Serine	Ser	S
Asparagine	Asn	N	Isoleucine	Ile	I	Threonine	Thr	T
Aspartic acid	Asp	D	Leucine	Leu	L	Tryptophan	Trp	W
Cysteine	Cys	C	Lysine	Lys	K	Tyrosine	Tyr	Y
Glutamine	Gln	Q	Methionine	Met	M	Valine	Val	V
Glutamic acid	Glu	E	Phenylalanine	Phe	F			

Contents

List of Figures

List of Tables

Chapter 1

General Introduction

Chapter 1

General Introduction

1.1 Introduction

One of the most essential properties of living systems is their ability to transform chemical energy into motion. This motion is essential in a myriad of biological functions: chemotaxis, cytokinesis, pinocytosis, signal transduction, vesicle transport and muscle contraction (Mermall, Post et al. 1998).

An extremely specialised and organised unit, called muscle, allows this phenomenon to occur. It has been widely accepted that muscle contraction occurs when two sets of interdigitating filaments, the thick filaments and the thin filaments, mainly composed of two proteins called myosin and actin, respectively, slide past each other in a highly organised and uniform manner.

While the basic mechanism of force generation in vertebrate muscle is well understood, the precise structure and function of numerous other proteins that contribute to muscle contraction, such as myosin binding protein C, are yet to be solved. Hence, many scientists endeavour to fill this gap, hoping that their discoveries will subsequently lead to a more focused approach to the understanding and management of muscle-related diseases, including familial hypertrophic cardiomyopathy.

1.2 Classification of Vertebrate Muscle

Vertebrate muscle is classified into two groups, striated and smooth muscle, according to their histological appearance, as shown in Figure 1.1. Striated muscle produces visible banding patterns that are not found in smooth muscle.

1.2.1 Striated Muscle

Vertebrate muscle consists of cells that exhibit cross-striations at the light microscope level. These striations are due to diffraction of light by highly organised repeating units in the muscle fibres called sarcomeres, which are further discussed in Section 1.3. Striated muscle tissue is further subclassified into 2 groups, skeletal and cardiac.

1.2.1.1 Skeletal Muscle

Skeletal muscles are attached to bones, organs (e.g. the eyeball), skin (e.g. facial muscles) and to the mucous membrane (e.g. intrinsic tongue muscles). They are voluntary and innervated by the somatic nervous system.

Fibres of skeletal muscle contain unbranched multinucleate myocytes resulting from fusion of many smaller cells during embryonic development. The muscle fibres lay parallel to each other, bundled together by connective tissue (Figure 1.1a). These fibres are 10-100 μm in diameter and extend the entire length of the muscle, from tendon to tendon; consequently they can be up to 35 cm in length. Longitudinally arrayed subunits called myofibrils make up the skeletal muscle fibres. These are the specialised contractile elements.

There are three types of skeletal muscle fibres: red, white and intermediate. Red fibres are small fibres making up slow-twitch motor units and can be found to be enriched, for example, in the legs of long distance runners. They are abundant in both mitochondria and myoglobin (a protein resembling haemoglobin), thus producing a red appearance. Since they are sustained by aerobic metabolism, the fibres have greater resistance to fatigue but produce less force than white fibres. White fibres, making up fast-twitch motor units and sustained by anaerobic metabolism, are more prone to fatigue, but generate more force than red fibres. Consequently, they are adapted for rapid contraction and precise movements and can be found to be enriched, for example, in the legs of sprinters. Intermediate fibres are intermediate between those of red and white fibres in size, amount of myoglobin and mitochondria

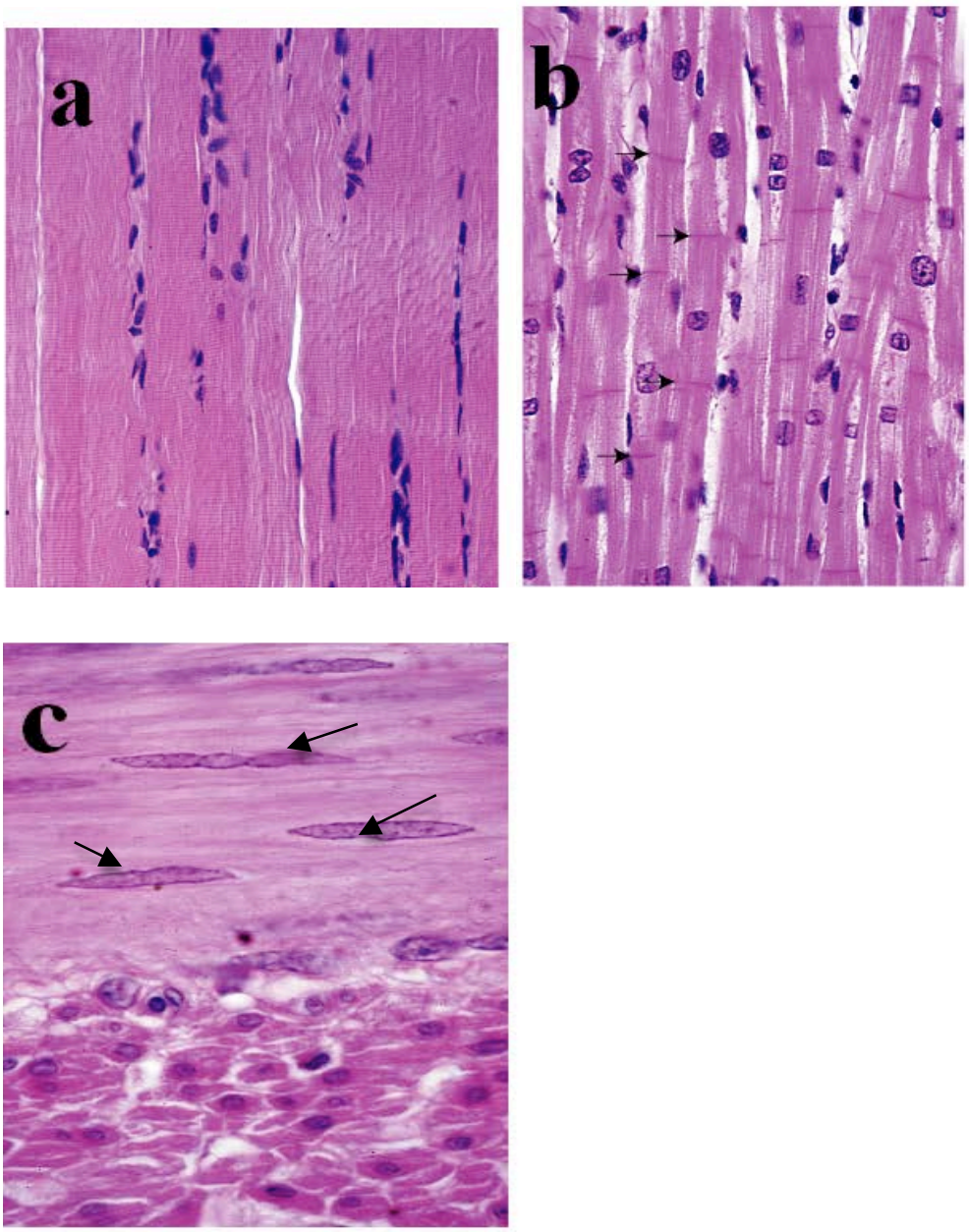

Figure 1.1. Haematoxylin and eosin stains of muscle viewed under the light microscope.

a) Longitudinal section of skeletal muscle. Muscle fibres are arranged parallel to each other; nuclei are located in the cytoplasm immediately beneath the plasma membrane and cross-striations of the muscle fibres are apparent.
b) Longitudinal section of cardiac muscle reveals the intercalated discs (arrows)
c) Longitudinal section of smooth muscle from small intestine. Note the centrally located nuclei (arrows) and their tapered ends. Image from (Ross, Kaye et al. 2003)

1.2.1.2 Cardiac Muscle

Cardiac muscle forms the muscular wall of the heart and has contractile filaments similar to skeletal muscle in its types and arrangement. Consequently, it appears striated when viewed under the microscope.

However, cardiac muscle differs from skeletal muscle in that it possesses a centrally located mononucleus and its fibres are smaller, only 100-200 μm in length and 15-20 μm in diameter. Furthermore, cardiac muscle fibres are branched and joined to their neighbouring fibres via intercalated discs through which the contractile signals are passed from cell to cell (Figure 1.1b).

Cardiac muscle fibres are involuntary and are innervated by the autonomic nervous system.

1.2.2 Smooth Muscle

Smooth muscle cells are between 20 – 500 μm in length and are composed of mononucleate cells. They are tapered at each end with nucleus located at the centre of the cell (Figure 1.1c). While smooth muscle cells also contain actin and myosin filaments like striated muscle cells, these filaments lack the aligned organisation that skeletal and cardiac muscle possess, thus lacking the striations.

Smooth muscle fibres are specialised for slow prolonged contraction and are innervated by the autonomic nervous system. They are also responsible for involuntary actions and can be found in the digestive tract, bladder, uterus and blood vessels walls.

1.3 The Sarcomere

1.3.1 Structure of the Sarcomere

Myofibrils are the functional unit of muscle cells and are made up of repeating units called sarcomeres. Sarcomeres occur in both skeletal and cardiac muscle and are very similar in structure in these two muscle types. However, in the sarcomere is lacking in smooth muscle. The sarcomere is a complex structure and is 2.2 μm in length in its relaxed state. It is composed of two cytoskeletal elements called thick and thin filaments. The thick filaments are approximately 1.5 μm long and are mainly composed of myosin, along with other proteins that bind to myosin, such as myosin binding protein C (MyBP-C). The thin filments are composed of actin and the

regulatory proteins tropomyosin and troponin and are attached to the Z-line, which defines the boundaries of the sarcomere (Figure 1.2). It is the overlapping of these two filaments that give it a striated appearance under the light microscope.

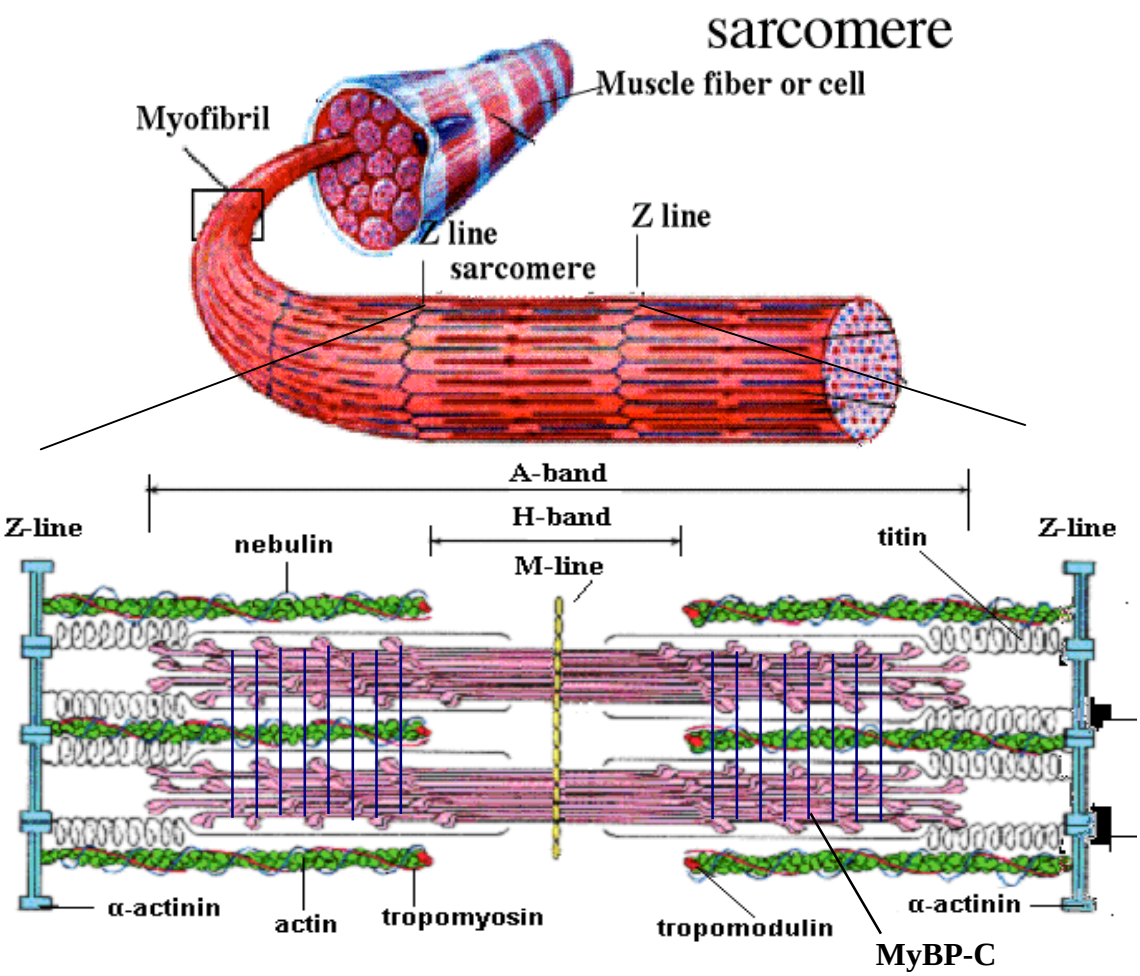

Figure 1.2. Structure and organisation of the sarcomere. Skeletal muscle consists of bundles of muscle fibres called fascicles, which in turn consists of a bundle of elongated muscle fibres called myofibrils. These myofibrils consist of thick and thin filaments and the overlap of these filaments creates various bands. Image modified from (Ross, Kaye et al. 2003)

The overall structure of a sarcomere can be viewed under the electron microscope (Figure 1.3), which manifests different zones of the sarcomere. The anisotropic A-band, the region where thick filaments are located, and which overlaps the thin filaments, is found as a dark zone. The isotropic I-band is a light zone, where thin filaments are found without the thick filaments. The H-band in the middle of the sarcomere is the region where thick filaments are found without thin filaments. Lastly,

the C-zone is the segment where the thick and thin filaments interdigitate, that is, the part of the thick filament that contains cross-bridges. In this C-zone, the thick filaments are aligned approximately 13 nm away from six neighbouring thin filaments. Thus, upon muscle contraction, the thick and thin filaments slide over one another and consequently, the length of sarcomere, I-band and H-zone shortens whereas the length of the A-band remains constant. In this anisotropic A-band, a protein called myosin binding protein-C (MyBP-C) is found in 7-9 transverse stripes 43 nm part (Figure 1.2.). This is the protein of interest in this thesis and will be discussed in details in Section 1.6.

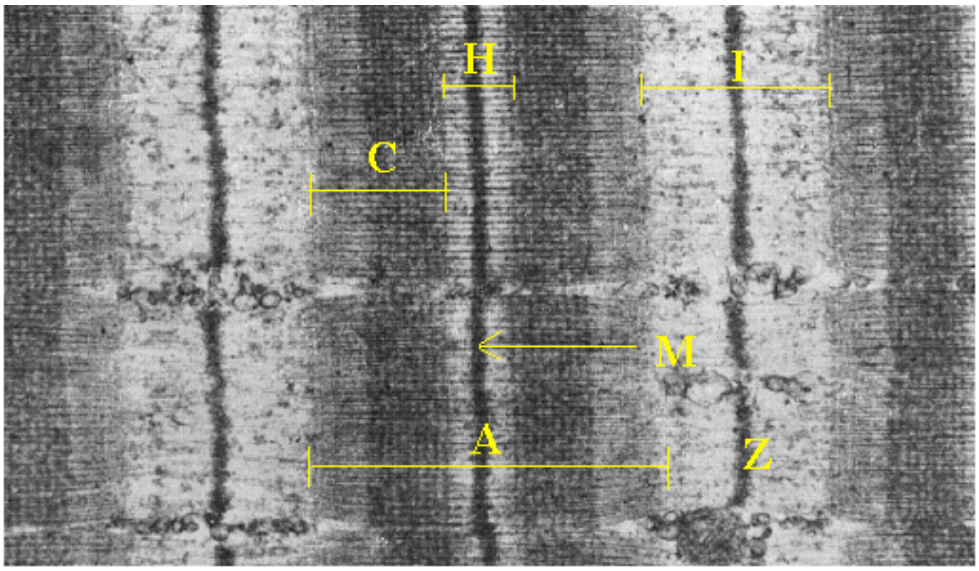

Figure 1.3. Electron micrograph of sarcomere. H: H-band; I: I-band; M: M-line; Z: Z-line; C: C-band and A: A-band. Image modified from (Ross, Kaye et al. 2003).

1.3.2 Components of the Sarcomere

1.3.2.1 Actin

Actin was discovered by Straub in 1942 from muscle tissue extracts and is now known to be found in all eukaryotes (Poglazov 1983). It is a highly conserved protein and plays a major role in a wide variety of functions in eukaryotes, including muscle contraction, ameboid movement, cytokinesis and mitotic division (Gunning, Ponte et al. 1983). Furthermore, its interactions with other actin monomers, tropomyosin, troponin and myosin maintain the structural integrity of the thin filament and supports the regulatory proteins.

Actin is the primary structural protein of the thin filament and was given its name due to its ability to “activate” myosin. Its simplest form is in the monomeric form, called G-actin, and it is globular in shape, approximately 4 nm in diameter with a molecular weight of 43 kDa. It is comprised of 375 amino acids (Gunning, Ponte et al. 1983). In the presence of physiological concentrations of salt and with the addition of divalent cations such as Ca^{2+} or Mg^{2+}, G-actin polymerises to form filamentous F-actin, consisting of 13 monomeric G-actin subunits for every six left-handed turns and a repeat of approximately 360 Å (Figure 1.4) (Egelman 1985). Actin is further described in Section 6.1.

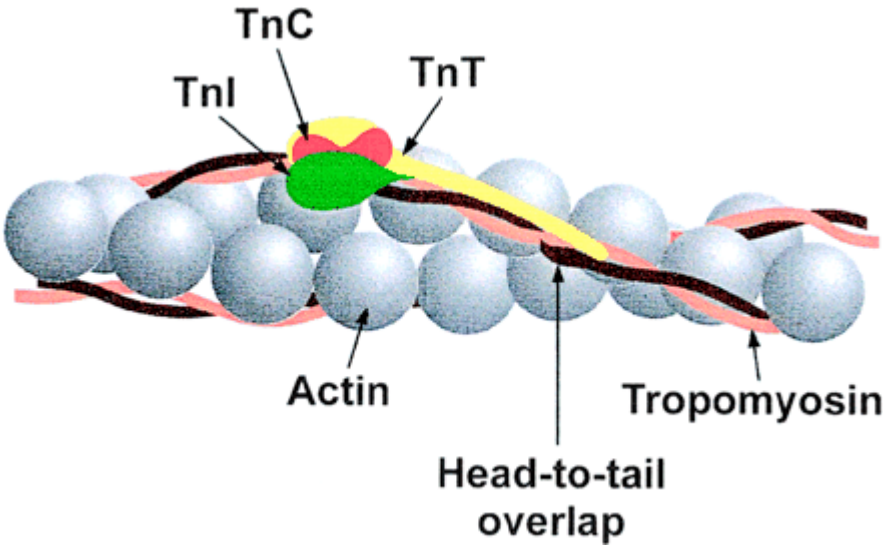

Figure 1.4. Schematic diagram of thin filament. Two strands of F-actin form a helical structure. Tropomyosin TM also form a helical coil by wrapping around the actin polymer and the troponin complex, which is made up of TnI (green), TnC (red) and TnT (yellow). This leads to coordinated interaction between actin, tropomyosin and the tropinin complex (Gordon, Homsher et al. 2000).

1.3.2.2 Tropomyosin

A threadlike protein, tropomyosin, is a double stranded α-helical, coiled-coil dimer with two 284 amino acid residue chains (Wolska and Wieczorek 2003). It lies in the grooves formed by the actin double-helix and wraps itself around by bridging approximately seven actin subunits (Figure 1.4). In the relaxed state (absence of Ca^{2+}), it binds strongly to actin via the troponin complex to block the actin-myosin interaction.

1.3.2.3 Troponin

Troponin is a heterotrimeric complex and was initially named as 'native tropomysin' (Ebashi 1963). The three subunits of troponin complex are troponin C (TnC), troponin I (TnI) and troponin T (TnT) (Figure 1.4), each of which performs a specific function. The troponin complex is directly affected by the Ca^{2+} concentration: in the low Ca^{2+} state, the troponin complex allows the tropomysin chain to lie over the myosin binding sites on the actin filaments. Once Ca^{2+} binding occurs, this interaction causes conformational changes, allowing the tropomyosin chain to slide away from the myosin binding sites and subsequently the myosin S1-actin interaction occurs, initiating the cross-bridge cycle. The atomic resolution structure of the core domains of the human cardiac components of the troponin complex has been determined (Takeda 2005).

TnC is a calcium binding subunit with molecular weight of approximately 18kDa. It is symmetrical in shape and belongs to the EF-hand protein with metal ion binding sites. The structure of TnC consists of two globular metal binding EF-hand domains joined by a central linker, giving the protein a dumbbell shape. TnC has N- and C-domains and each has two metal binding sites. The two binding sites on the C-domain have high affinity for Ca^{2+}/Mg^{2+} and are always occupied, hence anchoring TnC to TnI (Robertson, Johnson et al. 1982) whereas the two binding sites on the N-domain as low affinity for Ca^{2+} (Houdusse, Love et al. 1997, Soman, Tao et al. 1999) subsequently involved in the regulation of contraction. Although there is a high degree of homology between the skeletal and cardiac TnC isoforms, the two main differences are: cardiac TnC only has one N-domain Ca^{2+} binding EF-hand (van Eerd and Takahashi 1975, Li, Gagne et al. 1997) and the central linker between the N-domain and the C-domain in the cardiac TnC is more flexible (Slupsky and Sykes 1995, Takeda, Yamashita et al. 2003).

TnI is a flexible polypeptide chain (~24kDa) which inhibits the ATPase activity of actomyosin with at least two inhibitory sites (Filatov, Katrukha et al. 1999). Like TnC, TnI is an elongated protein and binds to TnC, TnT and actin. It consists of 181 amino acid residues in the skeletal isoform (both fast and slow) in contrast to 211 amino acid residues in the cardiac isoform, due mainly to the presence of an additional approximately 30 amino acid N-terminal peptide.

An elongated protein, TnT attaches its N-terminal tail end (TnT1) to tropomyosin laterally and its C-terminal end (TnT2) to both TnC and TnI to form

troponin's globular core domain (Greaser and Gergely 1971, Flicker, Phillips et al. 1982). Whilst its exact physiological role remains poorly understood, it is thought to play a role in anchoring the TnC and TnI complex to the thin filament, activation of actomyosin ATPase in a Ca^{2+} dependent manner (Potter, Sheng et al. 1995), regulating tropomyosin movement during muscle contraction (Gordon, Homsher et al. 2000) and stabilising the blocked state of cardiac thin filament in its cardiac isoform (Gollapudi, Mamidi et al. 2012).

1.3.2.4 Tropomyosin/Troponin Regulation

At low Ca^{2+} concentration, bilobed TnC binds weakly to the W-shaped TnI-TnT complex (Pirani, Vinogradova et al. 2006), but TnI binds strongly to actin thereby holding tropomyosin in the position that blocks the myosin binding site (Wolska and Wieczorek 2003). However, with an increase in Ca^{2+} concentration, the TnC-TnI interaction becomes dramatically stronger and the interaction between TnT-tropomyosin, TnI-actin and TnI-tropomyosin becomes weaker. Consequently, tropomyosin can shift to a non-blocking position, whereby the myosin binding site on actin is exposed and myosin binds to actin.

The structural interaction of Tm-Tn is known to involve TnI wrapping around the dumbbell-like TnC (Olah and Trewhella 1994). More recently, scientitsts have discovered the binding of Ca^{2+} to TnC leads to conformation changes, allowing a hydrophobic patch of the N-domain of TnC to open up (McKay, Tripet et al. 1997, Nakamura, Ueki et al. 2005, Ueki, Nakamura et al. 2005). Following this opening up, the hydrophobic patch of the N-domain of TnC binds to the hydrophobic switch peptide of TnI, thus releasing the TnI from its binding with the thin filament and forcing Tm to move away from the myosin binding sites and allowing contraction (Vassylyev, Takeda et al. 1998). Unfortunately, the structural organisation still remains unclear (Pirani, Vinogradova et al. 2006), although a very recent study has attempted to construct an atomic model by measuring distances between the proteins using fluorescence resonance energy transfer (FRET) (Miki, Makimura et al. 2012).

1.3.2.5 Myosin

Filamentous myosin is the major constituent of the thick filaments. It is one of the most conserved and ubiquitous proteins found in all eukaryotic cells. Since its discovery in 1859, a vast number of different molecules were identified with a great diversity of functions. Hence, myosins have been grouped into 24 unique categories based on the properties of the head domain (Foth, Goedecke et al. 2006). Myosin found in striated muscle is classified as myosin II.

Myosin II is a Y-shaped molecule with a molecular weight of 540 kDa. It is composed of two heavy chains (200 kDa), each comprising a globular head and a long thin tail and two pairs of light chains (17-25 kDa), called the essential and regulatory light chains (Figure 1.5). The two tail segments form a parallel, α-helical coiled coil that can interact with other myosin tails to form the backbone of the thick filament.

Myosin has two flexible regions that are proteolytically susceptible, called hinges that have both flexibility and/or a functional significance. In general, myosin can be cleaved into two fragments; heavy meromyosin (HMM) and light meromyosin (LMM). HMM can be further cleaved into S1, containing the two heads, and S2, containing a short segment of the tail. The ability to obtain fragments of myosin is experimentally invaluable as they enable the large molecule to be examined in smaller functionally distinct units. A schematic diagram of these components is illustrated in Figure 1.5.

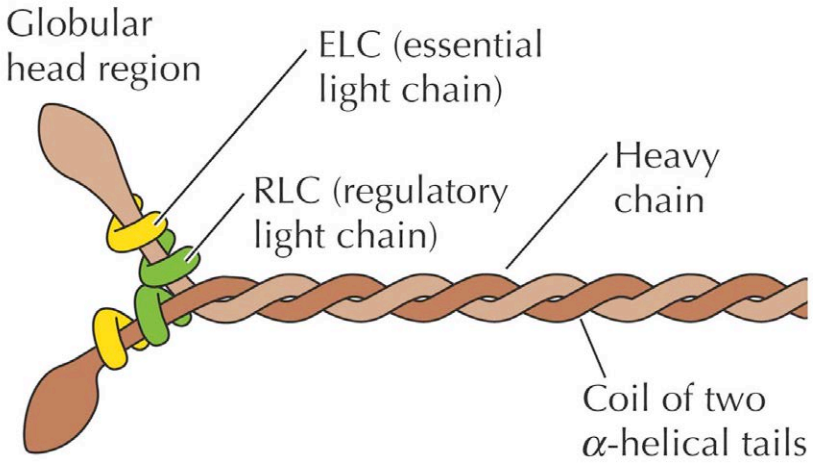

Figure 1.5. A schematic diagram of myosin II. Myosin II is made up of two myosin heavy chains coiled around each other to form a rod backbone and two heads. The two heads contain two light chains (ELC and RLC).
http://oregonstate.edu/instruction/bi314/summer09/Fig-12-25.jpg

Heavy Meromyosin

Heavy meromyosin (HMM) is a water soluble globular protein. It contains two identical N-terminal heads (S1) connected by two short C-terminal ends, the tails (S2).

Head (S1)

The myosin head is divided into two parts; the catalytic domain and the regulatory domain. The three-dimensional atomic resolution crystal structure of S1 is shown in Figure 1.6.

The catalytic domain, also known as the motor domain, contains binding sites for actin and Mg^{2+}-ATP. This domain undergoes a conformational change during muscle contraction in order to generate force.

The regulatory domain is slightly bent and like the catalytic domain, it undergoes conformational change upon muscle contraction by acting like a lever arm to maximise force generation. The regulatory domain consists of two light chains, the essential and regulatory light chains, wrapped around a single myosin heavy chain α-helix. Both light chains are homologous to calmodulin (Ca^{2+} binding).

The regulatory light chain is believed to wrap around the heavy chain and is stabilised by groups of hydrophobic residues: methionines, tryptophans and phenylalanines. This light chain is also the site of phosphorylation by myosin light chain kinase.

The essential light chain is wrapped around in a similar fashion to the regulatory light chain and dissociation of this chain from the myosin head results in the loss of the myosin ATPase activity.

In between the catalytic and regulatory domains, there is a converter domain (hinge). This domain transfers small changes in the motor domain to the regulatory domain. This mechanism is believed to increase the size of the power stroke (Rayment, Holden et al. 1993). Furthermore, S1 has been shown to be the minimum subfragment required to generate force in an *in vitro* motility assay (Toyoshima, Kron et al. 1987).

Tail (S2)

S2 is the neck of the myosin molecule, joining its head to the tail and hinged at each end. It is a short segment of α-helical coiled-coil. The tail of myosin (LMM) forms the myosin thick filament backbone, while the S2 segment projects out from the backbone, allowing the myosin head to reach out towards the thin filament. S2 also contains a binding site for the N-terminus of cardiac myosin binding protein-C and this interaction is known to be phosphorylation dependent (Gruen, Prinz et al. 1999, Kunst, Kress et al. 2000).

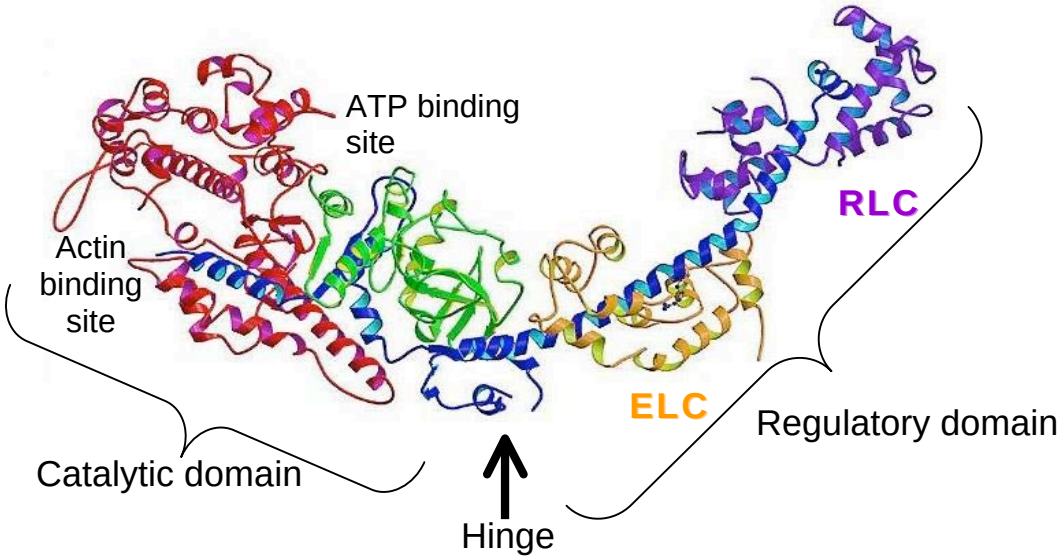

Figure 1.6. Ribbon diagram of the crystal structure of chicken skeletal muscle myosin S1. Myosin S1 consists of catalytic and regulatory domains. The catalytic domain contains the actin and ATP binding sites and the regulatory domain contains the two light chains – essential light chain (ELC) and regulatory light chain (RLC). Image modified from (Rayment, Rypniewski et al. 1993).

Light Meromyosin

Light meromyosin (LMM) is a water insoluble fibrous protein (Lowey 1964) and lacks ATPase activity and actin binding sites. It is the tail part of myosin, forming a rod-shaped molecule. These tails are electrostatically attracted to each other and assemble in a highly uniform manner, forming the backbone of the thick filament.

1.3.2.6 Titin

Titin, first known as connectin, is the largest known protein to date with a molecular weight of 3 MDa and the third most abundant component of the sarcomere in vertebrate striated muscle (Maruyama, Kimura et al. 1984, Wang 1985, Kurzban and Wang 1988). A single titin molecule is approximately 1 μm long and extends half the sarcomere, with the N-terminus at the Z-disc and the C-terminus located in the M-line. Thus, two molecules cover the entire length of the sarcomere from one Z-line to the other (Furst, Osborn et al. 1988, Nave, Furst et al. 1989). Titin is composed of immunoglobulin domains (IgI) and fibronectin domains (Fn): 165 IgI domains and 132 Fn domains in the skeletal isoform and 112 IgI and 132 Fn domains in the cardiac isoform (Labeit and Kolmerer 1995).

Interestingly, the functions of titin vary along its length and it is these variations that provide the sarcomeric alignment during muscle contraction and provides support in the assembly and regulation of the length of the thick filaments during myofibrillogenesis (Whiting, Wardale et al. 1989, Fulton and Isaacs 1991). In the I-band region it forms an elastic connection between the thick filaments and the Z-disc (Horowits, Maruyama et al. 1989, Funatsu, Kono et al. 1993), in the M-line it makes up an integral part of an extensive protein meshwork (Vinkemeier, Obermann et al. 1993) and in the A-band it interacts with myosin and other components of the thick filament (Labeit, Gautel et al. 1992, Soteriou, Gamage et al. 1993). As titin is known to be associated with myosin and myosin binding protein C at regular intervals, it is believed that titin also plays a role as a template for assembly of the thick filaments, acting as “the ruler for sarcomere” (Whiting, Wardale et al. 1989).

Titin has the ability to passively resist the stretching of the relaxed muscle and restore the thick and thin filament overlap at rest. This force is generated from three different sequence elements in the I-band region of titin: Ig domains, PEVK (Proline, Glutamine, Valine and Lysine) segments and the N2B sequence of cardiac titin. Of these three elements, PEVK contributes the most in passive tension (Cazorla, Freiburg et al. 2000, Freiburg, Trombitas et al. 2000).

1.3.2.7 Myosin Binding Protein-C

Myosin binding protein-C (MyBP-C) is found in all striated muscle. It is located in the portion of the A-band where the crossbridges are found (C-zone) in 7 to

9 transverse stripes, 43nm apart (Sjostrom and Squire 1977, Bennett, Craig et al. 1986), with each strip consisting of 2 to 4 MyBP-C molecules and it represents approximately 2% of the protein mass in the myofibril (Offer, Moos et al. 1973). MyBP-C belongs to the intracellular immunoglobulin superfamily and is composed of seven immunoglobulin (IgI) domains and three fibronectin type III (FnIII) domains. Functionally, it is known to interact with other sarcomeric proteins: myosin, actin and titin. MyBP-C is discussed in more detail in Section 1.6.

1.3.2.8 Cofilin

Cofilin is an actin binding protein that regulates actin polymerising and depolymerising activity. Although it is known to bind to both globular (G-actin) and filamentous (F-actin) actin, the exact binding sites of actin on cofilin are still under investigation. The major function of cofilin is its ability to depolymerise actin filaments at the minus end (pointed) and this activity is regulated by various factors, including phosphorylation (Nebl, Meuer et al. 1996), phosphatidylinositides (Yonezawa, Nishida et al. 1990) and pH (Yonezawa, Nishida et al. 1985). Cofilin has also been suggested to sever actin filaments and to be involved in nuclear translocation. However, precise mechanisms and significances are yet to be elucidated. Clinically, aggregation of cofilin is known to be associated with Alzheimer's disease (Minamide, Striegl et al. 2000), cancer (Sidani, Wessels et al. 2007) and asthma (Ruegg, Holsboer et al. 2004). Cofilin will be further discussed in Section 1.7.

1.4 Muscle Contraction

1.4.1 Force Generation

The most critical outcome of muscle contraction is force generation. According to the most widely accepted theory, the sliding filament theory, force is generated by the sliding of thin and thick filaments past one another (Hanson and Huxley 1953). Sliding occurs during muscle activation and is caused by the myosin crossbridges binding sequentially to the actin thin filaments, undergoing a conformational change and dissociating, with this process being repeated multiple times. The conformational change within the myosin crossbridge is powered by the

binding and hydrolysis of ATP. The mechanism of muscle contraction can be divided into five stages (Rayment, Holden et al. 1993, Sherwood 2004) (Figure 1.7).

1. Attached State: Initially, the myosin head is tightly bound to the actin molecule and adenosine triphosphate (ATP) is absent. This arrangement is called the rigor configuration. When death occurs, the absence of ATP continues permanently and does not proceed to the released state, resulting in muscle stiffening and rigidity. This is called rigor mortis.
2. Released State: Once ATP binds to the myosin head (S1), it induces conformational changes of the actin-binding site and reduces the affinity of the myosin head for the actin molecule. Therefore, the myosin head is now detached from the thin filament.
3. Cocked State: Hydrolysis of ATP into adenosine diphosphate (ADP) and inorganic phosphate (Pi) causes the myosin head to change its shape, such that there is a relative shift of a short distance (approximately 5 nm) of the tip of the myosin head relative to the neck. ADP and Pi are still attached to the myosin head.
4. Cross-Bridge State: As the myosin head shifts towards the neighbouring actin molecule, it binds very weakly and causes the intact Pi to be released.
5. Power-Stroke State: Once Pi is released, the myosin head again changes its conformation, causing the two filaments to slide past each other, which generates force within the muscle. Ultimately, the myosin head binds to the actin molecule strongly. Finally, ADP is released and the myosin and the myosin head assume the rigor conformation once again. The cycle then repeats.

Regulation of contraction is essential in order to avoid an endless cycling. The major regulatory mechanism in muscle contraction involves the tropomyosin - troponin complex, which responds to Ca^{2+} binding. This mechanism was discussed in depth in section 1.3.2.4.

It is important to note that during muscle contraction and relaxation, the lengths of the thick and thin filaments remain constant and it is only the length of the overlapping area that changes.

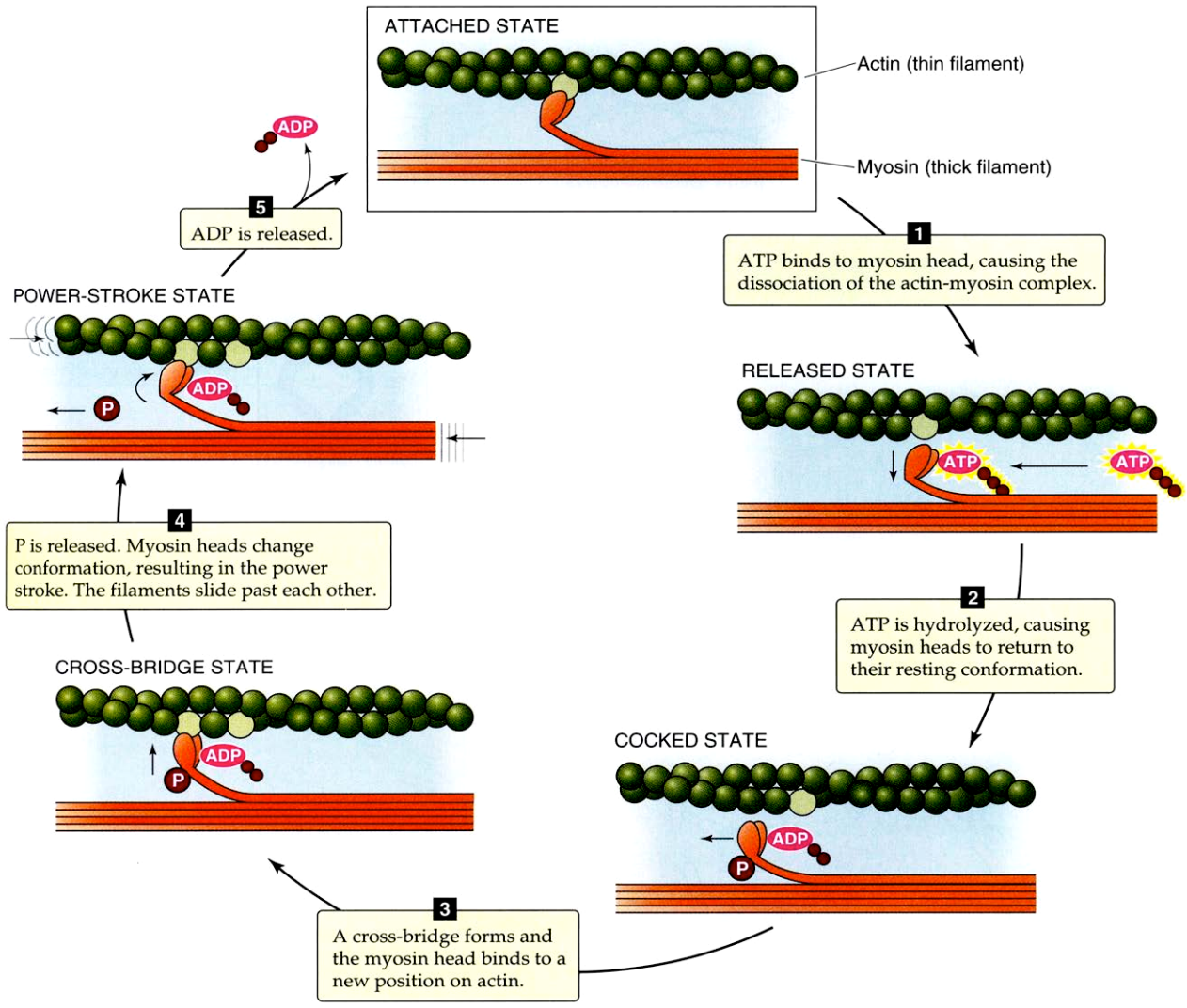

Figure 1.7 Schematic diagram of muscle contraction (Boron and Boulpaep 2005).

1.5 Familial Hypertrophic Cardiomyopathy

Familial hypertrophic cardiomyopathy (FHC) is one of the most frequently occurring congenital cardiac disorders (Maron, Gardin et al. 1995) and the most common cause of sudden cardiac death in young adults (Watkins, Seidman et al. 1995). It is an autosomal dominant disease, affecting both children and adults and characterised macroscopically, by an excessive thickening of the heart muscle, mainly by left ventricular hypertrophy, and microscopically, by myofibrillar and myocyte disarray and fibrosis (Davies 1984, Maron, Bonow et al. 1987). Studies over the last few decades have discovered that the causative mutations are located in genes

encoding numerous sarcomeric proteins and this is further discussed in Section 1.5.6. Unfortunately, the exact mechanisms by which these mutations in these genes cause FHC remain unclear.

1.5.1 History

Hypertrophic cardiomyopathy was first noticed by Vulpian in 1868 (Vulpian 1868) but it was not until the late 1950s that the unique clinical features of hypertrophic cardiomyopathy were systematically described (Teare 1958). Over the years its definition by World Health Organisation (WHO) has been changed from "diseases of different and often unknown etiology in which the dominant feature is cardiomegaly and heart failure" in 1968 (Abelmann 1984) to "an autosomal dominant (i.e. offsprings of affected individuals have 50 % chance of inheriting the gene mutation) heart muscle disease of unknown cause" in 1980 (Anonymous 1980). However, more recently, in 1995, the WHO redefined hypertrophic cardiomyopathy as a disease caused by mutations in sarcomeric contractile protein genes (Richardson, McKenna et al. 1996).

1.5.2 Epidemiology

Approximately 1 in 500 (0.2%) people are affected by hypertrophic cardiomyopathy (Maron, Gardin et al. 1996, Miura, Nakagawa et al. 2002, Maron, Towbin et al. 2006, Maron, Maron et al. 2012) and 60% of this cohort are believed to be familial (Fananapazir and Epstein 1995). Interestingly, the disease course is highly variable and unpredictable with the majority of the patients (~75%) living a normal life with few or no symptoms at all with only about 1% of cases of FHC leading to mortality (Maron, Olivotto et al. 2000). Nonetheless, FHC is the most common cause of sudden cardiac death in young competitive athletes (generally younger than 35 years old) (Maki, Ikeda et al. 1998, Maron, Olivotto et al. 2000).

1.5.3 Pathological Features

Familial hypertrophic cardiomyopathy (FHC) is characterised by thickening of the heart muscle without an obvious cause. The term "hypertrophy" denotes thickening of tissue due to an increase in the size of the constituent cells and the term "cardiomyopathy" denotes a disease of heart muscle. In general, hypertrophy occurs as a compensatory thickening of the left ventricle wall due to a physiological response

to either excessive haemodynamic burden (such as pressure overload due to hypertension and aortic valve disease) or a pathological state that compromises heart muscle function (Grossman, Jones et al. 1975). However in FHC, an inheritable disease, hypertrophy occurs in the absence of haemodynamic burden (Bashyam, Savithri et al. 2003). Usually this hypertrophy is asymmetrical and occurs in the left ventricle, especially in the intraventricular septum, although it can also occur in the apical area only, the base of the left ventricle, concentrically (spread throughout the left ventricle wall) or even in the right ventricle (Figure 1.8) (Bashyam, Savithri et al. 2003). Hypertrophy is common in many cardiac disorders but is usually due to an increase in the cardiac load. With the normal average thickness of the left ventricle wall being 12mm, the degree of hypertrophy in patients with FHC ranges from 13-15 mm in mild hypertrophy and up to 60 mm in the most extreme cases (Wigle, Sasson et al. 1985).

As a consequence of an increase in the wall size, reduction in the volume of the ventricular lumen occurs, which in turn leads to decreased volume of the blood ejected from the ventricle. Furthermore, although the left ventricle is usually not dilated in the absence of other systemic or cardiac diseases that are capable of producing the magnitude of the wall thickening evident, the atrial lumen is often dilated due to the resistance to filling of the ventricles.

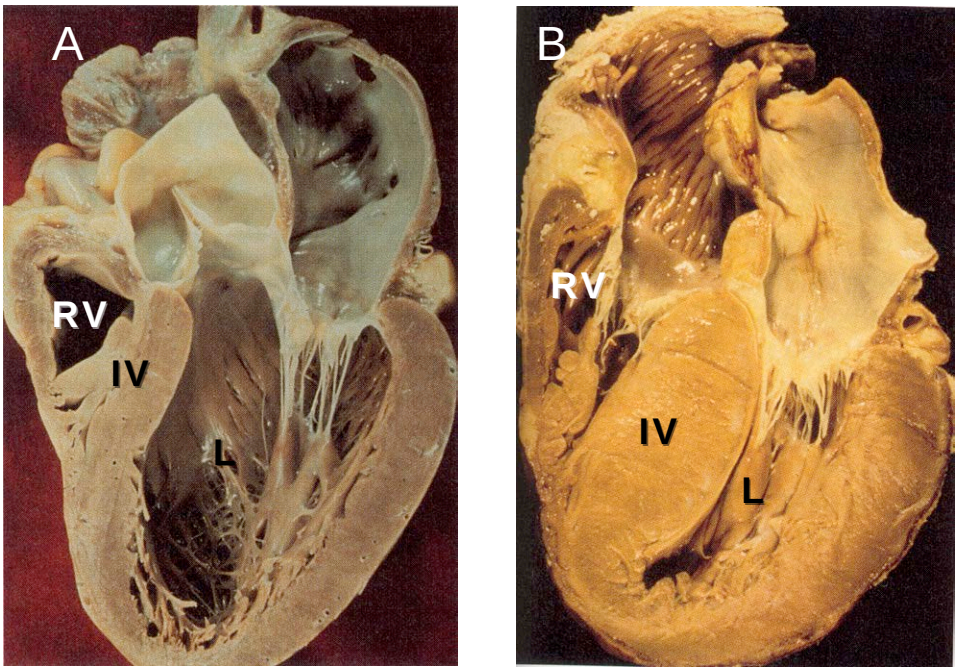

Figure 1.8. Interior view of the left ventricle in normal (a) and hypertrophic (b) human hearts. Compared to the normal heart (a), the hypertrophic heart (b) bas enlarged interventricular septus (IVS) and left ventriclur (LV) wall. There is also a decrease in the right ventricular (RV) volume (Seidman and Seidman 2001).

Histopathology techniques revealed that FHC manifests myofibrillar disarray and fibrosis (Thierfelder, Watkins et al. 1994). In a normal heart the muscle fibres are arranged in a highly uniform and organised manner to produce contraction and generate force in a uniform fashion (Figure 1.9a and c). However, in heart muscles with FHC, the fibres lose the normal orientation and move obliquely or perpendicularly. This occurs to approximately 25-35 % of fibres (Maron and Roberts 1979). Additionally, the myocytes are hypertrophied in an unusual shape (Figure 1.9b and d). This impairs the electrical impulses, leading to cardiac arrhythmias and the possibility of sudden cardiac death. Furthermore, this disarrary and fibrosis has also been shown in a recent study using cardiac magnetic resonance (CMR) (Todiere, Aquaro et al. 2012).

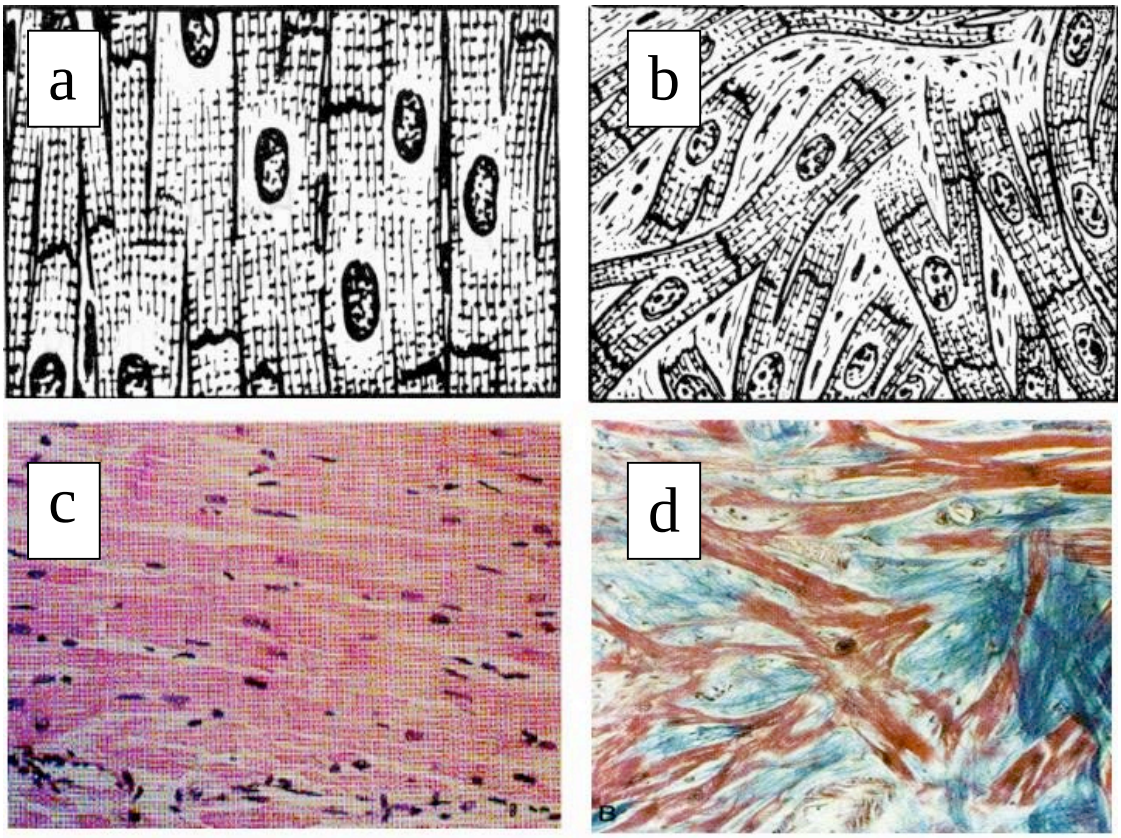

Figure 1.9. Microscopic appearance of normal and FHC myocardium

a) Drawing of normal myocytes. Cells are arranged in a uniform direction.
b) Drawing of disarrayed myocytes. Cells are at oblique and perpendicular angles to one another.
c) H & E stain of normal cardiac tissue.
d) FHC affected cardiac tissue. Note a large amount of fibrosis (seen as blue in this stain).

1.5.4 Clinical Features

1.5.4.1 Clinical Manifestations

Clinically, FHC can range from asymptomatic to severe. Due to the more common asymptomatic nature of the disease, it is usually discovered as an incidental finding, such as a murmur during a medical examination for insurance coverage or during clinical evaluation of a family (Murphy and Starling 2005) or even at *post mortem* (Maron, Shirani et al. 1996). However, the patients can present with some or all of the following symptoms, ranging from benign to severe (Bashyam, Savithri et al. 2003):

1. dyspnoea (breathlessness): thickening of the ventricular wall leads to an increase in left ventricular diastolic pressure, which in turn leads to increased

pulmonary pressure. This is usually linked to physical activity but can occur at rest and following meals.

2. angina (chest pain): there is an increased demand in oxygen supply due to the thickened muscle and chest pain occurs when this demand cannot be met. Angina can occur at rest or during sleep or can be brought on by exertion and relieved by rest.
3. syncope (fainting): thought to be due to an irregularity of the heartbeat or a fall in blood pressure leading to insufficient blood supply to the brain.
4. palpitations: patients may occasionally feel an extra beat or a skipped beat. This may start suddenly and be associated with sweating or light-headedness.
5. arrhythmias (irregular heartbeats): this is due to myocyte disarray, leading to disruption of the electrical conduction system of the heart

Furthermore, FHC is associated with an increased risk of sudden cardiac death (SCD) and is known to be the most common cause in young competitive athletes (Elliott, Poloniecki et al. 2000).

1.5.4.2 Clinical Diagnosis

The clinical diagnosis of FHC is based on medical history, physical examination and electrocardiography (ECG) and echocardiographic identification of the septal and left ventricular hypertrophy. However, due to the lack of specificity of ECG for FHC, a 2-dimensional echocardiogram is most commonly used for diagnostic purposes (Bashyam, Savithri et al. 2003). The diagnosis is based on the "presence of a hypertrophied and nondilated left ventricle in the absence of another cardiac or systemic disease capable of producing the magnitude of hypertrophy evident in the patient (usually ≥15 mm in an adult or the equivalent relative to body surface area in children)" (Gersh, Maron et al. 2011). Additionally, Doppler ultrasound is capable of producing a colour image of the blood flow within the heart and detect the presence of turbulent blood flow (Bashyam, Savithri et al. 2003).

Nowadays, there is an increase in the use of a more superior method called cardiovascular magnetic resonance (CMR) to diagnose FHC. CMR provides better spatial resolution than conventional 2-dimensional echocardiography, giving sharp contrast between blood and myocardium, and is thus able to more accurately characterise the presence and distribution of left ventricular hypertrophy. In addition,

studies have shown that hypertrophy confined to the apex may be difficult to visualise with echocardiography but is evident with CMR (Moon, Fisher et al. 2004, Maron, Finley et al. 2008).

Lastly, genetic testing is a powerful investigative tool for definitive diagnosis. Although it is now commercially available and represents best practice, it is often still confined to those who participate in research studies and in the identification of affected relatives in families known to have FHC (Gersh, Maron et al. 2011). Advances in the capacity of next-generation targeted exomic sequencing have allowed a much larger number of mutations to be screened simultaneously (Maron, Maron et al. 2012).

1.5.5 Management / Treatment

Due to the diversity of both clinical and genetic features, clinicians must individualise the treatment to the patient.

In asymptomatic patients, although most will achieve a normal life expectancy (Maron, Casey et al. 1999, Maron, Mathenge et al. 1999, Maron, Casey et al. 2003), it is essential to offer genetic counselling (Semsarian 2011) and educate these patients and their families about the disease process, including screening of first-degree relatives and avoiding particularly strenuous activity or competitive athletics (Spirito, Seidman et al. 1997). High doses of diuretics and vasodilators (e.g. for treatment of hypertension) should be avoided as these may exacerbate the degree of obstruction (Braunwald, Lambrew et al. 1964, Maron 2002).

For symptomatic patients, pharmaceutical therapy is widely used to alleviate symptoms of exertional dyspnoea, palpitations and angina. Beta-blockers are the mainstay and first-line of pharmacologic therapy due to their negative inotropic effects (Bonow, Dilsizian et al. 1985). These can be administered to both adults and children and work to decrease heart rate and increase diastolic filling time. Consequently this will result in an increase in stroke volume, maintenance of cardiac output and reduction in both angina and dyspnoea (Spirito, Seidman et al. 1997, Roberts and Sigwart 2001).

For those patients who do not respond to beta-blockers or cannot tolerate their side-effects, calcium channel blockers may be effective. Of such agents, verapamil has been the most thoroughly studied (Gersh, Maron et al. 2011) and diltiazem has also been shown to improve diastolic performance (Betocchi, Piscione et al. 1996)

and prevent or diminish myocardial ischemia (Sugihara, Taniguchi et al. 1998). However, both verapamil and diltiazem are not recommended in patients with severe outflow obstruction, elevated pulmonary artery wedge pressure and low systemic blood pressure, because a decrease in blood pressure with this treatment can trigger an increase in outflow obstruction, precipitate pulmonary oedema and serious haemodynamic complications (Epstein and Rosing 1981, Gersh, Maron et al. 2011).

Those patients who are unresponsive to pharmaceutical therapy have at least three surgical options (Maron, Bonow et al. 1987, Wigle, Rakowski et al. 1995, Gersh, Maron et al. 2011):

1. **Myoectomy** (removal of excess muscle from basal septum) is currently considered the most appropriate treatment for the majority of patients with obstructive hypertrophic cardiomyopathy (Gersh, Maron et al. 2011). Although surgical results have greatly improved in recent years, this surgery is limited to relatively few centres with extensive experience (Schoendube, Klues et al. 1995, Minakata, Dearani et al. 2004).
2. **Alcohol septal ablation** was first reported in 1995 (Sigwart 1995). In this procedure, 100% absolute alcohol is injected percutaneously into the branch of the coronary artery that perfuses the septum - the target point is the basal septum at the point of contact of the anterior mitral valve leaflet. Since alcohol is toxic to the heart muscle cells, it leads to a localised infarction and causes the thickened heart muscle to be replaced with thin scar tissue. As a result, there is a reduction in the obstruction of blood flow out of the left ventricle and associated mitral regurgitation, which simulates the results of surgical myoectomy. This procedure has been performed successfully in a large number of patients and is also particularly useful in patients where surgery is contraindicated (Fernandes, Nielsen et al. 2008, Kwon, Kapadia et al. 2008).
3. Insertion of a **dual-chamber pacemaker** is particularly recommended in patients with complications resulting from alcohol septal ablation surgery (Valettas, Rho et al. 2003). This procedure involves artificially exciting the septum in the left ventricle to decrease the pressure gradient by reducing the obstruction of the outflow blood.
4. In very severe cases of heart failure a **transplant** is also available

1.5.6 Genetic Basis of FHC

After intensive studies for more than two decades, 11 or more causative genes with greater than 1,400 mutations responsible for FHC have been found (Maron, Maron et al. 2012). These include both sarcomeric and non-sarcomeric proteins, although only the genes encoding sarcomeric proteins will be discussed in this thesis. Of the genes responsible for FHC, approximately 70% are found to have mutations in the two most common genes: beta-myosin heavy chain (MYH7) and myosin binding protein-C (MyBP-C). Table 1.1 (Maron, Maron et al. 2012) shows the list of genes found to cause FHC, listed from strongest to lesser evidence of pathogenicity. Although most people have been found to carry a single gene mutation, multiple mutations in an individual have been identified recently and these individuals were associated with more severe disease expression and adverse prognosis (Ingles, Doolan et al. 2005, Kelly and Semsarian 2009, Maron, Maron et al. 2012)

Table 1.1. List of FHC causing genes and their prevalence. (Maron, Maron et al. 2012)

Table 1 Molecular Substrate of HCM

Strongest evidence for pathogenicity	
Thick filament	
1. β-myosin heavy chain	MYH7
2. Regulatory myosin light chain	MYL2
3. Essential myosin light chain	MYL3
Thin filament	
4. Cardiac troponin T	TNNT2
5. Cardiac troponin I	TNNI3
6. Cardiac troponin C	TNNC1
7. α-tropomyosin	TPM1
8. α-cardiac actin	ACTC
Intermediate filament	
9. Cardiac myosin-binding protein C	MYBPC3
Z-disc	
10. α-actinin 2	ACTN2
11. Myozenin 2	MYOZ2
Lesser evidence for pathogenicity	
Thick filament	
12. α-myosin heavy chain	MYH6
13. Titin	TTN
Z-disc	
14. Muscle LIM protein	CSRP3
15. Telethonin	TCAP
16. Vinculin/metavinculin	VCL
Calcium handling	
17. Calsequestrin	CASQ2
18. Junctophilin 2	JPH2

HCM = hypertrophic cardiomyopathy.

1.5.6.1 β-Myosin Heavy Chain

The gene encoding β-myosin heavy chain (βMyHC) is called MYH7 and mutations in this gene account for about 30% of all FHC causing mutations (Watkins, Seidman et al. 1995, Sivaramakrishnan, Ashley et al. 2009)

A missense mutation in MYH7 was the first mutation to be identified in FHC (Geisterfer-Lowrance, Kass et al. 1990, Tanigawa, Jarcho et al. 1990) and since then several distinct missense mutations have been identified in this gene resulting in the substitution of conserved amino acids (Watkins, Rosenzweig et al. 1992, Vikstrom and Leinwand 1996). Of these mutations, several of them are clustered in the globular head region and may occur in regions that form functionally important domains. A significant fraction of mutations were also detected in the tail-helix region that lies in the rod region of βMyHC (Bashyam, Savithri et al. 2003).

Phenotypes of the mutations occurring in MYH7 vary from benign to severe, leading to sudden cardiac death. Out of these, a missense mutation resulting in an amino acid change from arginine to glutamine at position 403 (R403Q) is known to be one of the highest penetrance and most severe clinical phenotypes of FHC mutations, (Chuan, Sivaramakrishnan et al. 2012). Although the exact mechanism is yet to be elucidated (Chuan, Sivaramakrishnan et al. 2012), studies have shown that this mutation occurs at a highly conserved residue in close proximity to the actin-binding interface of the myosin motor domain (Volkmann, Lui et al. 2007) and these patients have a high incidence of morbidity and early mortality (Epstein, Cohn et al. 1992). Furthermore, a recent independent study has proposed that missense mutations of MYH7 will “probably affect actin or nucleotide binding” (Bashyam, Purushotham et al. 2012).

1.5.6.2 Myosin Binding Protein C

The link between hypertrophic cardiomyopathy and the locus containing myosin binding protein C (MyBP-C) on chromosome 11 was first made in 1993 (Carrier, Hengstenberg et al. 1993). Shortly thereafter, specific mutations within the MyBP-C gene were identified (Bonne, Carrier et al. 1995, Watkins, Conner et al. 1995) and to date, more than 200 MyBP-C mutations have been identified (Marston 2011, Schlossarek, Mearini et al. 2011). Furthermore, the β-myosin heavy chain

(MYH7) and myosin binding protein C genes are estimated to account for approximately 60-70% of all FHC cases (Xu, Dewey et al. 2010).

Mutations identified in MyBP-C include splice site mutations, nucleotide deletion/insertion, exon duplications, missense mutations and premature stop codons resulting in a truncated protein (Bashyam, Savithri et al. 2003, Flashman, Redwood et al. 2004, Morita, Nagai et al. 2010). The mechanism(s) by which these defects lead to FHC remains controversial (Knoll 2012), but some of the proposed mechanisms include: structural changes with or without altering its function (Morita, Nagai et al. 2010); deletions or insertions may render the messenger RNA or protein unstable, which can lead to reduction in the total amount of MyBP-C within sarcomeres (Morita, Nagai et al. 2010) and perhaps in turn may inhibit myosin binding (Bashyam, Purushotham et al. 2012) – studies have shown that a 50% reduction in normal MyBP-C levels will lead to myofibrillar architecture disruption and impact the sarcomere function by unknown mechanisms (Flavigny, Souchet et al. 1999, Marston, Copeland et al. 2009, van Dijk, Dooijes et al. 2009).

For awhile, FHC due to mutations in MyBP-C were thought to be of late onset, low penetrance and good prognosis (Charron, Dubourg et al. 1998, Niimura, Bachinski et al. 1998). However, several studies recently have demonstrated that the spectrum of clinical phenotypes of FHC due to MyBP-C mutations is broad and variable, including severe phenotypes, with all patterns and degrees of hypertrophy observed (Konno, Shimizu et al. 2006, Page, Kounas et al. 2012). These studies also proposed that these differences could not be explained by either the gene-specific or the mutation-specific data, hence highlighting the importance of nongenetic factors (such as hormones and environmental factors). Consequently, the current genotype-phenotype data should be used cautiously, especially by clinicians when counselling at risk family members, since the applicability of such data and the role of genetic predictive testing still remains uncertain.

1.5.6.3 Troponin T

Cardiac troponin T (cTnT) gene on chromosome 1 was first recognised to be related to hypertrophic cardiomyopathy in 1994 (Thierfelder, Watkins et al. 1994). Since then more than 30 mutations have been identified with the majority of them caused by missense mutations and a few due to truncated protein (Thierfelder,

Watkins et al. 1994). Unlike beta-myosin heavy chain (MYH7) and MyBP-C, the clinical phenotype due to the gene encoding troponin T (TNNT2) is similar and characterised by mild ventricular hypertrophy and a high incidence of sudden death (Fujino, Shimizu et al. 2002), especially at a young age (Varnava, Elliott et al. 2001, Richard, Charron et al. 2003).

1.5.6.4 Troponin I

The troponin I gene, TNNI3 is located on chromosome 19 and mutations in this gene have been reported in 2-7% of hypertrophic cardiomyopathy cases (Van Driest, Ellsworth et al. 2003, Mogensen, Murphy et al. 2004).

Troponin I has three binding sites: one for troponin T (residue 61-112), another for troponin C (residue 113-164) and the third one for actin-tropomyosin (residue 130-148; 173-181) (Mogensen, Murphy et al. 2004). Troponin I is the inhibitory subunit of the troponin complex and this inhibitory effect is released by calcium binding to troponin C. This triggers a series of events: altered interaction within the actin-troponin-tropomyosin binding complex, displacement of the myosin head along the thin filament and adenosine triphosphate (ATP) hydrolysis, leading to force generation. Furthermore, TNNI3 is known to be exclusively expressed in cardiac muscles and plays an important role in cardiac muscle contraction and relaxation in response to changes in intracellular calcium (Bhavsar, Brand et al. 1996).

Several mutations in TNNI3 leading to FHC have been identified (Kimura, Harada et al. 1997, Niimura, Patton et al. 2002, Murphy and Starling 2005) with the majority of them being missense mutations (Bashyam, Savithri et al. 2003). Some of the mechanisms by which these mutations lead to FHC include: hypercontractility with diastolic dysfunction (Cooke 1998, James, Zhang et al. 2000, Lang, Gomes et al. 2002), impaired relaxation (Elliott, Watkins et al. 2000) and increased calcium sensitivity of cardiac muscle contraction (Takahashi-Yanaga, Morimoto et al. 2001). Generally, FHC due to mutations in TNNI3 result in mild symptoms (Morner, Richard et al. 2000) but studies have shown that the Lys^{183} deletion has high significant disease penetrance and can lead to sudden cardiac death (Kokado, Shimizu et al. 2000).

1.5.6.5 Troponin C

The first FHC causing mutation in troponin C was identified in 2001 (Hoffmann, Schmidt-Traub et al. 2001). This mutation, $Leu^{29}Gly$, was found in a 60 year old patient with septal hypertrophy and atrial fibrillation. Subsequent studies have shown that mutations in this gene lead to significant effects on the kinetics of opening and closing of the conformation of the regulatory N-domain and elimination of the inotropic effect of PKA phosphorylation of cardiac troponin I on the transition, thus suggesting an antagonistic role in the effect of phosphorylation signalling from cardiac troponin I to cardiac troponin C (cTnC) (Dong, Xing et al. 2008). Another independent study has demonstrated that the $Leu^{29}Gly$ mutation increases the calcium binding characteristics of cTnC and this alters myocyte contractility, however, the exact mechanism of changes in myofilament calcium sensitivity and the etiology of FHC is unknown (Liang, Chung et al. 2008).

1.5.6.6 α-Tropomyosin

The gene encoding α-Tropomyosin is on chromosome 15 and mutations in this gene were first linked to hypertrophic cardiomyopathy in 1994. A few missense mutations have now been indentified and out of these, the two most common mutations are $Asp^{175}Asn$ and $Glu^{180}Gly$, which occur in highly conserved residues. Studies have shown that these mutations increase the bending flexibility of tropomyosin both locally and globally (Li, Suphamungmee et al. 2012, Loong, Zhou et al. 2012, Ly and Lehrer 2012). Extrapolating this finding further, scientists are proposing that this increase in flexibility is likely to increase accessibility of the myosin-binding sites on F-actin, leading to destabilisation the low-Ca^{2+} relaxed state of cardiac muscle and this imbalance will lead to enhanced systolic activity, diastolic dysfunction and cardiac compensation associated with hypertrophic cardiomyopathy and heart failure (Li, Suphamungmee et al. 2012). Similarly, another study also proposed that increased flexibility together with hypersensitivity of calcium could overwork cardiac muscle, resulting in FHC (Loong, Zhou et al. 2012).

Clinical phenotypes vary from mild hypertrophy to severe hypertrophy and unfortunately, both the mechanism by which the mutations cause FHC and differences in phenotypes are not yet clear (Kremneva, Boussouf et al. 2004).

1.5.6.7 Myosin Essential Light Chain

Mutations in myosin light chains are much less frequent and account for less than 5% of hypertrophic cardiomyopathies (Keren, Syrris et al. 2008).

The gene encoding myosin essential light chain is MYL3 and to date, ten mutations have been shown to cause hypertrophic cardiomyopathy. Of these, four missense mutations are located in exon 3 (E56G, A57G, V79L and R81H) and the rest are located in exon 4 (G128C, E143K, M149V, E152K, R154H and H155D) (Andersen, Hedley et al. 2012).

Poetter *et al* (Poetter, Jiang et al. 1996) first identified the two MYL3 mutations causing FHC (M149V and R154H) and these mutations were shown to be associated with a rare FHC phenotype. This involved marked papillary muscle hypertrophy and an unusually pronounced midventricular wall thickening, leading to midcavity obstruction.

Generally, the clinical phenotypes are shown to vary greatly, from mild to sudden cardiac death (A57G and M149V) and the penetrance is shown to be high in middle-aged mutation carriers (Hernandez, Jones et al. 2007). However, one novel mutation identified recently (V79L) was demonstrated to be present with low expressivity and late onset (Andersen, Hedley et al. 2012)

1.5.6.8 Myosin Regulatory Light Chain (RLC)

In 1996, mutations in the gene encoding myosin regulatory light chain (MYL2) causing hypertrophic cardiomyopathy were first identified, along with mutations in MYL3 (Poetter, Jiang et al. 1996). Since then, 10 mutations have been identified (Harris, Lyons et al. 2011): eight missense mutations (A13T, F18L, E22K, N47K, R58Q, P95A, L103E and D166V) and two splice acceptor site mutations (IVS6-1G>C and IVS5-2A>G).

Although the exact mechanism of the above mutations leading to FHC remains unclear, studies have found some effects of these mutations that could contribute to FHC causation. Three of the above mutations, E22K, N47K and R58Q, were found to alter the Ca^{2+} binding of RLC, whereas the A13T mutation was found to alter the phosphorylation of RLC (Szczesna, Ghosh et al. 2001, Szczesna-Cordary, Guzman et al. 2004). More recent studies have also found that the E22K mutation has no effect on mechanical properties of cross bridges (Dumka, Talent et al. 2006) and the R58Q

mutation lowers both the kinetic rates of cardiac myofibril contractility and force per cross-sectional area of the muscle fibre and thus compromises the ability of the heart to pump blood efficiently (Mettikolla, Calander et al. 2011).

Most MYL2 mutations appear to cause mild or benign clinical phenotypes (Harris, Lyons et al. 2011), except R58Q, D166V and IVS5-2 mutations, which have been shown to be associated with malignant phenotypes at earlier ages and/or with sudden cardiac death (Flavigny, Richard et al. 1998, Kabaeva, Perrot et al. 2002, Morner, Richard et al. 2003, Richard, Charron et al. 2003). Furthermore, mid-cavity obstruction and papillary muscle thickening were both shown to be linked to MYL2 mutations (Poetter, Jiang et al. 1996, Flavigny, Richard et al. 1998).

1.5.6.9 Actin

Point mutations in the gene encoding the α-cardiac actin gene (ACTC) are known to cause FHC, albeit rarely (Mogensen, Murphy et al. 2004). In 1999, the first mutation, A295S, was found that results in impaired myosin binding, which leads to impaired force generation and compensatory hypertrophy (Mogensen, Klausen et al. 1999). Since then, nine point mutations leading to hypertrophic cardiomyopathy have been identified (Muller, Mazur et al. 2012): H90Y, R97C, E99K, P164A, Y166C, A232V, A295S, M305L and A331P.

Not much is known about the functional significance of the above mutations but since actin is highly conserved and plays an important role in muscle contraction, mutations in the gene encoding this protein could affect the mechanics, kinetics and/or regulation of the actomyosin interaction (Debold, Saber et al. 2010). Studies of specific mutations have shown that the E99K mutant decreases both the binding affinity to the myosin S1-subfragment and actin filament velocity in an *in vitro* motility assay (Bookwalter and Trybus 2006). Recent studies further demonstrated that E99K inhibits the activation of the thin filament (Debold, Saber et al. 2010), increases the myofilament Ca^{2+} sensitivity and decreases the PKA phosphorylation response of troponin I (Song, Dyer et al. 2011). Additionally, mutations Y166C and M305L are shown to stimulate the cardiac ß-myosin ATPase to only 50% of wild-type (WT) cardiac F-actin and this might be the basis for the initiation of hypertrophy (Muller, Mazur et al. 2012). Although gene specific phenotypes need to be

investigated, the E99K mutant is shown to be linked with apical hypertrophy (Song, Dyer et al. 2011).

1.5.6.10 Titin

So far, only two mutations in the gene encoding titin (TTN) have been identified. Mutation R740L, (Satoh, Takahashi et al. 1999) is a missense mutation and is proposed to cause FHC by an altered affinity to α-actin. Mutation Ser3799Tyr is shown to increase the titin binding to FHL2 (four and half LIM protein 2) and as FHL2 is known to tether metabolic enzymes to N2-B and is 2 regions of titin/connectic, this altered binding capacity is proposed to lead to altered recruitment of metabolic enzymes to the sarcomere, thus contributing to FHC (Matsumoto, Hayashi et al. 2006).

1.6 Myosin Binding Protein C

Myosin binding protein C (MyBP-C) is a thick filament protein consisting of 1274 amino acid residues (149kDa) and it was first discovered in 1973 (Offer, Moos et al. 1973). Since its discovery, it was largely ignored by researchers until the link between mutations in the gene encoding its cardiac isoform and familial hypertrophic cardiomyopathy (FHC) was made in 1993 (Carrier, Hengstenberg et al. 1993). While the basic structural organisation of the protein and some basic functions have been proposed, its precise tertiary structure, function and therefore, how the mutations in it lead to FHC are yet to be resolved.

1.6.1 Isoforms of MyBP-C

MyBP-C has three isoforms: slow skeletal, fast skeletal and cardiac. These are encoded by the genes MyBP-C1, MyBP-C2 and MyBP-C3, respectively and are located in different chromosomes: 12, 19 and 11, respectively. Since the three isoforms map to different chromosomes, this suggests that the isoforms are not the result of alternative splicing (Winegrad 1999). Amino acid sequence analysis of all three human isoforms revealed a high homology (39.6%) (Vydyanath, Gurnett et al. 2012). This thesis will focus on the cardiac isoform of MyBP-C (cMyBP-C).

1.6.2 Location of MyBP-C

MyBP-C molecules are present in the myofibrils of all striated muscle and are responsible for approximately 1~2% of the myofibrillar mass (Offer, Moos et al. 1973). They are located in a portion of the A-band where crossbridges are found, namely the C-zone (Figure 1.10a), in 7 to 9 transverse stripes 43 nm apart (Sjostrom and Squire 1977, Bennett, Craig et al. 1986). This can be clearly seen under the electron microscope (Figure 1.10b).

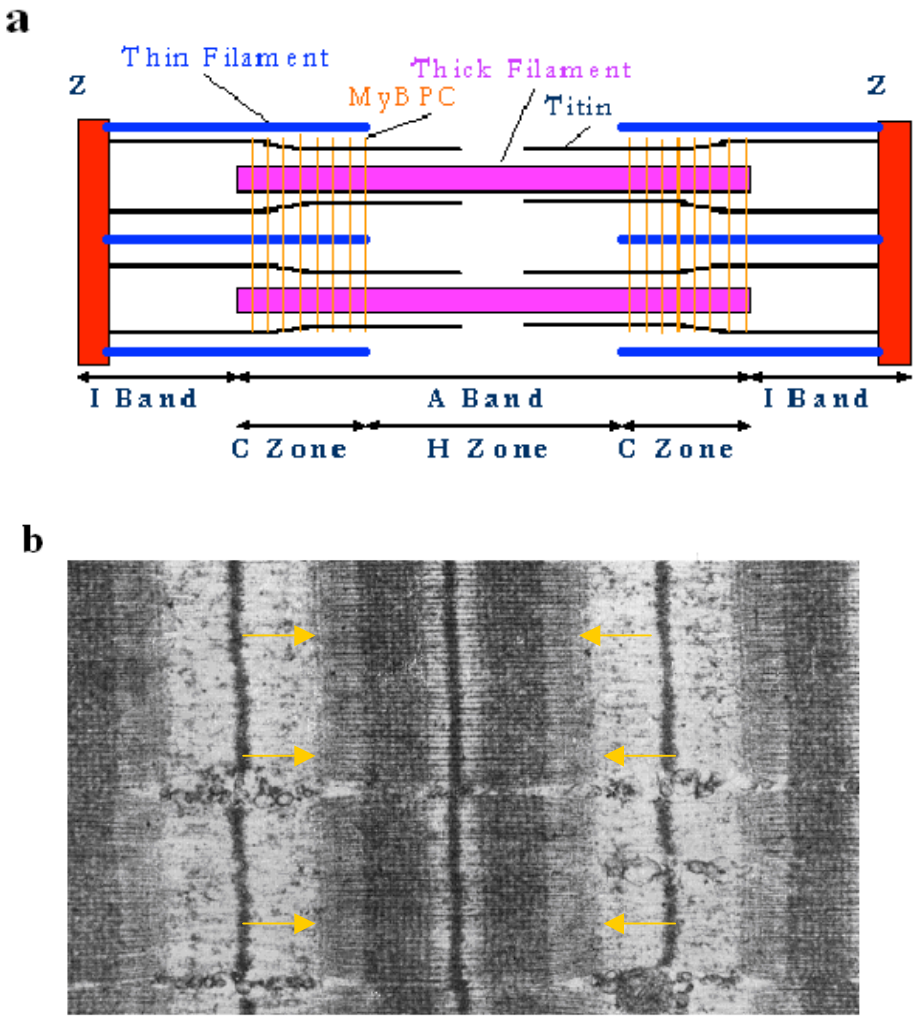

Figure 1.10. Location of MyBP-C.

a) Position of cMyBP-C. Image from (Oakley, Hambly et al. 2004)

b) Electron micrograph of cardiac muscle stained with antibody to MyBP-C. Eleven stripes are present in the A-band where 7 to 9 of these are believed to be due to MyBP-C (arrow). Image modified from (Craig and Offer 1976).

1.6.3 Structure of MyBP-C

Cloning and sequencing of different isoforms of MyBP-C from human (main focus of this thesis), chicken, rabbit and mouse have led to the determination of its basic structure (Weber, Vaughan et al. 1993, Yasuda, Koshida et al. 1995, Alyonycheva, Mikawa et al. 1997).

MyBP-C belongs to the intracellular immunoglobulin superfamily. All three isoforms share conserved architectural features, composed of seven immunoglobulin (IgI) domains and three fibronectin type III (FnIII) domains, arranged in a uniform order Ig-Ig-Ig-Ig-Ig-Fn-Fn-Ig-Fn-Ig. The domains are numbered from the N-terminus as C1 to C10 (Figure 1.11) with a 105 amino acid myosin binding protein motif in between the domains C1 and C2. In this region, a proline and alanine rich (PA) domain is located, as well as a single phosphorylation site in the two skeletal isoforms (c.f. more than one phosphorylation site in cardiac isoform).

The structure of the cardiac isoform differs from the two skeletal isoforms in 4 ways (Yamamoto and Moos 1983, Winegrad 1999):

1. cMyBP-C has an additional immunoglobulin module (C0) with 101 residues at the N-terminus
2. There are three phosphorylation sites, not one, in the linker between C1-C2 (Gautel, Zuffardi et al. 1995). However, recent studies have suggested additional phosphorylation sites for calmodulin kinase II, protein kinase C, protein kinase D and the 90-kDa ribosomal S6 kinase (Bardswell, Cuello et al. 2012, Knoll 2012, Kuster, Bawazeer et al. 2012).
3. A 25 residue loop is found in C5
4. cMyBP-C is longer than skeletal isoforms, being approximately 40 to 44 nm in length

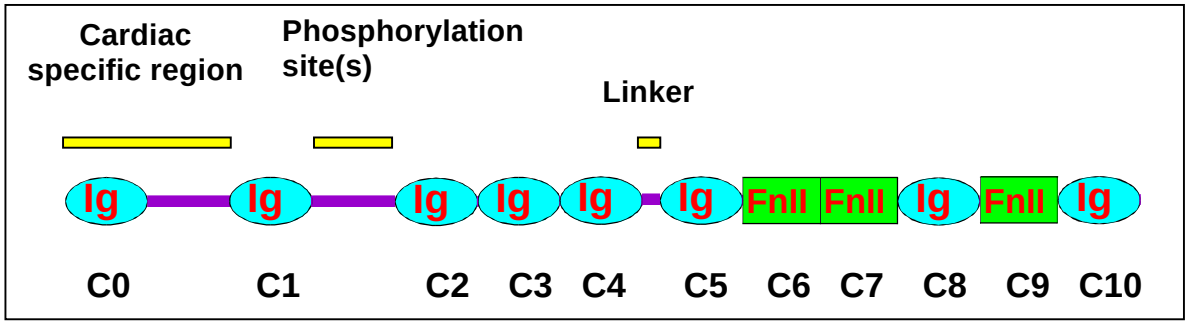

Figure 1.11 Structure of cMyBP-C. It is made up of eight IgI domains and three Fn domains. C0 is a cardiac specific site. Three phosphorylation sites between C1-C2 and myosin and titin binding sites between C7-C10 are present.

1.6.4 Binding Partners of MyBP-C

MyBP-C has no enzymatic activity. This suggests that MyBP-C must fulfil its biological function in the heart through interactions with other relevant molecules. Since there is little or no sequence or structural evidence that MyBP-C binds with molecules such as zinc, calcium, nucleic acids and sugars, it is most likely that protein-protein interactions remain the most plausible main mechanism of its function (Pfuhl and Gautel 2012).

Myosin

Studies have shown that phosphorylation of the MyBP-C motif (region between C1 and C2 domains) (Gautel, Zuffardi et al. 1995) affects the structure of the thick filament by changing the arrangement of the S1 heads (Weisberg and Winegrad 1996, Levine, Weisberg et al. 2001), which in turn affects the formation of cross bridges. The crossbridges appear to be able to move further from the thick filament backbone. Recently, this theory was further supported by high-resolution observations of changes in the shape of thick filaments (Farman, Gore et al. 2011, Palmer, Sadayappan et al. 2011).

A number of binding sites for MyBP-C on myosin have been identified to possibly achieve the above regulatory mechanism.

1. C10 domain in the C-terminus is shown to interatct with light meromyosin (LMM) via positively charged amino acids on its surface (Miyamoto, Fischman et al. 1999). Although C10 is the essential domain required for binding (Brown, Singh et al. 2002), this does not achieve the maximal binding to myosin. Hence, the three adjacent domains, C7-C9, also bind to LMM for maximum affinity and to ensure correct incorporation into the A-band (Gilbert, Kelly et al. 1996, Welikson and Fischman 2002).
2. Domains C1-C2 (including the phosphorylatable linker region) in the N-terminus have been shown to bind to S2 (Gruen and Gautel 1999). This interaction is phosphorylation dependent (Gruen, Prinz et al. 1999, Kunst, Kress et al. 2000) where binding occurs when the linker region is un-phosphorylated. A corresponding effect of phosphorylation on force generation was also demonstrated (McClellan, Kulikovskaya et al. 2001).

3. A recent study demonstrated an interaction between the cardiac-specific domain C0 and the myosin regulatory light chain (RLC) (Ratti, Rostkova et al. 2011). This interaction correlates well with previous experimental studies (Margossian 1985, Flavigny, Souchet et al. 1999, Gruen and Gautel 1999, Herron, Rostkova et al. 2006).

Actin

Shortly after the discovery of MyBP-C binding to myosin, its binding with F-actin was also discovered (Moos, Mason et al. 1978, Moos 1981, Yamamoto 1986). However, where exactly this binding occurs on MyBP-C, especially on cMyBP-C still remains unclear with a lot of controversial data (Weith, Sadayappan et al. 2012).

Based on electron microscopy and sequence analysis, this binding was initially thought to occur in the linker between the C0 and C1 domains (Squire, Luther et al. 2003, Squire, Roessle et al. 2004) where the sequence of this linker is Pro/Ala rich and was proposed to form a rod like, actin-binding structure, based on similarity to the N-terminal extension of the essential light chain (ELC) which is another proposed actin-binding site (Timson, Trayer et al. 1998). However, subsequent studies revealed a completely different interaction of the ELC N-terminus to actin (Pliszka, Redowicz et al. 2001, Lowey, Saraswat et al. 2007). In addition,an NMR study (Jeffries, Lu et al. 2011) showed an unstructured and collapsed rather than an extended, rod-like formation, making the original hypothesis less straightforward. This interaction still remains unresolved as no further experimental or theoretical evidence for a Pro/Ala sequence as an actin-binding site has been looked at since (Pfuhl and Gautel 2012).

Subsequently, the cardiac specific domain C0 was proposed as the actin-binding site (Kulikovskaya, McClellan et al. 2003). This was based on *in vitro* binding assays that showed no binding for the C1-C2 fragment. Since then, this work was further supported by more precise studies, such as small angle solution X-ray scattering (Whitten, Jeffries et al. 2008), electron microscopy (Kensler, Shaffer et al. 2011, Mun, Gulick et al. 2011) and NMR spectroscopy (Lu, Kwan et al. 2011), which have all shown C0 as the binding site.

Contradictory to the above data, several studies have shown F-actin binding to C1-C2 and C0-C2, but no or very weak binding for C0-C1 (Razmumova et al 2006, Rybakova et al 2011, Shaffer et al 2009 on p85 Pfuhl & Gautel), suggesting that

domain C0 and the C0-C1 linker do not play a significant role in F-actin binding. Furthermore, the linker region between C1 and C2 domains was also proposed as an F-actin binding site (Razumova, Bezold et al. 2008, Saber, Begin et al. 2008, Whitten, Jeffries et al. 2008, Weith, Sadayappan et al. 2012), where the interaction was demonstrated to be negatively regulated by phosphorylation of the MyBP-C motif region (Shaffer, Kensler et al. 2009).

Recently, one article concluded that no specific interaction of any N-terminal fragment with F-actin could be demonstrated but instead, the C-terminal half was shown to be able to bind to F-actin with high affinity (Rybakova, Greaser et al. 2011). However, this is yet to be confirmed and somewhat difficult to study as the C-terminal half is unequivocally associated with myosin and titin.

Titin

MyBP-C also binds to titin but much more weakly. This interaction occurs through domains 8-10 (Freiburg and Gautel 1996), specifically the first IgI domain in each eleven-domain super-repeat of titin, which defines the ~43 nm interval of MyBP-C localisation in the C-zone (Freiburg and Gautel 1996).

Myosin binding protein-C

Moolman-Smook *et al* (Moolman-Smook, Flashman et al. 2002) proposed intermolecular interaction of MyBP-C which forms the basis of one of the models of MyBP-C within the sarcomere – the collar model. This will be further explained in Sectin 1.6.5.

1.6.5 Assembly of cMyBP-C within the Sarcomere

The precise organisation of MyBP-C within the sarcomere is yet to be resolved (Vydyanath, Gurnett et al. 2012). However, there are currently two different models explaining the organisation of the cardiac isoform of MyBP-C (cMyBP-C) within the sarcomere: the axial and collar models.

Collar Model

In the collar model, also known as the “trimeric” collar model, three cMyBP-C molecules form a collar/ring around the thick filament backbone with intermolecular interactions. These intermolecular interactions are thought to stabilise the cMyBP-C around the thick filament and occur between domains C5 and C8, and C7 and C10 (Figure 1.12) (Moolman-Smook, Flashman et al. 2002). One study has demonstrated that the addition of exogenous C5 to skinned myocytes impairs MyBP-C function (McClellan, Kulikovskaya et al. 2004) and since C5 does not bind to actin or myosin, this impairment suggests that the addition of exogenous C5 disrupts the C5:C8 interaction and, therefore, the assembly of MyBP-C onto the think filament. This model also proposes that domains C0-C4 project outward to interact with the S2 neck of myosin and possibly actin in the thin filament.

However, this model has a few challenges that are yet to be clarified. Firstly, there is a mismatch of the circumference of the thick filament backbone (approximately 41-47 nm) and the diameter of cMyBP-C wrapped around the thick filament. This model proposes the wrapping of 9 immunoglobulin domains of cMyBP-C around the thick filament backbone. Since the diameter of these immunoglobulin domains is approximately 3.4-3.9 nm (Pfuhl and Pastore 1995, Improta, Politou et al. 1996), the diameter of cMyBP-C that is wrapped around the backbone is estimated to be 35-36nm, which is 5-12 nm shorter than the estimated circumference of the thick filament. Currently, there is no data suggesting the possible stretch of the C-terminal motifs of MyBP-C. Secondly, this model lacks an explanation for how cMyBP-C binds to titin and LMM via domains C8-C10. Additionally, both X-ray diffraction and EM reconstructions do not support this model (Squire, Luther et al. 2003, Luther, Winkler et al. 2011, Vydyanath, Gurnett et al. 2012).

Axial Model

This model suggests that C-terminal domains bind to the thick filament by running along it axially and the N-terminal domains project toward the thin filament perpendicularly (Figure 1.13) (Squire, Luther et al. 2003). In contrast to the collar model, this model incorporates the involvement of C7-C10 binding to titin by suggesting that the two proteins can run parallel to each other.

Recent studies using electron microscopy (EM) reconstructions (Vydyanath, Gurnett et al. 2012) and electron tomography (Luther, Winkler et al. 2011) have strongly suggested the axial distribution of MyBP-C on the thick filament. Furthermore, Vydyanath *et al* (Vydyanath, Gurnett et al. 2012) has also shown that mutations in MyBP-C leading to hypertrophic cardiomyopathies do not alter its mean axial distribution along the thick filament (Vydyanath, Gurnett et al. 2012).

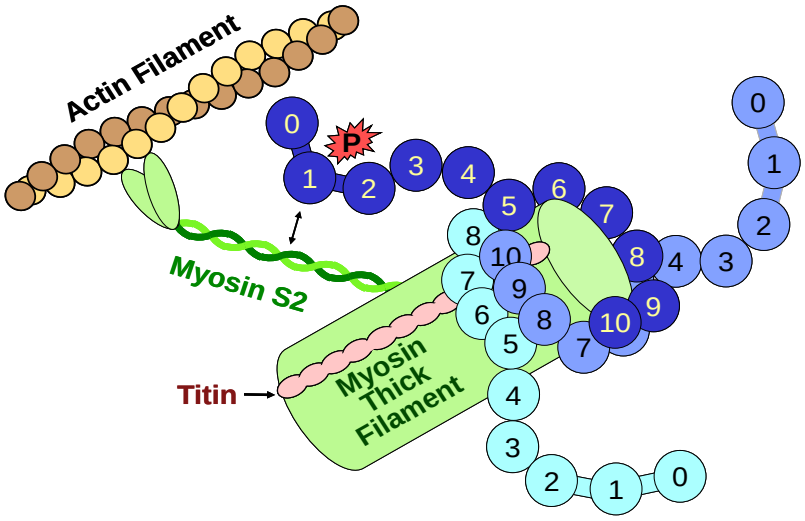

Figure 1.12. Collar model of MyBP-C arrangement in sarcomere. Image from (Oakley, Hambly et al. 2004).

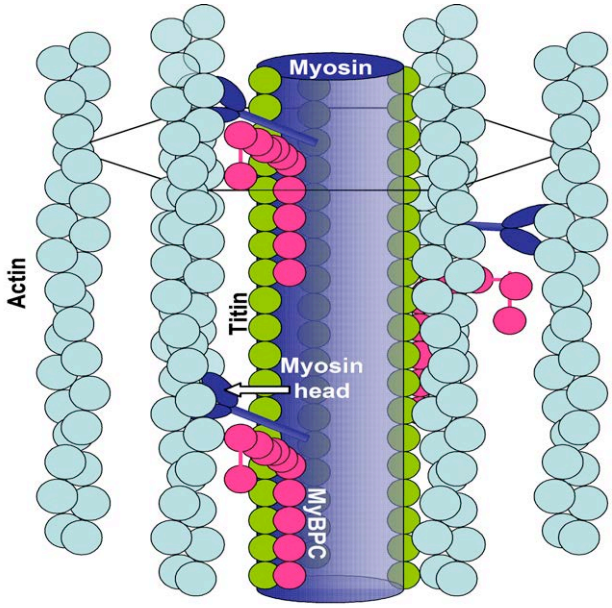

Figure 1.13. Axial model of MyBP-C arrangement in sarcomere. C7-C10 runs axially along the myosin backbone and interacts with titin. Image from (Oakley, Hambly et al. 2004)

1.6.6. Functional Implications for MyBP-C

Sarcomere Assembly

MyBP-C plays an important role in sarcomere assembly, for example, studies with knockout mice have demonstrated greater sensitivity and loss of order in the filaments (Kensler and Harris 2008, Zoghbi, Woodhead et al. 2008). One study demonstrated that in the presence of MyBP-C, synthetic myosin filaments display an increase in length, a decrease in diameter and an increase in the uniformity of diameters (Koretz 1979). Another study has demonstrated the presence of defective formation of sarcomeres when the titin and/or myosin binding sites of MyBP-C are missing (Gilbert, Kelly et al. 1996, Yang, Sanbe et al. 1998).

Furthermore, MyBP-C is not found in non-striated myofibrils and it has been shown that MyBP-C first appears in the myofibril around the time when non-striated myofibrils evolve into mature myofibrils (Schultheiss, Lin et al. 1990, Lin, Lu et al. 1994, Ehler, Rothen et al. 1999). The only type of striated cell in which MyBP-C is not present is the Purkinje cells in the heart whose function is electrical conduction not contraction. Instead, these cells have MyBP-H, which is homologous to the C-terminal domains of MyBP-C (domains C7-C10) (Vaughan, Weber et al. 1993, Alyonycheva, Mikawa et al. 1997). MyBP-H is also found in skeletal muscle. These findings suggest that the role of MyBP-C in sarcomere assembly is perhaps mediated by the C-terminus.

ATPase Activity

Another vital function of MyBP-C is its ability to regulate muscle contraction by alteration of myosin ATPase activity. This regulation of MyBP-C on ATPase activity has been shown to depend on the isoform of myosin as well as being dose dependent (Table 1.2). Cardiac or skeletal MyBP-C added to skeletal myosin at low ionic strength has been shown to decrease the ATP hydrolysis (Moos and Feng 1980, Yamamoto and Moos 1983) whereas the addition of MyBP-C to skeletal myosin at normal ionic strengths increased the ATPase activity slightly. However, the effect of cardiac or skeletal MyBP-C on cardiac myosin is an increase in ATPase activity at all molar ratios (Yamamoto and Moos 1983). Furthermore, no significant change has been found in the MyBP-C modified ATPase activity in the absence of actin or if one

part of the entire myosin molecule (rod, neck, head or light chains) is missing (Moos and Feng 1980, Hartzell 1985, Margossian 1985). Hence, the mechanism by which MyBP-C is thought to alter ATPase activity is believed to be related to an increase in the ordering of the filaments.

Table 1.2. Summary of the effect of MyBP-C on myosin ATPase activity.

Myosin	MyBPC isoform	Effect on myosin ATPase activity
Skeletal	Skeletal	↓ at low ionic strengths
	Skeletal	Small ↑ at normal ionic strengths
	Skeletal - phosphorylated	Same effect as when dephosphorylated
	Cardiac	↓ at low ionic strengths
	Cardiac	Small ↑ at normal ionic strengths
	Cardiac - phosphorylated	Same effect as when dephosphorylated
Cardiac	Skeletal	↑ ATPase activity
	Cardiac	↑ ATPase activity
	Cardiac - phosphorylated	↑ ATPase activity but not as great as when cMyBPC is dephosphorylated

The relationship between the MyBP-C regulated ATPase rate and MyBP-C phosphorylation has also been studied. Both phosphorylation and dephosphorylation of cMyBP-C resulted in an inhibitory effect on the skeletal muscle ATPase rate, but resulted in an increase of the cardiac muscle ATPase rate, with greater effect when cMyBP-C was dephosphorylated (Hartzell 1985, Lim and Walsh 1986, Venema and Kuo 1993). Additionally, transgenic mice lacking the crucial phosphorylation site have revealed a decrease in the phosphorylation of myofibril samples and an increase in the maximal ATPase (Yang, Hewett et al. 2001). Other effects of phosphorylation on thick filament structure and MyBP-C contraction are discussed in the next section.

Phosphorylation

The phosphorylation of MyBP-C was discovered in 1980 (Jeacocke and England 1980) when a protein with a molecular weight of 150 kDa was found to contain a small amount of ^{32}P in rat heart perfusate. Subsequently, this protein was found to increase with exposure to adrenaline, phosphorylated in response to α and β-adrenergic stimulation, endothelin and Ca^{2+} and dephosphorylated in response to cholinergic receptor stimulation (Hartzell and Glass 1984).

Phosphorylation Sites

MyBP-C can be phosphorylated by a number of kinases. These are listed below with phosphorylation sites in the mouse isoform and predicted sites in humans in brackets:

1. protein kinase A (PKA): serines 273 (275), 282 (284), 302 (304) (Gautel, Zuffardi et al. 1995)
2. protein kinase C (PKC): serines 273 (275), 302 (304) (Mohamed, Dignam et al. 1998)
3. calmodulin dependent kinase II (CamKII): serine 302 (304) (Gautel, Zuffardi et al. 1995)
4. protein kinase D (PKD): serine 302 (304) (Bardswell, Cuello et al. 2010)
5. ribosomal S6 kinase (RSK): serine 282 (284) (Cuello, Bardswell et al. 2011)

In skeletal MyBP-C, there is only one phosphorylation site and this is predicted to be at Ser^{172} in the human fast isoform and Ser^{178} in the human slow isoform. In contrast to the widely accepted presence of only one phosphorylation site in the skeletal MyBP-C, the number of phosphorylation sites on the cardiac isoform is still debatable (Knoll 2012). Nonetheless, there are three accepted phosphorylation sites (A-C) in the linker region that are found to be highly conserved between species and these correspond to Ser^{275} (A), Ser^{284} (B) and Ser^{304} (C) in human isoforms. The phosphorylation sites in skeletal isoforms align with site A in the cardiac isoform (Lim and Walsh 1986, Oakley, Hambly et al. 2004). More interestingly, these conserved sites appear to show substrate preferences or even absolute specificity for the different kinases (please refer to the previous paragraph) and not to be functionally equivalent - for example, Ser-282 is shown to markedly decrease the total cMyBP-C phosphorylation when it’s deleted or mutated (Gautel, Zuffardi et al. 1995, Kunst, Kress et al. 2000), possibly suggesting its role as a switch to allow the other phosphorylatable residues more or less access to the relevant kinases (Gautel, Zuffardi et al. 1995, Kunst, Kress et al. 2000).

Function of Phosphorylation

One of the most significant functions of MyBP-C is its ability to modulate filament orientation and contractile mechanics via phosphorylation/dephosphorylation (Winegrad 2003, Decker, Decker et al. 2005).

When viewed under the electron microscope, PKA phosphorylation of isolated thick filaments resulted in several changes:

1. increase in optical diffraction and filament thickness in the C-zone (Weisberg and Winegrad 1996, Weisberg and Winegrad 1998, Levine, Weisberg et al. 2001)
2. Myosin heads appeared extended from the backbone
3. Increase in the degree of order
4. Change in orientation

Thus, it has been suggested by Weisberg and Winegrad (1998) that perhaps the change in myosin head position and its flexibility upon MyBP-C phosphorylation regulates myosin ATPase rate.

The effects of partial phosphorylation of cMyBP-C on the thick filament have been studied by Levine et al (Levine, Weisberg et al. 2001). This study showed:

1. the addition of the first phosphate on MyBP-C (most likely to be at site B) induced a change from a disordered structure (myosin heads extending at different angles from the backbone) to a tight structure (myosin heads lie along the backbone).
2. di- and tri-phosphorylated cMyBP-C resulted in a loose thick filament structure

Therefore, these data support the idea that the cardiac isoform of MyBP-C plays a more significant role in muscle contraction than the skeletal isoform of MyBP-C.

The relationship between MyBP-C phosphorylation and the regulation of muscle contractility, by affecting the force and Ca^{2+} sensitivity, is of considerable interest. It has been shown that as the level of MyBP-C phosphorylation increases, the maximum Ca^{2+} activated force (F_{max}) increases (McClellan, Kulikovskaya et al. 2001) and conversely, the addition of un-phosphorylated C1-C2 to single skinned fibres decreases the F_{max} (Kunst, Kress et al. 2000). In line with the above findings, MyBP-C phosphorylation has been shown to increase the Ca^{2+}-sensitivity, meaning a lower

concentration of Ca^{2+} is required to achieve the same muscle contractile force. Several animal model studies found:

1. when the three phosphorylation sites, along with two adjacent sites that could be potentially phosphorylated, were replaced with alanines, thus leading to unphosphorylation of MyBP-C, there was contractile dysfunction (Sadayappan, Gulick et al. 2005)
2. when the three phosphorylation sites (serines) were replaced with alanines, it resulted in hypertrophic systolic and diastolic defects, further supporting the idea that PKA phosphorylation of cMyBP-C is important for myocardial function (Tong, Stelzer et al. 2008).
3. When the phosphorylation motif "LAGGGRRTS" was completely deleted, there was an increase in contractility and relaxation of about 22%. An increase in the phosphorylation of the remaining cMyBP-C and other proteins such as troponin I and phospholamban was also observed (Yang, Hewett et al. 2001)

Upon dephosphorylaton of MyBP-C, it binds to myosin-S2 via some part of the N-terminal C1-C2 sequence. Tri-phosphorylation of cMyBP-C has been shown to interrupt this interaction (Gruen, Prinz et al. 1999) and subsequently it has been suggested that the myosin heads with MyBP-C attached are released from any steric constraint imposed by MyBP-C upon phosphorylation, which then may enable MyBP-C to reach out and interact more readily with actin. Extrapolating these data, some suggest that phosphorylation enhances cMyBP-C interaction with the thin filament (Kulikovskaya, McClellan et al. 2003, Shaffer, Kensler et al. 2009).

As well as the above tethering mechanism of MyBP-C, it has also been demonstrated to play a role in non-tethering mechanisms. When C1-C2 was added to MyBP-C knockout mice myofibrils, there was an increase in the myocyte Ca^{2+} sensitivity that the phosphorylation of C1-C2 reduced (Harris, Rostkova et al. 2004), suggesting a role of the N-terminus of MyBP-C in regulating contraction, independent of tethering, but perhaps dependant on binding to myosin-S2.

Lastly, an interesting association between MyBP-C phosphorylation and protein degradation has been demonstrated. Decker *et al* (Decker, Decker et al. 2005) found that in ischaemic tissue, there was an increase in dephosphorylation along with a degraded N-terminus of MyBP-C, found mostly in unphosphorylated MyBP-C. This

perhaps suggests that another role of MyBP-C phosphorylation is to protect the protein from degradation.

1.7 Cofilin

1.7.1 Amino Acid Sequence of Cofilin

Cofilin was first discovered and purified from embryonic chicken brain extracts (Bamburg, Harris et al. 1980). Since then, the family has grown to include a number of related proteins sharing considerable (30-40%) amino acid sequence identity.

There are two known isoforms of cofilin: muscle and non-muscle. The amino acid sequence of these two isoforms and their sequence comparison are presented in Figure 1.14

```
                      1       10        20        30        40        50        60
                      |--------+---------+---------+---------+---------+---------|
Cofilin(non-muscle)   MASGVAVSDGVIKVFNDMKVRKSSTPEEVKKRKKAVLFCLSEDKKNIILEEGKEILVGDV
    Cofilin(muscle)   .....T.N.E.............Q..I...........D..RQ..V..A.Q.....I

                      61      70        80        90        100       110       120
                      |--------+---------+---------+---------+---------+---------|
Cofilin(non-muscle)   GQTVDDPYATFVKMLPDKDCRYALYDATYETKESKKEDLVFIFWAPESAPLKSKMIYASS
    Cofilin(muscle)   .D..E...TS...L..LN.....................................

                      121   130       140       150       160   166
                      |--------+---------+---------+---------+-----|
Cofilin(non-muscle)   KDAIKKKLTGIKHELQANCYEEVKDRCTLAEKLGGSAVISLEGKPL
    Cofilin(muscle)   .......F......W.V.GLDDI...S..G.....NV.V.......
```

Figure 1.14. Sequence comparison of the two isoforms of human cofilin.

1.7.2 Distribution of Cofilin

Cofilin exists not only in all eukaryotic cells but also in the cytoplasm of quiescent cells. It is active within subcellular regions in which the actin cytoskeleton is highly dynamic, such as the cleavage furrow of dividing cells, the leading edge of ruffled membranes, and advancing neuronal growth cones (dos Remedios, Chhabra et al. 2003). Cofilin plays a crucial role in cytokinesis and is therefore widely distributed among tissues of developing animals and plants. Cofilin levels are especially found to be higher in haematopoietic tissues, osteoclasts and fibroblasts (Yonezawa, Nishida et al. 1987).

1.7.3 Structure of Cofilin

Atomic structures of yeast (Fedorov, Lappalainen et al. 1997) and human (Pope, Zierler-Gould et al. 2004) cofilin have been determined. Cofilin is part of the Actin Binding Proteins (ABPs) where structures in this family share a structural similarity – i.e. a central six-stranded mixed ß-sheets, flanked by several α-helices contributed to by residues at the N- and C- terminus (Gorbatyuk, Nosworthy et al. 2006). Hence, not surprisingly, the atomic resolution structure of cofilin showed that cofilin consists of six-stranded ß-sheet, located in the centre with several α-helices surrounding the ß-sheets (Figure 1.15).

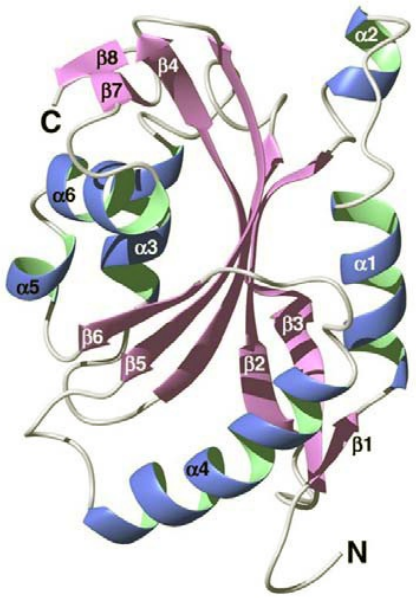

Figure 1.15. The atomic structure of cofilin. Cofilin comprises of a central six-stranded mixed ß-sheet, surrounded by six α-helices around N- and C- terminus.

1.7.4 Cofilin Binding to F-actin

Initially, it was thought that cofilin was primarily an F-actin binding protein. However, it is now known that cofilin is capable of binding to both G- and F-actin and also depolymerises F-actin (Yonezawa, Nishida et al. 1985).

Studies have shown that the upper binding site is the G/F-actin binding site and binds to the actin monomer on subdomains 1 and 3, whereas the lower binding site is the F-actin binding site and binds to the actin monomer on subdomains 1 and 2 (Figure 1.16) (McGough and Chiu 1999). Together these interactions provoke a twist

change in F-actin and weaken both lateral (McGough and Chiu 1999) and longitudinal (Bobkov, Muhlrad et al. 2002) contacts between subunits, promoting filament severing.

The two cofilin-F-actin binding sites are located at opposite ends of the long axis of cofilin (McGough and Chiu 1999, Pope, Zierler-Gould et al. 2004). The G/F-actin binding site is located within the half of cofilin that includes the mobile N-terminus (Pope, Zierler-Gould et al. 2004) and consists primarily of residues located within the long, kinked α4 helix, with contributions from residues located in the β1 strand near the N-terminus and within β6, the intervening loop and α5. The F-actin binding site, located at the opposite end of cofilin, involves residues from the N-terminal segment of the β5 strand and the α6 helix, with a contribution from the adjacent C-terminal residues (Pope, Zierler-Gould et al. 2004).

Phosphorylation at Ser3 in the N-terminus causes minor conformational alterations in 7 residues within α4, which forms much of the G/F-actin binding site, suggesting a structural mechanism by which phosphorylation prevents actin binding (Gorbatyuk, Nosworthy et al. 2006). On the other hand, phosphoinositide (PI) binding perturbs residues located in the C-terminal part of the sequence between β6 and β8, with Lys132 and His133, adjacent to the β6 strand, being directly involved in PI binding (Gorbatyuk, Nosworthy et al. 2006). This region of cofilin overlaps both the G/F-actin and F-actin binding sites. Therefore, PI binding probably prevents actin binding by perturbing residues in both the G/F-actin and F-actin binding sites.

A model has been proposed for the mechanism by which cofilin binds to F-actin and involves cofilin first binding to a monomer within F-actin via the G/F-actin binding site. The model proposes that the C-terminal F-actin binding site is then stabilised via an allosteric conformational change, allowing cofilin to bind to the adjacent actin monomer within the filament (Ono, McGough et al. 2001, Pope, Zierler-Gould et al. 2004). This allosteric effect is thought to be mediated by the β5 strand that bridges the G/F-actin and F-actin binding sites. Thus, the model proposes that binding through the G/F-actin binding site is a pre-requisite for F-actin binding.

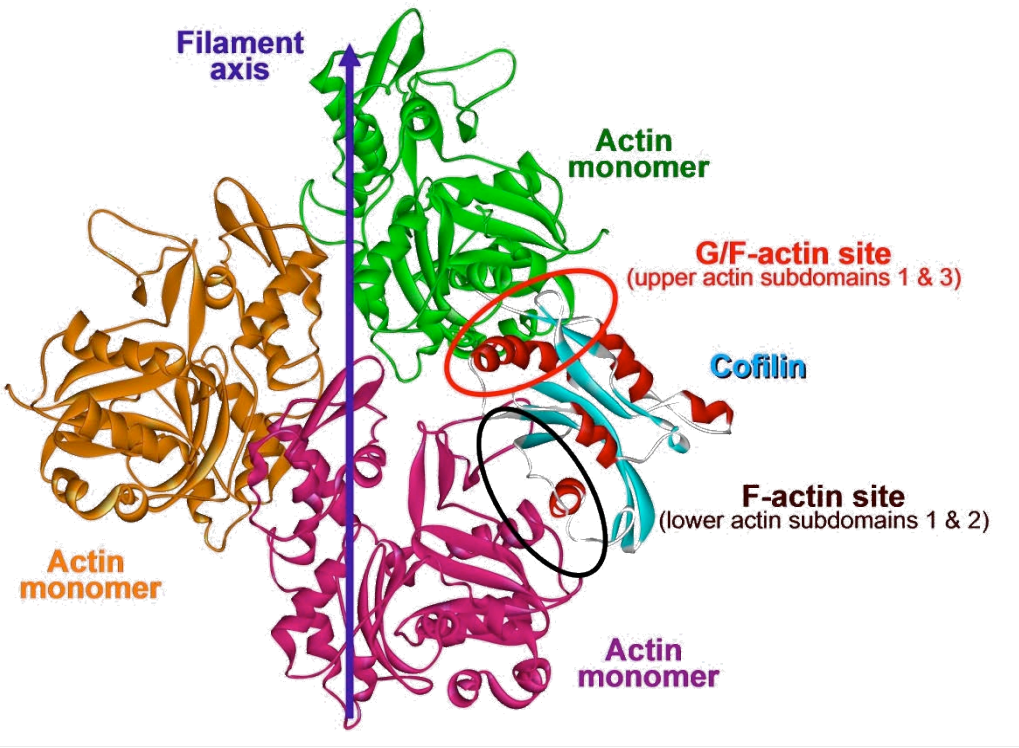

Figure 1.16. Model of cofilin binding sites on F-actin. The upper binding site is the G/F-actin binding site and binds to the green actin monomer on subdomains 1 and 3. The lower binding site is the F-actin binding site and binds to the pink actin monomer on subdomains 1 and 2.

1.7.5 Cellular Functions of Cofilin

1.7.5.1 Depolymerisation

Cofilin binds and depolymerises F-actin in a pH sensitive manner (Yonezawa, Nishida et al. 1985). The extent of this action depends on several factors, for example, different isoforms may have differing pH sensitivities (McGough, Pope et al. 2001) and other ABPs may compete with cofilin for binding to actin due to overlapping binding sites.

The high rate of treadmilling of monomers in actin filaments *in vivo* is achieved in part by increasing, by 30-fold, the off-rate (Ressad, Didry et al. 1998) at the pointed ends of filaments without changing the off-rate at the barbed ends (Carlier, Laurent et al. 1997). The resulting elevated concentration of cofilin-G-actin in the cytoplasm can be rapidly recycled at the barbed end of filaments, provided that ATP can replace the actin-bound nucleotide.

1.7.5.2 Severing

It remains unclear whether cofilin can sever actin filaments like true severing proteins or whether the highly co-operative binding of cofilin at sub-stoichiometric ratios, makes the filaments 'brittle' at the points where the decorated and undecorated regions meet (Bamburg 1999). However, current opinion seems to favour the severing ability of cofilin (Pavlov, Muhlrad et al. 2007, Elam, Kang et al. 2013).

1.7.5.3 Nucleation of Polymerisation

Cofilin is capable of nucleating the assembly of actin (Du and Frieden 1998). Cofilin's ability to nucleate actin polymerisation is probably pH-dependent and may vary between different isoforms of ADF/cofilin. Nonetheless, its precise mechanism is yet to be resolved.

1.7.5.4 Recycling of Actin Filaments

The faster rate of elongation at the barbed end of the actin filament than the pointed end means that subunits at the pointed end are likely to be older than at the barbed end. Consequently, the majority of subunits at the pointed end would contain bound ADP and the majority of subunits at the barbed end would contain ATP or ADP-Pi.

Cofilin binds ADP-actin with about two orders of magnitude greater affinity than actin containing bound ATP or ADP-Pi in both the globular and filamentous forms (Carlier, Laurent et al. 1997). This allows for selection and turnover of older filaments that are more susceptible to disassembly than newly polymerised actin. Cofilin has been shown to inhibit nucleotide exchange (Nishida 1985) of actin monomers. This suggests that cofilin not only depolymerises older filaments, but by preventing nucleotide exchange, the rate-limiting step in the recycling of disassociated F-actin subunits (Teubner and Wegner 1998), prevents repolymerisation (Figure 1.17). Sequestering of monomers by cofilin allows a concentration of monomeric actin, higher than the critical concentration to exist *in vivo*.

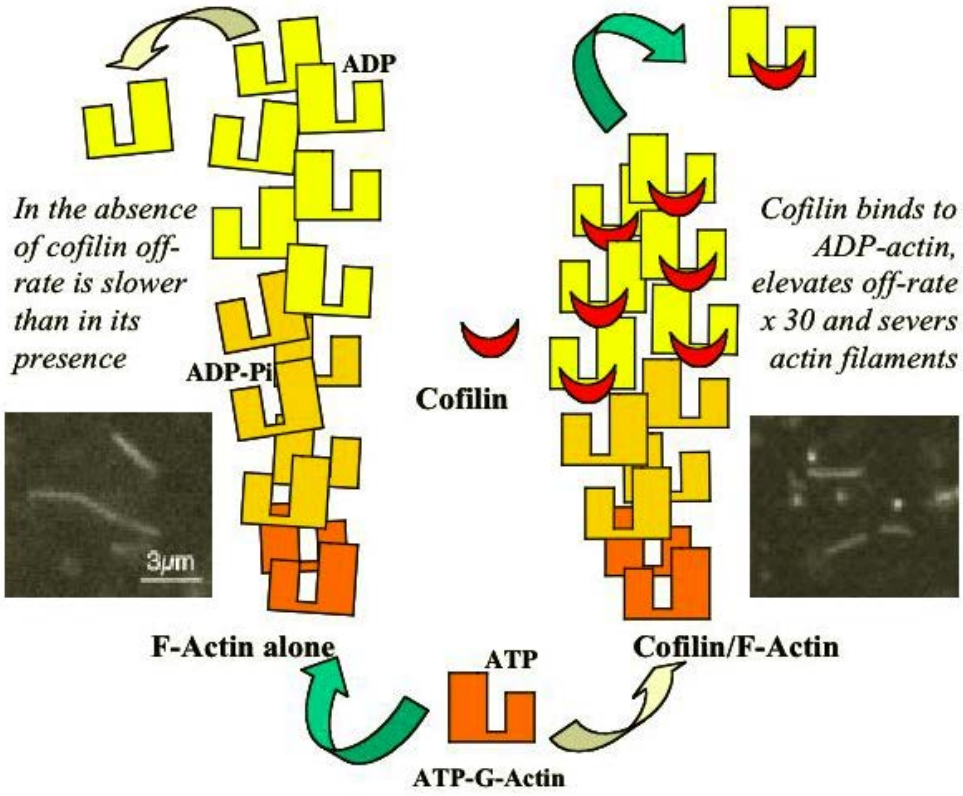

Figure 1.17. Schematic illustration of actin filament dynamics. Left diagram represents in the absence of cofilin and the right diagram represents in the presence of cofilin.

1.7.5.5 Nuclear Translocation

The cofilin sequence contains a putative nuclear localisation sequence (NLS) that enables it to migrate from its normal location in the cytoplasm to the nucleus under conditions of cellular stress (Nishida, Iida et al. 1987). Heat shock and other forms of stress are likely to affect a few residues immediately preceding the NLS. Subsequently, this will promote binding to a nuclear transport factor and thus passage through the nuclear pores (Bowman, Nodelman et al. 2000). Transport is an active process and actin accompanies cofilin into the nucleus, although the significance of this remains unclear.

1.7.5.6 Phosphorylation

Cofilin contains a residue capable of phosphorylation at Ser3 (Nebl, Meuer et al. 1996). Phosphorylated cofilin is dispersed throughout the cytoplasm, and dephosphorylation correlates to its translocation into the nucleus. Translocation is

mediated by a stretch of five basic residues (30-34, KKRKK) comprising the nuclear localisation sequence (Iida, Matsumoto et al. 1992). Phosphorylation of cofilin reduces its affinity for actin by 10-30 fold (Morgan, Lockerbie et al. 1993).

Phosphorylation of cofilin does not alter the tertiary structure of the protein, suggesting that abolition of actin-binding is a result of a steric hindrance (Blanchoin, Robinson et al. 2000).

ADP exchange in G-actin is strongly inhibited by cofilin, but once cofilin is phosphorylated, the released ADP-actin monomer can exchange with cytoplasmic ATP, and it is now ready for reincorporation at the barbed-end of a growing filament. Typically, this occurs at the interface of the microfilaments and the membrane at the leading edge of the moving cell. Thus, cellular microfilament turnover can potentially be regulated by cycles of phosphorylation and dephosphorylation.

Phosphorylation of vertebrate cofilin is by LIM-kinase proteins 1 and 2 (LIMK-1 and LIMK-2). LIMK-1 is predominantly neuronal, whereas LIMK-2 is more widespread (Bernard, Ganiatsas et al. 1994). Although the signalling pathway for activation of the LIM kinases is not yet fully understood, it is known that LIMK-1 is under the control of the small GTPase, Rac (Arber, Barbayannis et al. 1998, Yang, Sanbe et al. 1998), whereas LIMK-2 is regulated by both cdc42 and rho (Bamburg 1999). Dephosphorylation of cofilin in mediated by Slingshot, a protein phosphatase with F-actin binding ability (Niwa, Nagata-Ohashi et al. 2002).

1.8 Aims

The focus of this thesis lies in investigating two actin binding proteins: cMyBP-C and cofilin. The specific aims of this thesis are:

1. Clone and express a fragment of cMyBP-C, C1-L, and its FHC mutants using a recombinant protein expression technology (Chapter 3).
2. Assess binding capacity of C1-L and its FHC mutants to F-actin and myosin using a co-sedimentation assay and gel electrophoresis, subsequently finding the minimum domains required for binding (Chapter 4).
3. Gain insight into the tertiary structure of the linker region of cMyBP-C using nuclear magnetic resonance (NMR) (Chapter 5).
4. Design functional cofilin mutants suitable for selective labelling with extrinsic fluorescent spectroscopic probes for distance measurements (Chapter 6).

5. Determine secondary structure of a mutant cofilin using Circular Dichroism (CD) Spectroscopy (Chapter 6).
6. Perform binding assays to determine the binding status of cofilin mutants to actin, both before and after labelling (Chapter 6)
7. Use FRET spectroscopy to measure distances both within cofilin and between cofilin and actin (Chapter 6).

Chapter 2

General Methods and Materials

Chapter 2

General Methods and Materials

2.1 General Methods

2.1.1 Chemicals and Media

All chemicals and reagents used were of analytical grade unless otherwise stated. Water was purified by reverse osmosis followed by ion exchange/organic filtration (Millipore RO and Milli Q). All media and water used for PCR, cloning and bacterial growth were autoclaved at 1.5 kg f/cm^2 for a minimum of 20 minutes at 122^{o}C. The heat labile solutions such as antibiotics and IPTG were sterilised by passing the solution through a sterile 0.22 µM filter. These were then stored at -20^{o}C.

2.1.2 Tissue Samples for Muscle Proteins

Fresh skeletal muscle was acquired from male New Zealand White rabbits aged between 2-3 months and weighing 2.5 – 3 kg. Once the animal had been sacrificed using procedures approved by the University of Sydney Animal Care and Ethics Committee (ACEC K20/3-2006/3/4323), the back and leg muscles were obtained and immediately chilled on ice. The muscle was then minced to extract myosin and/or actin.

Generally multiple tissues were harvested from each carcass for a range of unrelated projects. The ACEC permitted this arrangement, principally because it avoided unnecessary euthanasia.

2.1.3 Lyophilisation of Proteins

Lyophilisation or freeze drying is a process by which water is removed from a snap-frozen protein sample. Purified G-actin was lyophilised and stored at -20^{o}C for up to three months. As freeze drying biological material primarily results in a dry product, enzymatic, bacterial and chemical changes are largely avoided.

Prior to lyophilisation, the protein solutions were placed in a round bottom flask ensuring the volume of protein did not exceed 10 % of the flask volume. The solution in the flask was then snap frozen by rotating the flask rapidly in a liquid nitrogen bath. Once all the protein solution was frozen, the flask was immediately connected to a Braun Christ Alpha 1-4 freeze-drying unit (B.Braun Biotech International) and vacuum was generated by a Javac double stage teflon-lined vacuum pump. Water was removed under a vacuum of 0.31 mBar or less for at least 12 hours (usually left overnight).

2.1.4 Determination of DNA Concentration

Concentration of DNA was measured either using a BioPhotometer (Eppendorf) or a NanoDrop 1000 spectrophotometer (Thermo Scientific). All measurements were done according to the manufacturer's instructions.

Diluent buffer was used as a blank irrespective of which machine was used. Absorption measurements were carried out in the ultraviolet and visible light ranges (260 nm), where an absorption of 1 corresponds to 50 µg/ml dsDNA. The BioPhotometer calculates the concentration of an unknown sample by using the following equation (Equation 2.1):

$$\textbf{dsDNA con (µg/ml)} = \mathbf{A_{260\ nm} \times 50 \times dilution\ factor} \qquad \text{Equation. 2.1}$$

Purity analysis was assessed by calculating the ratios of various absorption values.

i. $A_{260\ nm}/A_{280\ nm}$: protein contamination can be measured as proteins absorb maximally at 280 nm

: ideal value is 1.8. This value will decrease with increased protein contamination

ii. $A_{260\ nm}/A_{230\ nm}$: absorption at 230 nm reflects impurities of peptides, phenols, carbohydrates or aromatic compounds

: ideal value is >2.0 for pure samples

iii. $A_{320\ nm}$: dirty cuvettes and dust particles cause light scatter at 320 nm which can impact the absorbance at 260 nm. Since neither proteins nor nucleic acids absorb at 320 nm, BioPhotometer performs a background correction by making readings from a blank at 320 nm.

: ideal value is 0 for pure samples

2.1.5 Determination of Protein Concentration

2.1.5.1 UV-Vis Spectroscopy

Protein concentration was measured using a Varian Cary 50 Bio spectrophotometer. The UV lamp was turned on 30 minutes prior to use to obtain uniform light emission. The machine was blanked with the diluent buffer and the samples were measured at 280 nm. However, any samples which contained ATP, such as actin, were measured at 290 nm to avoid the absorbance of bound and free nucleotide. Using the extinction coefficients provided in Table 2.1, concentrations in mg/ml were calculated according to the following equation (Equation 2.2):

$$\mathbf{A = \varepsilon\ c\ l} \qquad \text{Equation 2.2}$$

A: absorbance; ε: extinction coefficient; c: concentration (mg/ml); l: path length of the cuvette (cm)

Table 2.1. Protein standard extinction coefficients.

Absorbance wavelength	Protein	Extinction Coefficient	Reference
290 nm	G-actin	0.63 cm^{-1}	(Lehrer and Kerwar 1972)
280 nm	Myosin	0.56 cm^{-1}	(Chock 1979)
280 nm	HMM	0.60 cm^{-1}	(Margossian and Lowey 1982)

2.1.5.2 Protein Assay

Concentrations for proteins without published extinction coefficients were determined using a Pierce BCA protein assay kit (Quantum Scientific Pty Ltd., Paddington, QLD). The method used was as recommended by the manufacturer. A standard curve was prepared using known concentrations of bovine serum albumin

(BSA). The reagent solution (which produces a colour change in the presence of protein) was added to both the standards and samples of unknown concentrations. Following an incubation period of 30 minutes at 37^{o}C, the absorbance was measured at 562 nm using a Varian Cary 50 Bio spectrophotometer. Ultimately, the unknown concentrations were obtained from the standard curve.

2.2 Electrophoresis

Gel electrophoresis is a powerful analytical technique for assessing the purity and content of both protein and DNA samples. The samples are able to move through a gel matrix under the influence of an electric field. The rate at which the molecules migrate is dependent on their size, shape and charge, as well as the composition and the pH of the gel.

In this project, gel electrophoresis was also used for preparative techniques to partially purify molecules prior to use for cloning (Chapter 3) and mass spectrometry (Chapter 3). All components required for electrophoresis are listed in Table 2.2.

2.2.1 Agarose Gel Electrophoresis

Agarose gels were used to visualise DNA samples. The percentage of agarose gel used depended on the size of the DNA fragment of interest and hence, by adjusting the concentration of agarose, the pore size of the gel is altered, consequently changing the sieving properties of the gel.

The rate at which the DNA fragments depends on 3 factors:

1. size

   Adjust the pore size of the gel by adjusting the concentration of agarose

2. charge

   DNA has a negatively charged backbone. Generally, this is distributed evenly under alkaline conditions, such as in the presence of TAE buffer (pH8.0). Thus, the DNA migrates from cathode to anode.

3. shape

   The conformation of the DNA affects the separation of DNA fragments, with supercoiled, linear and nicked circular DNA of the same molecular weight migrating at different rates. Supercoiled DNA moves the fastest due to its tight packing and smaller hydrodynamic radius and nicked

circular runs the slowest having lost all its superhelicity (Thorne 1967, Johnson and Grossman 1977).

The appropriate amount of agarose was added to 1 x TAE buffer and the agarose/buffer solution was heated until the agarose was completely dissolved. The solution was then partially cooled before pouring. Prior to loading, the samples were mixed with 6x DNA sample buffer and loaded into the wells of the gel. A standard size marker ladder was also loaded to verify the relevant DNA fragment length. The gel was run at 80 V in TAE buffer for approximately 1 hour. Lastly, the gel was stained with ethidium bromide and visualised under UV illumination.

Table 2.2. Components for SDS-PAGE, native-PAGE and agarose electrophoresis.

	SDS-PAGE	**NATIVE-PAGE**	**AGAROSE GELS**
Stacking gel	0.125 M Tris-HCl pH 6.8 0.1% SDS 4% acrylamide-bis	80 mM Tris-HCl, pH 6.8 4% acrylamide-bis	NA
Separating gel	0.375 M Tris-HCl pH 8.8 0.1% SDS 12-15% acrylamide-bis	80 mM Tris-HCl, pH 8.8 10% acrylamide-bis	1 – 1.5% w/v agarose in 1 × tank buffer (TAE)
Sample Buffer	**5×** 50 mM Tris-HCl pH 6.8 2% w/v SDS 10% glycerol 5% β-mercaptoethanol 0.01% w/v bromophenol blue	**5×** 0.25 M Tris-HCl, pH 6.8 20% glycerol 0.1% w/v bromophenol blue	**6×** 10mM Tris-HCl pH 7.5 15% Ficoll® 400 50mM EDTA pH 8.0 0.4% orange G 0.03% bromophenol blue 0.03% xylene cyanol FF
Tank buffer	25 mM Tris, pH 8.3 0.192 M glycine 0.1% w/v SDS	**10×** 25 mM Tris, pH 8.6 0.192 M glycine	**TAE** 4 mM Tris-HCl, pH 8.0 1% v/v acetic acid 2mM EDTA
Staining	**Stain** (overnight) 0.1% Coomassie Blue R-250 40% v/v methanol 10% v/v acetic acid **Destain** (~6 hours) 40% v/v methanol 10% v/v acetic acid	**Stain** (overnight) 0.1% Coomassie Blue R-250 40% v/v methanol 10% v/v acetic acid **Destain** (~6 hours) 40% v/v methanol 10% v/v acetic acid	**Stain** (30 minutes) 2mg/L ethidium bromide in TAE **Destain** (5 minutes) ddH_2O

2.2.2 SDS-PAGE

Sodium dodecyl sulphate-polyacrylamide gel electrophoresis (SDS-PAGE) separates proteins according to the length of their polypeptide chain, thus according to their molecular weights. SDS, being an anionic detergent, binds, solubilises, partially unfolds and coats proteins. Therefore the proteins acquire a negative charge approximately proportional to their molecular weights. As this negative charge (acquired by binding with SDS) is very saturated, the contribution of intrinsic charge of the protein to its rate of migration through the gel is negligible.

The concentration of acrylamide and its cross-linker, bis-acrylamide, determines the pore size of the gel matrix. For low molecular weight proteins, a 15-17% separating gel was used and for high molecular weight proteins, an 8-12% gel was used. A 30% stock solution of acrylamide was diluted to the desired concentration and polymerised by the addition of 1% (w/v) ammonium persulphate (APS) and 0.2% (v/v) N,N,N',N'-trimethylethylenediamine (TEMED).

In this thesis, all the SDS-PAGE gels used were of a discontinuous type (Laemmli 1970), that is, there were different stacking and running gels. The acrylamide concentration for the upper stacking gel was 4% and pH 6.8. The pH for the lower running/separating gels was 8.8. The difference in pH values creates a chloride gradient and sharpens the bands, resulting in better resolution. Gels, 80 mm wide and 0.75 mm thick, were cast using the mini-gel caster for the Bio-Rad Mini PROTEAN II system (Bio-Rad Laboratories Pty. Ltd., Regents Park, NSW).

Prior to loading, the samples were mixed with 5 x SDS-reducing buffer containing 5% (v/v) β-mercaptoethanol and 2.5% (w/v) SDS. The mixture was boiled for 4 minutes to reduce the disulphide bonds. Gels were run at 160 V in electrode buffer for approximately 60 minutes or until the bromophenol dye reached the bottom of the gel. A standard molecular weight marker set (Promega) was also used to estimate the molecular weight of the proteins of interest.

Gels were stained with 0.1% Coomassie brilliant blue stain in 40% methanol and 10% acetic acid for approximately 1 hour and destained using two changes of 40% ethanol and 10% acetic acid.

2.2.3 Native PAGE

Native PAGE is run in the absence of SDS and without boiling the samples. Consequently, the proteins are not denatured and do not have additional negative charge surrounding them. As a result, the mobility of proteins depends not primarily on their molecular weights but mainly on the protein's charge and conformation. In this thesis, native-PAGE was used to analyse binding activities in order to not disturb the non-covalent interactions between proteins. All components of stacking and separating gels, sample buffer and running buffer are listed in Table 2.2.

2.2.4 Gel Documentation

Coomassie blue stained protein bands were visualised and photographed under transilluminating white light using a UVP GDS 8000 gel documentation system (UVP Inc., Cambridge, UK) and an orange filter. The agarose gels were visualised and photographed under UV light using the same system.

2.3 Protein Preparation

2.3.1 Myosin Preparation

Myosin was prepared using an adapted method from Margossian and Lowey (Margossian and Lowey 1982) and this is outlined in Figure 2.1. The separation of myosin from other proteins is achieved by a series of precipitations and sedimentations. This method is based on differential solubility of myosin and other proteins at different ionic strengths.

Briefly, rabbit back muscle (approximately 350 g) taken from male New Zealand White rabbits, as described in section 2.1.2, was chilled on ice and minced thoroughly. Prior to mincing the muscle, any fat and connective tissue was removed and the minced meat was extracted in a high salt buffer with constant stirring and then centrifuged at 5,000 x g. The resultant supernatant was then filtered to ensure any remaining fat and large lumps of muscle were removed. The filtrate was then subjected to a series of precipitations and sedimentations in low salt and resuspended in high salt. In low salt conditions (<0.3 M), myosin is insoluble due to the hydrophobic rod region. In salt concentrations similar to physiological conditions (~0.15 M), myosin aggregates to form bipolar thick filaments and precipitates out of solution. At high salt concentrations (>0.3 M) myosin becomes fully soluble. Finally,

myosin was further clarified by centrifuging at 156,000 x g for 2 hours. Purified myosin was snap frozen by adding drop-wise into liquid nitrogen and stored at -80^{o}C for up to 3 months. The whole procedure was carried out at 4^{o}C.

Remove ~350 g of rabbit back muscle and place on ice for ~10 minutes

↓

Mince the muscle by passing through a meat mincer

↓

Extract the rabbit mince in 3 volumes of solution 1 for 30 minutes on ice with stirring

↓

Centrifuge the homogenate at 5,000 x g for 15 minutes at 4^{o}C

↓

Filter the supernatant though a fine cheese-cloth. Store the pellet at -20^{o}C or perform acetone powder preparation immediately (for thin filament proteins)

↓

Precipitate the supernatant by adding 10 volumes of cold H_2O and 0.2 mM DTT. Leave to stand until the precipitate settles (1-12 hours)

↓

Decant the supernatant

↓

Centrifuge the remainder at 5,000 x g for 15 minutes at 4^{o}C

↓

Completely dissolve the pellet in solution 2 (final [KCl] = 0.4 M) with stirring

↓

Decrease the [KCl] from 0.4 M to 0.28 M by adding water. Stir gently for ~15 minutes

↓

Centrifuge at 51,000 x g for 30 minutes at 4^{o}C

↓

Add 10 volumes of water to the supernatant

↓

Centrifuge at 5,000 x g for 15 minutes at 4^{o}C

↓

Dissolve the pellet in solution 3

↓

Centrifuge at 156,000 x g for 120 minutes at 4^{o}C

↓

Snap freeze the myosin by adding drop-wise to liquid N_2 and store at -80^{o}C

Solution1: 0.3 M KCl, 0.1 M K-PO_4, pH 6.8, 2 mM ATP, 1 mM $MgCl_2$, 0.2 mM DTT and 0.5 mM PMSF

Solution 2: 2.4 M KCl, 20 mM K-PO_4, pH 6.8, 0.2 mM DTT

Solution 3: 0.6 mM KCl, 10 mM K-Pyrophosphate pH 7.0, 0.5 mM DTT, 1 mM NaN_3

Figure 2.1 Myosin preparation. All steps were carried out at 4^{o}C unless otherwise stated.

2.3.2 HMM Preparation

The heavy meromyosin fragment of myosin was prepared using an adapted method from Margossian and Lowey (Margossian and Lowey 1982) and is outlined in Figure 2.2.

Snap frozen myosin was rapidly defrosted in a 30^{o}C water bath and diluted to 10 mg/ml in 0.5 M KCl and 50 mM K-PO_4 pH 6.5 (solution 1). The diluted myosin was then digested with α-chymotrypsin. The digestion process was terminated by adding the protease inhibitor PMSF and the solution was then dialysed in a low salt buffer (solution 2). During this dialysis, undigested myosin and myosin rod are precipitated and digested myosin containing HMM stays in solution. HMM is purified by centrifugation at 100,000 x g for 60 minutes at 4^{o}C. HMM is either used immediately or is snap frozen in liquid N_2 and stored at -80^{o}C for up to 3 months.

Rapidly defrost the snap frozen myosin in 30^{o}C water bath

↓

Dilute myosin to 10 mg/ml in 0.5 M KCl and 50 mM K-PO_4, pH 6.5 (solution 1)

↓

Digest myosin for 90 seconds with stirring by adding 0.05 mg/ml α-chymotrypsin

↓

Terminate digestion by adding PMSF to 0.5 mM

↓

Dialyse the digested myosin for 24 hours at 4^{o}C in 20 mM KCl, 10 mM K-PO_4, pH 7.0, 1.5 mM DTT with 2 x 1 L changes (solution 2)

↓

Centrifuge at 100,000 x g for 60 minutes at 4^{o}C (supernatant contains HMM)

↓

Snap freeze HMM in liquid N_2 and store at -80^{o}C

Figure 2.2 HMM preparation. All steps were carried out at room temperature unless otherwise stated.

2.3.3 S2 Preparation

S2 was prepared using a method adapted from Lowey and Slayter (Lowey, Slayter et al. 1969) and this is outlined in Figure 2.3

Briefly, HMM was digested with α-chymotrypsin and the reaction was terminated by adding PMSF. The protein was precipitated by adding ethanol and then pelleted by centrifugation. The pellet was then dissolved in 20 mM K-PO_4, pH 6.22 and dialysed in 20 mM K-PO_4, pH 6.22. The solubilised protein was obtained by centrifugation (located in supernatant) and dialysed in 20 mM K-acetate, pH 4.5 to precipitate the protein of interest. Finally, the desired protein, S2 was pelleted by centrifugation and dissolved in 40 mM KCl, 20 mM Tris-HCl, pH 8.0, 0.2 mM DTT, 0.2 mM $CaCl_2$, 2 mM $MgCl_2$. To further remove contaminants, the dissolved S2 was centrifuged one more time.

Digest HMM for 3.5 minutes by adding 0.05 mg/ml α-chymotrypsin. Gently stir

↓

Terminate digestion by adding PMSF to 0.5 mM

↓

Precipitate protein by adding 3 volumes of 100 % ethanol

↓

Centrifuge at 15,000 x g for 15 minutes at 4^oC

↓

Dissolve the pellet in 20 mM K-PO_4, pH 6.2 with stirring for ~3 hours at 4^oC (solution 1)

↓

Dialyse in 20 mM K-PO_4, pH 6.2 at 4^oC overnight (2 x 1 L changes) (solution 2)

↓

Centrifuge at 100,000 x g for 30 minutes at 4^oC

↓

Dialyse the supernatant in 20 mM K-acetate buffer, pH 4.5 overnight at 4^oC
(2 x 1 L changes)

↓

Centrifuge at 50,000 x g for 30 minutes at 4^oC (pellet contains S2)

↓

Dissolve pellet in 40 mM KCl, 20 mM Tris-HCl, pH 8.0, 0.2 mM DTT, 0.2 mM $CaCl_2$, 2 mM $MgCl_2$ with stirring at 4^oC for ~1 hour (solution 3)

↓

Centrifuge at 100,000 x g for 30 minutes at 4^oC (supernatant contains S2)

↓

Store S2 at -20^oC in aliquots

Figure 2.3 S2 preparation. All steps carried out at room temperature unless otherwise stated.

2.3.4 Acetone Powder Preparation

Acetone powder was prepared as described by Carsten and Mommaerts (Carsten and Mommaerts 1963) and this is outlined in Figure 2.4. Finely minced rabbit back muscle was extracted in high salt solution and filtered though a double layer of cheese cloth supported by a 300 mm diameter Buchner funnel. The extract was put through several washes and then dehydrated with sequential washes of ice cold acetone followed by acetone at room temperature and air dried overnight. Once the extract was completely dry, it was blended into a fine powder. Lastly, the powder was stored for actin preparation in a sealed container at -20^{o}C for up to 3 months.

Mince ~350 g of rabbit back muscle

↓

Extract in 3 volumes of 0.5 M KCl, 0.15 M K-PO_4 buffer, pH 6.4 for 30 minutes

↓

Centrifuge at 6,370 x g for 15 minutes at 4^{o}C

↓

Wash pellet in 5 volumes of 0.4 % sodium HCO_3 for 15 minutes at room temperature (x2)

↓

Filter through double cheese cloth

↓

Wash residue in 3 volumes of cold water for 5 seconds

↓

Filter through double cheese cloth

↓

Wash residues in 3 volumes of cold water for 2 hours

↓

Centrifuge at 6,370 x g for 15 minutes at 4^{o}C

↓

Wash pellet in 4 volumes of cold acetone for 5 seconds (x 2)

↓

Filter through double cheese cloth

↓

Wash in 4 volumes of acetone at room temperature for 15 minutes (x 3)

↓

Filter through double cheese cloth

↓

Air dry overnight at room temperature

↓

Blend at high speed for 20 seconds

↓

Store at -20^{o}C

Figure 2.4 Acetone powder preparation. All steps were carried out at 4^{o}C unless otherwise stated

2.3.5 Actin Preparation

Actin was prepared using the method of Spudich and Watt (Spudich and Watt 1971) with slight modification (Barden and dos Remedios 1984) and the steps are outlined in Figure 2.5. Actin was extracted from acetone powder and centrifuged. The supernatant, containing G-actin was then subjected to a polymerisation/depolymerisation process. G-actin is polymerised to F-actin by adding 0.1 M KCl and 4 mM $MgCl_2$. Then F-actin was sedimented by centrifuging at high speed. F-actin was again depolymerised into G-actin by homogenising the pellet using a Teflon-glass homogeniser and dialysed in G-buffer (2mM Tris pH 8.0, 0.2mM ATP, 0.2mM $CaCl_2$). Finally, G-actin was clarified by high speed centrifugation to remove any polymerised actin and other protein aggregates. The purified G-actin was lyophilised and stored at -20^{o}C.

Extract 10 g acetone powder in 1 mM Tris, pH 8.0 for 15 minutes

↓

Centrifuge at 31,000 x g for 30 minutes

↓

Take supernatant and add KCl to 0.1 M and $MgCl_2$ to 4 mM. Leave for 1 hour at 25^{o}C

↓

Increase [KCl] to 0.6-0.8 M. Leave for 2 hours at 25^{o}C

↓

Centrifuge at 130,000 x g for 90 minutes at 15^{o}C

↓

Homogenise the pellet in 60 mL of G-buffer

↓

Dialyse against G-buffer overnight (2 x 1 L changes) (x2)

↓

Centrifuge at 130,000 x g for 90 minutes at 4^{o}C

↓

Lyophilise the G-actin and store at -20^{o}C

G-buffer: 2 mM Tris-HCl, pH 8.0, 0.2 mM $CaCl_2$, 0.2 mM ATP, 0.2 mM DTT

Figure 2.5 Actin preparation. All steps were carried out at 4^{o}C unless otherwise stated.

2.4 Molecular Biology Methods

2.4.1 Media Components

The required amount of Luria Bertani (LB) broth or Terrific Broth (TB) was measured and autoclaved at 1.5 kgf/cm^2 for a minimum of 20 minutes at 122^{o}C. Once it was cooled to below 50^{o}C, selective media was prepared by adding chloramphenicol and ampicillin or kanamycin to 50 μg/mL each.

LB-agar plates were prepared by adding 20 g Bacto-agar to 1 L LB media. The mixture was then autoclaved. Once, the appropriate antibiotics were added, approximately 30 mL of the solution was decanted into sterile petri-dishes. The plates

were allowed to set at room temperature and dried for 30 minutes at 37^{o}C. The entire procedure was carried out in a sterile environment.

Super Optimal broth with Catabolite repression (SOC) media containing tryptone, yeast extract, NaCl and KCl was also autoclaved. Once it was cooled, filter sterilised heat labile ingredients were added. These are $MgCl_2$, $MgSO_4$ and glucose. Lastly, the final solution was filtered through a 0.2 µm filter unit and stored as aliquots at -20^{o}C.

All components required for media and stock solutions are listed in Table 2.3.

Table 2.3. Components of bacterial media and stock solutions used for protein preparation

Bacterial Media & Stock Solutions	Components
Ampicillin	50 mg/ml in sterile H_2O; filter sterilise; store in aliquots at -20^{o}C
Kanamycin	50 mg/ml in sterile H_2O; filter sterilise; store in aliquots at -20^{o}C
Chloramphenicol	50 mg/ml in sterile H_2O; filter sterilise; store in aliquots at -20^{o}C
LB media	1 L consists of 10 g tryptone, 5 g yeast extract, 5 g NaCl, adjust pH with 5 M NaOH; autoclave at 122^{o}C and 1.5 kgf/cm^2 for 20 minutes, allow to cool before adding antibiotics
TB Media	1 L consists of 12 g tryptone, 24 g yeast extract, 4 g proprietary carbon source, 12.54 g K_2HPO_4, 2.31 g KH_2PO_4; autoclave at 121^{o}C and 1.5kgf/cm^2 for 20 minutes, allow to cool before adding antibiotics
LB agar	LB medium with 20 g/L Bacto-agar; autoclave at and 1.5 kgf/cm^2 for 20 minutes, allow to cool (<50 ^{o}C) before adding antibiotics
SOC media	100 mL consists of 2 g tryptone, 0.5 g yeast extract, 1 mL of 1M NaCL, 0.25 mL 1 M KCl; autoclave at and 1.5 kgf/cm2 for 20 minutes, allow to cool (<50 ^{o}C) before adding 1 mL of 1 M MgCl2/1 M MgSO4 and 1 mL 2 M glucose (all filter sterilised through 0.2 µm filter unit); store in aliquots at -20 ^{o}C
IPTG	1 M stock consist of 238 mg/ml in sterile H2O; filter sterilise, store in aliquots at -20 ^{o}C

2.4.2. Glycerol Stocks for Storage of Bacteria

For long term storage, the bacterial cell lines containing the expression plasmids were stored as glycerol stocks at -70^{o}C. Cells were grown overnight in LB media with appropriate antibiotics at 30^{o}C with shaking (200 rpm). In a sterile cryovial, glycerol was added to the overnight cultures to 15 % v/v. The solution was thoroughly mixed, avoiding formation of any air bubbles, and submerged in liquid nitrogen for 2 minutes before storage at -70^{o}C.

2.4.3 Primer Design and Synthesis

In this thesis, primers were used for mutagenesis, cloning into bacterial expression vectors and sequencing. The critical elements to consider when designing primers are;

1. Primer length: between 18 to 30 bases
2. GC content: between 45 to 60 %
3. Complementary primer sequences: avoid inter-primer homology to prevent primer dimer formation
   : avoid intra-primer homology beyond 3 base pairs to prevent loop formation
4. Avoid PolyG and PolyC stretches to prevent non-specific annealing
5. Avoid PolyA and PolyT as these can lower the efficiency of amplification
6. Melting temperature: the primer pairs should have similar melting temperature.
   : the following equation was used to calculate the melting temperature

   $$Tm = 59.9 + 0.41 (\%G+C) – 675/length \qquad \text{Eqn 2.3}$$

   : the above formula can be used under standard PCR conditions where the Na^{+} or K^{+} concentration is 50 mM.
7. The 3’ terminals were designed to be a G or C residue as this provides a “GC clamp” which helps to ensure correct binding at the 3’ end due to stronger hydrogen bonding of G/C residues. This was not possible for all the primers used in this thesis but maximum effort was made to meet this requirement.

All primers used in this thesis were commercially synthesised by GeneWorks Pty Ltd (Adelaide, SA) and were desalted following production on a 40 nmole scale.

2.4.4 Polymerase Chain Reaction

The polymerase chain reaction (PCR) is an extremely useful molecular biology technique. It allows amplification of specific regions of a DNA strand from a very small amount of DNA *in vitro*.

PCR was cycled 20-40 times through a three-step process of denaturaion, annealing and extension. In the first step, denaturation, was performed at 94^{o}C. During this step, the hydrogen bonds that connect the two template DNA strands are broken. In the second step, annealing is usually performed at 55^{o}C. This temperature depends on the melting temperature of the primers. The annealing process allows the primers to pair with their complementary sequences on the template DNA. Lastly, DNA is synthesised during the extension step at 72^{o}C. Taq polymerase extends optimally at 72^{o}C. A sample program is outlined in Table 2.4.

Table 2.4 Basic thermal cycling program for PCR amplification. ^ The annealing temperature depended on the melting temperature (TM) of the primers. * The initial denaturation time depended on the type of DNA polymerase used.

STEP	TEMPERATURE	TIME	NUMBER OF CYCLES
Initial denaturation	94^{o}C	45 sec – 10 min*	1 cycle
Denaturation	94^{o}C	30 seconds	20 – 40 cycles
Annealing	55^{o}C – 68^{o}C^	30 seconds	
Extension	72^{o}C	2 -5 minutes	
Final extension	72^{o}C	5 – 7 minutes	1 cycle
Soak	4^{o}C	indefinite	

The components required for PCR are outlined in Table 2.5. The components are: template DNA, a synthetic primer pair, thermostable DNA polymerase, the four deoxyribonucleotides (dNTP), $MgCl_2$, a reaction buffer and nuclease-free water. Nuclease-free water was prepared by autoclaving distilled (MilliQ) water at 1.5 kgf/cm^2 for 20 minutes at 121^{o}C. The PCR reaction was set up as outlined in Table 2.4 in a sterile 0.5 mL microcentrifuge tube. The PCR cycles were controlled using a GeneAmp PCR System 9700 machine (P.E. Applied Biosystems). A mineral oil overlay, used to prevent evaporation, was not necessary when using this system as it has a heated lid.

Table 2.5 Reaction volumes and final concentrations for PCR reactions.

COMPONENT	VOLUME	FINAL CONCENTRATION
$MgCl_2$ (25 mM)	3 μL	1.5 mM
10 × reaction buffer (500 mM KCl, 100 mM Tris-HCl pH 9.0, 1.0% Triton® X-100)	5 μL	1 ×
dNTP mix (10 mM each)	2 μL	400 μM each
Forward primer (100 ng/μL)	1 μL	2 μM
Reverse primer (100 ng/μL)	1 μL	2 μM
DNA polymerase (5 U/μL)	0.5 μL	2.5 U
Template DNA	variable	< 0.5 μg
Nuclease free water to a final volume of	50 μL	

2.4.5 Polymerase Chain Reaction Optimisation

Since PCR is very sensitive, it is crucial to obtain optimal conditions that take into account both specificity and yield. The optimal conditions were achieved by manipulating several factors. Decreasing the concentration of $MgCl_2$ or DNA polymerase reduces non-specific amplification but decreases product yield. Likewise, decreasing the number of cycles and/or increasing the annealing temperature increases specificity but may decrease product yield.

The annealing temperature depends on the melting temperature (Tm) of the primers, which then depends on its length and content. Generally, the annealing temperature was 5^oC less than the calculated Tm of the primers. However, by starting with a higher annealing temperature and reducing it after a number of cycles, formation of non-specific products could be reduced without a great reduction in yield.

The length of extension depends on the length of the target sequence. The longer the target sequence, the more time required to synthesise it.

Specific optimised PCR protocols are included in the relevant sections.

2.4.6 DNA Sequencing

DNA sequencing and analysis of plasmids was performed on an ABI PRISM 3730 automatic sequencer by the Sydney University and Prince Alfred Hospital Macromolecular Analysis Centre (SUPAMAC, N.S.W). Prior to sequencing, plasmids were purified from cell lines using the Midi QLA-filter plasmid kit (QIAGEN) according to the manufacturer's instructions. Following the purification, the

concentrations of the purified plasmids were determined by UV spectrophotometry as described in Section 2.1.4.

2.4.7 Concentration of DNA Samples

DNA samples with concentrations less than 0.15 mg/mL were concentrated for convenience. Firstly, DNA was mixed with 1/10 volume of 3 M sodium acetate, pH 5.2, and then 2.5 volume (calculated after salt addition) of ice-cold 100 % ethanol was added. After leaving the mixture at room temperature for 30 minutes, it was centrifuged at maximum speed (14,500 rpm) for 20 minutes. The supernatant was discarded and the pellet was washed with 1 mL of room temperature 70 % ethanol to remove salts and small organic molecules. The mixture was then centrifuged again at a maximum speed (14,500 rpm) for 5 minutes. The supernatant was discarded and the pellet was dried in a heat block at 90^{o}C for 1 minute. Lastly, the dried pellet was dissolved in TE buffer to be stored indefinitely. TE buffer contains 10 mM Tris-HCl, pH 7.5 and 1 mM EDTA.

2.4.8 Concentration of protein Samples

Protein was concentrated using commercially available Amicon Ultra-15 Centrifugal Filter Units from Millipore (North Ryde, NSW). The unit concentrates the protein by using a filtration membrane to separate molecules of different molecular weights. The unit containing the protein to be concentrated was centrifuged in a fixed angle rotor at 5000 x g. The time of centrifugation was dependent on the volume and molecular weight of the protein. This was determined by using the graph in Figure 2.6.

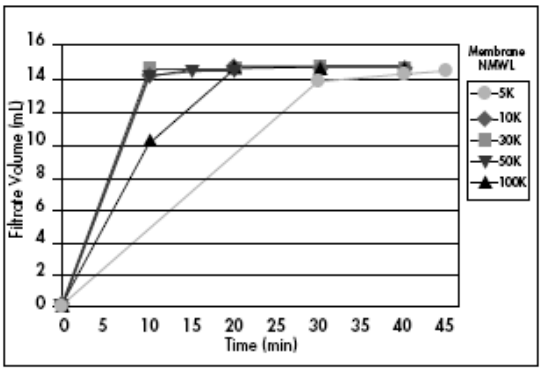

Figure 2.6. Centrifugation times for protein concentration.
(http://www.millipore.com/userguides.nsf/docs/pr01780)

2.5 Chromatography

Proteins expressed in bacteria were purified using ion exchange.

2.5.1 Ion Exchange Chromatography

Ion exchange chromatography separates proteins based on their molecular surface charge. This type of chromatography is further subdivided into two types;

1) cation exchange chromatography: positively charged ions bind to a negatively charged resin
2) anion exchange chromatography: negatively charged ions bind to a positively charged resin

Once the proteins are bound, they are eluted using a gradient of buffer that steadily increases the ionic strength of the buffer. Thus, the various proteins that have bound to the resin will be progressively eluted, from the least strongly bound to the most strongly bound proteins. The eluted proteins are collected as individual fractions and analysed separately. In this thesis, SP-Sepharose, a cation exchange chromatography media, was used to purify C1-L and its FHC mutants using BioLogic LP chromatography system (Bio-Rad).

Chapter 3

Cloning of C1-L of cMyBP-C and its FHC Mutants

Chapter 3

Cloning of C1-L of cMyBP-C and its FHC Mutants

3.1 Introduction

There are many advantages in expressing proteins *in vitro*. These include: high protein yield, ability to generate pure samples, relatively rapid production, inexpensive and the most relevant aspect to this thesis is the ease of manipulation of the gene sequence. The expression of recombinant protein has allowed the preparation of smaller domains or fragments of functional regions of large proteins for subsequent analysis. This is particularly useful in preparation of protein for structural and functional analyses as there is often an upper limit on the size that can be studied (e.g. for NMR). Furthermore, smaller proteins have fewer folding complications and are expressed more easily.

This chapter describes the preparation of a fragment of cMyBP-C, C1-L and its FHC mutants using a recombinant technology. C1-L is composed of one IgI domain (C1) joined by a 100 amino acid linker (L). This region is known to contain the phosphorylation sites, hence playing an important role in the regulation of cardiac muscle contraction. Previously, in this laboratory and in others (Oakley, Hambly et al. 2004), the entire C1-C2 region has been cloned, expressed and functionally characterised. Therefore, comparison of structural and functional analyses of C1-C2 and C1-L will also form part of this thesis. Additionally, C1-L contains a number of residues which, when mutated, have been linked to familial hypertrophic cardiomyopathy (FHC). These point mutations are listed in Table 3.1 with the phenotypes associated with each mutation (Oakley, Hambly et al. 2004). Once the

samples had been prepared, attempts were made to assess their structural and functional properties and these are described in the remainder of this thesis.

The vector used for the protein expression of all the samples in this thesis was a pET3a vector (Novagen). The pET vector system is one of the most powerful systems developed for cloning and expression of recombinant proteins in *E. coli*. The vectors are called pET for 'Plasmid for Expression by T7 RNA polymerase' and as the name suggests, pET vectors use T7 RNA polymerase to direct expression of cloned genes and this expression is controlled by a strong bacteriophage T7 promoter. T7 RNA polymerase is very specific for T7 promoters and it does no recognise DNA from other sources as these promoter sequences are very rare. Also, termination signals for T7 RNA polymerase are rare, hence long transcripts can be made without premature truncation. The pET-3a vectors are translation vectors (Figure 3.1), that is, they contain a highly efficient ribosome binding site from the phage T7 major capsid protein and are used for the expression of target genes without their own ribosomal binding site. This vector has an ampicillin resistant gene and the vector does not incorporate a His-tag into the cloned sequence. The latter is of particular importance as extra amino acids can affect the folding, binding and function of native proteins.

In order for the pET vector system to work, a source of T7 RNA polymerase must be supplied to the cells and in this project, *E. coli* strain BL21(DE3)pLysS has been used. The BL21(DE3) hosts are lysogenic for a fragment of the phage DE3 and this fragment contains the lacI gene, the lac UV5 promoter, the start of lacZ (β-galactosidase) and the T7 RNA polymerase gene. The lac UV5 promoter is responsible for driving the expression of T7 RNA polymerase and this is inducible by adding IPTG (isopropyl-β-D-thiogalactoside). BL21(DE3)pLysS contains pLysS plasmid, which contains the gene encoding T7 lysozyme. T7 lysozyme minimises the background expression level of target genes under the control of the T7 promoter but does not interfere with the level of expression achieved following induction with IPTG. Another advantage of using *E. coli* strain BL21(DE3) is that these strains do not contain the *lon* protease and are also deficient in the outer membrane protease, OmpT. The lack of these two key proteases reduces degradation of heterologous proteins expressed in the strains.

Table 3.1. Summary of FHC point mutations in cMyBPC. Table from (Oakley, Hambly et al. 2004)

Region (Motif)	Mutation	Phenotype	Reference
C0	$Thr^{59}Ala$	Mild, elderly onset	(Niimura, Patton et al. 2002)
C1	$Asp^{228}Asn$	Rare form of midventricular hypertrophy	(Andersen, Havndrup et al. 2001)
C1	$Tyr^{237}Ser$	Mild hypertrophy	(Morner, Richard et al. 2003)
C1 or Linker 1-2	$His^{257}Pro$	No specific information	(Richard, Charron et al. 2003)
C1 or Linker 1-2	$Glu^{258}Lys$	Delayed onset	(Niimura, Bachinski et al. 1998, Nanni, Pieroni et al. 2003, Girolami, Olivotto et al. 2006)
Linker 1-2	$Gly^{278}Glu$	No specific information	(Richard, Charron et al. 2003)
Linker 1-2	$Gly^{279}Ala$	No specific information	(Richard, Charron et al. 2003)
Linker 1-2	$Arg^{326}Gln$	Elderly onset. Also seen in healthy controls (Jaaskelainen, Kuusisto et al. 2002, Niimura, Patton et al. 2002)	(Maron, Niimura et al. 2001, Daehmlow, Erdmann et al. 2002, Morner, Richard et al. 2003)
Linker 1-2	$Leu^{352}Pro$	No specific information	(Richard, Charron et al. 2003)
C2	$Glu^{451}Gln$	Delayed onset, incomplete penetrance, long life expectancy	(Niimura, Bachinski et al. 1998)
C3	$Arg^{495}Gln$	Delayed onset, incomplete penetrance, long life expectancy	(Niimura, Bachinski et al. 1998, Maron, Niimura et al. 2001)
C3	$Arg^{502}Gln$ $Arg^{502}Trp$	Delayed onset, incomplete penetrance, long life expectancy	(Niimura, Bachinski et al. 1998, Richard, Charron et al. 2003)
C5	$Arg^{654}His$	Mild hypertrophy, elderly onset	(Moolman-Smook, Mayosi et al. 1998)
C5	$Arg^{668}His$	Early onset, one instance of sudden death	(Morner, Richard et al. 2003)
C5	$Asn^{755}Lys$	Severe	(Yu, French et al. 1998)
C6	$Arg^{810}His$	Mild	(Nanni, Pieroni et al. 2003)
C6	$Lys^{811}Arg$	No specific information	(Richard, Charron et al. 2003)
C6	$Arg^{820}Gln$	Burnt out phase in elderly left ventricular dysfunction/dilation	(Konno, Shimizu et al. 2003, Nanni, Pieroni et al. 2003)
C6	$Ala^{833}Val$ $Ala^{833}Thr$	Mild hypertrophy, lacks definite proof of being disease causing	(Morner, Richard et al. 2003, Richard, Charron et al. 2003)
C7	$Pro^{873}His$	Mild / moderate	(Nanni, Pieroni et al. 2003)
C7	$Val^{896}Met$	May disease causing or modifying (Jaaskelainen, Kuusisto et al. 2002, Richard, Charron et al. 2003).	(Moolman-Smook, De Lange et al. 1999, Morner, Richard et al. 2003)
C7	$Asn^{948}Thr$	Dilated, severe	(Daehmlow, Erdmann et al. 2002)
C8	$Arg^{1002}Gln$	Mild, elderly onset	(Niimura, Patton et al. 2002)
C10	$Ala^{1194}Thr$	No specific information	(Richard, Charron et al. 2003)
C10	1253 insert GGIYVC	Early onset, one instance of sudden death	(Watkins, Conner et al. 1995)
C10	$Ala^{1255}Thr$	No specific information	(Richard, Charron et al. 2003)

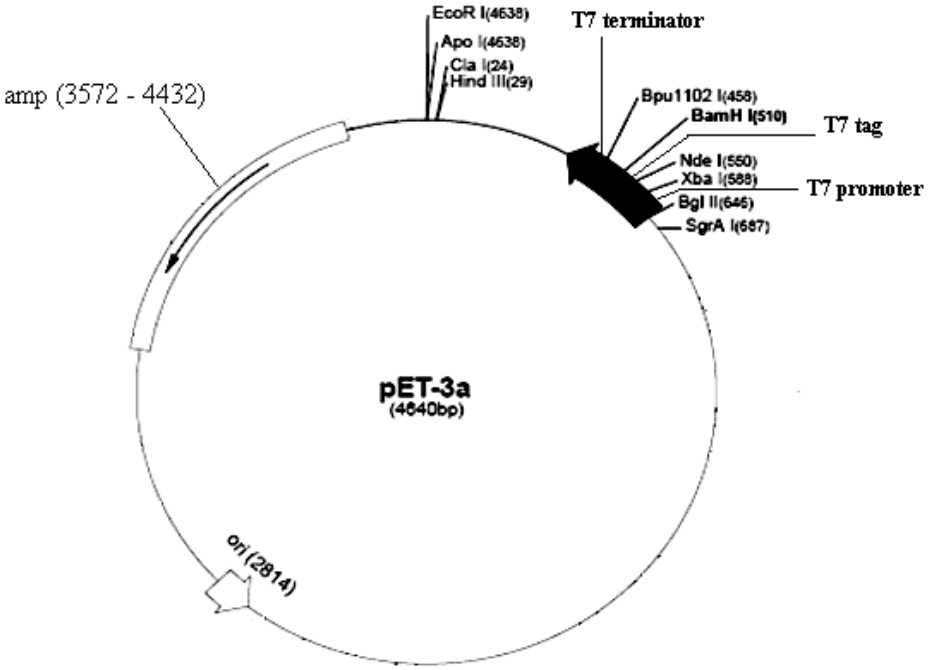

Figure 3.1. pET-3a expression vector. The location of the origin of replication (ori), ampicillin resistant gene marker (amp), T7 promoter (615-631), T7 tag coding sequence (519-551) and T7 terminator (404-450) are shown. The arrow indicates the direction of transcription.
Image modified from http://www.emdbiosciences.com/docs/docs/PROT/TB026.pdf

3.2 Materials and Methods

3.2.1 Gel Electrophoresis

The gel electrophoresis technique used in this chapter is described in Section 2.2. Agarose gels (1.0 – 2.0%) were used to analyse and purify DNA samples (Section 2.2.1). 12% discontinuous SDS-PAGE was used to locate the expressed protein and also to analyse the purity of expressed and purified proteins (Section 2.2.2). All the components of the electrophoresis are outlined in Table 2.2. For both methods, molecular weight markers were used to estimate the size of the samples of interest. A UVP GDS8000 gel documentation system was used to view the gels (Section 2.2.4) and Phoretix 1D Advanced Version 3.01 (Phoretix International) was used to estimate the molecular weight of expressed proteins.

3.2.2 Expression Vectors, Bacterial Strain and Enzymes

The expression vectors used for all cMyBP-C samples in this thesis was the pET-3a vector, purchased from Novagen.

Initial plasmid transformations of C1-L and its FHC mutants in pET-3a vector were carried out in *E.coli* strains DH5α™ - $T1^R$ (Invitrogen) and XL1-Blue supercompetent cells (Stratagene), respectively. For protein expression, BL21(DE3)pLysS competent cells (Promega) were used for all the samples.

DNA polymerases *PfuUltra* HF DNA polymerase and *Taq* DNA polymerase with their 10x reaction buffers were purchased from Stratagene and Invitrogen, respectively. DNA methylase with 10 x methylation buffer, T4 DNA ligase with 10 x ligase were purchased from Invitrogen. The restriction enzymes NcoI and Dpn I with their 10 x digestion buffers were purchased from Roche and Strategene, respectively. All media and agar plates were prepared as described in Section 2.4.1. All other chemicals were of analytical grade.

3.2.3 Preparation of plasmid C1-L

3.2.3.1 Selection of Module Boundaries for C1-L

cMyBP-C has been predicted to contain a series of domains which are homologous to IgI and FnIII motifs (Einheber and Fischman 1990, Weber, Vaughan et al. 1993). The protein of interest in this thesis, C1-L, contains the IgI domain C1 and then a 100 amino acid linker. The appropriate boundary for C1-L was selected from a previous analysis of the published sequence of human cMyBP-C (Oakley, Hambly et al. 2004) and was found to be from Pro^{152} to Asp^{358} . However, the final C1-L construct was N and C- terminally extended, as part of the C4-C5 linker was shown to be integral to the IgI fold of C5 (Idowu, Gautel et al. 2003). Therefore, the C1-L was boundaries were from Thr ^{145} to Lys ^{361}.

3.2.3.2 cMyBP-C DNA Template

C1-linker-C2 (C1-C2) DNA template in pET-3a vector was produced by Dr Cecily Oakley (Department of Pathology, University of Sydney) and this template was used to produce C1-linker (C1-L).

3.2.3.3 Site Directed Mutagenesis for C1-L

C1-L was prepared by inserting a stop codon (TGA) at the end of the linker in the C1-C2 construct. A commercially available kit, GeneTailor™ Site-Directed

Mutagenesis System (Invitrogen), was used to prepare C1-L and the method used was as recommended by the manufacturer.

Prior to mutagenesis, C1-C2 plasmid was methylated for 1 hour at 37^{o}C where DNA methylase methylates cytosine residues within a specific sequence throughout the double-stranded DNA. Then, mutagenesis was performed with the methylated plasmid, the forward and reverse mutagenic primers (Table 3.2) and *Taq* polymerase. During this process, it was important to ensure that the primer concentration was always in excess of the template, i.e. the methylated plasmid. The primers (Table 3.2) were designed as described in Section 2.4.3 with some additional specifications:

1. primers had an overlapping region at the 5' ends of 15-20 nucleotides for efficient end-joining of the mutagenesis product
2. the mutation site was located on only one of the primers, downstream from and adjacent to the overlapping region
3. on the mutagenic primer, at least 10 nucleotides downstream of the mutation site was ensured for efficient annealing

An example of primer design is illustrated in Figure 3.2.

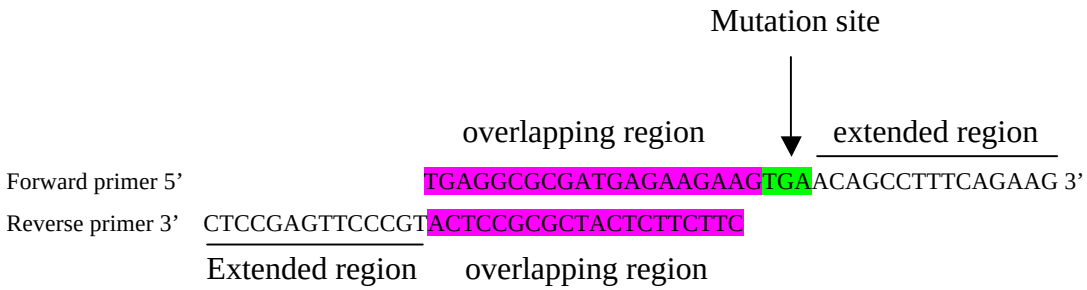

Figure 3.2. Primer design of C1L. Adequate overlapping and extended regions were incorporated to ensure optimal mutagenesis.

A single PCR cycle was used and this is shown in Table 3.3.

One of the advantages of using this kit was that there was no need for an *in vitro* digestion step after the mutagenesis reaction to get rid of the methylated DNA template. Instead, the DH5α™ - T1^{R} cells used during transformation and immediately after the mutagenesis reaction, had an inherent *Mcr*BC endonuclease that digests the methylated template DNA, leaving only the unmethylated mutated product.

A mutagenesis control was also performed to test the mutagenesis efficiency. The control plasmid (3.4 kb) contains the *lac*Zα gene, whose wild type produces blue colonies on plates containing LB + ampicillin (100 μg/ml) + X-gal (400 μg/ml). However upon mutagenesis, a *Hind* III site and stop codon within the *lac*Zα gene is produced, hence the stop codon generates a truncated LacZα protein which produces white colonies on plates containing X-gal. Finally, the mutagenesis efficiency (ME) for the control plasmid was calculated using the following formula:

$$ME = \frac{\text{number of white colony forming units}}{\text{total number of colony forming units}} \times 100\ \%$$

Lastly, the mutated C1-L DNA was concentrated as described in Section 2.4.7.

Table 3.2. Primers for C1-L mutagenesis and sequencing into pET-3a vector.

Primer	Sequence (5' → 3')
C1-L forward	TGAGGCGCGATGAGAAGAAG**TGA**ACAGCCTTTCAGAAG
C1-L reverse	CTTCTTCTCATCGCGCCTCATGCCCTTGAGCCTC
Forward sequencing	TAATACGACTCACTATAGGG
Reverse sequencing	GCTAGTTATTGCTCAGCGG

Table 3.3. PCR cycle for C1-L mutagenesis.

STEP	TEMPERATURE	TIME	NUMBER OF CYCLES
Initial denaturation	94^{o}C	2 min	1 cycle
Denaturation	94^{o}C	30 seconds	20 cycles
Annealing	55^{o}C	30 seconds	
Extension	68^{o}C	5 minutes	
Final extension	68^{o}C	10 minutes	1 cycle
Soak	4^{o}C	indefinite	

3.2.3.4 Detecting the Presence of the Insert: Restriction Enzyme Digest

Restriction digestion was carried out by adding 500 ng DNA with the appropriate restriction enzyme and its buffer. The final volume was made up to 20 μL

using autoclaved ddH_2O. The mixture was gently mixed using a pipette and incubated at 37^oC for 1.5 hours. The samples were analysed on a 1% agarose gel.

An appropriate restriction enzyme is one that cuts the prepared DNA but does not cut the vector. A list of restriction enzymes that cut the pET-3a vector was obtained from their manufacturer. A list of restriction enzymes that cut C1-L was obtained by using online software program RestrictionMapper version3 (http://www.restrictionmapper.org/).

C1-L was digested with NcoI. It cuts the sequence CCATGG at its 5' end. It cuts C1-L at position 344 once.

3.2.3.5 Plasmid Constructs Sequencing

The DNA sequence for C1-L was confirmed as described in Section 2.4.6. Two sequencing reactions were performed for each plasmid, forward and reverse, using the sequencing primers for pET3a vector (Table 3.2). Once the mutagenesis had been confirmed by sequencing, the C1-L plasmid was transformed into suitable competent cells for protein expression as described in Section 3.2.5.1 and glycerol stocks were also prepared according to the method in Section 2.4.2.

3.2.4 Preparation of plasmid C1-L FHC mutants

Six FHC mutants were created based on disease causing missense mutations present in human cMyBP-C (Table 3.1).

3.2.4.1 Primers

FHC mutagenic primers were designed with the aid of an online software program, http://labtools.strategene.com/QC specifically for use in the QuickChange II Site-Directed mutagenesis kit (Strategene). The aspects considered were:

1. forward and reverse primers were made complementary and contained the desired mutation
2. the mutation was in the middle of the primer, flanked by 10 -17 bases of homologous sequence
3. All FHC mutant primers were designed to have a melting temperature (Tm) of 78^oC – 80^oC so that mutagenesis reactions could proceed in parallel

The FHC mutagenic primers are listed in Table 3.4.

Table 3.4. FHC mutagenic primers. The codons in blue indicate the mutations. The reverse primers were the reverse-complementary sequence of the forward primers.

FHC Mutation	Primer	Sequence
$Asp^{228}Asn$	Forward	GCTGCACATCACC**AAT**GCCCAGCCTG
$His^{257}Pro$	Forward	CTTCAATCTCACTGTC**CCT**GAGGCCATGGGCAC
$Gly^{278}Glu$	Forward	CGAGCCTGGCT**GAA**GGTGGTCGGCG
$Gly^{279}Ala$	Forward	CCTGGCTGGA**GCT**GGTCGGCGGA
$Arg^{326}Gln$	Forward	GTGGGAGATCCTA**CAG**CAGGCACCCCC
$Leu^{352}Pro$	Forward	GCATGCTAAAGAGG**CCC**AAGGGCATGAGG

3.2.4.2 PCR Mutagenesis

C1-L FHC mutants were prepared by mutagenesis using a QuickChangeII Site-Directed Mutagenesis Kit (Strategene), according to the manufacturer's instructions. Each C1-L FHC mutant PCR reaction consisted of: template DNA (30 ng of C1-L plasmid in pET3a vector), 125 ng of forward and 125 ng reverse primers (Table 3.4), dNTP mix, 10x reaction buffer and 2.5 units of *PfuUltra* HF DNA polymerase (Stratagene). For the PCR mixtures, it was important to ensure that the primer concentration was always in excess of the template. The PCR protocol used is outlined in Table 3.3. This cycle produced a mutated plasmid containing staggered nicks and the extension time (1 minute/kb of plasmid length) was lengthy in order to ensure that the whole plasmid was synthesised.

Once the PCR cycle was complete, the supercoiled plasmid was then digested with 10 units of a restriction enzyme called *Dpn* I for 60 minutes at 37^{o}C. This step digests methylated DNA and ensures the template DNA (which does not contain the mutation) is digested and the mutated plasmid (which is not methylated) remains intact to be transformed.

A mutagenesis control was also performed to test the mutagenesis efficiency. The control plasmid (pWhitescript 4.5 kb) contained a stop codon in the ß-galactosidase gene that converts the stop codon into a glutamine codon. Consequently, the control plasmid produced blue colonies on IPTG and X-gal supplemented plates and the mutagenesis efficiency (ME) was calculated by the following formula:

$$ME = \frac{\text{number of blue colony forming units (}cfu\text{)}}{\text{total number of colony forming units (}cfu\text{)}} \times 100\ \%$$

3.2.4.3 Transformation of FHC mutants

Upon completion of PCR cycle and restriction enzyme digestion of C1-L mutant plasmids, they were transformed into XL1-Blue supercompetent cells (Strategene) according to the method described in Section 3.2.5.1.

Single colonies obtained from this transformation step were used for plasmid purification (Promega), which were then used for plasmid sequencing (Section 3.2.4.2)

3.2.4.4 Sequencing of FHC mutants

The DNA sequence for C1-L FHC mutants was confirmed as described in Section 2.4.6. For all mutants, two sequencing reactions were performed for each plasmid, forward and reverse, using the sequencing primers for pET3a vector (Table 3.2). Once the mutagenesis had been confirmed by sequencing, the plasmids were transformed into suitable competent cells for protein expression as described in Section 3.2.5.1 and glycerol stocks were also prepared according to the method in Section 2.4.2.

3.2.5 Protein Expression and Purification of C1-L and its FHC mutants

3.2.5.1 Transformation of Plasmid Constructs into Host Cell Lines

Once the desired DNA fragments have been inserted into appropriate vectors, the plasmid constructs were transformed into *E. coli* competent BL21(DE3)pLysS (Promega) strain for protein expression.

Competent cells were thawed on ice and gently mixed by flicking the tube. Then either 1-50 ng of DNA or 1 µL of competent cell control DNA was added to 100 µL of competent cells. The mixture was mixed by gently flicking the tube several times and was incubated on ice for 10 minutes. To facilitate the uptake of plasmid DNA, the mixture was heat shocked at exactly 42^{o}C for 45 seconds (without shaking) and incubated on ice for another 2 minutes. 900 µL of cold (4^{o}C) SOC medium (Table 2.3) was then added to the transformation reaction and incubated at 37^{o}C for 60 minutes with shaking (225 rpm). Upon completion, the transformation reaction was plated on LB agar plates with ampicillin (50 µg/mL) and incubated overnight at 37^{o}C.

Different transformation volumes were plated to ensure well spaced colonies on at least one plate.

When working with competent cells, extreme care should be taken as these cells are highly sensitive to changes in temperature and mechanical lysis caused by pipetting. Hence, transformation should be started immediately after thawing the cells on ice and the reaction should be mixed by swirling or tapping the tube gently, not by pipetting.

3.2.5.2 Growth Media and Chemicals

Luria-Bertani (LB) broth and terrific broth powder (TB) were purchased from Sigma Aldrich and Mo Bio Laboratories, respectively. Isopropyl-β-D-thiogalactoside (IPTG) was purchased from Promega. SP-Sepharose resin for cation exchange chromatography was purchased from Pharmacia Biotech and a BioLogic LP chromatography system from Bio-Rad was used for chromatography. All other chemicals used were of analytical grade.

3.2.5.3 Protein Expression

A flamed wire loop was allowed to cool and a loop-full of glycerol stock was inoculated into 10 mL of LB broth with ampicillin (50 μg/mL) and chloramphenicol (34 μg/mL). This starter culture was grown to saturation (overnight) with shaking (250 rpm) at 37^{o}C. The overnight culture was then diluted into 500 mL of pre-warmed LB broth without any antibiotics in a 2L conical flask. This mixture was grown at 37^{o}C with shaking (200 rpm) until the optical density at 600 nm reached an absorbance of 0.1 cm^{-1}. Once the appropriate OD_{600} value has been reached, protein expression from the *lac* promoter/T7 RNA polymerase promoter was induced by adding 1 mM IPTG. The culture was grown for another 4 to 5 hours at room temperature with shaking (200 rpm). Finally the cells were harvested by centrifugation at 6,000 rpm for 10 minutes at 4^{o}C and stored at -20^{o}C. Samples were taken from before and after induction and analysed by SDS-PAGE electrophoresis. Additionally, a time course after induction was performed. The samples were analysed by SDS-PAGE electrophoresis to determine the optimal time for induction and protein expression.

3.2.5.4 Protein Location

The first step in purification of a recombinant protein from bacteria is to determine the location within the bacteria where the protein of interest is being expressed, that is, within the cytoplasm or within insoluble inclusion bodies. 1 mL of cells in LB broth was grown for 4 hours after induction, and then was centrifuged at 6,000 rpm at 4^{o}C for 10 minutes. The cell pellet was resuspended in 10 mL/g lysis buffer (300 mM NaCl, 20 mM Tris-HCl, pH 7.0), followed by sonication for 3 x 10 second bursts at 10 watts and then left on ice for 30 minutes. The mixture (lysate) was again centrifuged at 8,500 rpm at 4^{o}C for 30 minutes. The pellet was dissolved in 1 mL of 8 M urea, 20 mM Tris-HCl, pH 7.0. Both soluble fraction (supernatant) and insoluble fraction (pellet) were analysed by SDS-PAGE electrophoresis.

3.2.5.5 Cell Lysis and Cytoplasm Purification

In this project, adequate amounts of C1-L and its FHC mutant proteins were present in the cytoplasm for it to be used for purification.

The bacterial pellet containing the protein of interest in the cytoplasm was thawed and resuspended (10mL/1g of pellet) in buffer A (40 mM NaCl, 1 mM EDTA, 1 mM DTT, 20 mM Tris-HCl, pH 7.0). The mixture was sonicated for 3 x 10 second pulses and incubated on ice for about 30 mins. It was then centrifuged at 8,500 rpm for 30 minutes at 4^{o}C. The resulting supernatant contains the soluble protein and was therefore applied directly onto an appropriate column to be purified, in this case, SP-Sepharose cation exchange chromatography with approximately 30 mL in column size.

Once the lysed total cell protein was bound, it was eluted using a gradient of buffer that steadily increases the ionic strength of from 40 mM to 200 mM NaCl. The buffers used to achieve the optimal gradient were:

Buffer A: 40 mM NaCl, 1 mM EDTA, 1 mM DTT, 20 mM Tris-HCl, pH 7.0

Buffer B: 200 mM NaCl, 1 mM EDTA, 1 mM DTT, 20 mM Tris-HCl, pH 7.0

The protocol used for BioLogic LP chromatography system (Bio-Rad) varied according to the sample size but the typical protocol used is outlined in Table 3.5. The eluted proteins were collected as individual fractions for analysis by SDS-PAGE electrophoresis. Once the program was complete, the column was washed with a high salt concentration (1M NaCl) buffer to elute any proteins that were still adhering to

the column. These fraction/s were also collected for analysis. Finally, all the fractions collected were analysed by 12% SDS-PAGE electrophoresis.

Table 3.5. Method for C1-L purification.

Volume (mL)	Buffer	mL/min
0.00 to 70.00	Buffer A	2.00
70.00 to 250.00	0 – 100 % Buffer B	2.00
250.00 to 300.00	Buffer B	2.00

3.2.5.6 Mass Spectrometry

The presence of C1-L protein was confirmed by using Matrix-Assisted Laser Desorption/Ionisation Time-Of-Flight Mass Spectrometry (MALDI-TOF MS). Mass spectrometry reports both the mass and mass to charge ratios of peptides. This work was done in collaboration with Mr Alistair Edwards (Australian Proteome Analysis Facility, Cordwell Laboratory, Departments of Biochemistry and Pathology, University of Sydney).

The SDS-PAGE gel band corresponding to the approximate molecular weight of C1-L (24,000 Da) was excised and stored in ddH_2O until ready to be used. The excised band was destained with 25 µL wash buffer (40% acetonitrile, 30 mM NH_4HCO_3) for one hour and dried by vacuum centrifugation for 30 minutes. The dried band was then rehydrated in 12 µL 50 mM NH_4HCO_3 buffer with sequencing grade trypsin (12 ng/µL) for one hour at 4^oC, and excess trypsin-NH_4HCO_3 buffer was removed. Digestion was continued by adding 15 µL 50 mM NH_4HCO_3 and incubating at 37^oC overnight.

Peptides were concentrated and desalted by using C_{18} Zip-Tips (Millipore) and the method used was as recommended by the manufacturer. The peptides were analysed by MALDI-TOF MS and the peptide mass map was created using an ABI QSTAR mass spectrometer (Applied Biosystems). The result was confirmed by comparing it with predicted tryptic masses based on the simulated digest of the protein. The simulated digest was performed using the online software, PeptideMass (http://ca.expasy.org/tools/peptide-mass.html). This program displayed monoisotopic masses greater than 500 Da and allows for one missed cleavage.

3.3 Results

3.3.1 Preparation of C1-L and its FHC Mutants

3.3.1.1 C1-L and its FHC mutatagenic plasmids in pET-3a Vector

C1-L was generated using site-directed mutagenesis to insert a stop codon at the end of the C1-C2 fragment and the mutagenesis efficiency calculated from its control was 99.7 % (calculation below).

$$ME = \frac{\text{number of white colony forming units}}{\text{total number of colony forming units}} \times 100\ \%$$

$$= \frac{300}{301} \times 100\ \%$$

$$= 99.7\ \%$$

From the plates acquired during transformation, several single colonies were selected for mini-plasmid preparations. The plasmid achieved from here was concentrated and was analysed by 1 % agarose gel (Figure 3.3). The size of C1-L in pET-3a vector was 5246 bp. As C1-L was in circular form, it did not migrate according to its mass but formed two distinct bands as shown in lanes 2, 4 and 5 in Figure 3.3. The top and bottom bands correspond to the nicked circles and supercoiled forms, respectively. A negative control was also performed to check for contamination (lane 3). Lastly lanes 4 and 5 show the concentrated C1-L.

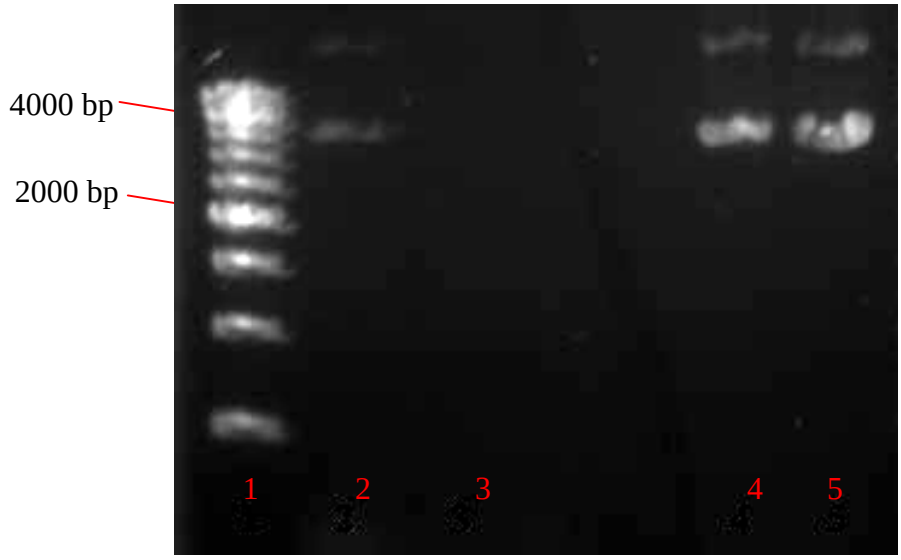

Figure 3.3 C1-L in pET-3a vector. Lane 1: molecular weight marker. Lane 2: C1-L in pET-3a vector before concentration. Lane 3: negative control. Lanes 4 and 5: C1-L in pET-3a vector after concentration.

C1-L FHC mutant plasmids were also generated as described in Section 3.2.4. The template used here was the correctly inserted C1-L in a pET3a vector and the mutagenesis efficiency calculated from mutagenesis control was 99.5% (calculation below).

$$ME = \frac{\text{number of blue colony forming units } (cfu)}{\text{total number of colony forming units } (cfu)} \times 100\ \%$$

$$= \frac{430}{432} \times 100\%$$

$$= 99.5\%$$

3.3.1.2 Restriction Enzyme Digest of C1-L with NcoI

Restriction enzyme digest of C1-L plasmid with NcoI was performed to confirm the presence of C1-L in the pET-3a vector and the samples were run on 1% agarose gel (Figure 3.4). The undigested circular C1-L produced two bands, nicked circles and supercoiled (lane 1). However, when plasmid C1-L was digested with NcoI, there was a shift in the band to 5246 bp (the nicked and supercoiled forms ran as one linear form) (lane 2).

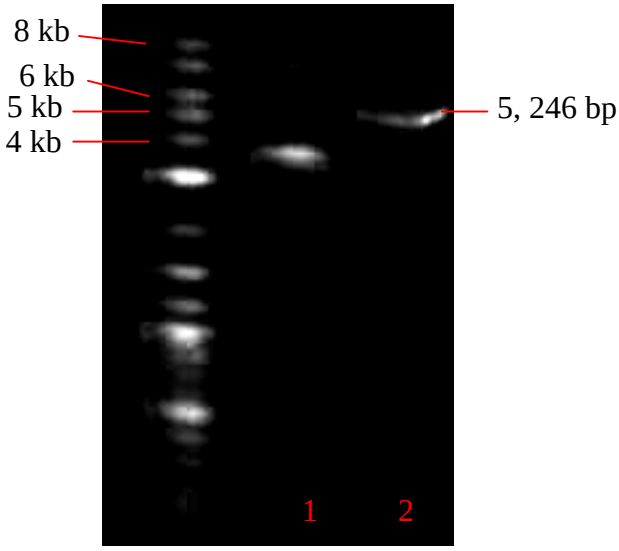

Figure 3.4 Restriction enzyme digest of C1-L with NcoI. Lane 1: undigested C1-L Lane 2: digested C1-L

3.3.1.3 C1-L and its FHC mutants: DNA Sequencing

The correct DNA sequence of C1-L and its FHC mutants was confirmed by the DNA sequencing method described in Section 2.4.6. The plasmids were prepared by selecting several single colonies from the plates acquired during transformation for mini-plasmid preparation. At the end of the analysis, an electrophoretogram was produced where each peak represents a single base. DNA sequencing for all the samples in this thesis was performed using both forward (Figure 3.5a) and reverse (Figure 3.5b) sequencing primers. Electrophoretograms generated from both analyses confirmed the correct sequence of C1-L and its FHC mutants. An example of electrophoretogram generated is shown in Figure 3.5.

ABI PRISM™ Model 3730
Version 3.3
KB.bcp
KB 1.2

a)

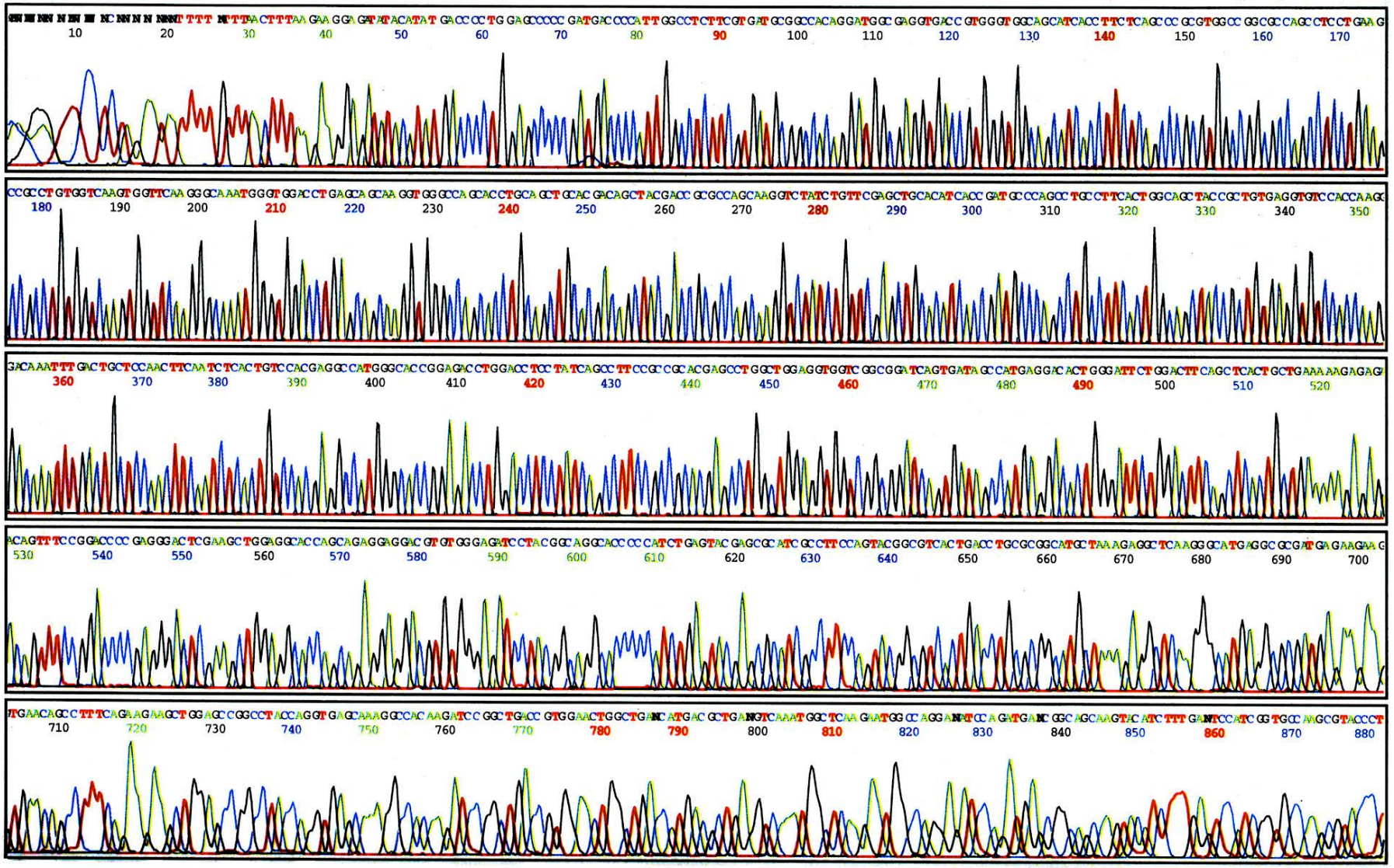

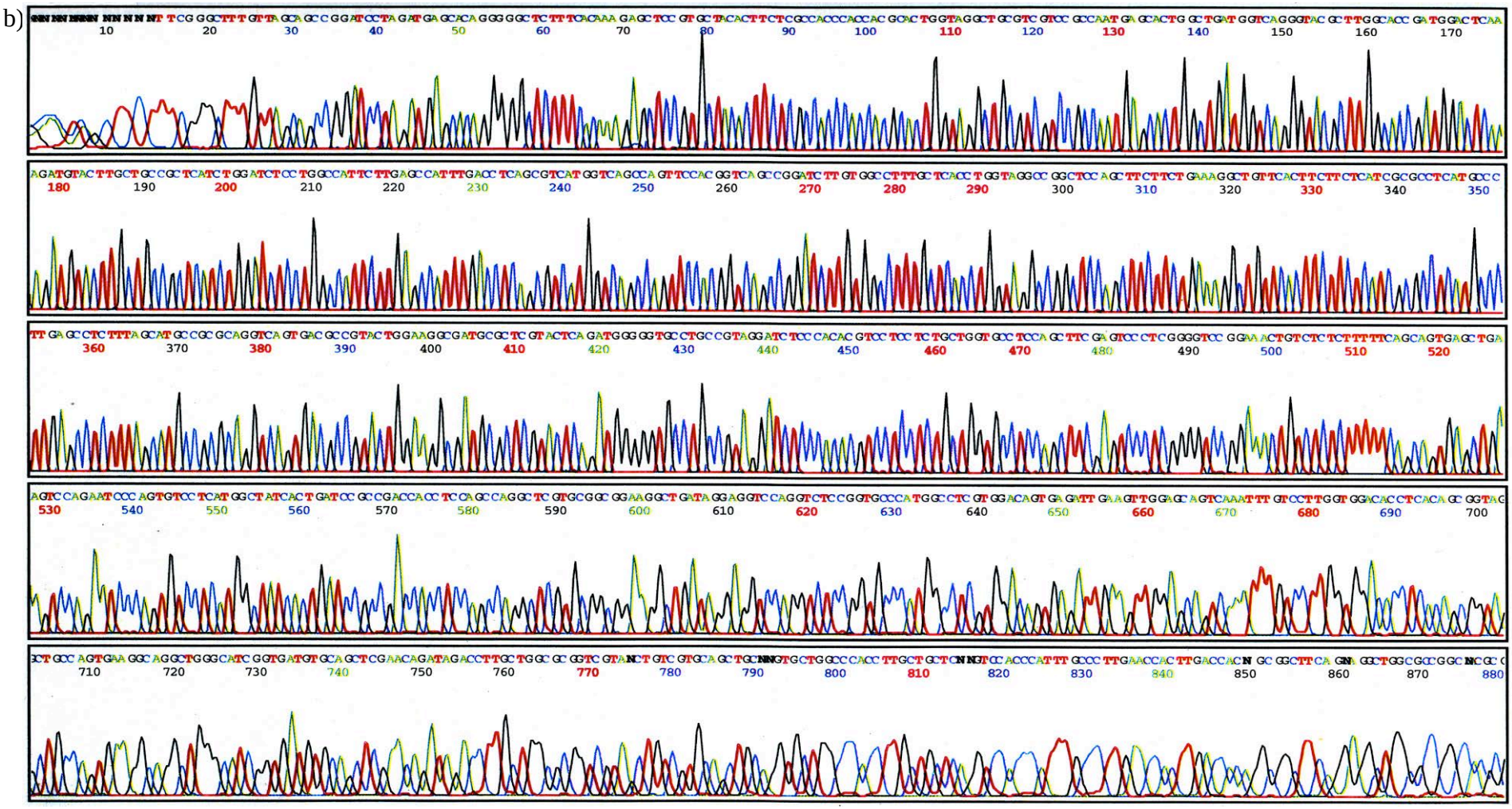

Figure 3.5 Electrophoretograms of C1-L with forward (a) and reverse (b) sequencing primers. Both have proven C1-L to consist of the correct sequence.

3.3.1.4 C1-L & its FHC Mutagenic Protein Expression and Location

Once the C1-L DNA sequence was confirmed, its protein was expressed according to the methods described in Section 3.2.5.3 using *E.coli* BL21(DE3)pLysS cells. The Optimisation of this method included a number of aspects:

1. Induction point

When C1-L protein was induced at OD_{600} = 3.0, i.e. at stationary phase, C1-L protein (24 kDa) was not expressed. On the contrary, C1-L protein was expressed when induced at both OD_{600} = 0.1 and 0.5 (mid log phase), although when induced at OD600 = 0.5, the protein of interest started to degrade faster. Furthermore, when the protein was grown overnight after induction, it resulted in degradation of the C1L protein. Therefore, the subsequent samples were induced at OD_{600} = 0.1 and grown for 3~4 hours. Figure 3.6 shows expression of C1-L protein at OD_{600} = 0.1, where C1-L was successfully expressed but started to degrade when left to grow overnight. Protein expression of C1-L FHC mutants yielded similar results.

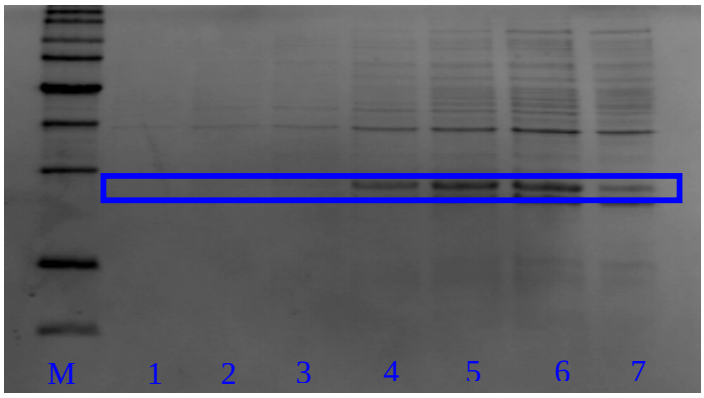

Figure 3.6. Expression of C1-L protein (Total Cell Protein). C1-L protein expression is presented in blue box. MW represents molecular weight marker. Lanes 1 to 7 corresponds to 0, 0.5, 1, 2, 3, 4 hours and overnight samples respectively after induction at OD_{600} = 0.1 with 1 mM IPTG at 37^{o}C.

2. Growth temperature

C1-L was left to grow at various temperatures: at room temperature (24^{o}C) and at 37^{o}C. Figure 3.7 shows that C1-L was capable of growing at both temperatures.

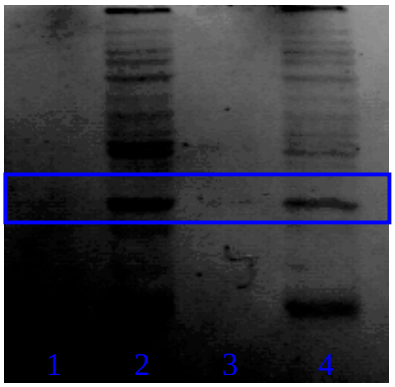

Figure 3.7. Expression of C1-L protein at various temperatures. Lanes 1 and 2 represent before and after induction at room temperature (24^{o}C) respectively. Lanes 3 and 4 represent before and after induction at 37^{o}C respectively. Protein of interest (C1-L) is highlighted in blue box.

3. Location of C1-L protein

An important issue for the expression of recombinant proteins in bacteria is the location of the accumulated expressed protein within the bacteria, either in the cytoplasm or within insoluble inclusion bodies. If the expressed protein is accumulated substantially within the cytoplasm, there is usually no need to use protein denaturants during purification, circumventing the need to consider the use of a re-folding strategy.

Prior to purification, the location of C1-L within the bacteria was determined as described in Section 3.2.5.4 and then the samples were analysed by 12 % SDS-PAGE electrophoresis. Figure 3.8 shows that when C1-L protein was grown at room temperature (24^{o}C), the majority of the protein was present in supernatant whereas at 37^{o}C, it was present in both supernatant and pellet.

Hence, the optimal growth condition for C1-L protein was for it to be induced at OD_{600} = 0.1, grown for 3 ~ 4 hours at room temperature (24^{o}C) and its supernatant (obtained after lysis) was used for purification

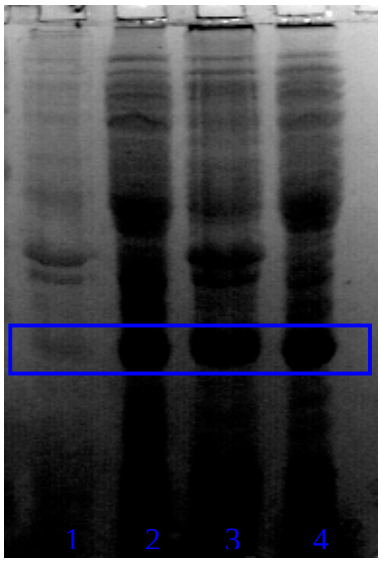

Figure 3.8. Location of C1-L Protein. Lanes 1 and 2 represent pellet and supernatant samples respectively grown at room temperature (24^{o}C). Lanes 3 and 4 represent pellet and supernatant samples respectively grown at 37^{o}C. Protein of interest (C1-L) is highlighted in blue box. Note that pellet contains the insoluble parts of the bacteria, mainly the insoluble inclusion bodies whereas the supernatant contains the soluble proteins from the cytoplasm.

Similarly, C1-L FHC mutagenic proteins were expressed using the same protocol as for C1-L protein. Its samples were analysed using 12% SDS-PAGE where it produced similar outcome to C1-L protein, i.e. all samples were shown to be expressed and were present in the soluble fraction in an adequate amount to be used for protein purification under the optimal condition described for C1-L protein.

3.3.1.5 C1-L & its FHC mutants: Protein Purification

C1-L and its FHC mutagenic proteins in the supernatant were purified using cation exchange chromatography as described in Section 3.2.5.1. Purification was done using BioLogic LP chromatography system (Bio-Rad) and this yielded a chromatogram consisting of two readings, conductivity and absorbance. Conductivity was measured to monitor the salt gradient and the unit used was milliSiemens per centimetre mS/cm where a Siemen is the standard unit for conductivity which is the reciprocal of resistance in electrical terms (1/Ohm). Absorbance was measured in optical density (OD). Figure 3.9a shows a typical chromatogram obtained during the purification. The first peak corresponds to the void peak and this contains part of the sample that was not retained by the SP-Sepharose resin. The second peak, which shoulders the first, contains DNA and the third peak corresponds to the elution of the

protein of interest, C1-L. At the end of each run, a high salt wash with 1M NaCl was performed (Figure 3.9b) to elute any remaining proteins from the column.

The salt gradient protocol was optimised each time according to the sample size to ensure that it began after the void peak and rose steadily until the end of the run. The isoelectric point (pI) of the sample determined the pH of the buffer and this pI was predicted using its amino acid sequence. Table 3.6. lists the predicted pI, salt gradient, pH of the buffer and the approximate salt conductivity at which the protein was eluted.

Table 3.6: Ion-exchange purification of C1-L and its FHC mutation constructs. The pH and salt conditions used to purify mutants is listed, along with the conductivity at which the protein eluted from the column.

Protein	**Predicted pI**	**Salt gradient**	**pH**	**Elutes @**
C1-L	7.78	40 – 200mM	7.0	16 mS/cm
FHC mutants				
$Asp^{228}Asn$ D84N	8.48	40 – 200mM	7.0	18 mS/cm
$His^{257}Pro$ H113P	7.76	40 – 200mM	7.0	16 mS/cm
$Gly^{278}Glu$ G134E	6.97	40 – 200mM	6.5	17 mS/cm
$Gly^{279}Ala$ G135A	7.78	40 – 200mM	7.0	16 mS/cm
$Arg^{326}Gln$ R182Q	6.97	40 – 200mM	6.5	17 mS/cm
$Leu^{352}Pro$ L208P	7.78	40 – 200mM	7.0	16 mS/cm

a)

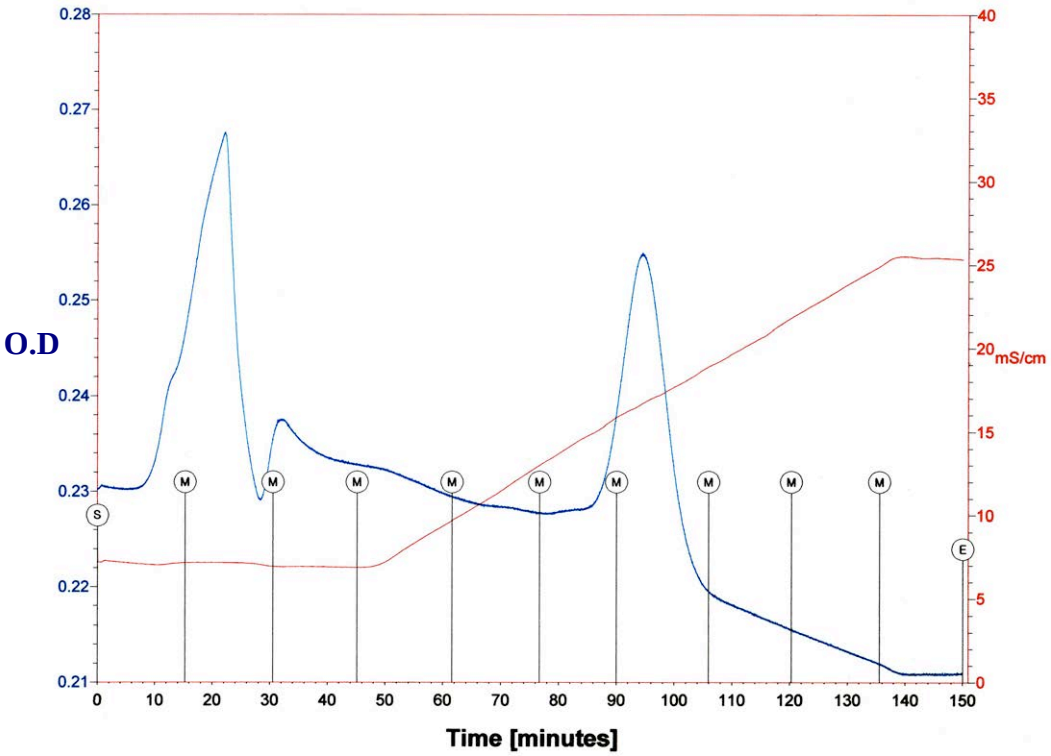

b)

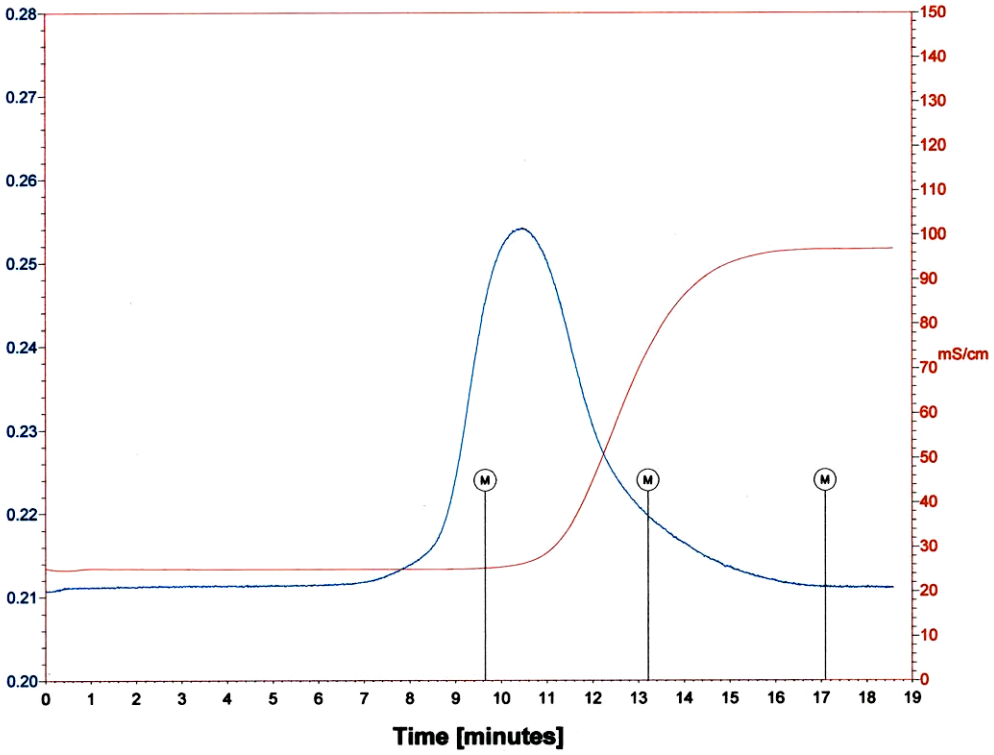

Figure 3.9. Chromatogram of C1-L. Ⓢ: start of the run, Ⓜ: event marker and Ⓔ: end of the run. a) Majority of C1-L was eluted in fraction 7 at 0.2550 O.D and 16.68 mS/cm. b) chromatogram of salt wash with 1 M NaCl

All fractions collected were analysed by 12 % SDS-PAGE and an example of this is shown in Figure 3.10. Figure 3.10 shows the purified C1-L protein in fractions 7 and 8. Lane a contains total cell protein sample of the cell culture after cell lysis, before purification. Lanes 1 and 2 contain the run-through from the chromatography column. C1-L FHC mutant proteins generated similar outcome to C1-L protein.

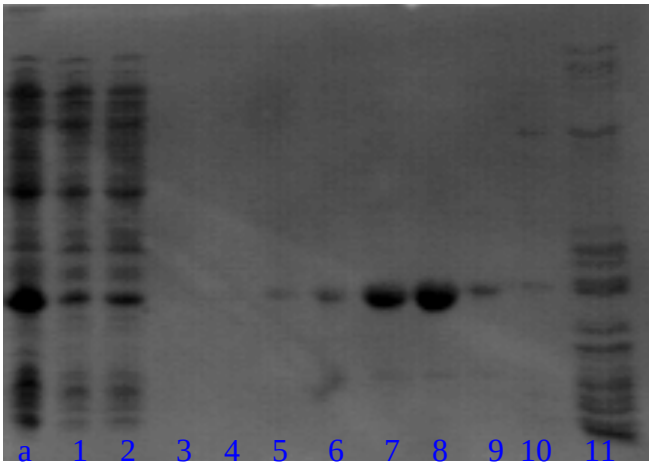

Figure 3.10. Purification of C1-L. Lane a contains total cell protein sample of the cell culture after cell lysis, before purification. Lanes 1 and 2 contain the run-through from the chromatography column. Purified C1-L protein is represented in lanes 7 and 8.

3.3.1.6 C1-L Protein Identification by Mass Spectrometry

The identity of C1-L protein was confirmed by MALDI-TOF MS with sequence coverage of 60 %. The sequence covered by mass spectrometry is highlighted in green in Figure 3.11 and the peaks in Figure 3.12 represent peptide masses generated by MALDI-TOF MS. The only two peptide masses that cover from position 1 (4678.4734: from 1 to 46 and 3418.6769: from 1 to 33) were too large for the machine to detect efficiently. Similarly, the peptide masses that cover from position 203 to 213 are less than 550. Hence the machine was not able to detect these peaks either.

```
1   MTPGAPDDPI GLFVMRPQDG EVTVGGSITF SARVAGASLL KPPVVKWFKG KWVDLSSKVG
61  QHLQLHDSYD RASKVYLFEL HITDAQPAFT GSYRCEVSTK DKFDCSNFNL TVHEAMGTGD
121 LDLLSAFRRT SLAGGGRRIS DSHEDTGILD FSSLLKKRDS FRTPRDSKLE APAEEDVWEI
181 LRQAPPSEYE RIAFQYGVTD LRGMLKRLKG MRRDEKKS
```

Figure 3.11. Amino acid sequence of C1-L. Sequences highlighted in green were covered by mass spectrometry.

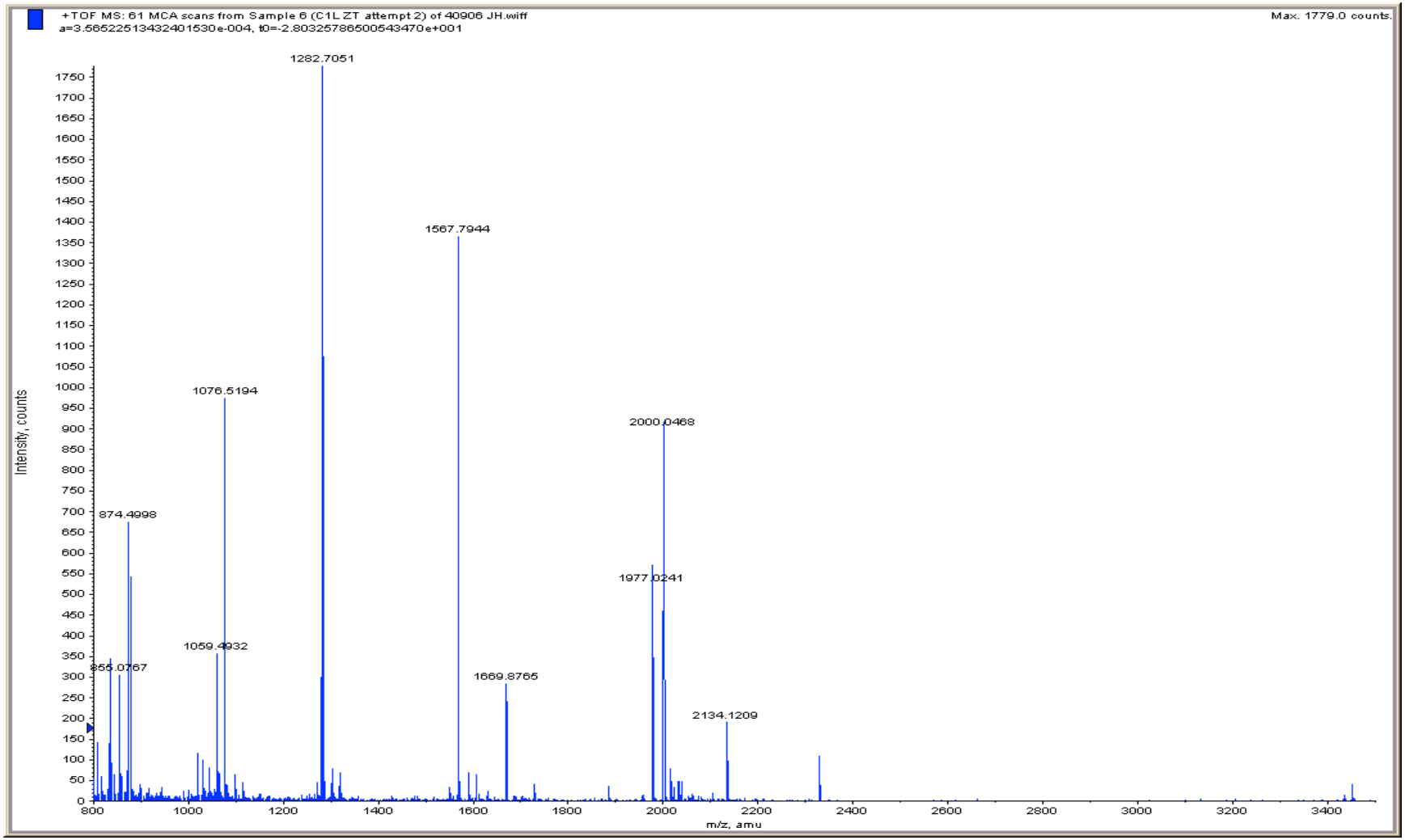

Figure 3.12. Tryptic mass/charge ratio of C1-L obtained by MALDI-TOF MS

3.4 Discussion

Fragments of the phosphorylation region of the N-terminus of cMyBP-C (C1-L and its FHC mutants) were generated successfully by site-directed mutagenesis.

Initial plasmid transformation of C1-L in a pET-3a vector was carried out in *E.coli* DH5α^{TM} – T1^{R} and there were advantages in selecting this cell. They were shown to produce sufficient colonies and generate high plasmid yield. Most importantly, use of this cell line made an *in vitro* digestion step after the mutagenesis reaction redundant. This is due to its inherent *Mcr*BC endonuclease, where it digests the methylated template DNA, leaving only unmethylated, mutated product. FHC mutagenic plasmids on the other hand, were initially transformed into XL-1 Blue supercompetent cells which did not contain inherent endonuclease. Therefore, an extra digestion step with an appropriate restriction enzyme was necessary prior to its transformation. Regardless whether or not the cells contained the inherent endonuclease, both cells generated the desired plasmids with high mutagenesis efficiency (>99 % for both).

Following mutagenesis, the plasmid DNA was expressed into a bacterial expression system, BL21(DE3)pLysS. This system generally provides a higher yield of the expressed protein than eukaryotic systems. However, they are unable to make post-translational modifications to the expressed proteins, which may interfere with the correct folding of the expressed protein. Furthermore, the protein will most likely be packaged as insoluble inclusion bodies if the protein is toxic to the cell or large quantities are produced. In this work, the protein of interest was initially found to be present in inclusion bodies. This meant unfolding of the protein using urea was required during the purification step, followed by refolding by slowly decreasing the urea concentration to minimise the precipitation. This was not ideal for this project for a few reasons – firstly, unfolding and refolding of the protein can interfere with its structural analysis (Chapter 5) and secondly, it was not possible to produce high enough concentrations of the protein for use in nuclear magnetic resonance (NMR) experiment.

These problems were overcome by inducing the protein at an early mid log phase (OD600 = 0.1) and growing at room temperature to maximise the yield in soluble form, that is, in cytoplasm. The purification protocol for FHC mutants were optimised mostly by trial and error but the buffer pH was predicted by calculating

each mutant's predicted pI. This was to ensure sufficient binding of the protein to the column.

The Novagen pET-3a expression vector used did not have any fusion or purification tags. Although this has an advantage of not having to remove the tag, it also necessitates the protein identification of the purified product by MALDI-TOF mass spectrometry. This identification was a crucial step as functional and structural analyses will be performed in subsequent experiments. Mass spectrometry performed using the corresponding gel band from SDS-PAGE gels (24kDa and this was the major protein in the cell lysates) and the resultant peptide map confirm the identity.

In conclusion, both the pET3a expression vector and BL21(DE3)pLysS cells were proven to be effective in producing C1-L and its FHC mutagenic proteins. The desired proteins were present in the soluble form in an adequate amount for the structural and functional analyses, which form the rest of this thesis.

Chapter 4

Binding Studies of C1-L and its FHC mutants

Chapter 4

Binding Studies of C1-L and its FHC mutants

4.1 Introduction

Myosin binding protein C (MyBP-C) is a thick filament protein and interest in it began to rise when researchers found the link between mutations in the gene encoding it's cardiac isoform and familial hypertrophic cardiomyopathy (FHC). Its precise tertiary structure and function is not well understood and therefore, little is known concerning how the mutations in it lead to the FHC phenotype.

MyBP-C has been shown to bind to myosin, actin and titin, however the specific binding site(s) remain to be determined. MyBP-C includes an N-terminal region, which projects out from the thick filament and is believed to be able to interact with both actin and the myosin crossbridge. Of this N-terminal region, domains C1 and C2 and the motif (linker) region connecting the two domains (collectively denoted as C1-C2) are of interest in this thesis. C1-C2 is of special interest as its cardiac isoform (related to FHC) contains multiple phosphorylation sites (phosphorylates in response to α and ß adrenergic stimulation) and controls S2 binding, which in turn allows an increase in systolic force. Phosphorylation may also regulate actin binding, thus making this region a crucial component of MyBP-C function.

Furthermore, the C2 domain alone has been shown to have minimal capacity to bind to actin, raising the question whether the minimum functional unit is the C1 domain and motif (linker). Numerous confirming and confounding studies have been discussed in detail in Sections 1.6.

Therefore, C1-linker and its FHC mutants of cMyBP-C were constructed (Chapter 3) and experiments presented in this chapter aim to address their *in vitro* functional activities.

4.2 Materials and Methods

4.2.1 Proteins

cMyBP-C C1-L and its FHC mutagenic proteins were expressed and purified from the pET3a protein expression vector as described in Chapter 3.

Briefly, the cMyBP-C C1-C2 protein was produced from its glycerol stock (see Section 2.4.2), which was kindly provided by Dr Cecily Oakley. General protein expression and purification steps for C1-L also applied to C1-C2. A starter culture of 10 mL LB broth with 50 μg/mL ampicillin was inoculated with a bacterial glycerol stock scraping and this culture was incubated for 16 hours (overnight) at 37^{o}C with shaking (250 rpm). The saturated culture was then diluted in 500 mL TB with ampicillin in a 2 L conical flask and was grown at 37^{o}C with shaking (200 rpm) until the optical density at 600 nm reached an absorbance of 0.5 – 0.8 cm^{-1}. Once the desired optical density was reached, T7 RNA polymerase promoter was induced by the addition of 1 mM IPTG. The culture was let to grow for additional 4-5 hours before harvesting by centrifugation at 6,000 rpm at 4^{o}C for 20 minutes. The cell pellet was stored at -20^{o}C until purification. C1-C2 was purified using the same protocol except for the salt gradient concentration, which was from 40 – 150 mM NaCl.

Filamentous (F)-actin was prepared from lyophilised (freeze dried) globular (G)-actin as described in sections 2.1.3 and 2.3.5. An adequate amount of freeze dried G-actin was dissolved (on ice) and dialysed in G-buffer (2 mM Tris, pH 8.0, 0.2 mM ATP, 0.2 mM $CaCl_2$) overnight at 4^{o}C. The following day, the solution was clarified by high speed centrifugation, 100 000xg at 4^{o}C for 60 minutes and the concentration was determined as described in section 2.1.5.1. Lastly, its salt concentration was increased to 100 mM KCl and 5 mM $MgCl_2$ to polymerise the G-actin to F-actin.

Myosin used in this chapter was prepared by myosin mini-filament preparation using the myosin prepared as described in section 2.3.1. The snap frozen myosin balls were rapidly defrosted in 30^{o}C water bath and placed on ice. The protein concentration was determined by UV/Vis-spectroscopy (section 2.1.5.1) and was diluted to 5 mg/mL in a high salt buffer (0.5 M NaCl, 50 mM K-PO_4, pH 6.5) and

dialysed extensively at 4^{o}C against the co-sedimentation buffer to form mini-filaments.

All proteins used for binding studies were dialysed against the same buffer prior to the binding assay and its concentrations were measured by using a BCA protein assay (section 2.1.5.2).

4.2.2. Sedimentation Binding

Binding studies of cMyBP-C samples with actin or myosin mini-filaments were performed using a co-sedimentation assay, where both components were mixed in varying molar ratios and incubated at room temperature for 30 minutes to allow adequate binding to take place. Following the incubation period, the mixtures were then centrifuged at 14,000xg for 30 minutes at 4^{o}C for binding studies with myosin or at 100,000xg for 30 minutes at 4^{o}C for binding studies with actin. Pellets were dissolved in an equal volume of 8 M urea and finally, both the soluble supernatant and the dissolved pellet samples were analysed by 12 % SDS-PAGE.

Specifically, a fixed concentration of actin (5 μM) and myosin (7 μM) were used in each binding assay sample, to which increasing concentrations of C1-C2 or C1-L were added, in the range 0 – 6-fold molar excess for the actin binding studies, and 0 – 2-fold molar excess for the myosin binding studies.

To quantitate the amount of protein in the gel bands the gels were digitised and the bands were quantitated using ImageJ V1.42q software (National Institutes of Health, USA). The values obtained for each band were then normalised by the molecular weight of the protein, and a molar binding ratio was derived. Additionally, the association/dissociation constants were calculated by using GraphPad Prism Version 6 using the non-linear fit of saturation binding data module (San Diego, USA).

4.3 Results

4.3.1 Binding Interactions with F-actin

4.3.1.1 Binding between C1-C2 and F-actin

The interaction between MyBPC fragments and F-actin has been demonstrated using a co-sedimentation assay between F-actin and C1-C2. The different molar ratios analysed were C1-C2:actin = 1:0, 0:1, 0.5:1, 1:1 and 2:1 in low ionic strength buffer

(40 mM KCl, 20 mM Tris-HCl, pH 7.0, 1 mM DTT, 1 mM EGTA). Upon centrifugation, F-actin is expected to sediment and form a pellet, whereas C1-C2 is expected to be present in the supernatant. However, if binding occurs between C1-C2 and F-actin, C1-C2 will co-sediment with F-actin and thus, be present in the pellet. Samples were taken after interaction and were analysed by 12 % SDS-PAGE (Figure 4.1).

As shown in Figure 4.1, all supernatant samples contained C1-C2 (34 kDa), except 0:1 sample as this sample did not contain C1-C2. A small proportion of F-actin was also present in all supernatant samples that contained F-actin, as not all F-actin has sedimented, due to the F-actin critical concentration. All pellet samples, except the 1:0 sample, contained F-actin (43 kDa) as expected. Additionally, C1-C2 was present in pellet samples, 0.5:1, 1:1 and 2:1. Thus, C1-C2 binds to F-actin. Notably, the binding of C1-C2 to F-actin is not stoichiometric, suggesting a low affinity interaction.

Quantification of the result showed that at a molar ratio of 1:1 65 % of the C1-C2 remained in the supernatant, consistent with weak binding (K_d = 6.93 ± 0.36 μM).

In order to determine the minimum fragment required to bind to F-actin, binding studies of F-actin with smaller fragments of C1-C2 were performed as a next step.

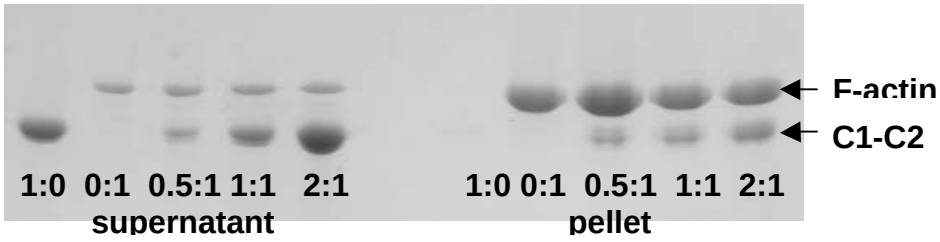

Figure 4.1. Binding study of C1-C2 with F-actin. Presence of C1-C2 in pellet with F-actin suggests binding interaction between the two proteins.

4.3.1.2 Binding between C1-L and F-actin

A sedimentation binding study of C1-L with F-actin was performed using the same method described for C1-C2 with F-actin.

As shown in Figure 4.2, all supernatant samples contained C1-L (24 kDa), except the 0:1 sample as this did not contain C1-L. A small quantity of F-actin was

also present in all supernatant samples that contained F-actin, as not all F-actin has sedimented.

All pellet samples, except the 1:0 sample, contained F-actin (43 kDa) as expected. Additionally, C1-L was present in pellet samples, 0.5:1, 1:1 and 2:1. Thus, C1-L binds to F-actin.

Quantification of the result showed that at a molar ratio of 1:1 75 % of the C1-L remained in the supernatant, consistent with weak binding (K_d = 6.6 ± 0.4 μM). This value was very similar to the binding affinity for C1-C2 (K_d = 6.93 ± 0.36 μM).

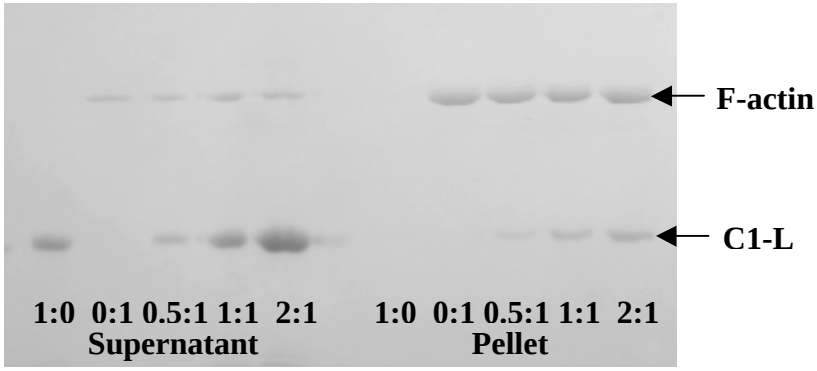

Figure 4.2. Binding study of C1-L with F-actin. Presence of C1-L in pellet with F-actin suggests binding interaction between the two proteins.

4.3.1.3 Binding between C1-L FHC mutants and F-actin

The impact of FHC-causing mutations on cMyBP-C fragment C1-L on F-actin binding was studied using a co-sedimentation assay between F-actin and C1-L constructs containing various FHC mutations.

The binding affinity of the five mutant constructs of C1-L containing FHC mutations were determined using the same method as described for C1-L WT. All the mutants bound to F-actin, but with a lower affinity than C1-L WT, yielding substantially higher K_d values (Figure 4.3 and Table 4.1). Specifically, the $Leu^{352}Pro$ mutant bound with a 3 fold lower affinity (K_d = 19.5 ± 0.5 μM), while the other mutants bound with affinities between 30 and 50 μM. Examples of the pellet fraction showing the binding of mutant C1-L are shown in Figure 4.4.

Table 4.1. K_d values of F-actin binding interaction with C1-L and its FHC mutants.

	C1-L	$Asp^{228}Asn$	$Gly^{278}Glu$	$Gly^{279}Ala$	$Arg^{326}Gln$	$Leu^{352}Pro$
K_d	6.6	38.0	37.1	30.1	47.3	19.5

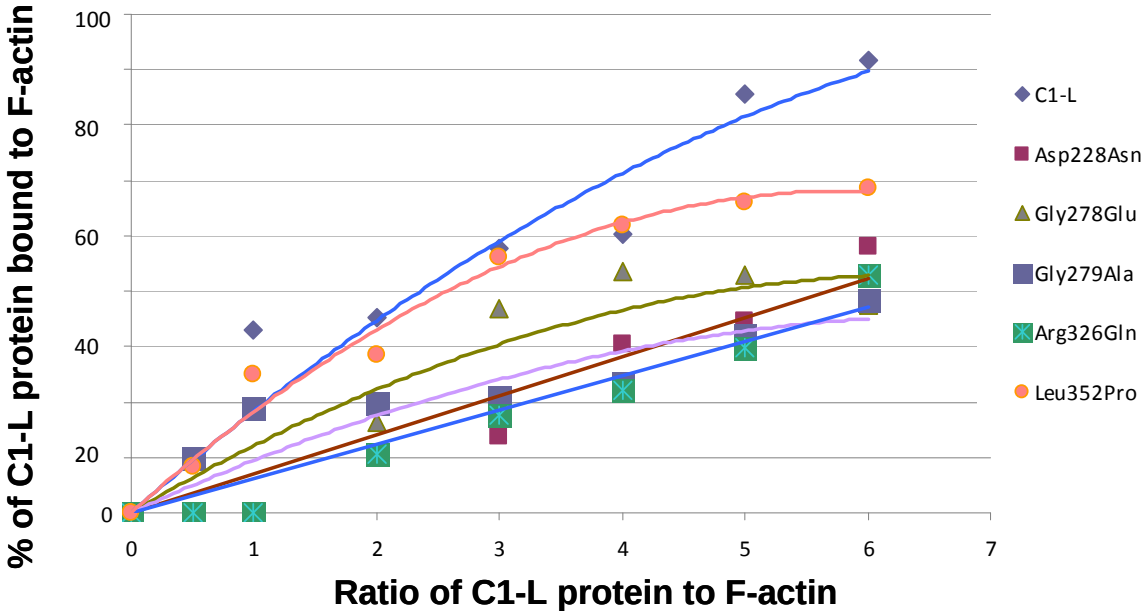

Figure 4.3. Binding curve of C1-L and its FHC mutants to F-actin. All C1-L FHC mutants bind to F-actin, but with lower affinity than C1-L WT.

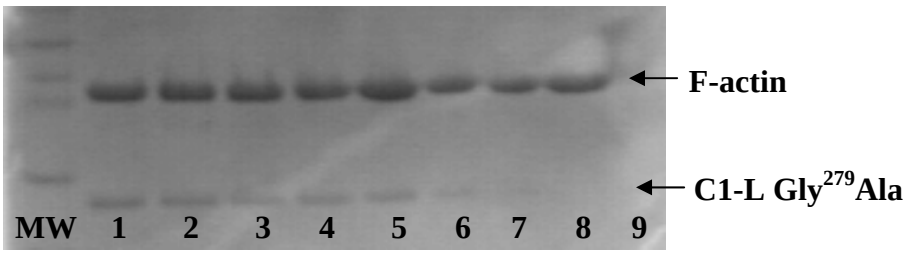

Figure 4.4. Pellet samples of co-sedimentation binding assay of C1-L FHC mutant $Gly^{279}Ala$ with F-actin. Lanes 1 to 9 represent a decrease in C1-L over F-actin. More precisely, the lanes correspond to molar ratios of C1-L $Gly^{279}Ala$ to F-acin of 6:1, 5:1, 4:1, 3:1, 1:1, 0.5:1, 0:1 and 1:0 respectively. Presence of C1-L $Gly^{279}Ala$ in pellet with F-actin suggests binding interaction of the two proteins.

4.3.2 Binding Interactions with Myosin

4.3.2.1 C1-C2 and myosin

The binding of C1-C2 to myosin was examined using a centrifugation binding assay as described in Section 4.2.4. Myosin molecule concentration was 7 μM. Five different molar ratios were examined: C1-C2:myosin = 1:0, 0:1, 0.5:1, 1:1 and 2:1. Upon centrifugation, myosin is expected to sediment and form a pellet, whereas C1-C2 is expected to stay in the supernatant. However, if binding of C1-C2 to myosin occurs, C1-C2 will co-sediment with myosin and be present in the pellet. Samples were taken for analyses by 12 % SDS-PAGE (Figure 4.5) and quantitation using ImageJ software.

All supernatant samples contained C1-C2 (34 kDa), except the 0:1 sample, where C1-C2 had not been added. Myosin was absent in all supernatant samples (Figure 4.5).

All pellet samples, except the 1:0 sample, contained myosin (150 kDa), as expected. Note that the volume of the pellet samples that were loaded on the gels was 5 times less than the supernatant samples. Importantly, C1-C2 was present in all pellet samples, 0.5:1, 1:1 and 2:1, with the amount of C1-C2 present in the pellet increasing in proportion to the loading. Thus, C1-C2 bound to myosin.

Figure 4.6 shows the binding curve for C1-C2 binding to myosin. This curve yields an affinity constant of $K_d = 6.1 \pm 0.9$ μM.

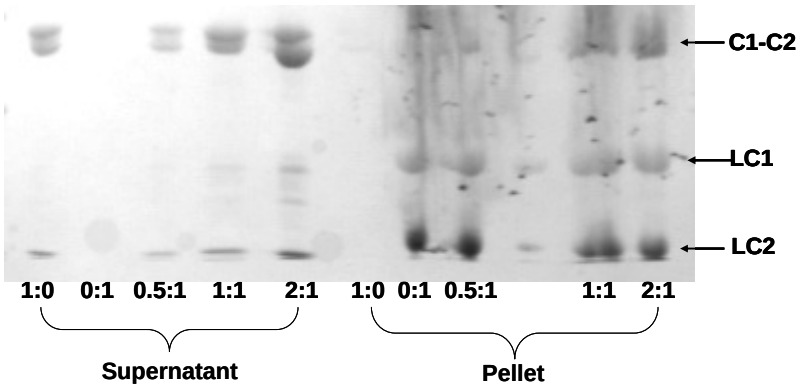

Figure 4.5 Binding assay of C1-C2 with myosin. LC1 denotes myosin light chain 1 and LC2 denotes myosin light chain 2. The presence of C1-C2 in the pellet suggests binding of C1-C2 to myosin. Note: trace of low molecular weight contaminants within the dye front are seen in the supernatant.

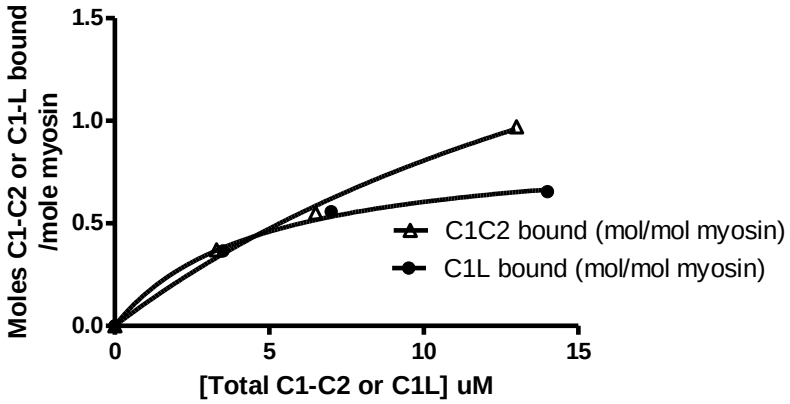

Figure 4.6. Binding curve of C1-L to myosin. C1-C2 binds to myosin with similar affinity to C1-L binds to myosin.

4.3.2.2 C1-L and myosin

Binding studies of C1-L with myosin were performed in order to determine the minimum construct required for binding with myosin. This binding study was performed using the same method as used for C1-C2 with myosin.

Figure 4.7 shows that myosin was absent in all the supernatant samples. This was as expected as myosin sediments upon centrifugation at low ionic strengths. C1-L was present in all supernatant samples, except in 0:1 sample as it did not contain C1-L.

Myosin was present in all pellet samples except in the 1:0 as myosin had not been added. The pellet was very concentrated, so the band representing myosin heavy chain could not be viewed as a single band, but rather as a smear. Pellets obtained from samples that contained both C1-L and myosin (0.5:1, 1:1 and 2:1) contained both C1-L and myosin, consistent with C1-L binding to myosin.

Interestingly, the light chains of myosin in this gel are well visualised. This gel shows that the myosin LC1 (myoLC1) band has a similar density to the C1-L band, consistent with the stoichiometry of binding of both C1-L and myoLC1 to the myosin heavy chain being similar (their molecular weights are very similar, which facilitates comparison).

Notably, if C1-L is binding stoichiometrically to the myosin heavy chain, the myoLC1 band should be slightly more intense (approximately 30%) than the C1-L band. The explanation for this is that myoLC1 binds the myosin heavy chain with a stoichiometry of approximately 0.7 (the other 0.3 is contributed by the other essential light chain, myoLC3), while we predict that C1-L will bind the myosin heavy chain

with a stoichiometry of 0.5, ie since the S2 region of myosin consists of both heavy chains, two myosin heavy chains are required for the binding of each C1-L fragment.

The densitometry analysis in Figure 4.6 revealed that the strength of the interaction between myosin and C1-L (K_d = 23.36 ± 9.2 μM) was similar to C1-C2 and myosin (K_d = 6.1 ± 0.9 μM). Although the K_d differs by 3 fold, the observation that C1-L can bind to myosin tells us that the C2 domain is not essential for the interaction between C1-C2 and myosin.

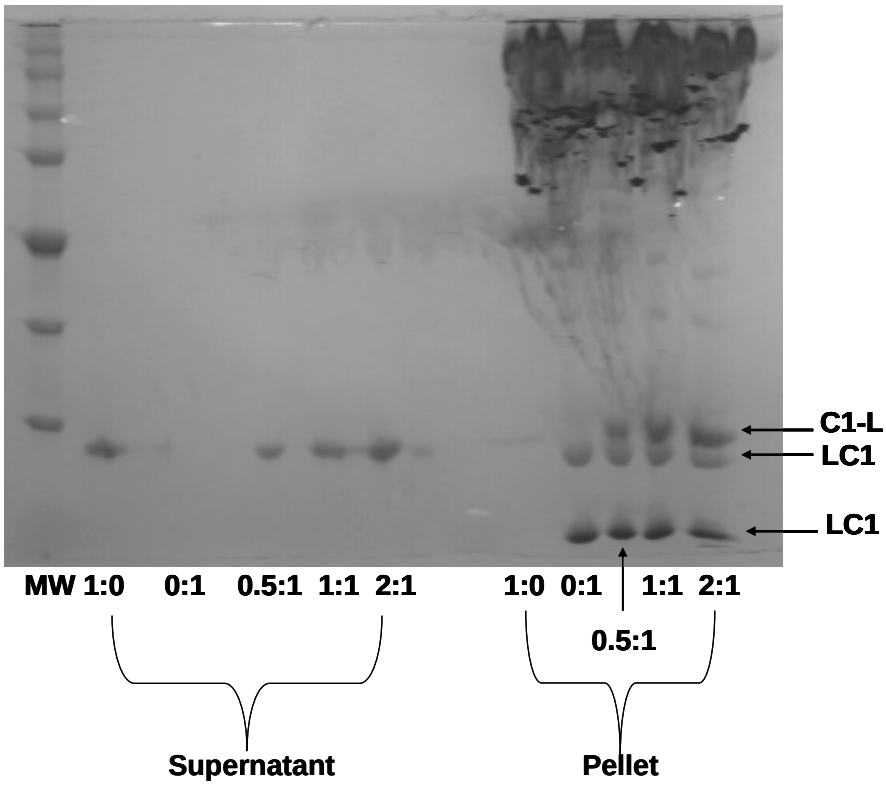

Figure 4.7. Binding assay of C1-L with myosin. LC1 denotes myosin light chain 1 and LC2 denotes myosin light chain 2. The presence of C1-L in the pellet suggests binding of C1-L to myosin.

4.4 Discussion

Our data show that C1-L is able to bind to both actin and myosin with similar, affinity to the C1-C2 construct. Both constructs bind with low affinity (~10 μM) to both F-actin and myosin. When mutants of C1-L were tested for binding affinity to F-actin, all mutants were found to bind with lower affinity than the C1-L WT. Mutant C1-L ($Leu^{352}Pro$) bound to F-actin with an affinity close to WT (3-fold reduction in

affinity), while all other C1-L mutants bound to F-actin with affinities close to an order of magnitude lower.

Similar data were obtained previously for the binding of the full C1-C2 construct to F-actin (K_d 10.9 μM) (Shaffer, Kensler et al. 2009). The majority of mutant C1-C2 constructs bound with much lower affinities to F-actin, with the exception of $Asp^{228}Asn$ C1-C2. This contrasts with the data obtained in this study, where C1-L ($Leu^{352}Pro$) [K_d 19.5 μM] was found to bind with an affinity close to WT C1-L [K_d 6.6 μM]. On the other hand, $Asp^{228}Asn$ C1-L bound with a substantially reduced affinity.

The reasons for these differences are unclear. $Leu^{352}Pro$ is located in the linker region, close to its C-terminus. It is predicted to be located centrally within an α-helical segment. $Leu^{352}Pro$ bound with near normal affinity in the mutant form of C1-L, but demonstrated substantially impaired binding in the mutant form of C1-C2. The insertion of a Pro residue into an α-helix is highly likely to disrupt helical structure, since Pro residues are secondary structure breakers (Chou and Fasman 1978). The disruption of the predicted α-helix within the linker, located close to the C2 domain in the C1-C2 construct, would be likely to disrupt the folding of this part of the linker. On the other hand, it is possible that the absence of the C2 domain in the C1-L construct may have allowed this part of the linker to become more unstructured, hence reducing the impact of the $Leu^{352}Pro$ mutation on the binding configuration of the C1-L structure when binding to F-actin.

$Asp^{228}Asn$ is located in the C1 domain, in the loop between the E and F ß-strands, involving the loss of an acidic residue. This mutation in the C1-C2 construct had a minimal impact on F-actin binding, but in the C1-L construct, $Asp^{228}Asn$ substantially impaired binding. There is no obvious explanation for this difference in binding. Notably, $Asp^{228}Asn$ is known to impair binding of C1 to the S2 region of myosin (Ababou, Rostkova et al. 2008).

The four other mutations of C1-L ($Gly^{278}Glu$, $Gly^{279}Ala$, $Arg^{326}Gln$ and $Leu^{352}Pro$) are all located within the linker region. With the exception of the C-terminally located $Leu^{352}Pro$, the three other linker mutations bound to F-actin with much lower affinity. These data would support the hypothesis that all these residues are involved in binding to F-actin, either directly, or by contributing to the overall fold of the linker region. Two of these mutations, studied here, $Gly^{278}Glu$ and $Gly^{279}Ala$ (Richard, Charron et al. 2003) occur within the conserved, cardiac-specific

LAGGGRRIS sequence (Gautel, Zuffardi et al. 1995), and are in close proximity to two of the phosphorylation sites (site A - Ser^{275} and site B - Ser^{284}). The $Arg^{326}Gln$ mutation is also located within a predicted α-helix within the linker region, likely to be involved in the fold of the linker.

Our data also show that the C1-L construct bound to the myosin molecule with similar affinity to C1-C2. Unfortunately, time constraints prevented us from further investigations into the effects of FHC mutations on this interaction.

The binding affinity of C1-L to other contractile proteins has only been evaluated for the binding of C1-L to F-actin (Shaffer, Kensler et al. 2009, Kensler, Shaffer et al. 2011). The affinity constant for the binding of C1-C2 and C1-L to F-actin obtained in our study was similar to that obtained previously (K_d 10.9 vs 6.93 μM for C1-C2 and 8.7 vs 6.6 μM for C1-L) (Shaffer, Kensler et al. 2009). These data have led to the conclusion that C2 makes little contribution to the binding of the C1-C2 construct to F-actin. However, the capacity of the C1-L to bind to myosin has never previously been determined. The data obtained in our study, showing that the binding of C1-L is similar to the binding of C1-C2 to myosin, supports the conclusion that the C2 domain also makes little contribution to the binding of C1-C2 to myosin.

In summary, our data have shown that C1-L is capable of binding to both F-actin and myosin with a similar affinity to the full C1-C2 construct, albeit with a weak, μmolar affinity. These data are consistent with the hypothesis that the C2 domain makes little contribution to binding to F-actin or myosin. Additionally, our data have shown that FHC mutations result in reduced binding to F-actin, suggesting that, at least in part, these mutations may exert their effects on sarcomeric function by inhibiting normal physiological interactions with F-actin during the contractile cycle. From a physiological point of view, the capacity of the linker region to bind to F-actin appears to be sufficiently important that when this fails to take place efficiently the resulting stress on the heart is sufficient to cause pathological cardiac hypertrophy.

Chapter 5

Structure Prediction of cMyBP-C C1-L

Chapter 5

Structure Prediction of cMyBP-C C1-L

5.1. Introduction

The C1-linker domain of cMyBP-C plays functionally important roles in a number of ways. Most importantly, it contains phosphorylatable residues, where the phosphorylation of these sites controls the interaction of cMyBP-C with myosin-S2 and possibly with actin (Shaffer, Kensler et al. 2009). In-depth discussion of the functional implications of this domain is presented in Section 1.6.6.

Despite the functional importance of the C1-linker domain, its structure remains unclear. Therefore, experiments have been conducted by a previous PhD candidate in our laboratory, using circular dichroic (CD) spectroscopy, to investigate the secondary structure content of the linker region. The results of these experiments showed that the linker region contains some α-helix, but is mostly random coil. In contrast to our CD data, small-angle X-ray scattering has been interpreted as suggesting that the linker domain is compact and has dimensions that are consistent with the immunoglobulin fold superfamily of proteins (Jeffries, Whitten et al. 2008). Furthermore, these data were further supported by homology modelling, calculated using the PHYRE protein structure prediction server. This modelling concluded that the amino acid sequence of the linker region fits into an immunoglobulin-like predicted structure, where a major characteristic of that structure was the absence of any α-helix (Jeffries, Whitten et al. 2008). This inconsistency of data compared to our own data led us to attempt our own modelling using an homology approach, where there is no bias towards a particular structure.

The online homology protein structure prediction program Robetta (http://robetta.bakerlab.org/) was used to generate ten different possible models of the linker region. Multiple sequence alignment of these ten models is presented in Figure 5.1, where the locations of α-helix, β-sheet and random coil are coloured in red, blue

and grey, respectively. Figure 5.2 shows a collage of the ten structures generated by Robetta. Some common features of many of the diverse structures predicted include the presence of at least some α-helix in the C-terminal half of the linker (probably at least three α-helices), while variable predictions of the N-terminal half of the linker have tended to suggest almost any secondary structure, but certainly a significant amount of random coil. Therefore, although the homology approach has revealed no unique structure, this approach did support the exclusion of an immunoglobulin-like structure and demonstrated the consistent presence of several α-helices. Additionally, the modelled structures suggested that the N-terminal half of the linker seems to be more random than the C-terminal half. While this homology prediction was able to provide some constraints to the final structure, in the form of the high likelihood of α-helix, the variety of tertiary structures generated propelled us towards attempting to use an atomic resolution method to determine the structure, in this case we used nuclear magnetic resonance (NMR).

The aim of this chapter is to gain insight into the tertiary structure of the linker region of cMyBPC, by using the C1-L construct described in Chapter 3. The rationale for using the C1-L construct was that this construct appears to be the minimum construct required for functional binding to F-actin and myosin (see Chapter 4). Ideally, NMR spectroscopy is most effective if the minimum sized, functional construct is used, since this will reduce the number of resonances in the NMR spectrum. Thus, we eliminated the C2 domain. Additionally, we aimed to evaluate the binding of C1-L to myosin-S2 (the putative myosin binding site for C1-L) using NMR, both to demonstrate specific binding to this region, and to detect any structural change that may be induced in C1-L upon myosin-S2 binding. Since our CD data and our homology modelling had suggested that the linker region may be poorly structured in solution, we hypothesised that binding may stabilise the structure of the linker region.

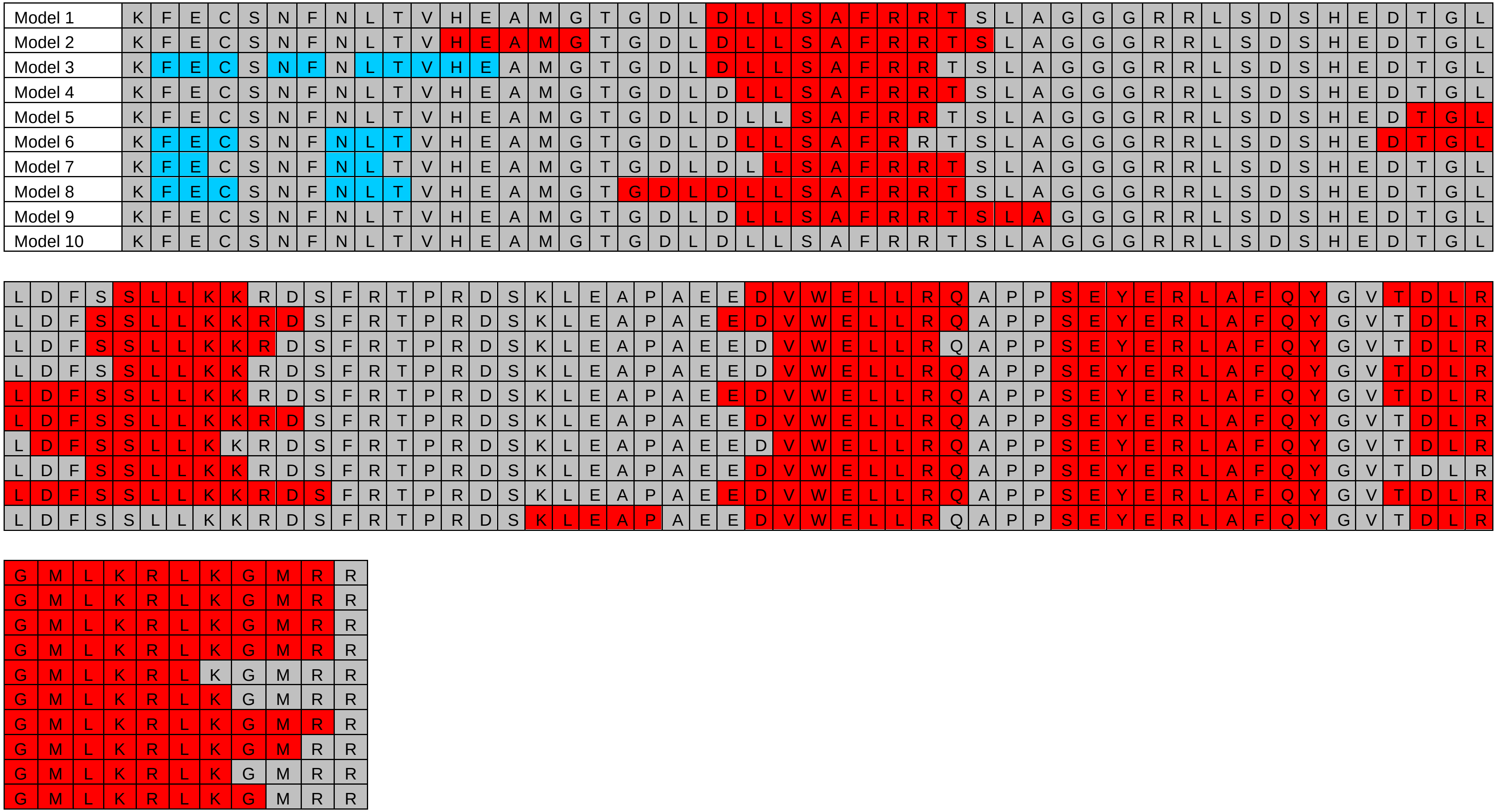

Figure 5.1. Multiple sequence alignment of the linker region based on the ten models. The locations of α-helix, β-sheet and random coil are coloured in red, blue and grey, respectively.

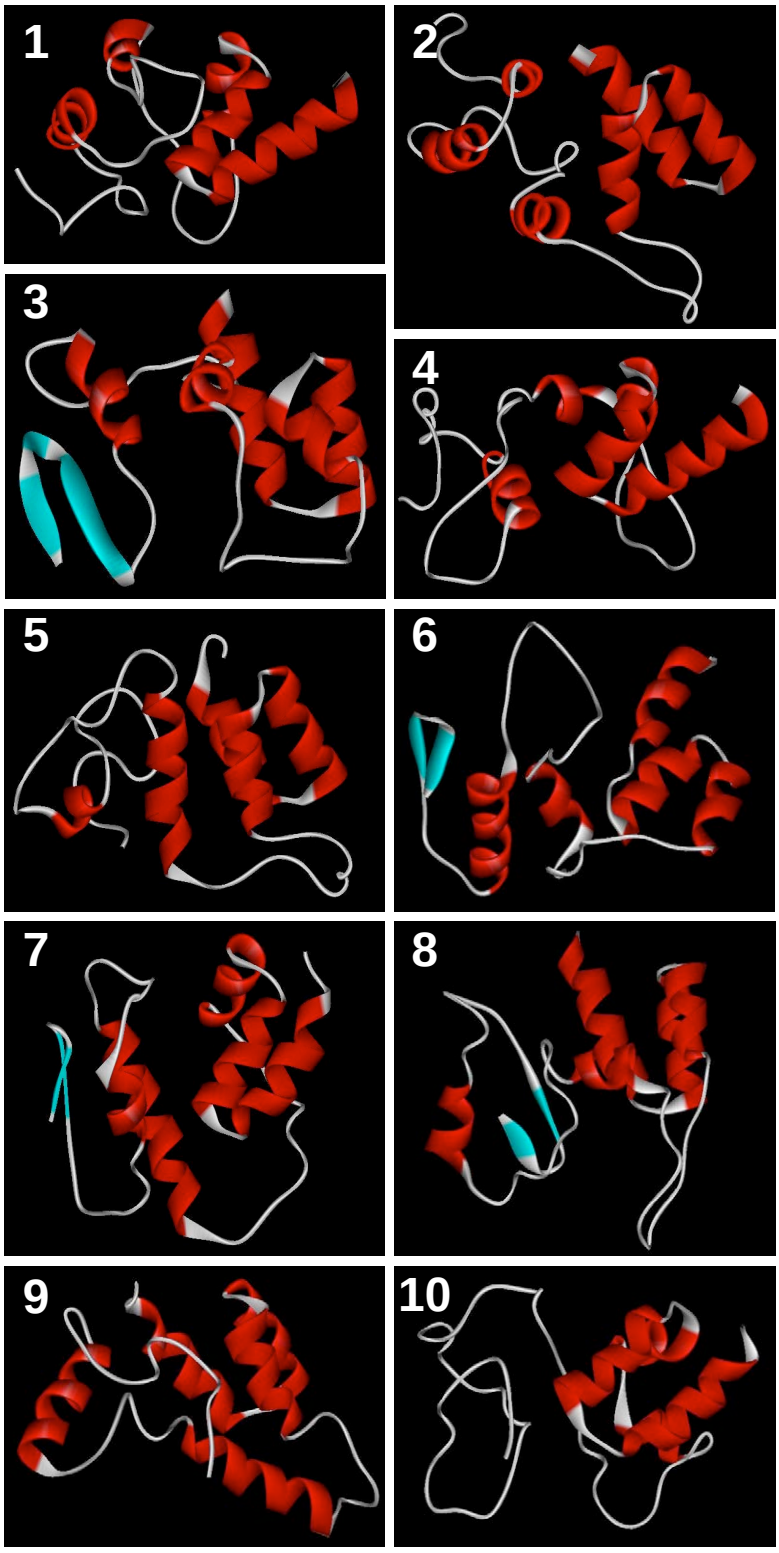

Figure 5.2. Ten structural models of the linker region between C1 and C2 of cMyBP-C. Red = α-helix, blue = ß sheet and grey = random coil. Each model has the N-terminal to the left of the picture and the C-terminal to the right. The models were produced by Robetta and are displayed in solid ribbon format.

5.2. Methods

5.2.1. Media Components

All components of media and stock solutions required for sample preparation for NMR are listed in Table 5.1.

Table 5.1. Components of media and stock solutions used for protein preparation for NMR.

Bacterial Media & Stock Solutions	Components
Ampicillin	50 mg/ml in sterile H_2O; filter sterilise; store in aliquots at -20^oC
LB media	1 L consists of 10 g tryptone, 5 g yeast extract, 5 g NaCl, adjust pH with 5 M NaOH; autoclave at 122^oC and 1.5 kgf/cm^2 for 20 minutes, allow to cool before adding antibiotics.
5x M9 salts	100 mL consists of 3.39 g Na_2HPO_4, 1.5 g KH_2PO_4, 0.25 g NaCl. Autoclave at 122^oC and 1.5 kgf/cm^2 for 20 minutes, allow to cool before adding antibiotics.
Minerals Mixture	2.2 mL consists of 0.1232 g/mL $MgSO_4$, 6.25 mM $ZnSO_4$, 0.25 mM $FeCl_3$. Each of these components were filter sterilised.
100x BME Vitamins Solution	This solution was purchased from Sigma (B6891). This product contains (/L): 0.1 g D-Biotin, 0.1 g choline chloride, 0.1 g folic acid, 0.2 g myo-Inositol, 0.1 g Niacinamide, 0.1 g D-Pantothenic Acid•1/2 Ca, 0.1 g Pyridozal.HCl, 0.01 g riboflavin, 0.1 g thiamine•HCl, 8.5 g NaCl.
Minimal Media	25mL consists of 5mL 5x M9 salts, 5 g/L C^{13}D-glucose, 0.25 mL 100x BME, 0.1 mL minerals mix, 0.1 mM $CaCl_2$, 1 g/L $^{15}NH_4Cl$, 50 µg/mL ampicillin. Each of the components are either autoclaved or filter sterilised.
IPTG	1 M stock consists of 238 mg/ml in sterile H2O; filter sterilise, store in aliquots at -20 ^oC.

5.2.2. Protein Preparation

5.2.2.1. C1-L

Starter culture of C1-L was prepared by inoculating C1-L from glycerol stock into 5 mL Luria Bertani (LB) media with ampicillin (50 μg/mL) and grown overnight at 37^{o}C. 2 mL of the above overnight grown starter culture was then added to 50 mL fresh minimal media and was left to grow at 37^{o}C. Once this culture reached oversaturation, the whole culture was added to 1 L fresh minimal media and left to grow at 37^{o}C until OD_{600} reached 0.1~0.3. The culture was then induced with 1 mM IPTG and left to grow overnight at room temperature. The following morning, the cells were harvested by centrifugation at 6,000 rpm for 10 minutes at 4^{o}C. Once the cells were harvested, they were resuspended and purified as described in Section 3.2.5.5. The concentration of protein was measured as described in Section 2.1.5.2.

The protein sample was concentrated to desired concentration as described in Section 2.4.8.

5.2.2.2. Myosin-S2

Myosin-S2 was prepared as described in Section 2.3.3. Myosin-S2 fragment is a considerably large fragment with a molecular weight of 60 kDa (Lowey, Slayter et al. 1969). Additionally, studies have shown that the proximal 126 residues of the myosin-S2 fragment, close to the lever arm domain of the myosin head is the cMyBP-C binding site (Gruen and Gautel 1999). Note that myosin-S2 is not labelled hence it will not be seen in the NMR spectrum.

5.2.3. NMR spectroscopy

NMR experiments were carried out on samples with protein concentrations of at least 100 μM in NMR phosphate buffer (20 mM $NaPO_4$, pH 7.0, 50 mM NaCl, 1 mM DTT, 1 mM EDTA). Both ^{15}N and $^{13}C^{15}N$ labelled C1-L protein samples were prepared but to date, experiments have only been performed on the ^{15}N sample.

A C1-L 2D ^{1}H-^{15}N heteronuclear single quantum coherence (HSQC) spectrum was acquired on a 600 MHz spectrometer (700 MHz Bruker at Florida State University, USA and 600 MHz Bruker at Macquarie University, Australia) in collaboration with Prof Tim Logan (Institute of Molecular Biophysics, Florida State University, USA). The samples were analysed for 2.5 hours at 20^{o}C. This experiment

provides correlations between the ^{1}H spins and their directly-attached ^{15}N spins of the protein backbone.

5.3. Results

5.3.1 ^{15}N and $^{13}C^{15}N$ labelled C1-L expression and purification

^{15}N and $^{13}C^{15}N$ labelled C1-L bacterial growth was initially attempted using minimal media for both the starter culture and the final grow-up media. However, it was observed that the nutrient in this media was not sufficient to supply growth for overnight cultures and this was evident by lack of protein expression shown in 12% SDS PAGE. Therefore, LB media was used as the starter culture to maximise the growth, then added to a smaller amount of minimal media, followed by addition to the larger grow-up media. This was found to provide sufficient nutrient for successful protein expression. Figure 5.3 shows successful C1-L protein expression.

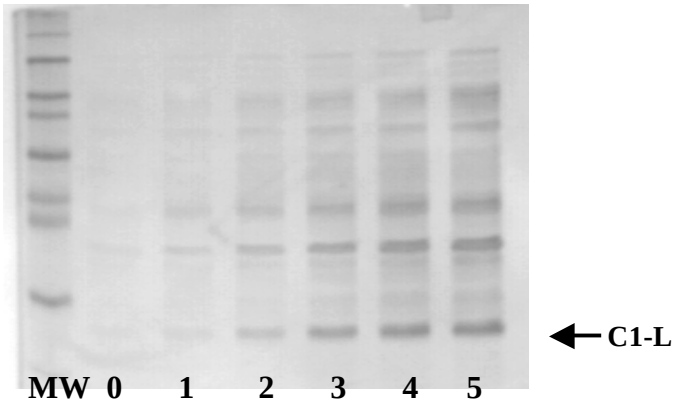

Figure 5.3. Protein expression of ^{15}N & ^{13}C labelled C1-L. MW represents molecular weight marker. Lane 0 represents before induction and lanes 1-5 represents 1, 2, 3, 4 and 5 hours after induction.

Following successful protein expression, C1-L was purified using a salt gradient with cation exchange chromatography. Figure 5.4. shows purified C1-L protein in lanes 4,5,6 and 7.

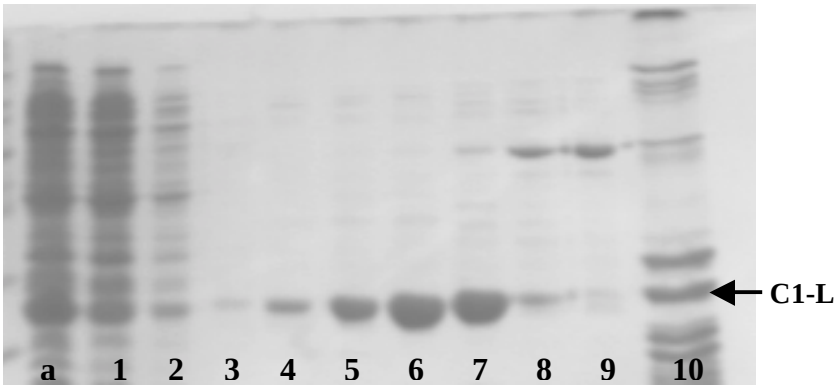

Figure 5.4. Purification of 15N & 13C labelled C1-L. Lane labelled a contains C1-L sample of before purification. Purified C1-L protein is present in lanes 4, 5, 6 and 7.

5.3.2. C1-L NMR spectroscopy

Both ^{15}N and $^{13}C^{15}N$ labelled C1-L protein samples were prepared but to date, experiments have only been performed on the ^{15}N sample. We planned to use the $^{13}C^{15}N$ labelled C1-L for structure determination, but this was not possible, as discussed later in this chapter.

The C1-linker protein with the ^{15}N labelled was examined using NMR spectroscopy. Initially, the sample was examined alone and later, in the presence of the S2 fragment of myosin, which is believed to be a binding target of C1-L. The 2D HSQC spectra (Figure 5.5) provide correlations between the ^{1}H spins and their directly-attached ^{15}N spins of the protein backbone, hence this experiment provides a fingerprint of the protein, but not the actual structure.

C1-L NMR

The 2D HSQC spectrum of C1-L (Figure 5.5) has shown a number of findings.

1. There is excellent chemical shift dispersion and good line-shapes. This high chemical shift dispersion is consistent with high β-strand content, as expected for the IgI C1 domain.
2. Wide dispersion suggests that C1 domain is structured and the pattern appears to correspond to the published data (Ababou, Zhou et al. 2004). Published data allows us to make tentative assignments that have yet to be confirmed.

3. Peaks clustered in the middle of the spectrum correspond to unstructured peptide, which in this case is the linker region. This is supported by published NMR structure of C1 domain (Ababou, Zhou et al. 2004), where it lacks this cluster in the middle of the spectrum. Hence, we deduce this region to be due to the linker region.
4. C1 domain does not seem to be interacting with the linker region as the identified published dispersed peaks from C1 domain have not been shifted. However, not all the peaks corresponding to C1 domain are visible as part of these are located in the central region that in our spectrum is dominated by the random coil in the linker.
5. There is a cluster of resonances at approximately 129 ppm in the ^{15}N and 8.2 ppm in the ^{1}H dimension. This is indicative of α-helix i.e. limited proton shift range and downfield shift in ^{15}N. Since this is not seen in the published C1 spectrum and C1 is known to contain no α-helix (Ababou, Zhou et al. 2004), we predict this α-helix to be located in the linker region, consistent with the hypothesis outlined in the introduction. The extent of the dispersion indicates that these helices are stable, but their interactions may also involve some tertiary contacts to stabilise the helices.

C1-L + myosin S2 NMR

Addition of the myosin S2 fragment resulted in some clear changes in the HSQC spectrum (Figure 5.5).

1. There were changes to the intensity of peaks. The peak intensity correlates with the number of protons of that type and is calculated by integration where line width is taken into account. The line width represents the rate of inter-conversion of conformers i.e. the rate of dynamic change.
2. There were changes to resonance frequency with some large and small shifts. Note these changes are population weighted averages.
3. The above two changes (intensity and resonance frequency) are consistent with interaction between two proteins, where many residues are involved, although many of these residues may not be in direct contact. Indeed, the largest changes probably correspond to residues that are in direct contact

leading to stabilisation of helices. This is evident with more red at the bottom of the spectrum.

4. The larger number of red resonances (C1-L in the presence of S2) and their generally greater intensity is consistent with an increase in structure as a consequence of myosin S2 binding. This is particularly apparent in the “helical region”, since the helix is more dispersed which makes it more visible.
5. The clustered region in the middle is extremely hard to evaluate and, hence, to determine whether there is more random coiled or not.
6. The cluster of resonance at approximately 121 ppm in the ^{15}N and 7.2 ppm in the ^{1}H dimension corresponds to a cluster of arginine (Arg) sidechains. Often this cluster is due to the His tag incorporated into the protein, however, C1-L does not contain a His tag. It is evident from the spectrum that this cluster of Arg sidechains in the C1-L spectrum (black) becomes dramatically dispersed on the addition and binding of myosin S2. This result is consistent with a significant change in structure and a possible charge interaction between the two proteins.

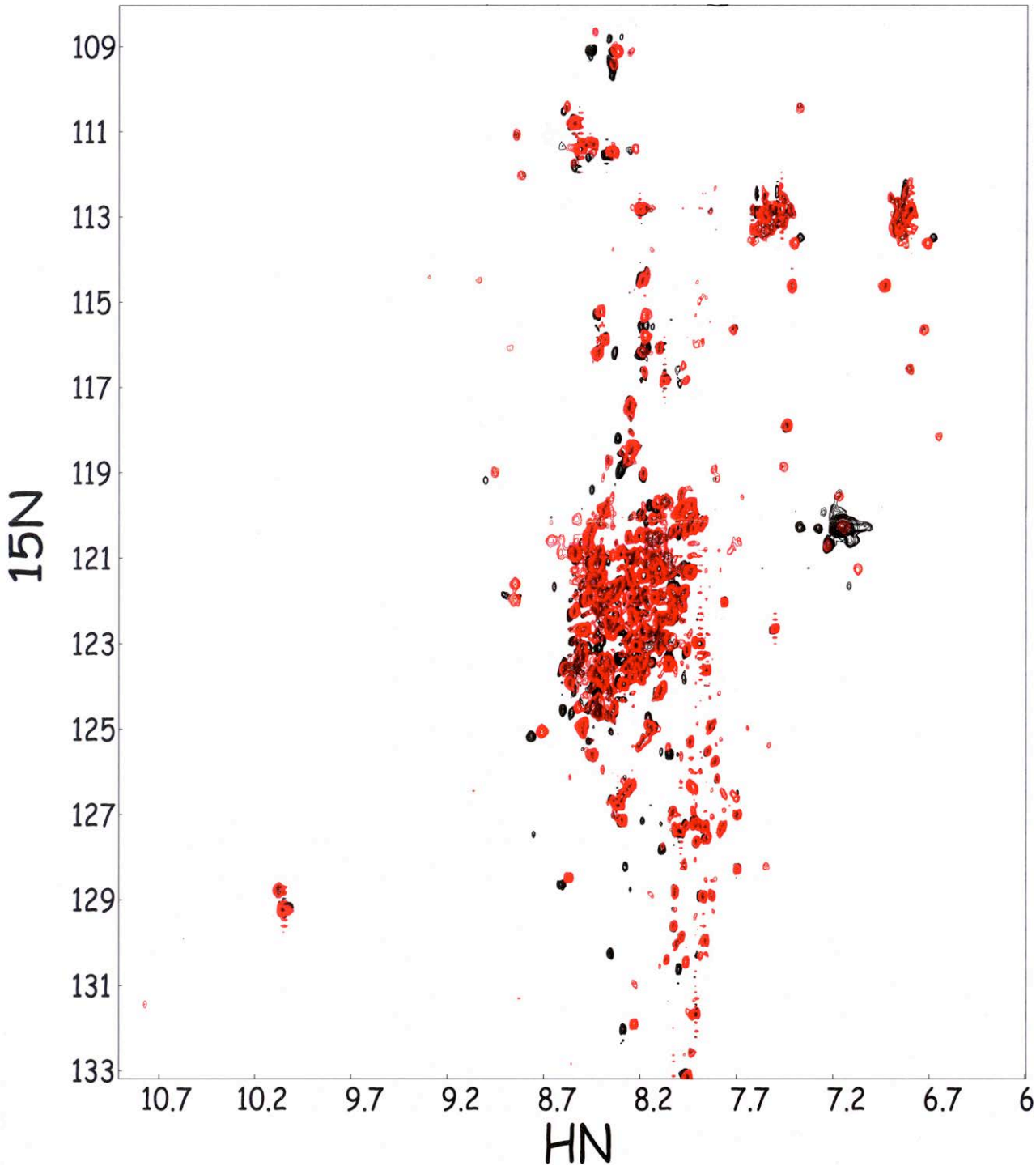

Figure 5.5. C1-L 2D 1H-15N HSQC spectra. Black represents C1-L by itself and red represents C1-L plus myosin-S2.

5.4. Discussion

Our data show that the NMR spectroscopy was able to identify dispersed resonances that corresponded well with the published spectrum of the C1 IgI domain. However, our NMR spectra had superimposed on them a cluster of poorly dispersed

resonances in the centre of the spectrum that were consistent with additional peptide, most likely corresponding to the linker region, that contained a substantial proportion of random coil. The poor dispersion of many of the resonances precludes their specific assignments to amino acids and thus this makes 3-D atomic resolution structure determination impossible. Importantly, our NMR spectra also revealed that there was a clear α-helical component within C1-L, and since no α-helix occurs within the known structure of the C1 IgI domain, this α-helix is almost certainly located within the linker region. Nonetheless the structure of the remainder of the linker region is unknown, although it is likely to be disordered given the high levels of dispersity for many of the remaining residues. Furthermore, when the binding target of C1-L, the myosin S2 α-helical coiled-coil was added to C1-L, the NMR spectrum revealed that a specific interaction took place, and that the interaction involved Arg residues.

Structure prediction obtained using the homology approach has shown that there are several areas of highly predicted α-helix and the rest of the linker region corresponds to no known structure. Since the homology structures obtained were not unique, except for the consistently predicted location of α-helices, it is highly likely that the linker region is highly disordered and flexible and lacks a globular structure. Secondary structure prediction (Figure 5.1) predicts the majority of remaining sequence to be random coil. The NMR data we have acquired is consistent with this structural interpretation. Additionally, the linker region also appears to have several well formed α-helices, interspersed with minimally structured random coil. These data contrast with published reports (Jeffries, Whitten et al. 2008) that the linker is a well-structured modified Ig domain, containing prominent β-sheets and no α-helices. Our NMR data show no evidence of β-sheet within the linker.

While this thesis was being written a report was published on the use of NMR to assess the structure of the linker region alone (we examined the linker plus the C1 IgI domain in this Chapter) (Howarth, Ramisetti et al. 2012). Our NMR data, which shows that the linker region is largely disorganised with some α-helical content, is in good agreement with the published data of Howarth *et al.* (2012), who believe that the linker region is divided into two regions: a well folded C-terminal end, containing three α-helices and an N-terminal end that is largely disordered and flexible (Figure 5.6). The three C-terminal α-helices correspond exactly with those predicted by us using the Robetta homology structure prediction programme (Figure 5.1).

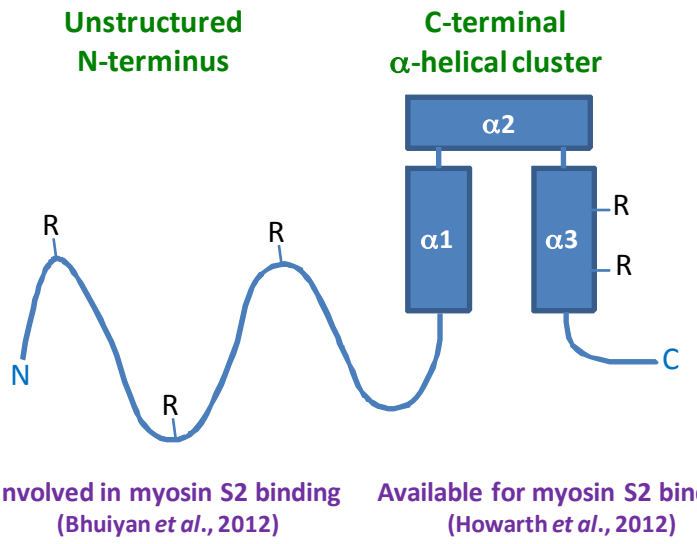

Figure 5.6. Schematic representation of the cMyBP-C linker region. Arg (R) residues that have been implicated in myosin S2 binding are shown.

Additionally, Howarth *et al.* (2012) believe that the C-terminal end of the linker region, containing three α-helices packed into a cluster, has an electrostatic surface including the α3 helix containing exposed Arg^{342}, Lys^{346}, Arg^{347} and Lys^{349}, combined with a largely hydrophobic belt around the middle of the structure, due to the packing of the helix bundles (Figure 5.6). These findings suggest the possibility of both hydrophobic and electrostatic interactions with either neighbouring molecules in cMyBP-C or sarcomeric proteins, for example myosin-S2. Of interest is the observation that eight out of the ten structures we generated using Robetta (Figure 5.2) show the three C-terminal helices (α1 – α3) packing into a cluster, similar to the cluster seen by Howarth *et al.* (2012).

Upon addition of myosin S2 to C1-L, there were changes in both intensity and resonance frequency, suggesting the specific interaction between the two proteins. Specifically, the resonances for several Arg residues became dispersed upon myosin S2 binding, directly implicating these residues in the process of binding, probably as part of the binding interface. This finding is supported by recent published data (Bhuiyan, Gulick et al. 2012), who have suggested a strong interaction between the linker region and myosin-S2. Furthermore, they were able to predict some critical residues required for binding, by mutating sets of amino acids to alanine. These residues were R266A, R270A, R271A, R279A, R280A, T281A, K298A, K299A and

R300A (in the mouse cMyBPC sequence). These charged residues are located in the unstructured N-terminal half of the linker region (Figure 5.6). Thus, these Arg residues may correspond to the Arg residues identified in our NMR spectra, that became dispersed upon myosin S2 binding. Taking these data together, Arg residues located in the N-terminal half of the linker region have been identified as being involved in myosin S2 binding (Bhuiyan, Gulick et al. 2012), and Arg residues on the surface of the C-terminal cluster of α-helices have been identified as being available for potential electrostatic interactions with other molecules (Howarth, Ramisetti et al. 2012). Our NMR data are consistent with these data that propose that electrostatic interactions involving Arg residues within the linker region are involved in myosin S2 binding.

In conclusion, the NMR studies have demonstrated that the linker region is important for the physiological interaction with myosin-S2. Thus, mutations of either the linker or myosin-S2 will interfere with this physiological interaction. This is the first time that NMR spectroscopy has been used to demonstrate specific binding between the linker and myosin-S2.

Chapter 6

Structural and Functional Studies of Cofilin

Chapter 6

Structural and Functional Studies of Cofilin

6.1. Introduction

Actin filaments (F-actin) are comprised of actin monomers (G-actin) and play many important roles in cellular processes including muscle contraction, cell motility, cell division, cytokinesis, vesicle and organelle movement, cell signaling, and the establishment and maintenance of cell junctions and cell shape. Actin is discussed in more depth in Section 1.3.2.1.

Cofilin is an actin binding protein that regulates actin polymerisation and depolymerisation and is known to play a crucial part in cell division, apoptosis and cancer. Although it is known to bind to both globular (G-actin) and filamentous (F-actin) actin, the exact binding sites and its quaternary structure are still yet to be solved. One of the major functions of cofilin is its ability to depolymerise actin filaments at the minus end (pointed) and this activity is regulated by various factors, including phosphorylation, phosphatidylinositides and pH. Furthermore, cofilin is known to sever actin filaments and is involved in nuclear translocation. Cofilin is discussed in more depth in Section 1.7.

One of our ultimate aims is to track cofilin interactions within the cytoplasm and the nucleus of cells. This objective has been hampered by our inability to attach extrinsic fluorescent probes to cofilin, while retaining the capacity to bind actin. Therefore, we aimed to design a cofilin that could be labelled with a fluorescent probe and still bind actin. Additionally, such probe sites can be used to elucidate the quaternary structure of the actin-cofilin complex.

The intrinsic Cys residue in cofilin is difficult to label and, after labelling, prevents actin binding. Consequently, we have designed several cofilin mutants to assess their capacity to bind actin when labelled. Additionally, these cofilin mutants have been utilised to investigate the quaternary structure of the actin-cofilin complex.

The role of cofilin in actin dynamics within the cell requires that an understanding at the molecular level should be determined. However, such an understanding is hampered by the lack of a high resolution structure of the complex. The most recent structure proposed from high-resolution electron microscopy, combined with dynamic molecular simulations has recently been published (Galkin, Orlova et al. 2011). We have generated an array of unique spectroscopic probe sites in cofilin, which when combined with known unique probe sites in actin, allow us to use spectroscopic techniques to measure distances within the quaternary complex, that can directly test the model of Galkin et al. (Galkin, Orlova et al. 2011).

Thus, the aims of this chapter were to:

1. Use fluorescent spectroscopic techniques to measure distances within the actin-cofilin quaternary complex to directly test the model of Galkin et al. (Galkin, Orlova et al. 2011). Thus, functional cofilin mutants suitable for selective labelling with extrinsic fluorescent spectroscopic probes were designed.

   The mutants generated were:

   i) N6-cys-cofilin: six additional amino acids including a Cys were added at the N-terminus
   ii) Cys170 cofilin: four additional amino acids including a Cys were added at the C-terminus (C170)
   iii) Cys170 W104 cofilin: Cys at the C-terminus (C170) + only the 1st Trp (W104) is present and the 2nd Trp W135 has been mutated to Leu
   iv) Cys170 W135 cofilin: Cys at the C-terminus (C170) + only the 2nd Trp (W135) is present and the 1st Trp W104 bas been mutated to Phe

2. Prior to performing spectroscopic measurements, structure and function of mutants were determined by:

   i) Circular Dichroism (CD) spectroscopy to compare the secondary structure content of the mutant cofilins to wild-type cofilin
   ii) Perform binding assays to determine the binding status of cofilin mutants to actin, both before and after labelling, compared to wild-type cofilin

The hypothesis was that the inter-molecular distances obtained in the actin-cofilin quaternary complex, using fluorescence spectroscopy, would correspond closely with those seen in the model of Galkin et al. (Galkin, Orlova et al. 2011).

6.2. Materials and Methods

6.2.1. Preparation of actin

Actin was prepared as described in Section 2.3.5.

6.2.2. Preparation of Cofilin Mutants

Plasmid encoding native cofilin (pCof) was a kind gift from Dr. Takashi Obinata (Chiba University, Japan). Recombinant avian embryonic skeletal muscle cofilin was prepared as previously described (Chhabra, Nosworthy et al. 2005). Purified cofilin was dialysed for 24 h against G-buffer without ATP (2 mM Tris, pH 8.0, 0.2 mM $CaCl_2$). The final concentration of native cofilin was determined from the OD_{280}, where $E^{0.1\%} = 0.93\ cm^{-1}$ (Abe, Endo et al. 1990).

The above native cofilin plasmid, in pGEX-2T vector, was used as a template for generating cofilin mutants used in this chapter. Prior to the preparation of the mutants, the native cofilin plasmid was amplified using Wizard Plus SV Minipreps DNA Purification System (Promega). The protocol was as suggested by the manufacturer and the culture used was an overnight LB culture with ampicillin (50 μg/ml) from fresh colonies obtained by transformation into Bl21(DE3) cells as described in section 3.2.5.1.

The four cofilin mutants generated were N6-cys-cofilin, Cys170 cofilin, Cys170 W104 cofilin and Cys170 W135 cofilin. For generation of N6-cys-cofilin, six additional residues (MACGCA) were cloned onto the N-terminus of native cofilin to produce cys-cofilin. N6-cys-cofilin is reported to have a reactive cysteine capable of conjugation with a fluorescent dye while retaining its actin-binding activity (Nagaoka, Kusano et al. 1995). The additional residues were coded for in the forward primer:
5’GGAATTCCATATGGCGTGCGGTTGCGCGATGGCTTCTGGAGTAACAGTG
For PCR amplification of the cDNA fragment for cloning the reverse primer was:
5’-CGCGGATCCTTATAAGGGTTTTCCTTCAAGTGAAACTAC. The forward and reverse primers contained Nde1 and BamH1 restriction sites, respectively. The PCR product was treated with Nde1 and BamH1 and inserted into a pET-3c vector that was pre-digested with Nde1 and BamH1. Integrity of the construct was confirmed by DNA sequencing. The rest of the mutants were all produced by site directed mutagenesis using the same method for C1-L preparation as described in section

3.2.3.3. The primers used for all mutants are listed in table 6.1. Upon completion of mutagenesis, the correct DNA sequence was confirmed as described in section 2.4.6.

Table 6.1. Primers for Cofilin mutagenesis and sequencing into pGEX-2T vector.

Primer	Sequence (5' → 3')
N6-cys-cofilin forward	GGAATTCCATATGGCGTGCGGTTGCGCGATGGCTTCTGGAGTAACAGTG
N6-cys-cofilin reverse	CGCGGATCCTTATAAGGGTTTTCCTTCAAGTGAAACTAC
Cys170 cofilin forward	AGGAAAACCCTTAGCGGGTTGCGCGTAAAAAGACA
Cys170 cofilin reverse	TAAGGGTTTTCCTTCAAGTGAAACTACCACGTTGCC
Cys170 W104 cofilin forward	CAGGTATTAAACATGAGCTGCAAGTAAATGGTTTGG
Cys170 W104 cofilin reverse	CCAAACCATTTACTTGCAGCTCATGTTTAATACCTG
Cys170 W135 cofilin forward	CCTGGTATTTATATTCTTTGCTCCTGAAAGCGCACC
Cys170 W135 cofilin reverse	GGTGCGCTTTCAGGAGCAAAGAATATAAATACCAGG
Forward sequencing	CGCGTGGATCCATGGCTTCTGGAGTAACAGTGA
Reverse sequencing	AGGAAAACCCTTAGCGGGTTGCGCGTAAAAAGACA

6.2.3. Transformation of Cofilin Mutants

Once the correct DNA sequence had been confirmed, the mutants were transformed into *Escherichia coli (E.coli)* BL21(DE3)pLysS cells for protein expression and glycerol stocks were prepared for long term storage as described in sections 3.2.5.1 and 2.4.2 respectively.

6.2.4. Protein Expression of Cofilin and its Mutants

Protein expression of all cofilin samples in this thesis was in *E.coli* BL21(DE3)pLysS cells as a glutathione-S-transferate (GST) fusion protein.

A flamed wire loop was allowed to cool and a loop-full of glycerol stock was inoculated into 10 mL of LB broth with ampicillin (50 µg/mL) and chloramphenicol (34 µg/mL). This starter culture was grown to saturation (overnight) with shaking (250 rpm) at 37^{o}C. The overnight culture was then diluted into 500 mL of pre-warmed LB broth with ampicillin (50 µg/mL) and chloramphenicol (34 µg/mL) in a 2L conical flask and was let to grow at 37^{o}C with shaking (200 rpm) until the optical density at 600 nm reached an absorbance of 0.5 cm^{-1}. Once the appropriate OD_{600} value had

been reached, protein expression from the *lac* promoter/T7 RNA polymerase promoter was induced by adding 1 mM IPTG and the culture was grown for another 4 to 5 hours at room temperature with shaking (200 rpm). Finally the cells were harvested by centrifugation at 6,000 rpm for 10 minutes at 4^{o}C and stored at -20^{o}C. Samples were taken from before and after induction and analysed by SDS-PAGE. Additionally, time courses after induction were performed. The samples were analysed by SDS-PAGE to determine the optimal time for induction and protein expression.

6.2.5. Protein Purification of Cofilin and its Mutants

The bacterial pellet containing the protein of interest in the cytoplasm was thawed and lysed in lysis buffer (50 mM Tris, pH8.0, 1mM EDTA, 0.5 mM PMSF, 1 mM DTT, 50 mM NaCl, 1 % Triton-X100). The mixture was sonicated for 3 x 10 second pulses and incubated on ice for about 30 mins. It was then centrifuged at 8,500 rpm for 30 minutes at 4^{o}C. The resulting supernatant contains the soluble protein and was therefore applied directly onto an appropriate column to be purified, in this case, glutathione Sepharose 4B column (Sigma).

Prior to loading the samples onto the column, the column was sequentially washed with three column volumes of Milli Q water, 20mM glutathione in 50 mM Tris, 8 M urea and phosphate buffered saline (PBS; 0.15 M NaCl, 2 mM KCl, 10 mM PO_4, pH 7.4) containing 0.5 mM PMSF and 1.0 mM EDTA. The supernatant was applied to the column and washed with three column volumes of thrombin buffer (50 mM Tris, 2.5 mM $CaCl_2$, 50 mM NaCl, pH 8.0). Following this, thrombin (100 U of thrombin/L of culture) was directly added into the column and was incubated at 4^{o}C overnight to cleave the GST tag. Finally, cofilin was eluted with two to three volumes of thrombin buffer the next day. Throughout the procedure, all the samples were collected for analysis using 12% SDS-PAGE gel. The protein concentration was measured and concentrated as described in Sections 2.1.5 and 2.4.8, respectively. Notably, after thrombin cleavage, two additional residues (G and S) remained at the N-terminus, compared to the native structure, but this has a negligible effect on the structure and function of cofilin, as demonstrated by subsequent CD and binding analysis (Section 6.3.4 – 6.3.8).

6.2.6. Fluorescent Labelling of Cofilin mutants and actin

Various fluorescent probes were used for this chapter. These include:

1. IAEDANS (5-({2-[(iodoacetyl) amino] ethyl} amino) naphthalene-1-sulphonic acid). The molecular weight of this probe is 434.25 with an extinction coefficient of 6100 $M^{-1}cm^{-1}$ at absorption maxima wavelength of 336 nm and a peak emission wavelength of 490 nm (Xing and Cheung 1995).

2. DABMI (4-dimethylaminophenylazophenyl-4'-maleimide). This probe is widely used for labelling of Cys sulphydryls. It has a molecular weight of 320.35 and has an extinction coefficient of 24,800 $M^{-1}cm^{-1}$ at an absorption maxima wavelength of 460nm (Xing and Cheung 1995).

3. DHNBS (dimethyl (2-hydroxy-5nitrobenzyl) sulphonium bromide). This is a chromophoric, water-soluble tryptophan-reactive reagent that does not fluoresce. It has a molecular weight of 294.2 and a large extinction coefficient of 18,000 $M^{-1}cm^{-1}$ at an absorption maxima wavelength at 410 nm, which makes it an excellent acceptor for FRET measurements (Barman and Koshland 1967).

4. εATP (1,N^6-ethenoadenosine 5'-triphosphate). This is an etheno ATP analog that can mimic ATP in both binding and function. This probe was used to label the nucleotide binding site of G-actin.

Table 6.2 shows list of fluorophores with its extinction coefficient and absorption maxima wavelength.

Table 6.2. Standard fluorophores' extinction coefficients and absorption maxima wavelengths.

Fluorophore	Absorption maxima	Extinction Coefficient	Reference
IAEDANS	336 nm	6,100 $M^{-1}cm^{-1}$	(Xing and Cheung 1995)
DABMI	460 nm	18,000 $M^{-1}cm^{-1}$	(Xing and Cheung 1995)
DHNBS	410 nm	24,800 $M^{-1}cm^{-1}$	(Barman and Koshland 1967)

Labelling N6-cys-cofilin with IAF

N6-cys-cofilin was labelled on a cysteine residue by overnight incubation at 4°C with a three-fold excess of fluorescein conjugated to iodoacetamide (5-IAF). The reaction was stopped by addition of DTT to a final concentration of 10 mM. Excess label was removed by overnight dialysis against 10 mM Pipes, pH 6.8, 1 mM EDTA, 1 mM EGTA, followed by passage through a Sephadex G-25 column. The resultant IAF-N6-cys-cofilin was dialysed for 24 h against G-buffer without ATP.

Labelling C170 cofilin with IAEDANS

Prior to labelling, the protein was dialysed against IAEDANS buffer (100 mM NaCl, 20 mM Na-PO_4, pH 8.0) and IAEDANS was dissolved in either DMF or DMSO. Cofilin C170 was then labelled with a 20x molar excess of IAEDANS at room temperature for 1.5 hours on a rocker. The reaction was stopped with 1 mM DTT and was dialysed exhaustively against appropriate buffers to remove any excess fluorophore probes. IAEDANS is a light sensitive fluorophore, hence the labelled samples were covered by foil at all times to prevent exposure to light, subsequently preventing photobleaching of the fluorophore.

Labelling cys170 W135 cofilin with DHNBS

Prior to labelling, the protein was dialysed against DHNBS buffer (100 mM NaCl, 20 mM Na-PO_4, pH 7.0) and DHNBS was dissolved in ddH_2O. Cofilin W104 was then labelled with a 20x molar excess of DHNBS at room temperature for 10 minutes on a rocker. The reaction was stopped with 1 mM DTT and was dialysed exhaustively against appropriate buffers to remove any excess fluorophore probes.

Labelling G-actin Cys374 with DABMI

DTT treated G-actin (incubate G-actin with 10 mM DTT for 4 hours on ice, then dialyse against G-buffer) was incubated with a 2 molar excess of DABMI overnight at 4^{o}C. Following the incubation, the protein was dialysed exhaustively against G-buffer to remove excess probes.

Labelling G-actin with IAEDANS

Prior to labelling, G-actin was dialysed against G-buffer containing no DTT and IAEDANS was dissolved in either DMF or DMSO. G-actin was then polymerised to F-actin by adding 50 mM KCl and 2 mM $MgCl_2$ for 1 hour on a rocker. Once the actin had been polymerised, it was incubated with a 7 molar excess of IAEDANS at room temperature for an hour and the reaction was stopped with 1 mM DTT. The solution was centrifuged at 100,000 xg for 90 minutes at 15^{o}C. The pellet, which contains F-actin, was dissolved in G-buffer and dialysed exhaustively against G-buffer to remove any excess fluorophores. IAEDANS is a light sensitive fluorophore, hence the labelled samples were covered by foil at all times to prevent exposure to light, subsequently preventing photobleaching of the fluorophore.

Labelling G-actin with εATP

Labelling of the nucleotide-binding site of G-actin with εATP was carried out as described by Miki et al (Miki, dos Remedios et al. 1987). Free ATP was removed from non-labelled G-actin by treating with 0.1 volumes of Dowex-1 by filtration at 0^{o}C for 10 minutes. Immediately after removing Dowex-1 by filtration, the actin solution was incubated with 0.5 mM εATP, 0.1 mM $CaCl_2$ and 1 mM Tris HCl, pH 8.0 and left overnight at 0^{o}C. This process was repeated again to ensure a complete replacement of bound ATP with εATP. Just before fluorescene measurements, free εATP were removed by another treatment with Dowex-1. Actin containing εATP was used in fluorescence experiments within one day of the final Dowex-1 treatment.

6.2.7. Binding interaction of Cofilin and its mutants with actin

6.2.7.1. Binding interaction of Cofilin and its mutants with G-actin

Native cofilin and its mutants were incubated with G-actin at room temperature for 1 h at equimolar concentration, unless otherwise stated. Upon completion of the binding, the samples were analysed by native-PAGE (non-denaturing gel) according to Section 2.2.3.

6.2.7.2. Binding interaction of N6-cys-cofilin with F-actin

The binding of N6-cys-cofilin to F-actin was examined by ultracentrifugation. G-actin (50 μM) was polymerised by addition of 0.1 M KCl and 5 mM $MgCl_2$ for 1 h at room temperature. The resultant F-actin solution was incubated with IAF-cys-cofilin (70 μM) for 10 min. The F-actin / cys-cofilin mixture was sedimented at 100,000 × g for 10 min and the resultant pellet was analysed by SDS-PAGE. SDS-PAGE was performed as described for native-PAGE with two important modifications: 1) 0.1% SDS was included in all buffers; and 2) protein samples were boiled for 10 minutes prior to electrophoresis. IAF-cys-cofilin was immediately visualised following electrophoresis using a UV-302 nm transilluminator (UVItec Limited, Cambridge, England). This was followed by Coomassie blue staining as described above.

6.2.8. Circular Dichroism (CD) Spectroscopy

Samples were prepared for CD spectroscopy by dialysis for 48 h at 4°C against CD buffer (10 mM Na-PO_4, pH 7.0, 30 mM NaF) with a change in dialysate after 24 h. Samples were diluted to 0.1 mg ml^{-1} in CD buffer and analysed using a Jasco J-720 CD spectropolarimeter (Jasco, Tokyo, Japan) calibrated with a known ammonium-D-camphor-10-sulphonic acid (CDA) reference standard. Protein samples were analysed in a 0.1 cm pathlength quartz cuvette, using a temperature regulated cuvette holder in a N_2 atmosphere. Four samples were collected over the range 260-190 nm using the following spectral parameters: resolution 0.2 nm, band width 1 nm, sensitivity 10 mdeg, response time 1 s and scan rate 20 nm min^{-1}.

Mean residue weight ellipticity (MRE) was calculated from raw ellipticity values using the following equation:

$$[\theta]_{MRE} = ([\theta] \times 100 \times MRW) / c \times d$$

Where [θ] is the baseline corrected ellipticity, MRW is the mean residue weight, *c* is the concentration of protein in mg ml^{-1}, and *d* is the optical pathlength in cm. $[\theta]_{MRE}$ has the units 10^{-3} × deg cm^2 $dmol^{-1}$. CD spectra were de-convoluted using CDSSTR, an online circular dichroism analysis program available from DichroWeb Department of Crystallography, University of London http://www.cryst.bbk.ac.uk/cdweb/html/home.html (Whitmore and Wallace 2004). Reference data set #4, incorporating 43 known protein spectra was used as it covered the relevant wavelength range

(Provencher and Glockner 1981, Pancoska and Keiderling 1991, Bonne, Carrier et al. 1995, Sreerama, Venyaminov et al. 1999).

6.2.9. Fluorescence Resonance Energy Transfer (FRET) Spectroscopy

FRET is a biophysical measurement that can be used to convert fluorescence measurements into distances. This method requires two probes: a donor and an acceptor, attached to specific loci on the molecule. Once the probes are attached, fluorescence occurs when the excited donor transfers some of its energy to the acceptor, which then emits energy at its own emission wavelength.

FRET experiments in this chapter were performed using Shimazu UV3600 steady-state photon counting fluorimeter, operated in the ratio mode. Samples were placed in 1 cm path quartz cuvettes at a concentration of 10 μM. The fluorescence emission spectra were recorded from 350 nm to 600 nm. The transfer of energy or quench was monitored at the emission maxima for each of the respective donor probes listed in Table 6.3. The emission spectra were plotted using Jandel Sigmaplot (V. 5.0). R_0 is the distance that corresponds to 50% quench of the donor fluorescence by the acceptor molecule. R_0values used were obtained from published data (Table 6.3), except for the probe pair ε-ATP and HNB. The overlap intergral for the probe pair ε-ATP – HNB was calculated from our absorption spectrum of HNB bound to cofilin and our fluorescence emission spectrum of ε-ATP bound to actin. The quantum yield (F_D) of G-actin labelled with ε-ATP was taken to be 0.8 (Miki, dos Remedios et al. 1987, Shaffer, Kensler et al. 2009). The overlap intergral was calculated as previously described (Palm, Sale et al. 1999).

Table 6.3. FRET spectroscopy parameters for probe pairs used.

Donor/ acceptor pairs label sites	Probe	Excitation maxima (Ex λ)	Emission maxima (Em λ)	R_o	Reference
Cof W104 (Donor)	Intrinsic W	280	340	24.2	(Boey, Huang et al. 1994)
Cof C170 (Acceptor)	IAEDANS				
Cof C170 (Donor)	IAEDANS	340	470	28.4	(Boey, Huang et al. 1994)
Cof W104 (Acceptor)	HNB				
Cof C170 (Donor)	IAEDANS	340	470	38	(Palm, Sale et al. 1999)
G-actin C374 (Acceptor)	DABMI				
G-actin C374 (Donor)	IAEDANS	340	470	28.4	(Boey, Huang et al. 1994)
Cof W104 (Acceptor)	HNB				
G-actin ATP (Donor)	ε-ATP	340	470	37.6	N/A (calculated by the author)
Cof W104 (Acceptor)	HNB				

6.3. Results

6.3.1. Cofilin Mutants: DNA Sequencing

The correct DNA sequence of cofilin mutants was confirmed by the DNA sequencing method described in section 2.4.6. This DNA sequencing confirmed successful mutagenesis.

6.3.2. Protein Expression

Once the DNA sequence was confirmed, its protein was expressed according to the method described in Section 6.2.4. Post-induction samples were taken at various time points to optimise the protein expression. These samples were then analysed using SDS-PAGE and an example is shown in Figure 6.1. Figure 6.1 shows an example of expression of native cofilin protein at various time points post-induction. The first lane contains molecular weight marker (MW) with the various weight markers labelled, then 0-4 represents number of hours after induction with IPTG. The cofilin is expressed as a fusion protein with GST, hence a molecular weight of approximately 47 kDa. The most intense band of cofilin protein expression was at 4 hours post induction, thus representing the optimal cofilin protein expression. Gels of other mutants showed similar expression profiles.

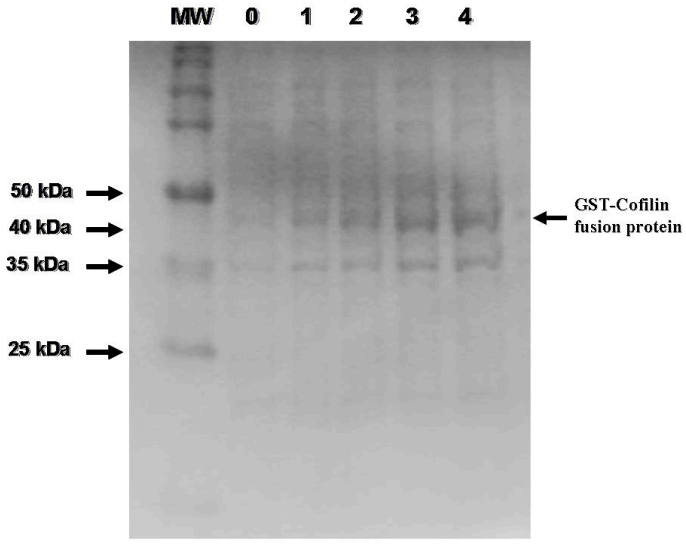

Figure 6.1. Expression of native cofilin. MW represents molecular weight marker with various molecular sizes labelled. Lanes 0-4 contain total cell protein samples taken at 0, 1, 2, 3 and 4 hours, respectively, post-induction of native cofilin. The most strongly expressed native cofilin protein (~47 kDa) is shown at 4 hours post-induction.

6.3.3. Protein Purification

All expressed cofilin samples, including native and its mutants were purified using a glutathione Sepharose 4B column, as described in Section 6.2.5. Samples were taken at various points for analysis using SDS-PAGE and an example of this is presented in Figure 6.2, with purified native cofilin labelled (lanes 5 and 6). Purification of other cofilin mutants generated a similar outcome.

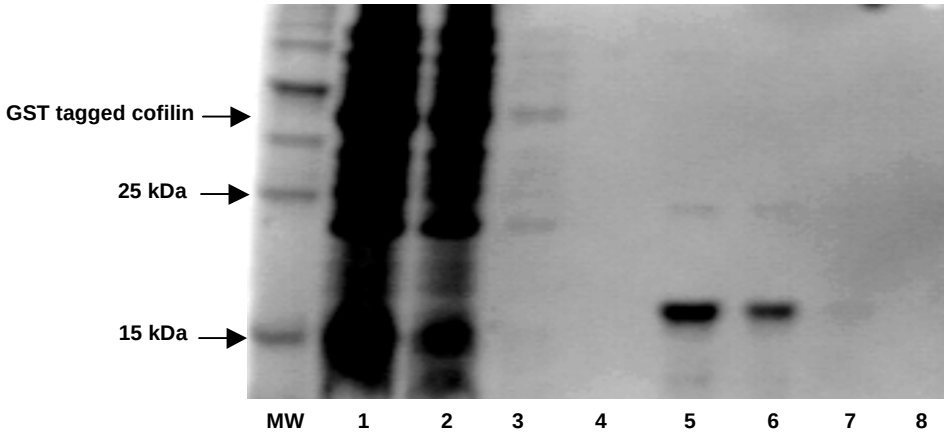

Figure 6.2. Purification of native cofilin. MW represents molecular weight markers. Lane 1 represents native cofilin protein sample before purification. Lane 2 contains run-through of the column. Lanes 3, 4, 7 and 8 represent samples obtained during wash phase of the column and lanes 5 and 6 shows the purified native cofilin protein (20 kDa).

6.3.4. Analysis of interaction between N6-cys-cofilin and G-actin

Native gel electrophoresis was used to determine the binding of native and mutant analogues of cofilin to G-actin. The advantage of using native gel electrophoresis is that the protein samples are not denatured, and hence when a protein complex is formed, the protein complex remains intact. The disadvantage of using native gel electrophoresis is that the direction and extent of migration of individual proteins and protein complexes is dependent on the net positive or negative charge of the complex under the running buffer conditions of the gel, in addition to its overall size. Thus, it can be difficult to predict the migration of a particular protein, so consequently the actual migration of a particular protein often has to be observed empirically.

Figure 6.3 shows a polyacrylamide gel run under non-denaturing conditions demonstrating the interactions of actin with native cofilin and with N6-cys-cofilin. Lane 1 contains 150 picomoles actin. Monomeric actin is seen as an intensely stained band running near the bottom of the gel. A small number of lighter staining bands are seen running above the G-actin band, probably corresponding to short oligomers of actin. Lane 2 contains 110 picomoles native cofilin. Due to the high isoelectric point of cofilin (≈ 8.0), the protein possesses a low net charge under the running conditions (pH = 8.3). Consequently, cofilin migrated relatively slowly and is seen as a light-staining band near the top of the gel. Lane 3 contains 70 picomoles N6-cys-cofilin. The addition of six residues at the N-terminus of cofilin has resulted in a slight shift in its migration. N6-cys-cofilin is observed as a light-staining band running slightly above native cofilin. Lane 4 contains a mixture of G-actin (150 picomoles) and native cofilin (110 picomoles). This results in formation of a new, intensely stained band comprising the native cofilin-actin complex. This correlates with removal of the isolated native cofilin band. Lane 5 contains a mixture of actin (150 picomoles) and N6-cys-cofilin (70 picomoles). The bands in this lane correspond to the sum of bands in lanes 1 and 3. In other words, no new bands are formed and no existing bands removed suggesting that monomeric actin and N6-cys-cofilin do not participate in formation of a complex. Lane 6 contains a mixture of actin (150 picomoles), native cofilin (110 picomoles) and N6-cys-cofilin (70 picomoles). The presence of N6-cys-cofilin has no effect on the interaction between actin and native cofilin.

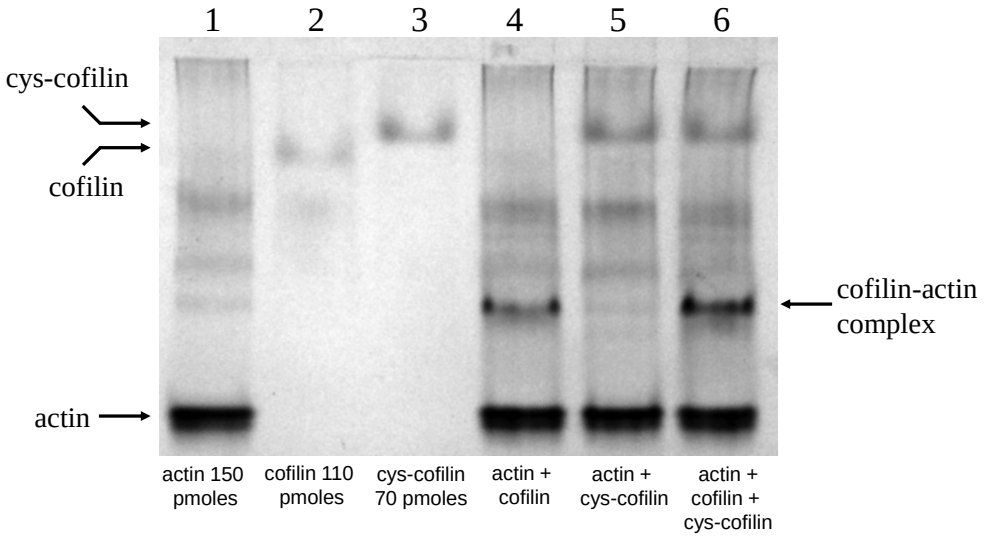

Figure 6.3. Non-denaturing polyacrylamide gel showing the interaction between G-actin, native cofilin and/or N6-cys-cofilin. Lane 1: actin (150 picomoles); Lane 2: native cofilin (110 picomoles); Lane 3: N6-cys-cofilin (70 picomoles); Lane 4: G-actin (150 picomoles) plus native cofilin (110 picomoles); Lane 5: actin (150 picomoles) plus N6-cys-cofilin (70 picomoles); Lane 6: actin (150 picomoles) plus native cofilin (110 picomoles) plus N6-cys-cofilin (70 picomoles). Electrophoresed at pH 8.3; stained with Coomassie Blue.

6.3.5. Analysis of interaction between N6-cys-cofilin and F-actin

Figure 6.4 shows a co-sedimentation assay of F-actin and IAF-N6-cys-cofilin upon (A) Coomassie blue staining and (B) UV transillumination. Panel A shows the migration of molecular weight standards (lane 1) and total protein in the pellet (lane 2); Panel B shows the presence of IAF-N6-cys-cofilin in the pellet. Co-sedimentation of F-actin and IAF-N6-cys-cofilin demonstrates the capacity of IAF-N6-cys-cofilin to bind to actin in its filamentous form.

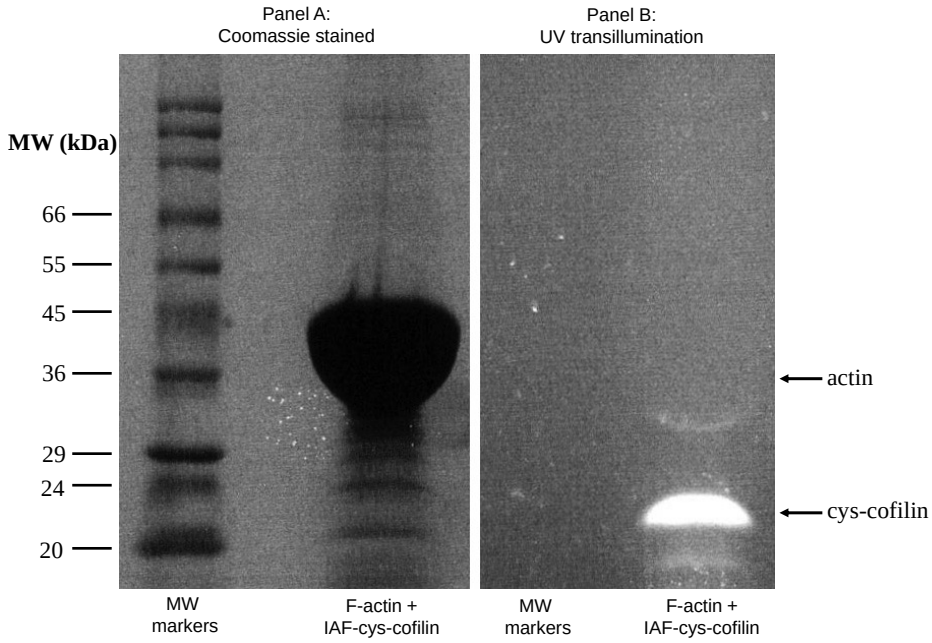

Figure 6.4. Co-sedimentation assay of F-actin and IAF-N6-cys-cofilin. Panel A: Coomassie blue staining; Lane 1: Molecular weight standards; Lane 2 total protein pellet after centrifugation of a mixture of F-actin and IAF-N6-cys-cofilin; Panel B: UV transillumination; Lanes are the same as in Panel A.

6.3.6 Circular dichroic spectroscopy of native and N6-cys-cofilin

The secondary structures of native cofilin and N6-cys-cofilin were investigated by circular dichroism (CD) spectroscopy.

The CD spectrum of native cofilin (Figure 6.5 – green trace) suggests the presence of both α-helical and β-strand contents. The negative intensities at 208 nm and 217 nm are indicative of α-helix and β-strand, respectively. The positive intensity at 193 nm is due to the presence of both α-helix (maximum intensity at 190 nm) and β-strand (maximum intensity at 195 nm). Upon de-convolution, the spectra yields 13% α-helix, 32% β-strand, 26% turns and 29% random coil with root mean square deviation (RMSD) of 0.069, where values less than 0.1 are considered reliable (Whitmore and Wallace 2004).

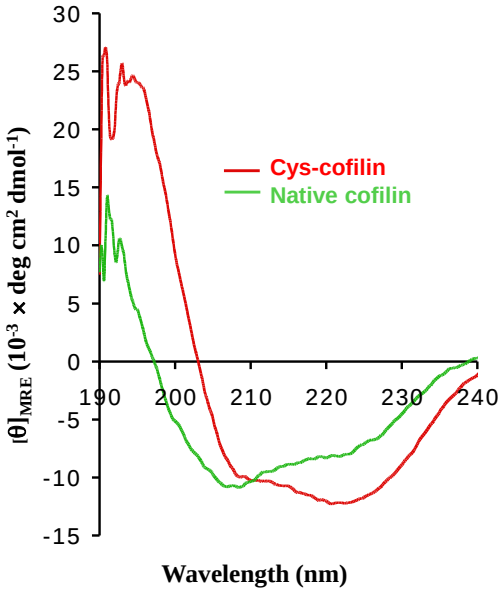

Figure 6.5. CD spectroscopy of native cofilin and N6-cys-cofilin. Green trace represents native cofilin and red trace represents N6-cys-cofilin.

The secondary structural content of N6-cys-cofilin was investigated in a similar manner (Figure 6.5 – red trace). When compared to the native cofilin spectrum, there is an increase in negative mean residue ellipticity at 220 nm, suggesting an increase in α-helical content for N6-cys-cofilin (58% compared to 13%). Likewise, an increase in positive mean residue ellipticity at 193 nm suggests an increase in the sum of α-helical and β-strand contents (77% compared to 45%). Upon de-convolution, the N6-cys-cofilin spectrum yields 56% α-helix, 21% β-strand, 2% turns and 20% random coil with RMSD of 0.002.

6.3.7. Binding Interactions between cofilin mutants and G-actin

Native gel electrophoresis was used to determine the binding of native and mutant analogues of cofilin to G-actin. As mentioned in Section 6.3.4., cofilin has severely limited mobility in the native gel electrophoresis used in this chapter and either does not enter or barely enters the native electrophoretic gel. Cofilin has a high pI (~8.0) and thus a very low net charge under the running conditions. In the case of this series of binding studies, part of cofilin did not enter the polyacrylamide running gel. The cofilin–actin complex is the dark-staining band that migrates essentially as reported previously (Chhabra, Nosworthy et al. 2005).

Figure 6.6 shows the electrophoretic mobility of G-actin, native cofilin, cofilin mutants and various cofilin - G-actin complexes. G-actin is clearly shown in lane 1 quite contrary to native cofilin and its mutants (from lanes 2-5) where the samples were barely able to enter the gel. When native cofilin and G-actin were added together (lane 6), a new band is observed corresponding to the cofilin – G-actin binary complex. Similarly, Cys170 cofilin – G-actin (lane 7) and Cys170 W104 cofilin – G-actin (lane 8) complexes produce new bands corresponding to these binary complexes. Note that these samples also produced a band corresponding to G-actin, suggesting unbound G-actin. Lastly, lane 9 represents the Cys170 W135 cofilin and G-actin interaction. The lack of a band corresponding to the cofilin – G-actin binary complex suggests that this mutant does not bind to G-actin.

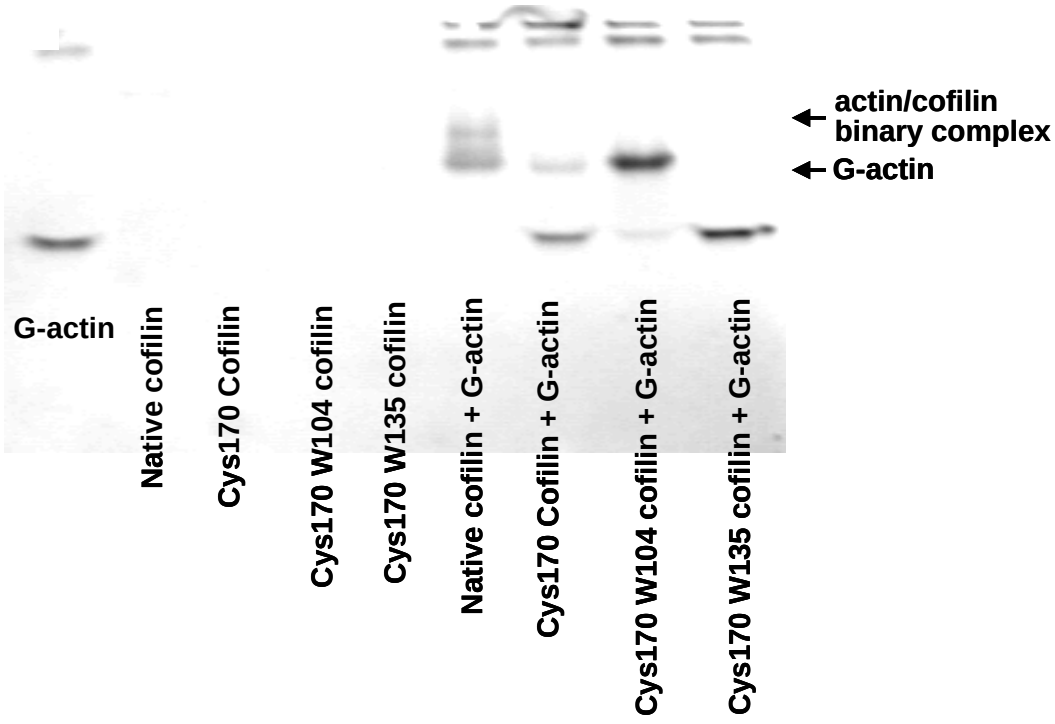

Figure 6.6. Binding assay of unlabelled native cofilin and its mutants with G-actin.

6.3.8. Fluorophores Labelled Cofilin/Actin Binding Assay

Modification of either cofilin or its mutants and/or G-actin with fluorescent probes could impair or abolish binding between these two proteins. Consequently, we tested this binding using native gel electrophoresis, as described above. In all cases,

labelling had no effect on binding. An example of a binding study using labelled cofilin and labelled actin is shown in Figure 6.7. In this figure, lanes 1 and 6 show the large mobility of DABM-labelled G-actin, lanes 2 and 7 show that labelled cofilin does not enter the gel, lanes 3-5 show the binding of Cys170-cofilin labelled with IAEDANS (at increasing molar ratios) to DABMI labelled G-actin and lanes 8-10 show the binding of Cys170-W104 cofilin labelled with HNB (at increasing molar ratios) to DABMI labelled G-actin.

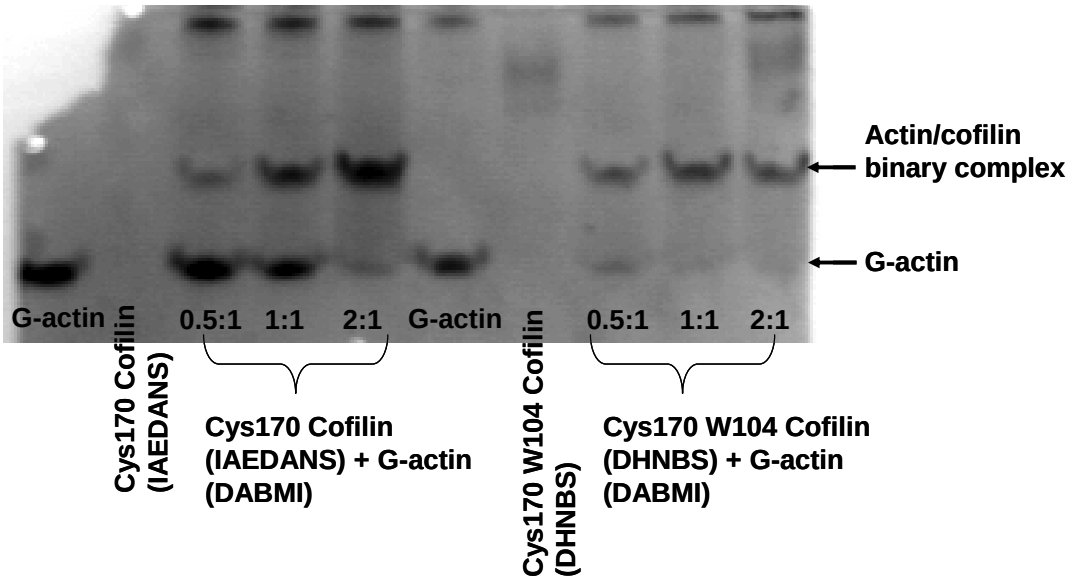

Figure 6.7. Binding assay of labelled mutants with G-actin.

6.3.9. FRET spectroscopy

Five distance measurements were performed using the labelled protein samples in various combinations.

Cys 170 cofilin to Cys170 W104 Cofilin

This distance was measured using 2 sets of probe pairs:

1. Cys170 cofilin labelled with IAEDANS as the acceptor, using the intrinsic fluorescence of the single W104, i.e. Cys170 W104 cofilin mutant, where W135 had been mutated into phenylalanine.
2. Cofilin Cys170 labelled with IAEDANS as the donor, using the single W104 residue on Cys170 W104 cofilin mutant labelled with HNB as the acceptor.

The donor fluorescence emission spectra for the intrinsic tryptophan fluorescence of the Cys170 W104 cofilin mutant and the absorption spectra for Cys170 cofilin +IAEDANS are shown in Figure 6.8. The donor fluorescence emission spectra for cofilin C170+IAEDANS and the absorption spectra for cofilin Trp104+HNB are shown in Figure 6.9.

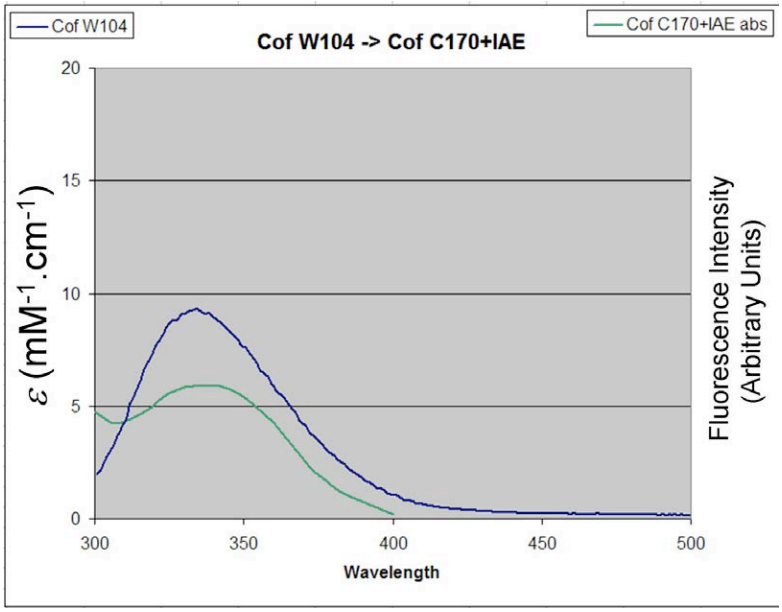

Figure 6.8. The intrinsic tryptophan fluorescence of the cys170 W104 cofilin and Cys170 cofilin (IAEDANS).

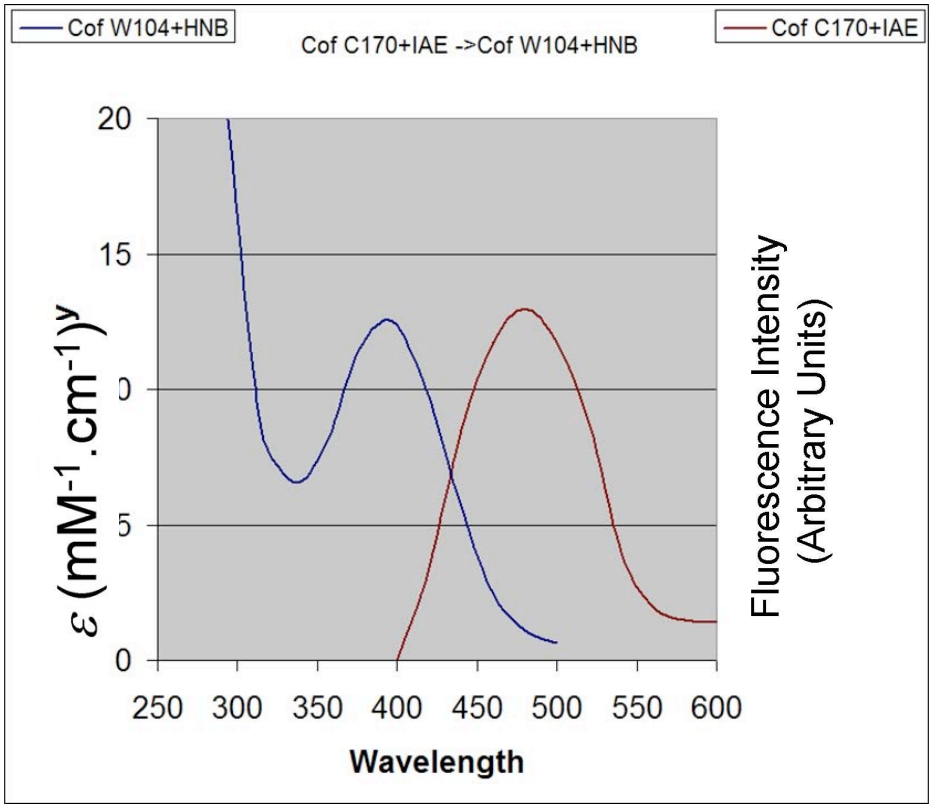

Figure 6.9. The donor fluorescence emission spectra for Cys170 cofilin and the absorption spectra for Cys170 W104 Cofilin (DHNBS).

To measure the distance between the various extrinsic probe pairs, the fluorescence emission of the donor was measured in the absence or presence of the acceptor, using a cofilin concentration of 5 μM. Figure 6.10 shows the intrinsic fluorescence intensity of the single Trp 104 of cofilin, excited at 280 nm, in the absence and presence of the acceptor IAEDANS bound to cofilin Cys 170. The extent of acceptor labelling was 76%. After correction for the extent of IAEDANS labelling the efficiency of transfer (E) was calculated to be 0.87. Note that an additional fluorescent peak can be seen at 470 nm in the IAEDANS-labelled sample, which corresponds to the IEADANS fluorescence as a result of FRET between the donor Trp and the IAEDANS acceptor.

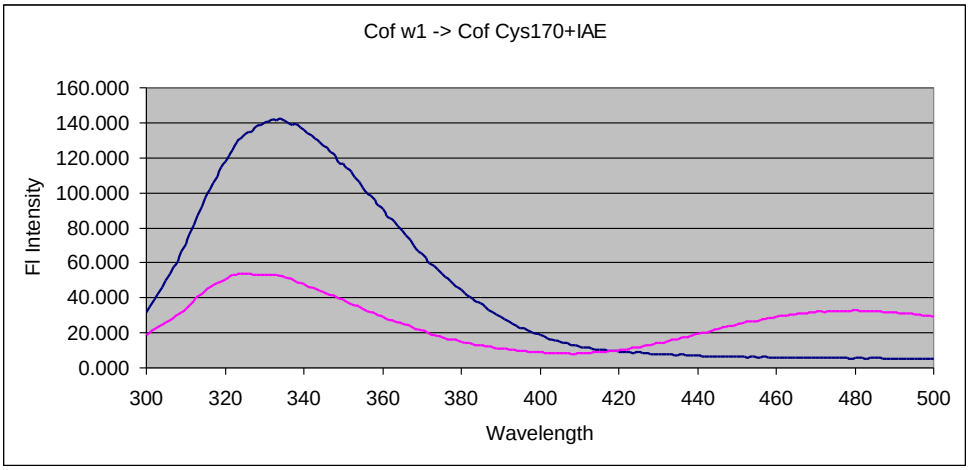

Figure 6.10. The intrinsic fluorescence intensity of the single W104 of cofilin, excited at 280 nm, in the absence and presence of the acceptor IAEDANS bound to Cys170 cofilin. Blue curve is the single W104 of Cys170 W104 cofilin sample being excited at 280 nm in the absence of the acceptor bound to Cys170 cofilin. Pink curve is single Cys170 W104 Cofilin excited at 280 nm in the presence of acceptor bound to Cys170 cofilin.

Figure 6.11 shows the fluorescence emission of IAEDANS bound to Cys170 of cofilin, in the absence and presence of the acceptor label HNB bound to W104. The extent of labelling of the IAEDANS was 100% and of the HNB was 71%. After correction for the extent of labelling, the efficiency of transfer was determined to be 0.94.

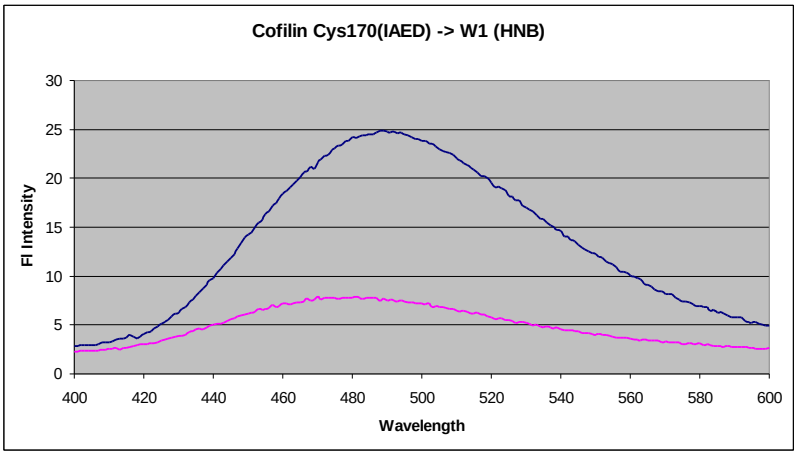

Figure 6.11. The fluorescence emission of IAEDANS bound to Cys170 cofilin in the absence and presence of the acceptor label HNB to Trp 104 of Cys170 W104 cofilin. Blue curve is 5 μM C170-IAEDANS cofilin (76% labelled) to Cys170 W104 cofilin. Pink curve is 5 μM Cof C170-IAEDANS (100% labelled) to Cys170 W104 cofilin-HNB (71% labelled).

Table 6.4 summarises the fluorescence data for these two experiments. Assuming a R_o of 28.4 Å, the measured distances were calculated to be 21 Å using the intrinsic Trp fluorescence as the donor, and 18.1 Å using IAEDANS as a donor.

Cofilin Cys 170 to G-actin Cys 374

This distance was measured using the following probe pair: Cys170 cofilin labelled with IAEDANS as the donor, and G-actin labelled at Cys 374 with DABMI as the acceptor. The donor fluorescence emission spectra for the Cys170 cofilin labelled with IAEDANS and the absorption spectra for G-actin labelled at Cys 374 with DABMI are shown in Figure 6.12.

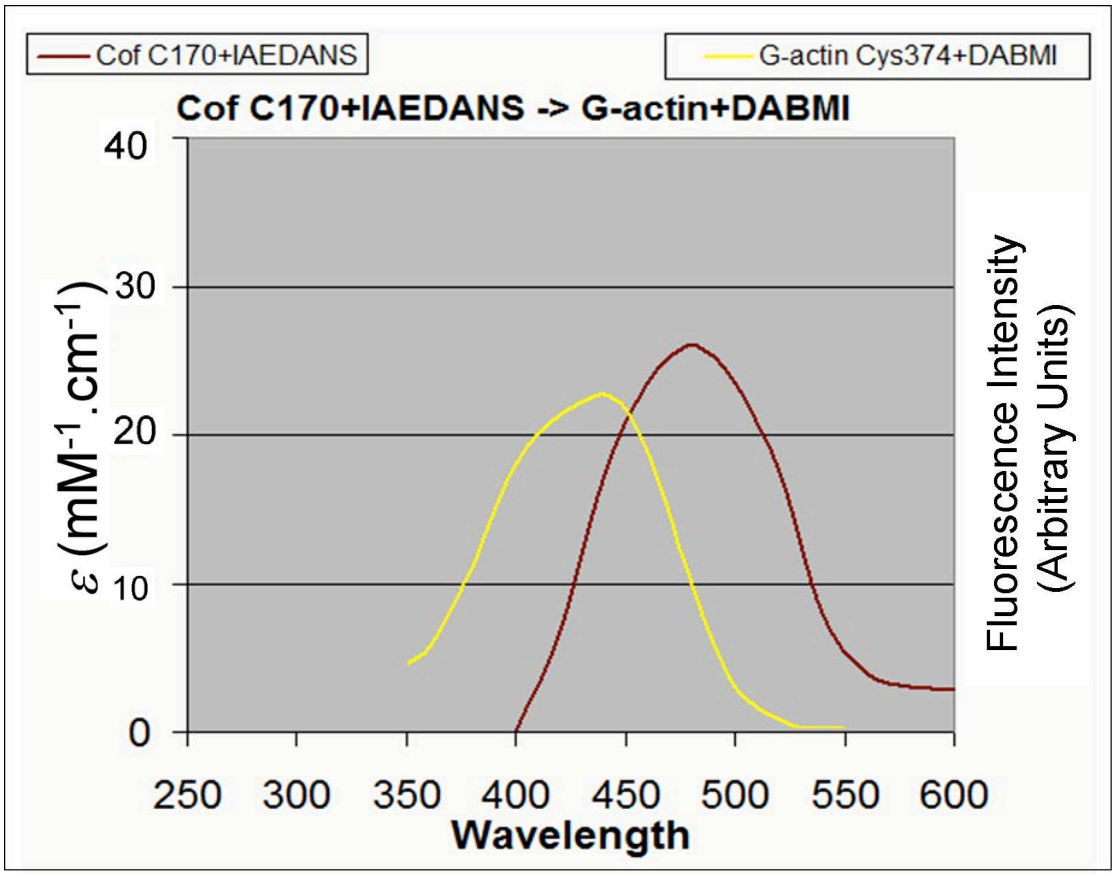

Figure 6.12. The donor fluorescence emission spectra for the Cys170 cofilin labelled with IAEDANS (red) and the absorption spectra for G-actin labelled at Cys 374 with DABMI (yellow).

To measure the distance between these two extrinsic probes, the fluorescence emission of the donor was measured in the absence or presence of the acceptor, using a fixed cofilin concentration of 5 μM and increasing concentrations of G-actin

Cys374+DABMI, ranging between 10 – 20 µM G-actin. A 2-4 fold excess of G-actin over cofilin was used, to ensure that all cofilin was bound to a G-actin molecule.

Figure 6.13 shows the fluorescence emission of IAEDANS bound to Cys170 cofilin, in the absence and presence of the acceptor label DABMI bound to G-actin Cys374+DABMI. Note that substantial quench is observed after the addition of a 2 fold molar excess of actin, with only a small additional quench observed after the addition of a 4 fold molar excess of actin, indicating that essentially all cofilin molecules had bound to G-actin at these concentrations. The extent of labelling of the DABMI on actin was 75%. After correction for the extent of labelling, the efficiency of transfer was determined to be 0.69.

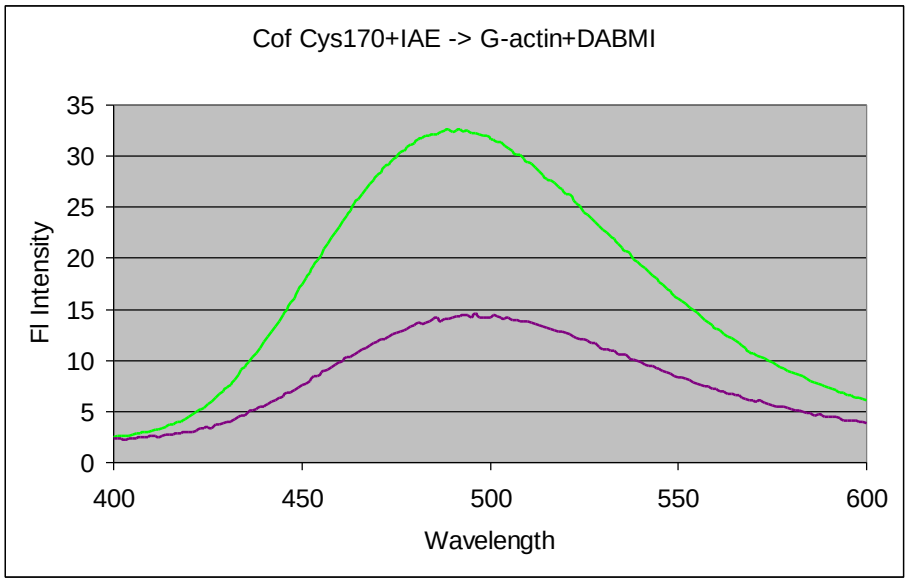

Figure 6.13. The donor fluorescence emission spectra for the Cys170 cofilin labelled with IAEDANS in the absence and presence of G-actin labelled at Cys 374 with DABMI. Green curve is 5 µM cof Cys170 cofilin IAEDANS and purple curve is 5 µM cof Cys170 cofilin IAEDANS + 20µM G-actin DABMI.

Table 6.4 summarises the fluorescence data for this experiment. Assuming a R_o of 38 Å, the measured distances were calculated to be 33.2 Å.

Cys170 W104 Cofilin to G-actin Cys 374

This distance was measured using the following probe pair: G-actin labelled at Cys 374 with IAEDANS as the donor, and W104 labelled with DHNBS as the acceptor. The donor fluorescence emission spectra for the G-actin Cys374 labelled

with IAEDANS and the absorption spectra for cofilin labelled at W104 with DHNBS are shown in Figure 6.14.

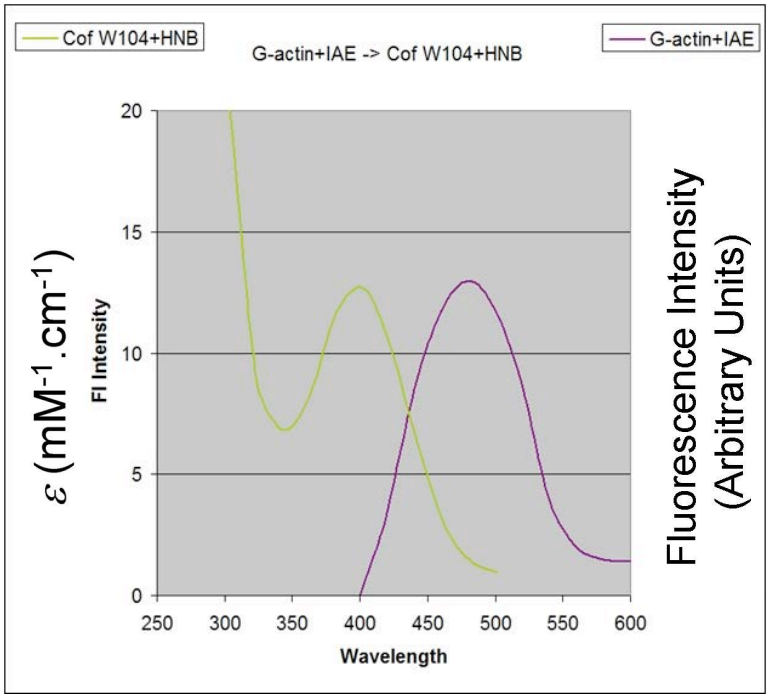

Figure 6.14. The donor fluorescence emission spectra for the G-actin Cys374 labelled with IAEDANS and the absorption spectra for cofilin labelled at W104 with HNB.

To measure the distance between these two extrinsic probes, the fluorescence emission of the donor was measured in the absence or presence of the acceptor, using a G-actin concentration of 5 μM and a 4 fold molar excess (20 μM) of cofilin W104+HNB, to ensure that all G-actin molecules were bound to a cofilin.

Figure 6.15 shows the fluorescence emission of IAEDANS bound to Cys374 of G-actin, in the absence and presence of the acceptor label HNB bound to cofilin W104. Substantial quench is observed after the addition of a 4 fold molar excess of cofilin. The extent of labelling of the HNB on cofilin was 78%. After correction for the extent of labelling, the efficiency of transfer was determined to be 0.6.

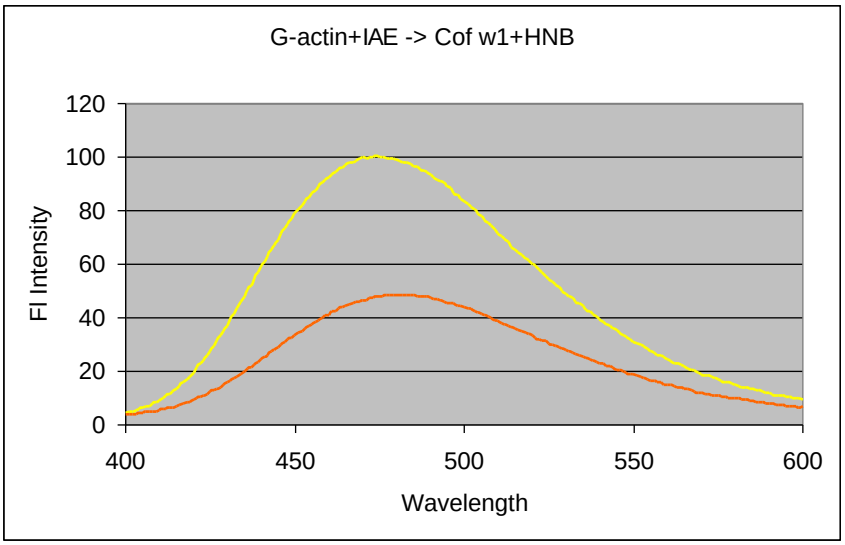

Figure 6.15. The fluorescence emission of IAEDANS bound to Cys374 of G-actin, in the absence and presence of the acceptor label HNB bound to W104 of Cys170 W104 cofilin. Yellow curve represents 5 µM G-actin IAEDANS and orange curve represents 5 µM G-actin IAEDANS + 20 µM Cys170 W104-HNB cofilin.

Table 6.4 summarises the fluorescence data for this experiment. Assuming a R_o of 28.4 Å, the measured distances were calculated to be 27.9 Å.

Cys170 W104 Cofilin to G-actin nucleotide (ATP) site

This distance was measured using the following probe pair: G-actin labelled at the nucleotide site with ε-ATP as the donor, and Cys170 W104 cofilin labelled with HNB as the acceptor. The donor fluorescence emission spectra for the G-actin ε-ATP and the absorption spectra for cofilin labelled at Trp104 labelled with HNB are shown in Figure 6.16.

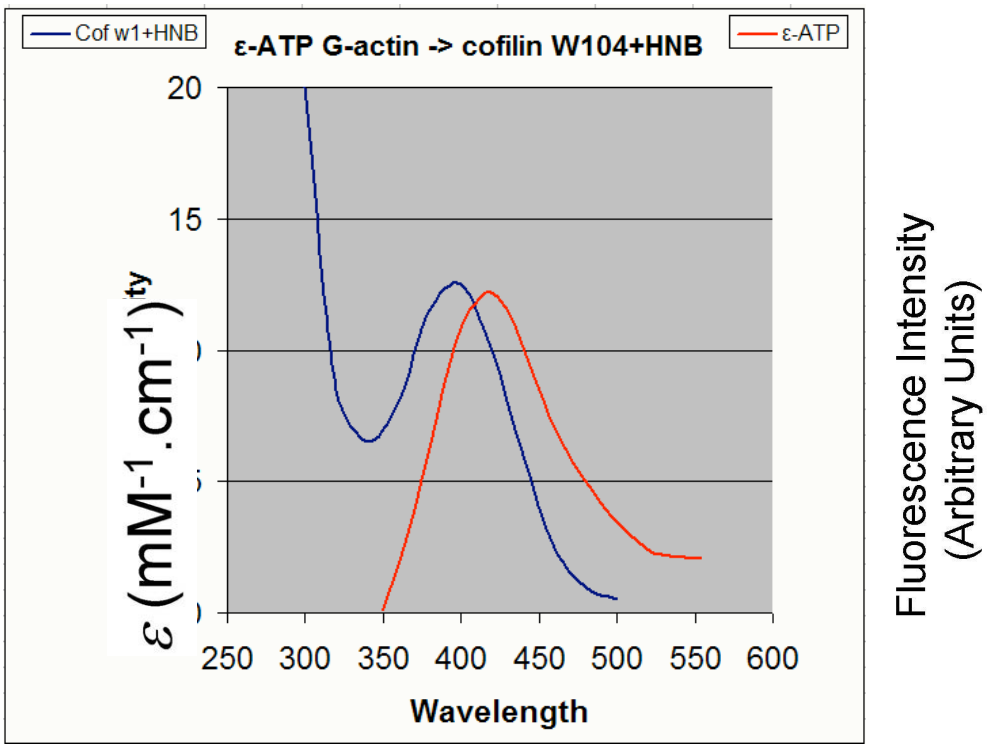

Figure 6.16. The donor fluorescence emission spectra for G-actin ε-ATP and the absorption spectra for cofilin labelled at W104 with HNB.

To measure the distance between these two extrinsic probes, the fluorescence emission of the donor was measured in the absence or presence of the acceptor, using a G-actin concentration of 1 μM and a 2-4 fold molar excess (2-4 μM) of Cys170 W104 cofilin+HNB, to ensure that all G-actin molecules were bound to a cofilin.

Figure 6.17 shows the fluorescence emission of ε-ATP bound to G-actin, in the absence and presence of the acceptor label HNB bound to W104. Substantial quench is observed after the addition of both 2 and 4 fold molar excess of cofilin. The extent of labelling of the HNB on cofilin was 70%. After correction for the extent of labelling, the efficiency of transfer was determined to be 0.65.

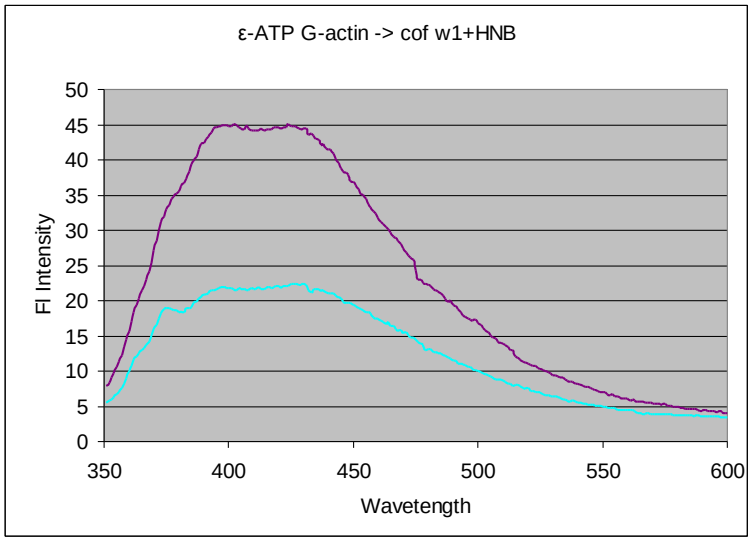

Figure 6.17. The fluorescence emission of ε-ATP bound to G-actin, in the absence and presence of the acceptor label HNB bound to W104 of Cys170 W104 cofilin. Purple curve represents 1 μM G-actin ε-ATP + 2 μM Cys170 W104 cofilin and bright blue curve represents 1 μM G-actin ε-ATP + 4 μM Cys170 W104 cofilin.

Table 6.4 summarises the fluorescence data for this experiment. Assuming a R_o of 37.6 Å, the measured distances were calculated to be 33.9 Å.

Table 6.4. Summary of distance measurements obtained using FRET spectroscopy.

Site	Probe	Label Ratio	Excitation maxima (Ex λ)	Emission maxima (Em λ)	E corr	R_o	R (2/3)	Galkin model distance
Cof W104	Intrinsic	1	280	340	0.87	24.2	17.6	Unknown
Cof C170	IAEDANS	0.76	Nil	Nil				
Cof C170	IAEDANS	0.76	340	470	0.94	28.4	18.1	Unknown [W104 to E151=18A]
Cof W104	HNB	0.71	Nil	Nil				
Cof C170	IAEDANS	0.76	340	470	0.69	38	33.17	Unknown [Actin C374 to cofilin E151 (α6 helix)=32 A]
G-actin C374	DABMI	0.75	Nil	Nil				
G-actin C374	IAEDANS	0.95	340	470	0.6	28.4	27.9	30.6
Cof W104	HNB	0.78	Nil	Nil				
G-actin ATP	ε-ATP	0.2	340	470	0.65	37.6	33.9	31.6
Cofilin W104	HNB	0.7	Nil	Nil				

6.4 Discussion

6.4.1 Summary of results

We were able to successfully mutate and express four mutant cofilins, that each contained unique spectroscopic probe sites. We were hampered in this process by the apparent sensitivity of the structure of cofilin to mutagenesis. Thus, we found

that mutagenesis of the N-terminus abolished G-actin binding, while still permitting F-actin binding. On the other hand, mutation of the C-terminus of cofilin and W135 had no effect on the binding of cofilin to G-actin, while mutation of W104 abolished G-actin binding. Fortunately, the mutant forms of cofilin that retained binding to G-actin (Cys170 cofilin and Cys170 W104 cofilin) retained their capacity to bind to G-actin after modification with extrinsic spectroscopic probes, allowing us to measure one distance within cofilin and three distances between cofilin and G-actin. The distances between cofilin and G-actin corresponded closely to the predicted distances from the Galkin model (Table 6.4).

6.4.2 Perturbation of actin-cofilin binding by mutagenesis of cofilin

Cofilin is believed to bind to F-actin via two sites. The upper actin monomer binds to cofilin at the G/F-actin binding site, spanning subdomains 1 and 3 of actin, whereas the cofilin F-actin binding site binds the lower actin and spans actin subdomains 1 and 2 (McGough and Chiu 1999) (Figure 6.18). The two cofilin-F-actin binding sites are located at opposite ends of the long axis of cofilin (McGough and Chiu 1999, Pope, Zierler-Gould et al. 2004).

The G/F-actin binding site is located within the half of cofilin that includes the mobile N-terminus (Pope, Zierler-Gould et al. 2004) and consists primarily of residues located within the long, kinked α4 helix, with contributions from residues located in the β1 strand near the N-terminus and within β6, the intervening loop and α5 (Figure 6.19).

The F-actin binding site, located at the opposite end of cofilin, involves residues from the N-terminal segment of the β5 strand and the α6 helix, with a contribution from the adjacent C-terminal residues (Pope, Zierler-Gould et al. 2004).

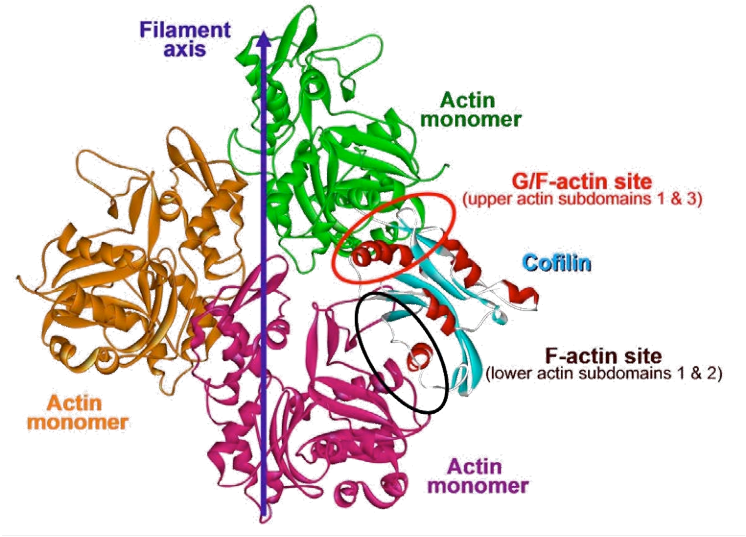

Figure 6.18. Model of cofilin binding sites on F-actin. The upper binding site is the G/F-actin binding site and binds to the green actin monomer on subdomains 1 and 3. The lower binding site is the F-actin binding site and binds to the hot pink actin monomer on subdomains 1 and 2.

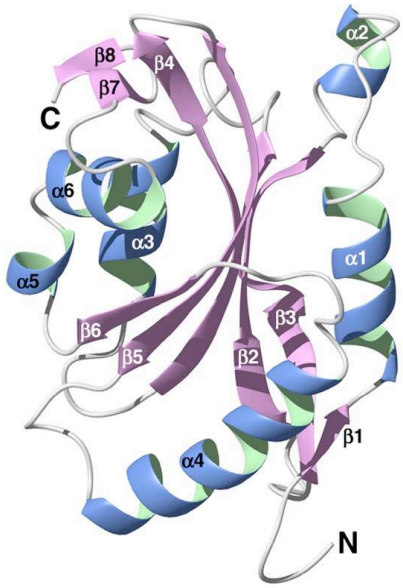

Figure 6.19. The atomic structure of cofilin. It comprises of a central six-stranded mixed β sheet, flanked by several α helices contributed by residues at the N- and C-terminus.

Phosphorylation at Ser3 in the N-terminus causes minor conformational alterations in 7 residues within α4, which forms much of the G/F-actin binding site, suggesting a structural mechanism by which phosphorylation prevents actin binding (Pope, Zierler-Gould et al. 2004, Gorbatyuk, Nosworthy et al. 2006). On the other

hand, PI binding perturbs residues located in the C-terminal part of the sequence between β6 and β8, with Lys132 and His133, adjacent to the β6 strand, being directly involved in PI binding (Gorbatyuk, Nosworthy et al. 2006). This region of cofilin overlaps both the G/F-actin and F-actin binding sites. Therefore, PI binding probably prevents actin binding by perturbing residues in both the G/F-actin and F-actin binding sites.

A model has been proposed for the mechanism by which cofilin binds to F-actin and involves cofilin first binding to a monomer within F-actin via the G/F-actin binding site. The model proposes that the C-terminal F-actin binding site is then stabilised via an allosteric conformational change, allowing cofilin to bind to the adjacent actin monomer within the filament (Ono, McGough et al. 2001, Pope, Zierler-Gould et al. 2004). This allosteric effect is thought to be mediated by the β5 strand that bridges the G/F-actin and F-actin binding sites. Thus, the model proposes that binding through the G/F-actin binding site is a pre-requisite for F-actin binding.

6.4.2.1 Mutant N6-cys-cofilin abolishes G-actin but not F-actin binding

The insertion of an N-terminal extension of six amino acids into cofilin (N6-cys-cofilin) was found to prevent binding of N6-cys-cofilin to G-actin, but not to F-actin. The N6-cys-cofilin structure also exhibited a substantial change (increase) in the secondary structure content compare to wild-type cofilin. This study is the first to demonstrate that a modification of cofilin can selectively uncouple G-actin, but not F-actin, binding. The location of the mutation within the N-terminus of cofilin confirms the importance of the N-terminus in regulating cofilin interactions with actin. We hypothesise that the uncoupling of G-actin binding from F-actin binding, by the N-terminal mutation, is due to an alteration in the structure of the G/F-actin binding site.

Several studies have shown that modifications in the F-actin binding site selectively abolish F-actin, but not G-actin, binding. A mutation at residues 95/96, located in the loop region between the β4 and β5 strands, can selectively abolish F-actin binding, while retaining G-actin binding (Pope, Zierler-Gould et al. 2004). Similarly, removal of the C-terminal region of cofilin (residues 100-166) (Boey, Huang et al. 1994) or removal of the C-terminal residue of UNC-60B (residue 152),

the nematode homologue of cofilin, (Ono, McGough et al. 2001) results in a loss of both F-actin binding and severing ability but still allows interaction with G-actin, suggesting that the C-terminus of cofilin is important for binding to F-, but not G-actin. The importance of the C terminus to the β4-β5 loop for F-actin binding is further supported by the observation that in twinfilin, which binds G-actin, but not F-actin, this loop is oriented away from the C terminus, and hence the F-actin binding surface of cofilin, rather than toward it (Paavilainen, Merckel et al. 2002).

The current model for cofilin binding to F-actin proposes that sequential binding of the G/F-actin, then the F-actin binding sites is mandatory for F-actin binding (Ono, McGough et al. 2001, Pope, Zierler-Gould et al. 2004). This model proposes that binding at the G/F-actin site induces a pre-requisite allosteric conformational change in the F-actin binding site on cofilin, possibly mediated via the β5 strand that extends the length of cofilin between the two sites. The data presented in this study, showing that F-actin binding of cofilin can be uncoupled from G-actin binding, argues against this current model. Binding to actin by the G/F binding site of cofilin may not be a pre-requisite for F-actin binding. The modification of the N-terminus of cofilin described in this study may be sufficient to alter the G/F-actin binding site, of which the N-terminus of cofilin is a part, without altering the F-actin binding site located at the other end of cofilin. This explanation also argues against a substantial pre-requisite allosteric conformational change occurring within the C-terminus of cofilin, following binding to actin via the G/F-actin binding site.

Alternatively, it is possible that the N-terminal modification selectively disrupts G/F-actin binding, while still inducing an appropriate allosteric conformational change within the C-terminus that promotes F-actin binding. Investigation of these possibilities will require atomic resolution studies to unequivocally validate a model for the structure and mechanism of cofilin binding to G- and F-actin.

In conclusion, the observation that modification of the N-terminus of cofilin can selectively uncouple G-actin binding from F-actin binding, argues against a model of cofilin binding to actin that requires sequential bind to the G/F-actin, then the F-actin binding sites. Additionally, the importance of the phosphorylatable N-terminus in the subtle regulation of cofilin binding to actin is emphasised.

6.4.2.2 Mutation of cofilin W104 abolishes G-actin binding, but mutation of W135 or the C-terminus has no effect on G-actin binding

W104 is highly conserved, being always present in cofilins from yeast to humans and the cofilin-like molecules actotrophin, coactosin and ADF (Wong and Sept 2011). On the other hand, W135 is poorly conserved, being present only in chick cofilin, and being replaced variously by Leu, Val, Ile or Phe in other isotypes and related molecules.

W104 is located at the C-terminal end of the β5 strand, which is part of the large, 5 stranded β-sheet that forms the hydrophobic core of cofilin. It is also immediately adjacent to the α4 helix, which is an essential binding element for the G/F actin binding site (Wong and Sept 2011). The α4 helix is stabilised by the underlying core β-sheet. Thus, a mutation of W104 is likely to perturb the structure of the hydrophobic core of the cofilin molecule and consequently alter the orientation, and possibly the stability, of the α4 helix.

Glu 107 is located within the loop that connects the β5 strand to the alpha4 helix and is predicted to be an actin contact point (Wong and Sept 2011).

Additionally, it has been proposed that for F-actin binding to take place an allosteric effect is thought to be mediated by the β5 strand that bridges the G/F-actin and F-actin binding sites, although the data we have presented above argues against this. Never the less, the mutation of W104, located at the C-terminal end of the β5 strand is likely to perturb any allosteric effect that may occur.

The F-actin binding site, located at the opposite end of cofilin, involves residues from the N-terminal segment of the β5 strand and the α6 helix, with a contribution from the adjacent C-terminal residues (Pope, Zierler-Gould et al. 2004). We did not observe any perturbation of binding of the C-terminal mutated cofilin. However, we only tested this cofilin for binding to G-actin, which does not involved the F-actin binding site. We expect that the C-terminal modification may interfere with F-actin binding.

6.4.3Measurement of distances within cofilin using FRET spectroscopy

We measured the distance between W104 and the mutant C-terminal Cys 170 using two sets of donor-acceptor pairs. The distances obtained were 17.6 and 18.1 Å. Since a four residue peptide that contains Cys 170 has been added to the C-terminus

of cofilin a corresponding residue is not available in the structure of cofilin. Consequently, we can only poorly predict the likely location of Cys 170, although we expect that it will be located on the surface of cofilin in the vicinity of the C-terminus. The distance obtained is consistent with this location. The distance between C-alphas of W104 and the C-terminal Leu 166 is 23.4 Å. Thus, it is likely that Cys 170 is adjacent to the α6 helix.

6.4.4. Measurement of distances between cofilin and G-actin using FRET spectroscopy

Cofilin is capable of binding to and severing F-actin, one of the most abundant and highly conserved eukaryotic proteins. The molecular mechanism by which cofilin binds to F-actin, and under appropriate conditions is able to sever F-actin, is unknown due to the absence of a high resolution atomic model of the complex of cofilin and G-actin or F-actin. A recent atomic resolution model of cofilin-F-actin proposes a possible mode of assembly of these proteins (Galkin, Orlova et al. 2011). We sought to test this model by undertaking distance measurements both within cofilin and between cofilin and G-actin.

FRET was used to measure distances between 4 loci, two located on cofilin and two on actin. Table 6.4 summarises these distances and compares them to the most recent model of cofilin bound to F-actin. Three distances were measured between cofilin and actin (and the corresponding predicted distances were):

- Actin Cys374 to cofilin W104 28 Å (30.6 Å)
- Actin nucleotide to cofilin W104 34 Å (31.6 Å)
- Actin Cys374 to cofilin Cys 170 33 Å (Unknown)

The distance between cofilin W104 and the two actin loci, actin Cys 374 and actin ATP were able to directly test the model of cofilin-G-actin binding. These measured distances corresponded very well with the model distances, provided strong support for the validity of the model proposed by (Galkin, Orlova et al. 2011). However, this model makes two assumptions. Firstly, the model is a structure of cofilin bound to F-actin. We assume that the cofilin binds to G-actin via the G/F cofilin binding site, which is highly likely (McGough and Chiu 1999). Secondly, we assume that no major re-orientation of cofilin occurs with respect to the actin monomer to which it is bound in the model F-actin structure.

Ideally, to more fully test the model a third distance measurement would be required to positively identify a unique position in space of loci within cofilin with respect to actin. Unfortunately, we did not have access to a suitable probe site. Additional mutagenesis would be required to insert a suitable probe site on cofilin. Other sites are available on actin, although these sites are more difficult to uniquely label.

The distance between actin Cys 374 and cofilin Cys 170 was found to be 33 Å (Table 6.4). As described above, we had no model location for Cys 170 within the cofilin structure. Therefore, we could not use this distance to test the model of actin cofilin binding. However, when we combine the intra-molecular distance between cofilin W104 with the inter-molecular distance between actin Cys 374 and cofilin Cys 170, a location in the vicinity of the cofilin surface residue Glu 151 meets these distance criteria. Glu 151 is located centrally in the α6 helix on the surface of cofilin near the C-terminus of cofilin. Thus, it is likely that cofilin Cys 170 is located near the α6 helix.

6.4.5. Conclusions

The mutagenesis studies described in this Chapter have allowed us to develop appropriate cofilin mutants (Cys170 cofilin and Cys170 W104 cofilin) that can be labelled with fluorescent probes and is still capable of binding to G-actin. These cofilin mutants are consequently suitable for intra-cellular localisation and intra-cellualar FRET studies in fixed cells with permeabilised cell membranes.

Our data also reinforced the importance of the N-terminus of cofilin in binding to actin. The discovery that mutation of W104 prevents actin binding highlights the importance of the β5 strand - α6 helix in actin binding via the G/F actin binding site on cofilin. As expected, the C-terminal mutation did not alter G-actin binding, consistent with this region of cofilin not being involved in the G/F binding site.

Finally, our inter-molecular distance measurements provide strong support for the cofilin-F-actin model of Galkin et al. (2011).

References

Ababou, A., E. Rostkova, S. Mistry, C. Le Masurier, M. Gautel and M. Pfuhl (2008). "Myosin binding protein C positioned to play a key role in regulation of muscle contraction: structure and interactions of domain C1." J Mol Biol **384**(3): 615-630.

Ababou, A., L. Zhou, M. Gautel and M. Pfuhl (2004). "Sequence specific assignment of domain C1 of the N-terminal myosin-binding site of human cardiac myosin binding protein C (MyBP-C)." J Biomol NMR **29**(3): 431-432.

Abe, H., T. Endo, K. Yamamoto and T. Obinata (1990). "Sequence of cDNAs encoding actin depolymerizing factor and cofilin of embryonic chicken skeletal muscle: two functionally distinct actin-regulatory proteins exhibit high structural homology." Biochemistry **29**(32): 7420-7425.

Abelmann, W. H. (1984). "Classification and natural history of primary myocardial disease." Prog Cardiovasc Dis **27**(2): 73-94.

Alyonycheva, T. N., T. Mikawa, F. C. Reinach and D. A. Fischman (1997). "Isoform-specific interaction of the myosin-binding proteins (MyBPs) with skeletal and cardiac myosin is a property of the C-terminal immunoglobulin domain." J Biol Chem **272**(33): 20866-20872.

Andersen, P. S., O. Havndrup, H. Bundgaard, J. C. Moolman-Smook, L. A. Larsen, J. Mogensen, . . . M. Christiansen (2001). "Myosin light chain mutations in familial hypertrophic cardiomyopathy: phenotypic presentation and frequency in Danish and South African populations." J Med Genet **38**(12): E43.

Andersen, P. S., P. L. Hedley, S. P. Page, P. Syrris, J. C. Moolman-Smook, W. J. McKenna, . . . M. Christiansen (2012). "A novel Myosin essential light chain mutation causes hypertrophic cardiomyopathy with late onset and low expressivity." Biochem Res Int **2012**: 685108.

Anonymous (1980). "Report of the WHO/ISFC task force on the definition and classification of cardiomyopathies." Br Heart J **44**(6): 672-673.

Arber, S., F. A. Barbayannis, H. Hanser, C. Schneider, C. A. Stanyon, O. Bernard and P. Caroni (1998). "Regulation of actin dynamics through phosphorylation of cofilin by LIM-kinase." Nature **393**(6687): 805-809.

Bamburg, J. R. (1999). "Proteins of the ADF/cofilin family: essential regulators of actin dynamics." Annu Rev Cell Dev Biol **15**: 185-230.

Bamburg, J. R., H. E. Harris and A. G. Weeds (1980). "Partial purification and characterization of an actin depolymerizing factor from brain." FEBS Lett **121**(1): 178-182.

Barden, J. A. and C. G. dos Remedios (1984). "The environment of the high-affinity cation binding site on actin and the separation between cation and ATP sites as revealed by proton NMR and fluorescence spectroscopy." J Biochem **96**(3): 913-921.

Bardswell, S. C., F. Cuello, J. C. Kentish and M. Avkiran (2012). "cMyBP-C as a promiscuous substrate: phosphorylation by non-PKA kinases and its potential significance." J Muscle Res Cell Motil **33**(1): 53-60.

Bardswell, S. C., F. Cuello, A. J. Rowland, S. Sadayappan, J. Robbins, M. Gautel, . . . M. Avkiran (2010). "Distinct sarcomeric substrates are responsible for protein kinase D-mediated regulation of cardiac myofilament Ca^{2+} sensitivity and cross-bridge cycling." J Biol Chem **285**(8): 5674-5682.

Barman, T. E. and D. E. Koshland, Jr. (1967). "A colorimetric procedure for the quantitative determination of tryptophan residues in proteins." J Biol Chem **242**(23): 5771-5776.

Bashyam, M. D., G. Purushotham, A. K. Chaudhary, K. M. Rao, V. Acharya, T. A. Mohammad, . . . C. Narasimhan (2012). "A low prevalence of MYH7/MYBPC3 mutations among familial hypertrophic cardiomyopathy patients in India." Mol Cell Biochem **360**(1-2): 373-382.

Bashyam, M. D., G. R. Savithri, M. S. Kumar, C. Narasimhan and P. Nallari (2003). "Molecular genetics of familial hypertrophic cardiomyopathy (FHC)." J Hum Genet **48**(2): 55-64.

Bennett, P., R. Craig, R. Starr and G. Offer (1986). "The ultrastructural location of C-protein, X-protein and H-protein in rabbit muscle." J Muscle Res Cell Motil **7**(6): 550-567.

Bernard, O., S. Ganiatsas, G. Kannourakis and R. Dringen (1994). "Kiz-1, a protein with LIM zinc finger and kinase domains, is expressed mainly in neurons." Cell Growth Differ **5**(11): 1159-1171.

Betocchi, S., F. Piscione, M. A. Losi, L. Pace, M. Boccalatte, P. Perrone-Filardi, . . . M. Chiariello (1996). "Effects of diltiazem on left ventricular systolic and diastolic function in hypertrophic cardiomyopathy." Am J Cardiol **78**(4): 451-457.

Bhavsar, P. K., N. J. Brand, M. H. Yacoub and P. J. Barton (1996). "Isolation and characterization of the human cardiac troponin I gene (TNNI3)." Genomics **35**(1): 11-23.

Bhuiyan, M. S., J. Gulick, H. Osinska, M. Gupta and J. Robbins (2012). "Determination of the critical residues responsible for cardiac myosin binding protein C's interactions." J Mol Cell Cardiol **53**(6): 838-847.

Blanchoin, L., R. C. Robinson, S. Choe and T. D. Pollard (2000). "Phosphorylation of Acanthamoeba actophorin (ADF/cofilin) blocks interaction with actin without a change in atomic structure." J Mol Biol **295**(2): 203-211.

Bobkov, A. A., A. Muhlrad, K. Kokabi, S. Vorobiev, S. C. Almo and E. Reisler (2002). "Structural effects of cofilin on longitudinal contacts in F-actin." J Mol Biol **323**(4): 739-750.

Boey, W., W. Huang, B. Bennetts, J. Sparrow, C. Dos Remedios and B. Hambly (1994). "Fluorescence resonance energy transfer within the regulatory light chain of myosin." Eur J Biochem **219**(1-2): 603-610.

Bonne, G., L. Carrier, J. Bercovici, C. Cruaud, P. Richard, B. Hainque, . . . K. Schwartz (1995). "Cardiac myosin binding protein-C gene splice acceptor site mutation is associated with familial hypertrophic cardiomyopathy." Nat Genet **11**(4): 438-440.

Bonow, R. O., V. Dilsizian, D. R. Rosing, B. J. Maron, S. L. Bacharach and M. V. Green (1985). "Verapamil-induced improvement in left ventricular diastolic filling and increased exercise tolerance in patients with hypertrophic cardiomyopathy: short- and long-term effects." Circulation **72**(4): 853-864.

Bookwalter, C. S. and K. M. Trybus (2006). "Functional consequences of a mutation in an expressed human alpha-cardiac actin at a site implicated in familial hypertrophic cardiomyopathy." J Biol Chem **281**(24): 16777-16784.

Boron, W. F. and E. L. Boulpaep (2005). Medical Physiology: a cellular and molecular approach Updated Edition. Philadelphia, USA, Elsevier Saunders.

Bowman, G. D., I. M. Nodelman, Y. Hong, N. H. Chua, U. Lindberg and C. E. Schutt (2000). "A comparative structural analysis of the ADF/cofilin family." Proteins **41**(3): 374-384.

Braunwald, E., C. T. Lambrew, S. D. Rockoff, J. Ross, Jr. and A. G. Morrow (1964). "Idiopathic Hypertrophic Subaortic Stenosis. I. A Description of the Disease Based Upon an Analysis of 64 Patients." Circulation **30**: SUPPL 4:3-119.

Brown, L. J., L. Singh, K. L. Sale, B. Yu, R. Trent, P. G. Fajer and B. D. Hambly (2002). "Functional and spectroscopic studies of a familial hypertrophic cardiomyopathy mutation in Motif X of cardiac myosin binding protein-C." Eur Biophys J **31**(5): 400-408.

Carlier, M. F., V. Laurent, J. Santolini, R. Melki, D. Didry, G. X. Xia, . . . D. Pantaloni (1997). "Actin depolymerizing factor (ADF/cofilin) enhances the rate of filament turnover: implication in actin-based motility." J Cell Biol **136**(6): 1307-1322.

Carrier, L., C. Hengstenberg, J. S. Beckmann, P. Guicheney, C. Dufour, J. Bercovici, . . . D. Pulvenis (1993). "Mapping of a novel gene for familial hypertrophic cardiomyopathy to chromosome 11." Nature Genetics **4**(3): 311-313.

Carsten, M. E. and W. F. Mommaerts (1963). "A study of actin by means of starch gel electrophoresis." Biochemistry **2**: 28-32.

Cazorla, O., A. Freiburg, M. Helmes, T. Centner, M. McNabb, Y. Wu, . . . H. Granzier (2000). "Differential expression of cardiac titin isoforms and modulation of cellular stiffness." Circ Res **86**(1): 59-67.

Charron, P., O. Dubourg, M. Desnos, M. Bennaceur, L. Carrier, A. C. Camproux, . . . M. Komajda (1998). "Clinical features and prognostic implications of familial hypertrophic cardiomyopathy related to the cardiac myosin-binding protein C gene." Circulation **97**(22): 2230-2236.

Chhabra, D., N. J. Nosworthy and C. G. dos Remedios (2005). "The N-terminal fragment of gelsolin inhibits the interaction of DNase I with isolated actin, but not with the cofilin-actin complex." Proteomics **5**(12): 3131-3136.

Chock, S. P. (1979). "The mechanism of the skeletal muscle myosin ATPase. III. Relationship of the H+ release and the protein absorbance change induced by ATP to the initial Pi burst." J Biol Chem **254**(9): 3244-3248.

Chou, P. Y. and G. D. Fasman (1978). "Prediction of the secondary structure of proteins from their amino acid sequence." Adv Enzymol Relat Areas Mol Biol **47**: 45-148.

Chuan, P., S. Sivaramakrishnan, E. A. Ashley and J. A. Spudich (2012). "Cell-intrinsic functional effects of the alpha-cardiac myosin Arg-403-Gln mutation in familial hypertrophic cardiomyopathy." Biophys J **102**(12): 2782-2790.

Cooke, R. (1998). "New angle on myosin." Proc Natl Acad Sci U S A **95**(6): 2720-2722.

Craig, R. and G. Offer (1976). "The location of C-protein in rabbit skeletal muscle." Proc R Soc Lond B Biol Sci **192**(1109): 451-461.

Cuello, F., S. C. Bardswell, R. S. Haworth, E. Ehler, S. Sadayappan, J. C. Kentish and M. Avkiran (2011). "Novel role for p90 ribosomal S6 kinase in the regulation of cardiac myofilament phosphorylation." J Biol Chem **286**(7): 5300-5310.

Daehmlow, S., J. Erdmann, T. Knueppel, C. Gille, C. Froemmel, M. Hummel, . . . V. Regitz-Zagrosek (2002). "Novel mutations in sarcomeric protein genes in dilated cardiomyopathy." Biochem Biophys Res Commun **298**(1): 116-120.

Davies, M. J. (1984). "The current status of myocardial disarray in hypertrophic cardiomyopathy." Br Heart J **51**(4): 361-363.

Debold, E. P., W. Saber, Y. Cheema, C. S. Bookwalter, K. M. Trybus, D. M. Warshaw and P. Vanburen (2010). "Human actin mutations associated with hypertrophic and dilated cardiomyopathies demonstrate distinct thin filament regulatory properties in vitro." J Mol Cell Cardiol **48**(2): 286-292.

Decker, R. S., M. L. Decker, I. Kulikovskaya, S. Nakamura, D. C. Lee, K. Harris, . . . S. Winegrad (2005). "Myosin-binding protein C phosphorylation, myofibril structure, and contractile function during low-flow ischemia." Circulation **111**(7): 906-912.

Dong, W. J., J. Xing, Y. Ouyang, J. An and H. C. Cheung (2008). "Structural kinetics of cardiac troponin C mutants linked to familial hypertrophic and dilated cardiomyopathy in troponin complexes." J Biol Chem **283**(6): 3424-3432.

dos Remedios, C. G., D. Chhabra, M. Kekic, I. V. Dedova, M. Tsubakihara, D. A. Berry and N. J. Nosworthy (2003). "Actin binding proteins: regulation of cytoskeletal microfilaments." Physiol Rev **83**(2): 433-473.

Du, J. and C. Frieden (1998). "Kinetic studies on the effect of yeast cofilin on yeast actin polymerization." Biochemistry **37**(38): 13276-13284.

Dumka, D., J. Talent, I. Akopova, G. Guzman, D. Szczesna-Cordary and J. Borejdo (2006). "E22K mutation of RLC that causes familial hypertrophic cardiomyopathy in heterozygous mouse myocardium: effect on cross-bridge kinetics." Am J Physiol Heart Circ Physiol **291**(5): H2098-2106.

Ebashi, S. (1963). "Third Component Participating in the Superprecipitation of 'Natural Actomyosin'." Nature **200**: 1010.

Egelman, E. H. (1985). "The structure of F-actin." J Muscle Res Cell Motil **6**(2): 129-151.

Ehler, E., B. M. Rothen, S. P. Hammerle, M. Komiyama and J. C. Perriard (1999). "Myofibrillogenesis in the developing chicken heart: assembly of Z-disk, M-line and the thick filaments." J Cell Sci **112 (Pt 10)**: 1529-1539.

Einheber, S. and D. A. Fischman (1990). "Isolation and characterization of a cDNA clone encoding avian skeletal muscle C-protein: an intracellular member of the immunoglobulin superfamily." Proc Natl Acad Sci U S A **87**(6): 2157-2161.

Elam, W. A., H. Kang and E. M. De La Cruz (2013). "Biophysics of actin filament severing by cofilin." Febs Letters **587**(8): 1215-1219.

Elliott, K., H. Watkins and C. S. Redwood (2000). "Altered regulatory properties of human cardiac troponin I mutants that cause hypertrophic cardiomyopathy." J Biol Chem **275**(29): 22069-22074.

Elliott, P. M., J. Poloniecki, S. Dickie, S. Sharma, L. Monserrat, A. Varnava, . . . W. J. McKenna (2000). "Sudden death in hypertrophic cardiomyopathy: identification of high risk patients." J Am Coll Cardiol **36**(7): 2212-2218.

Epstein, N. D., G. M. Cohn, F. Cyran and L. Fananapazir (1992). "Differences in clinical expression of hypertrophic cardiomyopathy associated with two distinct mutations in the beta-myosin heavy chain gene. A 908Leu----Val mutation and a 403Arg----Gln mutation." Circulation **86**(2): 345-352.

Epstein, S. E. and D. R. Rosing (1981). "Verapamil: its potential for causing serious complications in patients with hypertrophic cardiomyopathy." Circulation **64**(3): 437-441.

Fananapazir, L. and N. D. Epstein (1995). "Prevalence of hypertrophic cardiomyopathy and limitations of screening methods." Circulation **92**(4): 700-704.

Farman, G. P., D. Gore, E. Allen, K. Schoenfelt, T. C. Irving and P. P. de Tombe (2011). "Myosin head orientation: a structural determinant for the Frank-Starling relationship." Am J Physiol Heart Circ Physiol **300**(6): H2155-2160.

Fedorov, A. A., P. Lappalainen, E. V. Fedorov, D. G. Drubin and S. C. Almo (1997). "Structure determination of yeast cofilin." Nat Struct Biol **4**(5): 366-369.

Fernandes, V. L., C. Nielsen, S. F. Nagueh, A. E. Herrin, C. Slifka, J. Franklin and W. H. Spencer, 3rd (2008). "Follow-up of alcohol septal ablation for symptomatic hypertrophic obstructive cardiomyopathy the Baylor and Medical University of South Carolina experience 1996 to 2007." JACC Cardiovasc Interv **1**(5): 561-570.

Filatov, V. L., A. G. Katrukha, T. V. Bulargina and N. B. Gusev (1999). "Troponin: structure, properties, and mechanism of functioning." Biochemistry (Mosc) **64**(9): 969-985.

Flashman, E., C. Redwood, J. Moolman-Smook and H. Watkins (2004). "Cardiac myosin binding protein C: its role in physiology and disease." Circ Res **94**(10): 1279-1289.

Flavigny, J., P. Richard, R. Isnard, L. Carrier, P. Charron, G. Bonne, . . . B. Hainque (1998). "Identification of two novel mutations in the ventricular regulatory myosin light chain gene (MYL2) associated with familial and classical forms of hypertrophic cardiomyopathy." J Mol Med (Berl) **76**(3-4): 208-214.

Flavigny, J., M. Souchet, P. Sebillon, I. Berrebi-Bertrand, B. Hainque, A. Mallet, . . . L. Carrier (1999). "COOH-terminal truncated cardiac myosin-binding protein C mutants resulting from familial hypertrophic cardiomyopathy mutations exhibit

altered expression and/or incorporation in fetal rat cardiomyocytes." J Mol Biol **294**(2): 443-456.

Flicker, P. F., G. N. Phillips, Jr. and C. Cohen (1982). "Troponin and its interactions with tropomyosin. An electron microscope study." J Mol Biol **162**(2): 495-501.

Foth, B. J., M. C. Goedecke and D. Soldati (2006). "New insights into myosin evolution and classification." Proc Natl Acad Sci U S A **103**(10): 3681-3686.

Freiburg, A. and M. Gautel (1996). "A molecular map of the interactions between titin and myosin-binding protein C. Implications for sarcomeric assembly in familial hypertrophic cardiomyopathy." Eur J Biochem **235**(1-2): 317-323.

Freiburg, A., K. Trombitas, W. Hell, O. Cazorla, F. Fougerousse, T. Centner, . . . S. Labeit (2000). "Series of exon-skipping events in the elastic spring region of titin as the structural basis for myofibrillar elastic diversity." Circ Res **86**(11): 1114-1121.

Fujino, N., M. Shimizu, H. Ino, M. Yamaguchi, T. Yasuda, M. Nagata, . . . H. Mabuchi (2002). "A novel mutation Lys273Glu in the cardiac troponin T gene shows high degree of penetrance and transition from hypertrophic to dilated cardiomyopathy." Am J Cardiol **89**(1): 29-33.

Fulton, A. B. and W. B. Isaacs (1991). "Titin, a huge, elastic sarcomeric protein with a probable role in morphogenesis." Bioessays **13**(4): 157-161.

Funatsu, T., E. Kono, H. Higuchi, S. Kimura, S. Ishiwata, T. Yoshioka, . . . S. Tsukita (1993). "Elastic filaments in situ in cardiac muscle: deep-etch replica analysis in combination with selective removal of actin and myosin filaments." J Cell Biol **120**(3): 711-724.

Furst, D. O., M. Osborn, R. Nave and K. Weber (1988). "The organization of titin filaments in the half-sarcomere revealed by monoclonal antibodies in immunoelectron microscopy: a map of ten nonrepetitive epitopes starting at the Z line extends close to the M line." J Cell Biol **106**(5): 1563-1572.

Galkin, V. E., A. Orlova, D. S. Kudryashov, A. Solodukhin, E. Reisler, G. F. Schroder and E. H. Egelman (2011). "Remodeling of actin filaments by ADF/cofilin proteins." Proc Natl Acad Sci U S A **108**(51): 20568-20572.

Gautel, M., O. Zuffardi, A. Freiburg and S. Labeit (1995). "Phosphorylation switches specific for the cardiac isoform of myosin binding protein-C: a modulator of cardiac contraction?" Embo J **14**(9): 1952-1960.

Geisterfer-Lowrance, A. A., S. Kass, G. Tanigawa, H. P. Vosberg, W. McKenna, C. E. Seidman and J. G. Seidman (1990). "A molecular basis for familial hypertrophic cardiomyopathy: a beta cardiac myosin heavy chain gene missense mutation." Cell **62**(5): 999-1006.

Gersh, B. J., B. J. Maron, R. O. Bonow, J. A. Dearani, M. A. Fifer, M. S. Link, . . . L. G. Tarkington (2011). "2011 ACCF/AHA guideline for the diagnosis and treatment of hypertrophic cardiomyopathy: Executive summary: A report of the American College of Cardiology Foundation/American Heart Association Task Force on Practice Guidelines." The Journal of Thoracic and Cardiovascular Surgery **142**(6): 1303-1338.

Gilbert, R., M. G. Kelly, T. Mikawa and D. A. Fischman (1996). "The carboxyl terminus of myosin binding protein C (MyBP-C, C-protein) specifies incorporation into the A-band of striated muscle." J Cell Sci **109 (Pt 1)**: 101-111.

Girolami, F., I. Olivotto, I. Passerini, E. Zachara, S. Nistri, F. Re, . . . F. Cecchi (2006). "A molecular screening strategy based on beta-myosin heavy chain, cardiac myosin binding protein C and troponin T genes in Italian patients with hypertrophic cardiomyopathy." J Cardiovasc Med (Hagerstown) **7**(8): 601-607.

Gollapudi, SampathÂ K., R. Mamidi, SriÂ L. Mallampalli and M. Chandra (2012). "The N-Terminal Extension of Cardiac Troponin T Stabilizes the Blocked State of Cardiac Thin Filament." Biophysical Journal **103**(5): 940-948.

Gorbatyuk, V. Y., N. J. Nosworthy, S. A. Robson, N. P. Bains, M. W. Maciejewski, C. G. Dos Remedios and G. F. King (2006). "Mapping the phosphoinositide-binding site on chick cofilin explains how PIP2 regulates the cofilin-actin interaction." Mol Cell **24**(4): 511-522.

Gordon, A. M., E. Homsher and M. Regnier (2000). "Regulation of contraction in striated muscle." Physiol Rev **80**(2): 853-924.

Greaser, M. L. and J. Gergely (1971). "Reconstitution of troponin activity from three protein components." J Biol Chem **246**(13): 4226-4233.

Grossman, W., D. Jones and L. P. McLaurin (1975). "Wall stress and patterns of hypertrophy in the human left ventricle." J Clin Invest **56**(1): 56-64.

Gruen, M. and M. Gautel (1999). "Mutations in beta-myosin S2 that cause familial hypertrophic cardiomyopathy (FHC) abolish the interaction with the regulatory domain of myosin-binding protein-C." J Mol Biol **286**(3): 933-949.

Gruen, M., H. Prinz and M. Gautel (1999). "cAPK-phosphorylation controls the interaction of the regulatory domain of cardiac myosin binding protein C with myosin-S2 in an on-off fashion." FEBS Lett **453**(3): 254-259.

Gunning, P., P. Ponte, H. Okayama, J. Engel, H. Blau and L. Kedes (1983). "Isolation and characterization of full-length cDNA clones for human alpha-, beta-, and gamma-actin mRNAs: skeletal but not cytoplasmic actins have an amino-terminal cysteine that is subsequently removed." Mol Cell Biol **3**(5): 787-795.

Hanson, J. and H. E. Huxley (1953). "Structural basis of the cross-striations in muscle." Nature **172**(4377): 530-532.

Harris, S. P., R. G. Lyons and K. L. Bezold (2011). "In the thick of it: HCM-causing mutations in myosin binding proteins of the thick filament." Circ Res **108**(6): 751-764.

Harris, S. P., E. Rostkova, M. Gautel and R. L. Moss (2004). "Binding of myosin binding protein-C to myosin subfragment S2 affects contractility independent of a tether mechanism." Circ Res **95**(9): 930-936.

Hartzell, H. C. (1985). "Effects of phosphorylated and unphosphorylated C-protein on cardiac actomyosin ATPase." J Mol Biol **186**(1): 185-195.

Hartzell, H. C. and D. B. Glass (1984). "Phosphorylation of purified cardiac muscle C-protein by purified cAMP-dependent and endogenous Ca^{2+}-calmodulin-dependent protein kinases." J Biol Chem **259**(24): 15587-15596.

Hernandez, O. M., M. Jones, G. Guzman and D. Szczesna-Cordary (2007). "Myosin essential light chain in health and disease." Am J Physiol Heart Circ Physiol **292**(4): H1643-1654.

Herron, T. J., E. Rostkova, G. Kunst, R. Chaturvedi, M. Gautel and J. C. Kentish (2006). "Activation of myocardial contraction by the N-terminal domains of myosin binding protein-C." Circ Res **98**(10): 1290-1298.

Hoffmann, B., H. Schmidt-Traub, A. Perrot, K. J. Osterziel and R. Gessner (2001). "First mutation in cardiac troponin C, L29Q, in a patient with hypertrophic cardiomyopathy." Hum Mutat **17**(6): 524.

Horowits, R., K. Maruyama and R. J. Podolsky (1989). "Elastic behavior of connectin filaments during thick filament movement in activated skeletal muscle." J Cell Biol **109**(5): 2169-2176.

Houdusse, A., M. L. Love, R. Dominguez, Z. Grabarek and C. Cohen (1997). "Structures of four Ca^{2+}-bound troponin C at 2.0 A resolution: further insights into the Ca^{2+}-switch in the calmodulin superfamily." Structure **5**(12): 1695-1711.

Howarth, J. W., S. Ramisetti, K. Nolan, S. Sadayappan and P. R. Rosevear (2012). "Structural insight into unique cardiac myosin-binding protein-C motif: a partially folded domain." J Biol Chem **287**(11): 8254-8262.

Idowu, S. M., M. Gautel, S. J. Perkins and M. Pfuhl (2003). "Structure, stability and dynamics of the central domain of cardiac myosin binding protein C (MyBP-C): Implications for multidomain assembly and causes for cardiomyopathy." Journal of Molecular Biology **329**(4): 745-761.

Iida, K., S. Matsumoto and I. Yahara (1992). "The KKRKK sequence is involved in heat shock-induced nuclear translocation of the 18-kDa actin-binding protein, cofilin." Cell Struct Funct **17**(1): 39-46.

Improta, S., A. S. Politou and A. Pastore (1996). "Immunoglobulin-like modules from titin I-band: extensible components of muscle elasticity." Structure **4**(3): 323-337.

Ingles, J., A. Doolan, C. Chiu, J. Seidman, C. Seidman and C. Semsarian (2005). "Compound and double mutations in patients with hypertrophic cardiomyopathy: implications for genetic testing and counselling." J Med Genet **42**(10): e59.

Jaaskelainen, P., J. Kuusisto, R. Miettinen, P. Karkkainen, S. Karkkainen, S. Heikkinen, . . . M. Laakso (2002). "Mutations in the cardiac myosin-binding protein C gene are the predominant cause of familial hypertrophic cardiomyopathy in eastern Finland." Journal of Molecular Medicine **80**(7): 412-422.

James, J., Y. Zhang, H. Osinska, A. Sanbe, R. Klevitsky, T. E. Hewett and J. Robbins (2000). "Transgenic modeling of a cardiac troponin I mutation linked to familial hypertrophic cardiomyopathy." Circ Res **87**(9): 805-811.

Jeacocke, S. A. and P. J. England (1980). "Phosphorylation of a myofibrillar protein of Mr 150 000 in perfused rat heart, and the tentative indentification of this as C-protein." FEBS Lett **122**(1): 129-132.

Jeffries, C. M., Y. Lu, R. M. Hynson, J. E. Taylor, M. Ballesteros, A. H. Kwan and J. Trewhella (2011). "Human cardiac myosin binding protein C: structural flexibility within an extended modular architecture." J Mol Biol **414**(5): 735-748.

Jeffries, C. M., A. E. Whitten, S. P. Harris and J. Trewhella (2008). "Small-angle X-ray scattering reveals the N-terminal domain organization of cardiac myosin binding protein C." J Mol Biol **377**(4): 1186-1199.

Johnson, P. H. and L. I. Grossman (1977). "Electrophoresis of DNA in agarose gels. Optimizing separations of conformational isomers of double- and single-stranded DNAs." Biochemistry **16**(19): 4217-4225.

Kabaeva, Z. T., A. Perrot, B. Wolter, R. Dietz, N. Cardim, J. M. Correia, . . . K. J. Osterziel (2002). "Systematic analysis of the regulatory and essential myosin light chain genes: genetic variants and mutations in hypertrophic cardiomyopathy." Eur J Hum Genet **10**(11): 741-748.

Kelly, M. and C. Semsarian (2009). "Multiple mutations in genetic cardiovascular disease: a marker of disease severity?" Circ Cardiovasc Genet **2**(2): 182-190.

Kensler, R. W. and S. P. Harris (2008). "The structure of isolated cardiac Myosin thick filaments from cardiac Myosin binding protein-C knockout mice." Biophys J **94**(5): 1707-1718.

Kensler, R. W., J. F. Shaffer and S. P. Harris (2011). "Binding of the N-terminal fragment C0-C2 of cardiac MyBP-C to cardiac F-actin." J Struct Biol **174**(1): 44-51.

Keren, A., P. Syrris and W. J. McKenna (2008). "Hypertrophic cardiomyopathy: the genetic determinants of clinical disease expression." Nat Clin Pract Cardiovasc Med **5**(3): 158-168.

Kimura, A., H. Harada, J. E. Park, H. Nishi, M. Satoh, M. Takahashi, . . . T. Sasazuki (1997). "Mutations in the cardiac troponin I gene associated with hypertrophic cardiomyopathy." Nat Genet **16**(4): 379-382.

Knoll, R. (2012). "Myosin binding protein C: implications for signal-transduction." J Muscle Res Cell Motil **33**(1): 31-42.

Kokado, H., M. Shimizu, H. Yoshio, H. Ino, K. Okeie, Y. Emoto, . . . H. Mabuchi (2000). "Clinical features of hypertrophic cardiomyopathy caused by a Lys183 deletion mutation in the cardiac troponin I gene." Circulation **102**(6): 663-669.

Konno, T., M. Shimizu, H. Ino, N. Fujino, K. Uchiyama, T. Mabuchi, . . . H. Mabuchi (2006). "A novel mutation in the cardiac myosin-binding protein C gene is responsible for hypertrophic cardiomyopathy with severe ventricular hypertrophy and sudden death." Clin Sci (Lond) **110**(1): 125-131.

Konno, T., M. Shimizu, H. Ino, T. Matsuyama, M. Yamaguchi, H. Terai, . . . H. Mabuchi (2003). "A novel missense mutation in the myosin binding protein-C gene is responsible for hypertrophic cardiomyopathy with left ventricular dysfunction and dilation in elderly patients." J Am Coll Cardiol **41**(5): 781-786.

Koretz, J. F. (1979). "Effects of C-protein on synthetic myosin filament structure." Biophys J **27**(3): 433-446.

Kremneva, E., S. Boussouf, O. Nikolaeva, R. Maytum, M. A. Geeves and D. I. Levitsky (2004). "Effects of two familial hypertrophic cardiomyopathy mutations in alpha-tropomyosin, Asp175Asn and Glu180Gly, on the thermal unfolding of actin-bound tropomyosin." Biophys J **87**(6): 3922-3933.

Kulikovskaya, I., G. McClellan, J. Flavigny, L. Carrier and S. Winegrad (2003). "Effect of MyBP-C binding to actin on contractility in heart muscle." J Gen Physiol **122**(6): 761-774.

Kunst, G., K. R. Kress, M. Gruen, D. Uttenweiler, M. Gautel and R. H. Fink (2000). "Myosin binding protein C, a phosphorylation-dependent force regulator in muscle that controls the attachment of myosin heads by its interaction with myosin S2." Circ Res **86**(1): 51-58.

Kurzban, G. P. and K. Wang (1988). "Giant polypeptides of skeletal muscle titin: sedimentation equilibrium in guanidine hydrochloride." Biochem Biophys Res Commun **150**(3): 1155-1161.

Kuster, D. W., A. C. Bawazeer, R. Zaremba, M. Goebel, N. M. Boontje and J. van der Velden (2012). "Cardiac myosin binding protein C phosphorylation in cardiac disease." J Muscle Res Cell Motil **33**(1): 43-52.

Kwon, D. H., S. R. Kapadia, E. M. Tuzcu, C. M. Halley, E. Z. Gorodeski, R. J. Curtin, . . . M. Y. Desai (2008). "Long-term outcomes in high-risk symptomatic patients with hypertrophic cardiomyopathy undergoing alcohol septal ablation." JACC Cardiovasc Interv **1**(4): 432-438.

Labeit, S., M. Gautel, A. Lakey and J. Trinick (1992). "Towards a molecular understanding of titin." Embo J **11**(5): 1711-1716.

Labeit, S. and B. Kolmerer (1995). "Titins: giant proteins in charge of muscle ultrastructure and elasticity." Science **270**(5234): 293-296.

Laemmli, U. K. (1970). "Cleavage of structural proteins during the assembly of the head of bacteriophage T4." Nature **227**(5259): 680-685.

Lang, R., A. V. Gomes, J. Zhao, P. R. Housmans, T. Miller and J. D. Potter (2002). "Functional analysis of a troponin I (R145G) mutation associated with familial hypertrophic cardiomyopathy." J Biol Chem **277**(14): 11670-11678.

Lehrer, S. S. and G. Kerwar (1972). "Intrinsic fluorescence of actin." Biochemistry **11**(7): 1211-1217.

Levine, R., A. Weisberg, I. Kulikovskaya, G. McClellan and S. Winegrad (2001). "Multiple structures of thick filaments in resting cardiac muscle and their influence on cross-bridge interactions." Biophys J **81**(2): 1070-1082.

Li, M. X., S. M. Gagne, L. Spyracopoulos, C. P. Kloks, G. Audette, M. Chandra, . . . B. D. Sykes (1997). "NMR studies of Ca^{2+} binding to the regulatory domains of cardiac and E41A skeletal muscle troponin C reveal the importance of site I to energetics of the induced structural changes." Biochemistry **36**(41): 12519-12525.

Li, X. E., W. Suphamungmee, M. Janco, M. A. Geeves, S. B. Marston, S. Fischer and W. Lehman (2012). "The flexibility of two tropomyosin mutants, D175N and E180G, that cause hypertrophic cardiomyopathy." Biochem Biophys Res Commun **424**(3): 493-496.

Liang, B., F. Chung, Y. Qu, D. Pavlov, T. E. Gillis, S. B. Tikunova, . . . G. F. Tibbits (2008). "Familial hypertrophic cardiomyopathy-related cardiac troponin C mutation L29Q affects Ca^{2+} binding and myofilament contractility." Physiol Genomics **33**(2): 257-266.

Lim, M. S. and M. P. Walsh (1986). "Phosphorylation of skeletal and cardiac muscle C-proteins by the catalytic subunit of cAMP-dependent protein kinase." Biochem Cell Biol **64**(7): 622-630.

Lin, Z., M. H. Lu, T. Schultheiss, J. Choi, S. Holtzer, C. DiLullo, . . . H. Holtzer (1994). "Sequential appearance of muscle-specific proteins in myoblasts as a function of time after cell division: evidence for a conserved myoblast differentiation program in skeletal muscle." Cell Motil Cytoskeleton **29**(1): 1-19.

Loong, C. K., H. X. Zhou and P. B. Chase (2012). "Familial hypertrophic cardiomyopathy related E180G mutation increases flexibility of human cardiac alpha-tropomyosin." FEBS Lett **586**(19): 3503-3507.

Lowey, S. (1964). "Myosin Substructure: Isolation of a Helical Subunit from Heavy Meromyosin." Science **145**: 597-599.

Lowey, S., L. D. Saraswat, H. Liu, N. Volkmann and D. Hanein (2007). "Evidence for an interaction between the SH3 domain and the N-terminal extension of the essential light chain in class II myosins." J Mol Biol **371**(4): 902-913.

Lowey, S., H. S. Slayter, A. G. Weeds and H. Baker (1969). "Substructure of the myosin molecule. I. Subfragments of myosin by enzymic degradation." J Mol Biol **42**(1): 1-29.

Lu, Y., A. H. Kwan, J. Trewhella and C. M. Jeffries (2011). "The C0C1 fragment of human cardiac myosin binding protein C has common binding determinants for both actin and myosin." J Mol Biol **413**(5): 908-913.

Luther, P. K., H. Winkler, K. Taylor, M. E. Zoghbi, R. Craig, R. Padron, . . . J. Liu (2011). "Direct visualization of myosin-binding protein C bridging myosin and actin filaments in intact muscle." Proc Natl Acad Sci U S A **108**(28): 11423-11428.

Ly, S. and S. S. Lehrer (2012). "Long-range effects of familial hypertrophic cardiomyopathy mutations E180G and D175N on the properties of tropomyosin." Biochemistry **51**(32): 6413-6420.

Maki, S., H. Ikeda, A. Muro, N. Yoshida, A. Shibata, Y. Koga and T. Imaizumi (1998). "Predictors of sudden cardiac death in hypertrophic cardiomyopathy." Am J Cardiol **82**(6): 774-778.

Margossian, S. S. (1985). "Reversible dissociation of dog cardiac myosin regulatory light chain 2 and its influence on ATP hydrolysis." J Biol Chem **260**(25): 13747-13754.

Margossian, S. S. and S. Lowey (1982). "Preparation of myosin and its subfragments from rabbit skeletal muscle." Methods Enzymol **85 Pt B**: 55-71.

Maron, B. J. (2002). "Hypertrophic cardiomyopathy: a systematic review." JAMA **287**(10): 1308-1320.

Maron, B. J., R. O. Bonow, R. O. Cannon, 3rd, M. B. Leon and S. E. Epstein (1987). "Hypertrophic cardiomyopathy. Interrelations of clinical manifestations, pathophysiology, and therapy (2)." N Engl J Med **316**(14): 844-852.

Maron, B. J., S. A. Casey, R. G. Hauser and D. M. Aeppli (2003). "Clinical course of hypertrophic cardiomyopathy with survival to advanced age." J Am Coll Cardiol **42**(5): 882-888.

Maron, B. J., S. A. Casey, L. C. Poliac, T. E. Gohman, A. K. Almquist and D. M. Aeppli (1999). "Clinical course of hypertrophic cardiomyopathy in a regional United States cohort." JAMA **281**(7): 650-655.

Maron, B. J., J. M. Gardin, J. M. Flack, S. S. Gidding and D. E. Bild (1996). "HCM in the general population." Circulation **94**(3): 588-589.

Maron, B. J., J. M. Gardin, J. M. Flack, S. S. Gidding, T. T. Kurosaki and D. E. Bild (1995). "Prevalence of hypertrophic cardiomyopathy in a general population of young adults. Echocardiographic analysis of 4111 subjects in the CARDIA Study. Coronary Artery Risk Development in (Young) Adults." Circulation **92**(4): 785-789.

Maron, B. J., M. S. Maron and C. Semsarian (2012). "Double or compound sarcomere mutations in hypertrophic cardiomyopathy: a potential link to sudden death in the absence of conventional risk factors." Heart Rhythm **9**(1): 57-63.

Maron, B. J., M. S. Maron and C. Semsarian (2012). "Genetics of hypertrophic cardiomyopathy after 20 years: clinical perspectives." J Am Coll Cardiol **60**(8): 705-715.

Maron, B. J., R. Mathenge, S. A. Casey, L. C. Poliac and T. F. Longe (1999). "Clinical profile of hypertrophic cardiomyopathy identified de novo in rural communities." J Am Coll Cardiol **33**(6): 1590-1595.

Maron, B. J., H. Niimura, S. A. Casey, M. K. Soper, G. B. Wright, J. G. Seidman and C. E. Seidman (2001). "Development of left ventricular hypertrophy in adults in hypertrophic cardiomyopathy caused by cardiac myosin-binding protein C gene mutations." J Am Coll Cardiol **38**(2): 315-321.

Maron, B. J., I. Olivotto, P. Spirito, S. A. Casey, P. Bellone, T. E. Gohman, . . . F. Cecchi (2000). "Epidemiology of hypertrophic cardiomyopathy-related death: revisited in a large non-referral-based patient population." Circulation **102**(8): 858-864.

Maron, B. J. and W. C. Roberts (1979). "Quantitative analysis of cardiac muscle cell disorganization in the ventricular septum of patients with hypertrophic cardiomyopathy." Circulation **59**(4): 689-706.

Maron, B. J., J. Shirani, L. C. Poliac, R. Mathenge, W. C. Roberts and F. O. Mueller (1996). "Sudden death in young competitive athletes. Clinical, demographic, and pathological profiles." JAMA **276**(3): 199-204.

Maron, B. J., J. A. Towbin, G. Thiene, C. Antzelevitch, D. Corrado, D. Arnett, . . . J. B. Young (2006). "Contemporary definitions and classification of the cardiomyopathies: an American Heart Association Scientific Statement from the Council on Clinical Cardiology, Heart Failure and Transplantation Committee; Quality of Care and Outcomes Research and Functional Genomics and Translational Biology Interdisciplinary Working Groups; and Council on Epidemiology and Prevention." Circulation **113**(14): 1807-1816.

Maron, M. S., J. J. Finley, J. M. Bos, T. H. Hauser, W. J. Manning, T. S. Haas, . . . B. J. Maron (2008). "Prevalence, clinical significance, and natural history of left ventricular apical aneurysms in hypertrophic cardiomyopathy." Circulation **118**(15): 1541-1549.

Marston, S., O. Copeland, A. Jacques, K. Livesey, V. Tsang, W. J. McKenna, . . . H. Watkins (2009). "Evidence from human myectomy samples that MYBPC3 mutations cause hypertrophic cardiomyopathy through haploinsufficiency." Circ Res **105**(3): 219-222.

Marston, S. B. (2011). "How do mutations in contractile proteins cause the primary familial cardiomyopathies?" J Cardiovasc Transl Res **4**(3): 245-255.

Maruyama, K., S. Kimura, H. Yoshidomi, H. Sawada and M. Kikuchi (1984). "Molecular size and shape of beta-connectin, an elastic protein of striated muscle." J Biochem (Tokyo) **95**(5): 1423-1433.

Matsumoto, Y., T. Hayashi, N. Inagaki, M. Takahashi, S. Hiroi, T. Nakamura, . . . A. Kimura (2006). "Functional analysis of titin/connectin N2-B mutations found in cardiomyopathy." J Muscle Res Cell Motil: 1-8.

McClellan, G., I. Kulikovskaya, J. Flavigny, L. Carrier and S. Winegrad (2004). "Effect of cardiac myosin-binding protein C on stability of the thick filament." J Mol Cell Cardiol **37**(4): 823-835.

McClellan, G., I. Kulikovskaya and S. Winegrad (2001). "Changes in cardiac contractility related to calcium-mediated changes in phosphorylation of myosin-binding protein C." Biophys J **81**(2): 1083-1092.

McGough, A. and W. Chiu (1999). "ADF/cofilin weakens lateral contacts in the actin filament." J Mol Biol **291**(3): 513-519.

McGough, A., B. Pope and A. Weeds (2001). "The ADF/cofilin family: accelerators of actin reorganization." Results Probl Cell Differ **32**: 135-154.

McKay, R. T., B. P. Tripet, R. S. Hodges and B. D. Sykes (1997). "Interaction of the second binding region of troponin I with the regulatory domain of skeletal muscle troponin C as determined by NMR spectroscopy." J Biol Chem **272**(45): 28494-28500.

Mermall, V., P. L. Post and M. S. Mooseker (1998). "Unconventional myosins in cell movement, membrane traffic, and signal transduction." Science **279**(5350): 527-533.

Mettikolla, P., N. Calander, R. Luchowski, I. Gryczynski, Z. Gryczynski, J. Zhao, . . . J. Borejdo (2011). "Cross-bridge kinetics in myofibrils containing familial hypertrophic cardiomyopathy R58Q mutation in the regulatory light chain of myosin." J Theor Biol **284**(1): 71-81.

Miki, M., C. G. dos Remedios and J. A. Barden (1987). "Spatial relationship between the nucleotide-binding site, Lys-61 and Cys-374 in actin and a conformational change induced by myosin subfragment-1 binding." Eur J Biochem **168**(2): 339-345.

Miki, M., S. Makimura, Y. Sugahara, R. Yamada, M. Bunya, T. Saitoh and H. Tobita (2012). "A Three-Dimensional FRET Analysis to Construct an Atomic Model of the Actin-Tropomyosin-Troponin Core Domain Complex on a Muscle Thin Filament." Journal of Molecular Biology **420**: 40-55.

Minakata, K., J. A. Dearani, R. A. Nishimura, B. J. Maron and G. K. Danielson (2004). "Extended septal myectomy for hypertrophic obstructive cardiomyopathy

with anomalous mitral papillary muscles or chordae." J Thorac Cardiovasc Surg **127**(2): 481-489.

Minamide, L. S., A. M. Striegl, J. A. Boyle, P. J. Meberg and J. R. Bamburg (2000). "Neurodegenerative stimuli induce persistent ADF/cofilin-actin rods that disrupt distal neurite function." Nat Cell Biol **2**(9): 628-636.

Miura, K., H. Nakagawa, Y. Morikawa, S. Sasayama, A. Matsumori, K. Hasegawa, . . . Y. Inaba (2002). "Epidemiology of idiopathic cardiomyopathy in Japan: results from a nationwide survey." Heart **87**(2): 126-130.

Miyamoto, C. A., D. A. Fischman and F. C. Reinach (1999). "The interface between MyBP-C and myosin: site-directed mutagenesis of the CX myosin-binding domain of MyBP-C." J Muscle Res Cell Motil **20**(7): 703-715.

Mogensen, J., I. C. Klausen, A. K. Pedersen, H. Egeblad, P. Bross, T. A. Kruse, . . . A. D. Borglum (1999). "Alpha-cardiac actin is a novel disease gene in familial hypertrophic cardiomyopathy." J Clin Invest **103**(10): R39-43.

Mogensen, J., R. T. Murphy, T. Kubo, A. Bahl, J. C. Moon, I. C. Klausen, . . . W. J. McKenna (2004). "Frequency and clinical expression of cardiac troponin I mutations in 748 consecutive families with hypertrophic cardiomyopathy." J Am Coll Cardiol **44**(12): 2315-2325.

Mohamed, A. S., J. D. Dignam and K. K. Schlender (1998). "Cardiac myosin-binding protein C (MyBP-C): identification of protein kinase A and protein kinase C phosphorylation sites." Arch Biochem Biophys **358**(2): 313-319.

Moolman-Smook, J., E. Flashman, W. de Lange, Z. Li, V. Corfield, C. Redwood and H. Watkins (2002). "Identification of novel interactions between domains of Myosin binding protein-C that are modulated by hypertrophic cardiomyopathy missense mutations." Circ Res **91**(8): 704-711.

Moolman-Smook, J. C., W. J. De Lange, E. C. Bruwer, P. A. Brink and V. A. Corfield (1999). "The origins of hypertrophic cardiomyopathy-causing mutations in two South African subpopulations: a unique profile of both independent and founder events." Am J Hum Genet **65**(5): 1308-1320.

Moolman-Smook, J. C., B. Mayosi, P. Brink and V. A. Corfield (1998). "Identification of a new missense mutation in MyBP-C associated with hypertrophic cardiomyopathy." J Med Genet **35**(3): 253-254.

Moon, J. C., N. G. Fisher, W. J. McKenna and D. J. Pennell (2004). "Detection of apical hypertrophic cardiomyopathy by cardiovascular magnetic resonance in patients with non-diagnostic echocardiography." Heart **90**(6): 645-649.

Moos, C. (1981). "Fluorescence microscope study of the binding of added C protein to skeletal muscle myofibrils." J Cell Biol **90**(1): 25-31.

Moos, C. and I. N. Feng (1980). "Effect of C-protein on actomyosin ATPase." Biochim Biophys Acta **632**(2): 141-149.

Moos, C., C. M. Mason, J. M. Besterman, I. N. Feng and J. H. Dubin (1978). "The binding of skeletal muscle C-protein to F-actin, and its relation to the interaction of actin with myosin subfragment-1." J Mol Biol **124**(4): 571-586.

Morgan, T. E., R. O. Lockerbie, L. S. Minamide, M. D. Browning and J. R. Bamburg (1993). "Isolation and characterization of a regulated form of actin depolymerizing factor." J Cell Biol **122**(3): 623-633.

Morita, H., R. Nagai, J. G. Seidman and C. E. Seidman (2010). "Sarcomere gene mutations in hypertrophy and heart failure." J Cardiovasc Transl Res **3**(4): 297-303.

Morner, S., P. Richard, E. Kazzam, B. Hainque, K. Schwartz and A. Waldenstrom (2000). "Deletion in the cardiac troponin I gene in a family from northern Sweden with hypertrophic cardiomyopathy." J Mol Cell Cardiol **32**(3): 521-525.

Morner, S., P. Richard, E. Kazzam, U. Hellman, B. Hainque, K. Schwartz and A. Waldenstrom (2003). "Identification of the genotypes causing hypertrophic cardiomyopathy in northern Sweden." Journal of Molecular & Cellular Cardiology **35**(7): 841-849.

Morner, S., P. Richard, E. Kazzam, U. Hellman, B. Hainque, K. Schwartz and A. Waldenstrom (2003). "Identification of the genotypes causing hypertrophic cardiomyopathy in northern Sweden." J Mol Cell Cardiol **35**(7): 841-849.

Muller, M., A. J. Mazur, E. Behrmann, R. P. Diensthuber, M. B. Radke, Z. Qu, . . . H. G. Mannherz (2012). "Functional characterization of the human alpha-cardiac actin mutations Y166C and M305L involved in hypertrophic cardiomyopathy." Cell Mol Life Sci **69**(20): 3457-3479.

Mun, J. Y., J. Gulick, J. Robbins, J. Woodhead, W. Lehman and R. Craig (2011). "Electron microscopy and 3D reconstruction of F-actin decorated with cardiac myosin-binding protein C (cMyBP-C)." J Mol Biol **410**(2): 214-225.

Murphy, R. T. and R. C. Starling (2005). "Genetics and cardiomyopathy: where are we now?" Cleveland Clinic Journal of Medicine **72**(6): 465-466.

Nagaoka, R., K. Kusano, H. Abe and T. Obinata (1995). "Effects of cofilin on actin filamentous structures in cultured muscle cells. Intracellular regulation of cofilin action." J Cell Sci **108 (Pt 2)**: 581-593.

Nakamura, M., S. Ueki, H. Hara and T. Arata (2005). "Calcium structural transition of human cardiac troponin C in reconstituted muscle fibres as studied by site-directed spin labelling." J Mol Biol **348**(1): 127-137.

Nanni, L., M. Pieroni, C. Chimenti, B. Simionati, R. Zimbello, A. Maseri, . . . G. Lanfranchi (2003). "Hypertrophic cardiomyopathy: two homozygous cases with "typical" hypertrophic cardiomyopathy and three new mutations in cases with progression to dilated cardiomyopathy." Biochem Biophys Res Commun **309**(2): 391-398.

Nave, R., D. O. Furst and K. Weber (1989). "Visualization of the polarity of isolated titin molecules: a single globular head on a long thin rod as the M band anchoring domain?" J Cell Biol **109**(5): 2177-2187.

Nebl, G., S. C. Meuer and Y. Samstag (1996). "Dephosphorylation of serine 3 regulates nuclear translocation of cofilin." J Biol Chem **271**(42): 26276-26280.

Niimura, H., L. L. Bachinski, S. Sangwatanaroj, H. Watkins, A. E. Chudley, W. McKenna, . . . C. E. Seidman (1998). "Mutations in the gene for cardiac myosin-

binding protein C and late-onset familial hypertrophic cardiomyopathy." N Engl J Med **338**(18): 1248-1257.

Niimura, H., K. K. Patton, W. J. McKenna, J. Soults, B. J. Maron, J. G. Seidman and C. E. Seidman (2002). "Sarcomere protein gene mutations in hypertrophic cardiomyopathy of the elderly." Circulation **105**(4): 446-451.

Nishida, E. (1985). "Opposite effects of cofilin and profilin from porcine brain on rate of exchange of actin-bound adenosine 5'-triphosphate." Biochemistry **24**(5): 1160-1164.

Nishida, E., K. Iida, N. Yonezawa, S. Koyasu, I. Yahara and H. Sakai (1987). "Cofilin is a component of intranuclear and cytoplasmic actin rods induced in cultured cells." Proc Natl Acad Sci U S A **84**(15): 5262-5266.

Niwa, R., K. Nagata-Ohashi, M. Takeichi, K. Mizuno and T. Uemura (2002). "Control of actin reorganization by Slingshot, a family of phosphatases that dephosphorylate ADF/cofilin." Cell **108**(2): 233-246.

Oakley, C. E., B. D. Hambly, P. M. Curmi and L. J. Brown (2004). "Myosin binding protein C: structural abnormalities in familial hypertrophic cardiomyopathy." Cell Res **14**(2): 95-110.

Offer, G., C. Moos and R. Starr (1973). "A new protein of the thick filaments of vertebrate skeletal myofibrils. Extractions, purification and characterization." Journal of Molecular Biology **74**(4): 653-676.

Olah, G. A. and J. Trewhella (1994). "A model structure of the muscle protein complex $4Ca^{2+}$.troponin C.troponin I derived from small-angle scattering data: implications for regulation." Biochemistry **33**(43): 12800-12806.

Ono, S., A. McGough, B. J. Pope, V. T. Tolbert, A. Bui, J. Pohl, . . . A. G. Weeds (2001). "The C-terminal tail of UNC-60B (actin depolymerizing factor/cofilin) is critical for maintaining its stable association with F-actin and is implicated in the second actin-binding site." J Biol Chem **276**(8): 5952-5958.

Paavilainen, V. O., M. C. Merckel, S. Falck, P. J. Ojala, E. Pohl, M. Wilmanns and P. Lappalainen (2002). "Structural conservation between the actin monomer-binding sites of twinfilin and actin-depolymerizing factor (ADF)/cofilin." J Biol Chem **277**(45): 43089-43095.

Page, S. P., S. Kounas, P. Syrris, M. Christiansen, R. Frank-Hansen, P. S. Andersen, . . . W. J. McKenna (2012). "Cardiac myosin binding protein-C mutations in families with hypertrophic cardiomyopathy: disease expression in relation to age, gender, and long term outcome." Circ Cardiovasc Genet **5**(2): 156-166.

Palm, T., K. Sale, L. Brown, H. Li, B. Hambly and P. G. Fajer (1999). "Intradomain distances in the regulatory domain of the myosin head in prepower and postpower stroke states: fluorescence energy transfer." Biochemistry **38**(40): 13026-13034.

Palmer, B. M., S. Sadayappan, Y. Wang, A. E. Weith, M. J. Previs, T. Bekyarova, . . . D. W. Maughan (2011). "Roles for cardiac MyBP-C in maintaining myofilament lattice rigidity and prolonging myosin cross-bridge lifetime." Biophys J **101**(7): 1661-1669.

Pancoska, P. and T. A. Keiderling (1991). "Systematic comparison of statistical analyses of electronic and vibrational circular dichroism for secondary structure prediction of selected proteins." Biochemistry **30**(28): 6885-6895.

Pavlov, D., A. Muhlrad, J. Cooper, M. Wear and E. Reisler (2007). "Actin filament severing by cofilin." J Mol Biol **365**(5): 1350-1358.

Pfuhl, M. and M. Gautel (2012). "Structure, interactions and function of the N-terminus of cardiac myosin binding protein C (MyBP-C): who does what, with what, and to whom?" J Muscle Res Cell Motil **33**(1): 83-94.

Pfuhl, M. and A. Pastore (1995). "Tertiary structure of an immunoglobulin-like domain from the giant muscle protein titin: a new member of the I set." Structure **3**(4): 391-401.

Pirani, A., M. V. Vinogradova, P. M. Curmi, W. A. King, R. J. Fletterick, R. Craig, . . . W. Lehman (2006). "An atomic model of the thin filament in the relaxed and Ca^{2+}-activated states." J Mol Biol **357**(3): 707-717.

Pliszka, B., M. J. Redowicz and D. Stepkowski (2001). "Interaction of the N-terminal part of the A1 essential light chain with the myosin heavy chain." Biochem Biophys Res Commun **281**(4): 924-928.

Poetter, K., H. Jiang, S. Hassanzadeh, S. R. Master, A. Chang, M. C. Dalakas, . . . N. D. Epstein (1996). "Mutations in either the essential or regulatory light chains of myosin are associated with a rare myopathy in human heart and skeletal muscle." Nat Genet **13**(1): 63-69.

Poglazov, B. F. (1983). "Actin and coordination of metabolic processes." Biochem Int **6**(6): 757-765.

Pope, B. J., K. M. Zierler-Gould, R. Kuhne, A. G. Weeds and L. J. Ball (2004). "Solution structure of human cofilin: actin binding, pH sensitivity, and relationship to actin-depolymerizing factor." J Biol Chem **279**(6): 4840-4848.

Potter, J. D., Z. Sheng, B. S. Pan and J. Zhao (1995). "A direct regulatory role for troponin T and a dual role for troponin C in the Ca^{2+} regulation of muscle contraction." Journal of Biological Chemistry **270**(6): 2557-2562.

Provencher, S. W. and J. Glockner (1981). "Estimation of globular protein secondary structure from circular dichroism." Biochemistry **20**(1): 33-37.

Ratti, J., E. Rostkova, M. Gautel and M. Pfuhl (2011). "Structure and interactions of myosin-binding protein C domain C0: cardiac-specific regulation of myosin at its neck?" J Biol Chem **286**(14): 12650-12658.

Rayment, I., H. M. Holden, M. Whittaker, C. B. Yohn, M. Lorenz, K. C. Holmes and R. A. Milligan (1993). "Structure of the actin-myosin complex and its implications for muscle contraction." Science **261**(5117): 58-65.

Rayment, I., W. R. Rypniewski, K. Schmidt-Base, R. Smith, D. R. Tomchick, M. M. Benning, . . . H. M. Holden (1993). "Three-dimensional structure of myosin subfragment-1: a molecular motor." Science **261**(5117): 50-58.

Razumova, M. V., K. L. Bezold, A. Y. Tu, M. Regnier and S. P. Harris (2008). "Contribution of the myosin binding protein C motif to functional effects in permeabilized rat trabeculae." J Gen Physiol **132**(5): 575-585.

Ressad, F., D. Didry, G. X. Xia, Y. Hong, N. H. Chua, D. Pantaloni and M. F. Carlier (1998). "Kinetic analysis of the interaction of actin-depolymerizing factor (ADF)/cofilin with G- and F-actins. Comparison of plant and human ADFs and effect of phosphorylation." J Biol Chem **273**(33): 20894-20902.

Richard, P., P. Charron, L. Carrier, C. Ledeuil, T. Cheav, C. Pichereau, . . . M. Komajda (2003). "Hypertrophic cardiomyopathy: distribution of disease genes, spectrum of mutations, and implications for a molecular diagnosis strategy." Circulation **107**(17): 2227-2232.

Richard, P., P. Charron, L. Carrier, C. Ledeuil, T. Cheav, C. Pichereau, . . . E. H. F. Project (2003). "Hypertrophic cardiomyopathy: distribution of disease genes, spectrum of mutations, and implications for a molecular diagnosis strategy.[comment]." Circulation. **107**(17): 2227-2232.

Richardson, P., W. McKenna, M. Bristow, B. Maisch, B. Mautner, J. O'Connell, . . . P. Nordet (1996). "Report of the 1995 World Health Organization/International Society and Federation of Cardiology Task Force on the Definition and Classification of cardiomyopathies." Circulation **93**(5): 841-842.

Roberts, R. and U. Sigwart (2001). "New concepts in hypertrophic cardiomyopathies, part II." Circulation **104**(18): 2249-2252.

Robertson, S. P., J. D. Johnson, M. J. Holroyde, E. G. Kranias, J. D. Potter and R. J. Solaro (1982). "The effect of troponin I phosphorylation on the Ca^{2+}-binding properties of the Ca^{2+}-regulatory site of bovine cardiac troponin." J Biol Chem **257**(1): 260-263.

Ross, M. H., G. I. Kaye and W. Pawlina (2003). Histology: A text and Atlas with Cell and Molecular Biology. USA, Lippincott Williams & Wilkins.

Ruegg, J., F. Holsboer, C. Turck and T. Rein (2004). "Cofilin 1 is revealed as an inhibitor of glucocorticoid receptor by analysis of hormone-resistant cells." Mol Cell Biol **24**(21): 9371-9382.

Rybakova, I. N., M. L. Greaser and R. L. Moss (2011). "Myosin binding protein C interaction with actin: characterization and mapping of the binding site." J Biol Chem **286**(3): 2008-2016.

Saber, W., K. J. Begin, D. M. Warshaw and P. VanBuren (2008). "Cardiac myosin binding protein-C modulates actomyosin binding and kinetics in the in vitro motility assay." J Mol Cell Cardiol **44**(6): 1053-1061.

Sadayappan, S., J. Gulick, H. Osinska, L. A. Martin, H. S. Hahn, G. W. Dorn, 2nd, . . . J. Robbins (2005). "Cardiac myosin-binding protein-C phosphorylation and cardiac function." Circ Res **97**(11): 1156-1163.

Satoh, M., M. Takahashi, T. Sakamoto, M. Hiroe, F. Marumo and A. Kimura (1999). "Structural analysis of the titin gene in hypertrophic cardiomyopathy: identification of a novel disease gene." Biochem Biophys Res Commun **262**(2): 411-417.

Schlossarek, S., G. Mearini and L. Carrier (2011). "Cardiac myosin-binding protein C in hypertrophic cardiomyopathy: mechanisms and therapeutic opportunities." J Mol Cell Cardiol **50**(4): 613-620.

Schoendube, F. A., H. G. Klues, S. Reith, F. A. Flachskampf, P. Hanrath and B. J. Messmer (1995). "Long-term clinical and echocardiographic follow-up after surgical correction of hypertrophic obstructive cardiomyopathy with extended myectomy and reconstruction of the subvalvular mitral apparatus." Circulation **92**(9 Suppl): II122-127.

Schultheiss, T., Z. X. Lin, M. H. Lu, J. Murray, D. A. Fischman, K. Weber, . . . H. Holtzer (1990). "Differential distribution of subsets of myofibrillar proteins in cardiac nonstriated and striated myofibrils." J Cell Biol **110**(4): 1159-1172.

Seidman, J. G. and C. Seidman (2001). "The genetic basis for cardiomyopathy: from mutation identification to mechanistic paradigms." Cell **104**(4): 557-567.

Semsarian, C. (2011). "Guidelines for the diagnosis and management of hypertrophic cardiomyopathy." Heart Lung Circ **20**(11): 688-690.

Shaffer, J. F., R. W. Kensler and S. P. Harris (2009). "The myosin-binding protein C motif binds to F-actin in a phosphorylation-sensitive manner." J Biol Chem **284**(18): 12318-12327.

Sherwood, L. (2004). Human Physology: From cells to Systems. USA, Brooks/Cole-Thomson Learning.

Sidani, M., D. Wessels, G. Mouneimne, M. Ghosh, S. Goswami, C. Sarmiento, . . . J. Condeelis (2007). "Cofilin determines the migration behavior and turning frequency of metastatic cancer cells." J Cell Biol **179**(4): 777-791.

Sigwart, U. (1995). "Non-surgical myocardial reduction for hypertrophic obstructive cardiomyopathy." Lancet **346**(8969): 211-214.

Sivaramakrishnan, S., E. Ashley, L. Leinwand and J. A. Spudich (2009). "Insights into human beta-cardiac myosin function from single molecule and single cell studies." J Cardiovasc Transl Res **2**(4): 426-440.

Sjostrom, M. and J. M. Squire (1977). "Fine structure of the A-band in cryo-sections. The structure of the A-band of human skeletal muscle fibres from ultra-thin cryo-sections negatively stained." J Mol Biol **109**(1): 49-68.

Slupsky, C. M. and B. D. Sykes (1995). "NMR solution structure of calcium-saturated skeletal muscle troponin C." Biochemistry **34**(49): 15953-15964.

Soman, J., T. Tao and G. N. Phillips, Jr. (1999). "Conformational variation of calcium-bound troponin C." Proteins **37**(4): 510-511.

Song, W., E. Dyer, D. J. Stuckey, O. Copeland, M. C. Leung, C. Bayliss, . . . S. B. Marston (2011). "Molecular mechanism of the E99K mutation in cardiac actin (ACTC Gene) that causes apical hypertrophy in man and mouse." J Biol Chem **286**(31): 27582-27593.

Soteriou, A., M. Gamage and J. Trinick (1993). "A survey of interactions made by the giant protein titin." J Cell Sci **104 (Pt 1)**: 119-123.

Spirito, P., C. E. Seidman, W. J. McKenna and B. J. Maron (1997). "The management of hypertrophic cardiomyopathy." N Engl J Med **336**(11): 775-785.

Spudich, J. A. and S. Watt (1971). "The regulation of rabbit skeletal muscle contraction. I. Biochemical studies of the interaction of the tropomyosin-troponin complex with actin and the proteolytic fragments of myosin." J Biol Chem **246**(15): 4866-4871.

Squire, J. M., P. K. Luther and C. Knupp (2003). "Structural evidence for the interaction of C-protein (MyBP-C) with actin and sequence identification of a possible actin-binding domain." J Mol Biol **331**(3): 713-724.

Squire, J. M., M. Roessle and C. Knupp (2004). "New X-ray diffraction observations on vertebrate muscle: organisation of C-protein (MyBP-C) and troponin and evidence for unknown structures in the vertebrate A-band." J Mol Biol **343**(5): 1345-1363.

Sreerama, N., S. Y. Venyaminov and R. W. Woody (1999). "Estimation of the number of alpha-helical and beta-strand segments in proteins using circular dichroism spectroscopy." Protein Sci **8**(2): 370-380.

Sugihara, H., Y. Taniguchi, K. Ito, K. Terada, K. Matsumoto, N. Kinoshita, . . . M. Nakagawa (1998). "Effects of diltiazem on myocardial perfusion abnormalities during exercise in patients with hypertrophic cardiomyopathy." Ann Nucl Med **12**(6): 349-354.

Szczesna, D., D. Ghosh, Q. Li, A. V. Gomes, G. Guzman, C. Arana, . . . J. D. Potter (2001). "Familial hypertrophic cardiomyopathy mutations in the regulatory light chains of myosin affect their structure, Ca^{2+} binding, and phosphorylation." J Biol Chem **276**(10): 7086-7092.

Szczesna-Cordary, D., G. Guzman, S. S. Ng and J. Zhao (2004). "Familial hypertrophic cardiomyopathy-linked alterations in Ca^{2+} binding of human cardiac myosin regulatory light chain affect cardiac muscle contraction." J Biol Chem **279**(5): 3535-3542.

Takahashi-Yanaga, F., S. Morimoto, K. Harada, R. Minakami, F. Shiraishi, M. Ohta, . . . I. Ohtsuki (2001). "Functional consequences of the mutations in human cardiac troponin I gene found in familial hypertrophic cardiomyopathy." J Mol Cell Cardiol **33**(12): 2095-2107.

Takeda, S. (2005). "Crystal structure of troponin and the molecular mechanism of muscle regulation." J Electron Microsc (Tokyo) **54 Suppl 1**: i35-41.

Takeda, S., A. Yamashita, K. Maeda and Y. Maeda (2003). "Structure of the core domain of human cardiac troponin in the $Ca(^{2+})$-saturated form." Nature **424**(6944): 35-41.

Tanigawa, G., J. A. Jarcho, S. Kass, S. D. Solomon, H. P. Vosberg, J. G. Seidman and C. E. Seidman (1990). "A molecular basis for familial hypertrophic cardiomyopathy: an alpha/beta cardiac myosin heavy chain hybrid gene." Cell **62**(5): 991-998.

Teare, D. (1958). "Asymmetrical hypertrophy of the heart in young adults." Br Heart J **20**(1): 1-8.

Teubner, A. and A. Wegner (1998). "Kinetic evidence for a readily exchangeable nucleotide at the terminal subunit of the barbed ends of actin filaments." Biochemistry **37**(20): 7532-7538.

Thierfelder, L., H. Watkins, C. MacRae, R. Lamas, W. McKenna, H. P. Vosberg, . . . C. E. Seidman (1994). "Alpha-tropomyosin and cardiac troponin T mutations cause familial hypertrophic cardiomyopathy: a disease of the sarcomere." Cell **77**(5): 701-712.

Thorne, H. V. (1967). "Electrophoretic characterization and fractionation of polyoma virus DNA." J Mol Biol **24**(2): 203-211.

Timson, D. J., H. R. Trayer and I. P. Trayer (1998). "The N-terminus of A1-type myosin essential light chains binds actin and modulates myosin motor function." Eur J Biochem **255**(3): 654-662.

Todiere, G., G. D. Aquaro, P. Piaggi, F. Formisano, A. Barison, P. G. Masci, . . . M. Lombardi (2012). "Progression of myocardial fibrosis assessed with cardiac magnetic resonance in hypertrophic cardiomyopathy." J Am Coll Cardiol **60**(10): 922-929.

Tong, C. W., J. E. Stelzer, M. L. Greaser, P. A. Powers and R. L. Moss (2008). "Acceleration of crossbridge kinetics by protein kinase A phosphorylation of cardiac myosin binding protein C modulates cardiac function." Circ Res **103**(9): 974-982.

Toyoshima, Y. Y., S. J. Kron, E. M. McNally, K. R. Niebling, C. Toyoshima and J. A. Spudich (1987). "Myosin subfragment-1 is sufficient to move actin filaments in vitro." Nature **328**(6130): 536-539.

Ueki, S., M. Nakamura, T. Komori and T. Arata (2005). "Site-directed spin labeling electron paramagnetic resonance study of the calcium-induced structural transition in the N-domain of human cardiac troponin C complexed with troponin I." Biochemistry **44**(1): 411-416.

Valettas, N., R. Rho, J. Beshai, C. T. Lloyd, H. M. Ross, D. Kocovic and H. C. Herrmann (2003). "Alcohol septal ablation complicated by complete heart block and permanent pacemaker failure." Catheter Cardiovasc Interv **58**(2): 189-193.

van Dijk, S. J., D. Dooijes, C. dos Remedios, M. Michels, J. M. Lamers, S. Winegrad, . . . J. van der Velden (2009). "Cardiac myosin-binding protein C mutations and hypertrophic cardiomyopathy: haploinsufficiency, deranged phosphorylation, and cardiomyocyte dysfunction." Circulation **119**(11): 1473-1483.

Van Driest, S. L., E. G. Ellsworth, S. R. Ommen, A. J. Tajik, B. J. Gersh and M. J. Ackerman (2003). "Prevalence and spectrum of thin filament mutations in an outpatient referral population with hypertrophic cardiomyopathy." Circulation **108**(4): 445-451.

van Eerd, J. P. and K. Takahashi (1975). "The amino acid sequence of bovine cardiac tamponin-C. Comparison with rabbit skeletal troponin-C." Biochem Biophys Res Commun **64**(1): 122-127.

Varnava, A. M., P. M. Elliott, C. Baboonian, F. Davison, M. J. Davies and W. J. McKenna (2001). "Hypertrophic cardiomyopathy: histopathological features of sudden death in cardiac troponin T disease." Circulation **104**(12): 1380-1384.

Vassylyev, D. G., S. Takeda, S. Wakatsuki, K. Maeda and Y. Maeda (1998). "Crystal structure of troponin C in complex with troponin I fragment at 2.3-A resolution." Proc Natl Acad Sci U S A **95**(9): 4847-4852.

Vaughan, K. T., F. E. Weber, S. Einheber and D. A. Fischman (1993). "Molecular cloning of chicken myosin-binding protein (MyBP) H (86-kDa protein) reveals extensive homology with MyBP-C (C-protein) with conserved immunoglobulin C2 and fibronectin type III motifs." J Biol Chem **268**(5): 3670-3676.

Venema, R. C. and J. F. Kuo (1993). "Protein kinase C-mediated phosphorylation of troponin I and C-protein in isolated myocardial cells is associated with inhibition of myofibrillar actomyosin MgATPase." J Biol Chem **268**(4): 2705-2711.

Vikstrom, K. L. and L. A. Leinwand (1996). "Contractile protein mutations and heart disease." Curr Opin Cell Biol **8**(1): 97-105.

Vinkemeier, U., W. Obermann, K. Weber and D. O. Furst (1993). "The globular head domain of titin extends into the center of the sarcomeric M band. cDNA cloning, epitope mapping and immunoelectron microscopy of two titin-associated proteins." J Cell Sci **106 (Pt 1)**: 319-330.

Volkmann, N., H. Lui, L. Hazelwood, K. M. Trybus, S. Lowey and D. Hanein (2007). "The R403Q myosin mutation implicated in familial hypertrophic cardiomyopathy causes disorder at the actomyosin interface." PLoS One **2**(11): e1123.

Vulpian, A. (1868). "Contribution à l'étude des rétrécíssements de l'orifice ventriculo-aortique." Archives de Physiologie **3**: 456-457.

Vydyanath, A., C. A. Gurnett, S. Marston and P. K. Luther (2012). "Axial distribution of myosin binding protein-C is unaffected by mutations in human cardiac and skeletal muscle." J Muscle Res Cell Motil **33**(1): 61-74.

Wang, K. (1985). "Sarcomere-associated cytoskeletal lattices in striated muscle. Review and hypothesis." Cell Muscle Motil **6**: 315-369.

Watkins, H., D. Conner, L. Thierfelder, J. A. Jarcho, C. MacRae, W. J. McKenna, . . . C. E. Seidman (1995). "Mutations in the cardiac myosin binding protein-C gene on chromosome 11 cause familial hypertrophic cardiomyopathy." Nat Genet **11**(4): 434-437.

Watkins, H., A. Rosenzweig, D. S. Hwang, T. Levi, W. McKenna, C. E. Seidman and J. G. Seidman (1992). "Characteristics and prognostic implications of myosin missense mutations in familial hypertrophic cardiomyopathy." N Engl J Med **326**(17): 1108-1114.

Watkins, H., J. G. Seidman and C. E. Seidman (1995). "Familial hypertrophic cardiomyopathy: a genetic model of cardiac hypertrophy." Hum Mol Genet **4 Spec No**: 1721-1727.

Weber, F. E., K. T. Vaughan, F. C. Reinach and D. A. Fischman (1993). "Complete sequence of human fast-type and slow-type muscle myosin-binding-protein C (MyBP-C). Differential expression, conserved domain structure and chromosome assignment." Eur J Biochem **216**(2): 661-669.

Weisberg, A. and S. Winegrad (1996). "Alteration of myosin cross bridges by phosphorylation of myosin-binding protein C in cardiac muscle." Proc Natl Acad Sci U S A **93**(17): 8999-9003.

Weisberg, A. and S. Winegrad (1998). "Relation between crossbridge structure and actomyosin ATPase activity in rat heart." Circ Res **83**(1): 60-72.

Weith, A., S. Sadayappan, J. Gulick, M. J. Previs, P. Vanburen, J. Robbins and D. M. Warshaw (2012). "Unique single molecule binding of cardiac myosin binding protein-C to actin and phosphorylation-dependent inhibition of actomyosin

motility requires 17 amino acids of the motif domain." J Mol Cell Cardiol **52**(1): 219-227.

Welikson, R. E. and D. A. Fischman (2002). "The C-terminal IgI domains of myosin-binding proteins C and H (MyBP-C and MyBP-H) are both necessary and sufficient for the intracellular crosslinking of sarcomeric myosin in transfected non-muscle cells." J Cell Sci **115**(Pt 17): 3517-3526.

Whiting, A., J. Wardale and J. Trinick (1989). "Does titin regulate the length of muscle thick filaments?" J Mol Biol **205**(1): 263-268.

Whitmore, L. and B. A. Wallace (2004). "DICHROWEB, an online server for protein secondary structure analyses from circular dichroism spectroscopic data." Nucleic Acids Res **32**(Web Server issue): W668-673.

Whitten, A. E., C. M. Jeffries, S. P. Harris and J. Trewhella (2008). "Cardiac myosin-binding protein C decorates F-actin: implications for cardiac function." Proc Natl Acad Sci U S A **105**(47): 18360-18365.

Wigle, E. D., H. Rakowski, B. P. Kimball and W. G. Williams (1995). "Hypertrophic cardiomyopathy. Clinical spectrum and treatment." Circulation **92**(7): 1680-1692.

Wigle, E. D., Z. Sasson, M. A. Henderson, T. D. Ruddy, J. Fulop, H. Rakowski and W. G. Williams (1985). "Hypertrophic cardiomyopathy. The importance of the site and the extent of hypertrophy. A review." Prog Cardiovasc Dis **28**(1): 1-83.

Winegrad, S. (1999). "Cardiac myosin binding protein C." Circ Res **84**(10): 1117-1126.

Winegrad, S. (2003). "Myosin-binding protein C (MyBP-C) in cardiac muscle and contractility." Adv Exp Med Biol **538**: 31-40; discussion 40-31.

Wolska, B. M. and D. M. Wieczorek (2003). "The role of tropomyosin in the regulation of myocardial contraction and relaxation." Pflugers Arch **446**(1): 1-8.

Wong, D. Y. and D. Sept (2011). "The interaction of cofilin with the actin filament." J Mol Biol **413**(1): 97-105.

Xing, J. and H. C. Cheung (1995). "Internal movement in myosin subfragment 1 detected by fluorescence resonance energy transfer." Biochemistry **34**(19): 6475-6487.

Xu, Q., S. Dewey, S. Nguyen and A. V. Gomes (2010). "Malignant and benign mutations in familial cardiomyopathies: insights into mutations linked to complex cardiovascular phenotypes." J Mol Cell Cardiol **48**(5): 899-909.

Yamamoto, K. (1986). "The binding of skeletal muscle C-protein to regulated actin." FEBS Lett **208**(1): 123-127.

Yamamoto, K. and C. Moos (1983). "The C-proteins of rabbit red, white, and cardiac muscles." J Biol Chem **258**(13): 8395-8401.

Yang, Q., T. E. Hewett, R. Klevitsky, A. Sanbe, X. Wang and J. Robbins (2001). "PKA-dependent phosphorylation of cardiac myosin binding protein C in transgenic mice." Cardiovasc Res **51**(1): 80-88.

Yang, Q., A. Sanbe, H. Osinska, T. E. Hewett, R. Klevitsky and J. Robbins (1998). "A mouse model of myosin binding protein C human familial hypertrophic cardiomyopathy." J Clin Invest **102**(7): 1292-1300.

Yasuda, M., S. Koshida, N. Sato and T. Obinata (1995). "Complete primary structure of chicken cardiac C-protein (MyBP-C) and its expression in developing striated muscles." J Mol Cell Cardiol **27**(10): 2275-2286.

Yonezawa, N., E. Nishida, K. Iida, I. Yahara and H. Sakai (1990). "Inhibition of the interactions of cofilin, destrin, and deoxyribonuclease I with actin by phosphoinositides." J Biol Chem **265**(15): 8382-8386.

Yonezawa, N., E. Nishida, S. Koyasu, S. Maekawa, Y. Ohta, I. Yahara and H. Sakai (1987). "Distribution among tissues and intracellular localization of cofilin, a 21kDa actin-binding protein." Cell Struct Funct **12**(5): 443-452.

Yonezawa, N., E. Nishida and H. Sakai (1985). "pH control of actin polymerization by cofilin." J Biol Chem **260**(27): 14410-14412.

Yu, B., J. A. French, L. Carrier, R. W. Jeremy, D. R. McTaggart, M. R. Nicholson, . . . R. J. Trent (1998). "Molecular pathology of familial hypertrophic cardiomyopathy caused by mutations in the cardiac myosin binding protein C gene." J Med Genet **35**(3): 205-210.

Zoghbi, M. E., J. L. Woodhead, R. L. Moss and R. Craig (2008). "Three-dimensional structure of vertebrate cardiac muscle myosin filaments." Proc Natl Acad Sci U S A **105**(7): 2386-2390.